Towards Compostable Pressure Sensitive Adhesives

By

Maryam Movafagh

Thesis submitted to the University of Ottawa
in partial Fulfillment of the requirements for the
degree of Ph.D. in Chemical Engineering

Department of Chemical and Biological Engineering, Faculty of Engineering

University of Ottawa, Ottawa, Canada

Abstract

Polymers play a crucial role in modern society, yet their widespread use has led to environmental challenges, particularly due to their persistence and reliance on petroleum-based feedstocks. The transition toward sustainable polymer reaction engineering requires innovations in polymer synthesis, including water-based polymerization, bio-based monomers, and degradable structures that enable responsible end-of-life disposal. Among polymeric materials, pressure-sensitive adhesives (PSAs) are widely used in packaging, medical, and industrial applications, but conventional PSAs are synthesized via solution polymerization using petroleum-derived monomers, resulting in non-biodegradable materials that contribute to long-term waste accumulation.

This study develops sustainable, compostable PSAs via emulsion polymerization, incorporating bio-based monomers and renewable nanomaterials to achieve a balance between adhesive performance and environmental degradability. A key innovation is the integration of 2-methylene-1,3-dioxepane (MDO) into butyl acrylate (BA)/vinyl acetate (VAc) terpolymers, introducing hydrolyzable ester bonds to enhance degradability. The reactivity ratios of MDO, BA, and VAc were estimated using the Error-in-Variables Model (EVM) to provide crucial insights into monomer distribution and polymer structure. A major challenge in emulsion polymerization was MDO's hydrolysis sensitivity and ring retention, which was mitigated through optimized reaction conditions, including pH control (7.8–8.8) and reaction temperatures (40–50°C). These optimizations minimized ring retention, ensuring the effective incorporation of degradable linkages.

To further enhance PSA performance, carboxylated cellulose nanocrystals (cCNCs) were incorporated via post-polymerization blending, reinforcing the polymer matrix and simultaneously improving tack, peel strength, and shear adhesion without compromising sustainability and biodegradability. The biodegradability of these formulations was evaluated under controlled composting conditions following ASTM D5338, using a lab-scale composting setup. Among the tested formulations, BMV10-NEW-cCNC (containing 10 wt% MDO and cCNC) exhibited the highest degradation rate. The elevated polymerization temperature (50°C) led to nearly complete MDO ring opening, as confirmed by ^{13}C-NMR, with CO_2 evolution indicating 12.49 wt% biodegradation over 60 days. While these findings demonstrate the potential of MDO-based PSAs

for compostable adhesive applications, further improvements in MDO content and polymerization strategies are needed to achieve complete degradation under industrial composting conditions.

This study highlights the potential of integrating bio-based polymer chemistry, nanomaterials, and controlled water-based polymerization techniques to develop high-performance, compostable PSAs, advancing the field of sustainable polymer reaction engineering and contributing to a circular economy.

Résumé

Les polymères jouent un rôle crucial dans la société moderne, mais leur utilisation généralisée a entraîné des défis environnementaux, notamment en raison de leur persistance et de leur dépendance aux matières premières dérivées du pétrole. La transition vers l'ingénierie des réactions polymères durables nécessite des innovations dans la synthèse des polymères, y compris la polymérisation à base d'eau, les monomères biosourcés et les structures dégradables permettant une élimination responsable en fin de vie. Parmi les matériaux polymères, les adhésifs sensibles à la pression (PSAs) sont largement utilisés dans les applications d'emballage, médicales et industrielles, mais les PSAs conventionnels sont synthétisés par polymérisation en solution à l'aide de monomères dérivés du pétrole, ce qui donne des matériaux non biodégradables contribuant à l'accumulation de déchets à long terme.

Cette étude développe des PSAs durables et compostables par polymérisation en émulsion, intégrant des monomères biosourcés et des nanomatériaux renouvelables pour atteindre un équilibre entre les performances adhésives et la dégradabilité environnementale. Une innovation clé est l'intégration de 2-méthylène-1,3-dioxépane (MDO) dans des térpolymères acrylate de butyle (BA)/acétate de vinyle (VAc), introduisant des liaisons esters hydrolysables pour améliorer la dégradabilité. Les rapports de réactivité de MDO, BA et VAc ont été estimés à l'aide du modèle de l'erreur dans les variables (EVM) afin de fournir des informations cruciales sur la distribution des monomères et la structure du polymère. Un défi majeur de la polymérisation en émulsion était la sensibilité de MDO à l'hydrolyse et la rétention d'anneaux, ce qui a été atténué par des conditions de réaction optimisées, y compris le contrôle du pH (7,8–8,8) et des températures de réaction (40–50°C). Ces optimisations ont minimisé la rétention d'anneaux, assurant ainsi l'incorporation effective des liaisons dégradables.

Pour améliorer davantage les performances des PSAs, des nanocristaux de cellulose carboxylée (cCNCs) ont été incorporés par mélange post-polymérisation, renforçant la matrice polymère et améliorant simultanément l'adhérence, la résistance au pelage et l'adhésion au cisaillement sans compromettre la durabilité et la biodégradabilité. La biodégradabilité de ces formulations a été évaluée dans des conditions de compostage contrôlées suivant la norme ASTM D5338, en utilisant une installation de compostage à l'échelle du laboratoire. Parmi les formulations testées, BMV10-NEW-cCNC (contenant 10 % en poids de MDO et cCNCs) a montré le taux de dégradation le plus élevé. La température de polymérisation élevée (50°C) a conduit à

une ouverture quasi complète des anneaux de MDO, comme le confirme le ^{13}C-NMR, avec une évolution de CO_2 indiquant une biodégradation de 12,49 wt% sur 60 jours. Bien que ces résultats démontrent le potentiel des PSAs à base de MDO pour les applications d'adhésifs compostables, des améliorations supplémentaires dans la teneur en MDO et les stratégies de polymérisation sont nécessaires pour parvenir à une dégradation complète dans des conditions de compostage industriel.

Cette étude met en évidence le potentiel de l'intégration de la chimie des polymères biosourcés, des nanomatériaux et des techniques de polymérisation contrôlée à base d'eau pour développer des PSAs de haute performance et compostables, faisant progresser le domaine de l'ingénierie des réactions polymères durables et contribuant à une économie circula.

Dedication

To all Iranian women who have been denied the opportunity to pursue their dreams yet continue to fight with resilience and courage for every step forward. To those who have faced countless constraints yet refuse to be silenced, fighting not just for themselves but for a future where equality, education, and freedom are not privileges but fundamental rights—this work is for you. **Woman, Life, Freedom**.

To my best friend and soulmate, my husband, Ali, who has stood by my side through every challenge, offering love, encouragement, and endless support.

To my mom and dad, who have shown me the true meaning of hard work and perseverance, and whose support has shaped the person I am today.

To my sisters, Fatemeh and Sahar, my dear friends, and every person who has helped, guided, inspired, and encouraged me—your kindness, wisdom, and companionship have been my pillars of strength throughout this journey. Thank you for being part of my life.

Acknowledgements

I would like to express my deepest gratitude to my supervisors, Prof. Marc A. Dubé and Prof. Kelly M. Meek.

Marc was not only an incredible mentor but also one of the best people I have had the privilege to work with. Supportive, kind, and a man of his word, he created an environment where I could learn and grow with confidence. His encouragement, scientific insights, and unwavering support have shaped my journey, and I will always be grateful for the invaluable lessons he imparted, both academically and personally.

Kelly brought an energy to our discussions that made research exciting. Young, brilliant, and approachable, she felt more like a friend to brainstorm and explore science with rather than just a supervisor. Our conversations were always insightful, and her enthusiasm made every challenge feel like an opportunity.

I was truly fortunate to have Marc and Kelly by my side throughout my PhD journey. They made this experience not just educational but also enjoyable, reminding me that academia can be filled with fun, kindness, and truly great people. Their support, mentorship, and warmth will always stay with me, and I will forever cherish the time I spent working with them.

To my husband, Ali Fadaei, for his unwavering support, especially during moments of emotional breakdown and overwhelming challenges throughout my Ph.D. journey. He was my source of motivation and provided invaluable help, especially when I faced difficulties with computer-based problems, including coding-related challenges. His patience, encouragement, and technical expertise made a significant difference in my research, and I am incredibly grateful for his presence in my life.

I would also like to extend my gratitude to Dr. Fatemeh Abedi, my best friend since our bachelor's studies. She has been someone I could always turn to, whether for scientific discussions or personal challenges. Her support and encouragement have been invaluable throughout this journey.

A special thank you to Parisa Bayat, my labmate, officemate, and friend. We started our PhD journey together, and being the only two in the Polymer Reaction Engineering group who shared the same language made our bond even stronger. From long hours in the lab to navigating the challenges of research and adapting to life in a new country, her friendship has been a source of comfort and strength.

I would also like to thank Gerard Nina, Franco Ziroldo, and Patrick Pageau for their invaluable assistance in making ampoules and setting up the composting experiments in the lab.

I would like to acknowledge Prof. Alison J. Scott (Dalhousie University) for their valuable contributions to reactivity ratio measurements. Prof. Alison J. Scott contributed MATLAB-based simulations for calculating reactivity ratios.

This journey would not have been the same without the support, kindness, and generosity of these incredible people. I am deeply thankful to each and every one of them.

Statement of Contributions

I would like to acknowledge Prof. Emily D. Cranston (University of British Columbia), Prof. Michael Cunningham (Queen's University), and Prof. Pascale Champagne (Queen's University) for their valuable editorial comments and general experimental guidance on the work involving carboxylated cellulose nanocrystals. I also extend my appreciation to Parisa Bayat (University of Ottawa), Dr. Timothy Morse (Anomera Inc.), Michael Kiriakou (Anomera Inc.), and Dr. Sean George (BASF Corp.) for their collaboration and support in various aspects of this work.

I would like to acknowledge Prof. Alexander Penlidis (University of Waterloo) and Prof. Alison J. Scott (Dalhousie University) for their valuable contributions to reactivity ratio measurements.

I would also like to thank Vida A. Gabriel for building the composting setup, which provided the foundation for my composting work.

Finally, I am deeply grateful to my supervisors, Prof. Marc A. Dubé and Prof. Kelly M. Meek, for their scientific guidance, and invaluable contributions to the revisions and editing of the manuscripts presented in this thesis.

Statement of Originality

I certify that the research presented in this thesis is of my own work, and all referenced work performed by others is explicitly stated using standard methods.

Table of Contents

List of Figures

List of Tables

Nomenclature

2OA	2-Octyl acrylate monomer
2-EHA	2-Ethylhexyl Acrylate
AFM	Atomic force microscopy
AIBN	2,2'-Azobisisobutyronitrile
APS	Ammonium persulfate
ASTM	American Society for Testing and Materials
ATR-FTIR	Attenuated total reflectance-Fourier transform infrared spectroscopy
BA	Butyl acrylate
$CDCl_3$	Deuterated chloroform
cCNC	Carboxylated CNCs
CNC	Cellulose nanocrystal
CTA	Chain transfer agent
D_2O	Deuterium oxide
DDW	Distilled deionized water
DLS	Dynamic light scattering
DMA	Dynamic mechanical analysis
DSC	Differential scanning calorimetry
EDTA	Ethylenediaminetetraacetic Acid
HCl	Hydrochloric acid
ISO	International Organization for Standardization
KPS	Potassium persulfate
M_c	Molecular weight between crosslink
M_e	Entanglement molecular weight
M_w	Molecular weight
MMA	Methyl methacrylate
mol%	Mol percent
MWD	Molecular weight distribution
MDO	2-Methylene 1,3-dioxepane
NaOH	Sodium hydroxide
NMR	Nuclear magnetic resonance spectroscopy
phm	Parts per hundred parts of monomer
PLLA	Poly-L-lactic acid
ppm	Parts per million
PSA	Pressure-sensitive adhesive
PSD	Particle size distribution
PSTC	Pressure Sensitive Tape Council
SEM	Scanning electron microscopy
t-BHP	tert-Butyl hydroperoxide
TEM	Transmission electron microscopy
T_g	Glass transition temperature
TGA	Thermogravimetric Analysis
THF	Tetrahydrofuran
VAc	Vinyl Acetate
VOCs	Volatile organic compounds
wt.%	Weight percent

Chapter 1
Introduction

1.1 Sustainable polymer reaction engineering

Polymer materials offer unrivalled benefits to humanity, meeting a wide variety of needs over a range of applications. However, polymers present substantial environmental issues by contributing to climate change, air pollution, waste generation and water pollution due to their widespread use and existing production and disposal methods.[1] Polymer reaction engineering is an economically important and technologically broad topic that has significant potential for transformation toward better sustainability. There is no single, unique way to transform polymerization processes into more environmentally friendly ones; rather, a combination of multiple procedures can result in a more sustainable polymerization process. However, our concerns extend beyond the production of the polymer and include its end-of-life impact. The "12 Principles of Green Chemistry" (Figure 1.1) provide a guide towards achieving a more sustainable approach to the synthesis, use, and disposal of polymeric materials.[2] These principles were used to reexamine polymerization techniques by Salehpour and Dubé.[3] They determined that four of the principles have the most potential to provide a positive environmental impact: using safer solvents and reaction conditions (principle #8), using renewable feedstock (principle #4), building safer products (principle #2), and designing for less hazardous waste (principle #10). This has guided research to investigate the use of water-based (e.g, emulsion) synthesis methods as opposed to solvent-based ones, to replace traditional petroleum-based components with bio-based alternatives, and to use renewable, non-toxic means to modify polymer properties. Six years later, Dubé et al., provided an update on the most recent advances in the utilization of renewable polymer materials, process intensification initiatives, water-based polymerization, and approaches to dealing with the end of the polymer's application life. From that work, the issue of degradability, and more specifically, compostability, was identified as an avenue worthy of exploration.[1]

A class of polymeric materials of interest in this thesis was pressure sensitive adhesives (PSAs). PSAs can quickly adhere to solid surfaces under low pressure (i.e., finger pressure) and are viscoelastic polymeric materials having a low glass transition temperature (T_g) ranging from -70 to -20 ^{o}C.[4] They are used for labels, tapes, films, and other specialized applications, making

them vital in everyday life.[5] The worldwide demand for PSAs continues to grow. The world market for PSAs was evaluated at $9.8 billion in 2020 and is predicted to reach $17.6 billion by 2030. It shows a compound annual growth rate of 6.1% from 2021 to 2030.[6] Acrylic PSAs led the PSA market in 2016, accounting for 54.5% of the total 3.1 MT of PSAs manufactured that year, with a yearly growth rate of 5.6%.[7]

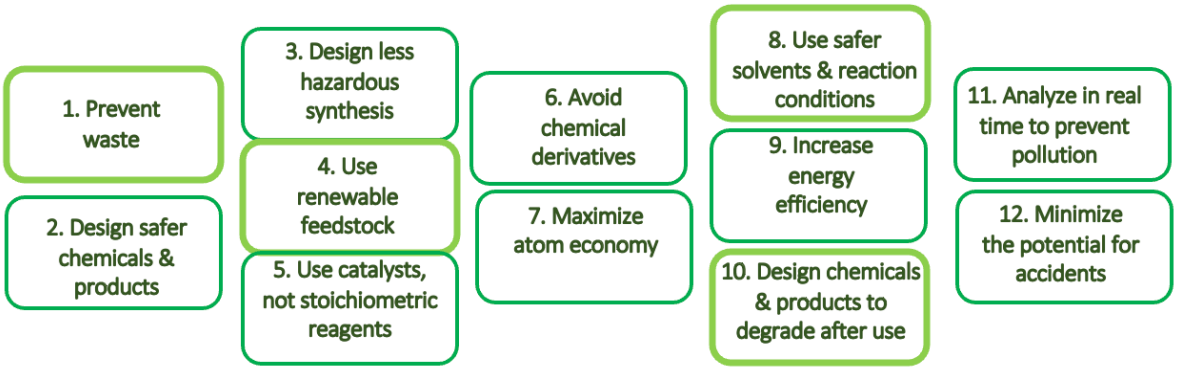

Figure 1.1. 12 Principles of Green Chemistry[2,3]

The adhesive and cohesive properties of PSAs are closely tied to their viscoelastic properties.[8] Firstly, the wetting of the substrate and the Van der Waals and polar forces between the PSA and the substrate give rise to adhesion. On the other hand, intermolecular forces, and covalent interactions, such as polymer crosslinks, influence the cohesion of a PSA. Often, these forces are impacted by various production factors in opposing ways, making the control of their properties challenging. To adjust adhesive characteristics in PSA formulations, a "hard monomer" (i.e., high polymer T_g), such as methyl methacrylate (MMA), can be copolymerized with a "softer" monomer (i.e., low polymer T_g) such as 2-ethyl hexyl acrylate (EHA).[9,10] The PSA market is dominated by polyacrylates made by free radical polymerization. Acrylic adhesives have the benefits of colorlessness, outstanding cohesive strength, adequate tack and peel strength, and good heat and aging resistance. The "soft" monomers typically provide the required flowability and wettability to give the PSA film tack and peel strength. The PSA gains hardness and internal strength from the "hard" monomers. Modifiers such as crosslinkers and chain transfer agents (CTAs) are often used to manipulate the polymer microstructure, which further impacts PSA performance.[11] Adding a CTA tends to boost polymer flexibility and mobility by lowering molecular weight and gel content level. On the other hand, an increase in crosslinker concentration

leads to a higher gel content, which increases both the stiffness and internal (or cohesive) strength of the PSA.[12,13]Moreover, PSAs typically require the use of additives, which often bring additional hazards to the synthesis, processing, application, and disposal stages.

Historically, PSAs have been produced using solution polymerization, which poses evident hazardous conditions both at the synthesis stage and during product application. Within the last few decades increased environmental concerns on the management of volatile organic compounds (VOCs) have resulted in tremendous growth in the use of emulsion polymerization to make latexes for water-borne coating applications as alternatives to solvent-borne coatings.[14] In a similar way, commercial PSA production is shifting to emulsion polymerization. Acrylic PSAs can be produced by the more sustainable free radical emulsion polymerization.[15] In addition to its environmental benefits (i.e., not using a toxic solvent), the water used as the medium in emulsion polymerization is effective as a heat sink for the highly exothermic polymerization reaction, provides a low viscosity/high polymer molecular weight product, and provides unique opportunities for product formulation due to the resulting sub-micron particle size and morphology (e.g., for film casting applications).[16]

Another approach to improve sustainability involves the synthesis of PSAs from renewable resources to reduce our reliance on petroleum, the common source for monomers. For this reason, biobased polymers have attracted the attention of industry, consumers, and governments.[17] There is a significant global demand for replacing petroleum-derived raw materials with renewable, bio-based materials in producing valuable polymeric products.[18] We must replace the most impactful components (i.e., petroleum-based monomers) with greener counterparts if we are to make our PSA formulation sustainable. While there are many options available, many of them are either too costly or are obtained through unsustainable pathways (e.g., the process for acquiring and isolating renewable monomers is sometimes less environmentally friendly than the process for its fossil-based counterpart),[1] thus defeating the purpose of this research. We propose to use 2-methylene-1,3-dioxepane (MDO) as a component of our PSA formulation because its physical properties make it suitable for PSA production, it is a bio-sourced monomer, and as will be discussed, it presents a possible pathway for degradability. MDO is considered a bio-based monomer because it is produced from starting materials such as 1,4-butanediol and diethylene glycol, which are themselves bio-sourced materials (i.e., produced from plant-derived glucose and fermentation of corn or sugarcane, respectively).[19] In addition, the

homopolymer of MDO has a low T_g, making it an ideal replacement for petroleum-based monomers in PSA formulations. Thus, we proposed to displace some of the petroleum-based, non-biodegradable components in a PSA formulation with MDO to increase the percentage of bio-based components in the formulation.

By changing from a solution-based technology to emulsion polymerization, there is an inevitable impact on polymer properties. In addition, changing a product formulation from a traditional monomer to a bio-sourced one often results in further property changes. As noted, these property changes usually are addressed by using additives such as CTAs and cross-linkers to modify the polymer microstructure and compensate for the changes. However, these additives often introduce further toxicity to the PSA formulation. As an alternative, the effectiveness of using a "green" nanomaterial, cellulose nanocrystals (CNCs), for PSA property modification has been shown. [20–23] In that pioneering work, petroleum-based monomers were still a substantial part of the reaction formulation. CNCs have attracted much attention in recent years due to their renewability, nontoxicity, and availability.[24] CNCs are hydrophilic, which makes them eminently compatible with emulsion polymerization. What makes them effective in PSA applications is their high aspect ratio, which allows them to form a network at an interface or in the continuous phase of a matrix rather than the typical close-packed monolayer seen when using spherical nanomaterials.[25] Thus, we proposed to use CNCs in this project to compensate for any PSA property changes resulting from changes in the formulation.

In our research group, carboxylated CNCs (cCNCs) called DextraCel (produced by Anomera Inc.) have been used in emulsion-based PSAs and have resulted in improvements to PSA properties.[23,26] DextraCel has a length of 100–200 nm and a width of 5 nm and can form stable colloidal suspensions in water. DextraCel has a lower surface charge and is somewhat shorter than CNCs produced by sulfuric acid hydrolysis or other commercial CNCs.[27] Moreover, the effect of DextraCel cCNCs on PSA properties requires further study.

A final consideration for aligning with the "12 Principles of Green Chemistry" is the end-of-life of the polymer. A major environmental drawback of polymer materials is that they do not readily decompose in the environment, resulting in their accumulation.[28] Synthetic polymer waste is a significant and growing environmental concern. It is difficult to naturally degrade polymers due to their high molecular weight.[29] The backbone chains of polymers produced via chain-growth polymerization are composed of carbon atoms and are highly resistant to hydrolytic

cleavage. These polymers are, therefore, deemed non-biodegradable.[30] On the other hand, the backbones of many polymers produced via step-growth polymerization (e.g., polyesters and polyurethanes) contain heteroatoms such as oxygen and nitrogen. Because of the hydrophilic amide or ester bond between the structural units of step-growth polymers, these polymers may be prone to hydrolytic cleavage. However, step-growth polymers will last at least decades, if not centuries, when disposed of in landfills because their molecular weights are also very high.[31] Biodegradation in nature is said to occur only at molecular weights of less than tens of thousands, which is regarded as relatively low for many industrial polymers.[32] Moreover, making a product biodegradable has no inherent value if it does not end up in a waste management system that takes advantage of the biodegradability features after the customer has used it.[33]

Composting is the controlled decomposition of heterogeneous organic materials by a mixed microbial population in a wet, warm, aerobic atmosphere. [34] The primary outcome of biodegradation of naturally occurring materials will be valuable compost, combined with water and CO_2. In the case of food waste, for example, because the CO_2 produced is already part of the biological carbon cycle, it does not contribute to an increase in greenhouse gases. This points to the importance of the source of the polymer material that one may wish to compost. If the polymer originates from a petroleum-based source, its conversion to CO_2 is not necessarily helpful from a greenhouse gas perspective. However, if one uses a bio-sourced material to produce biodegradable polymers, composting becomes an essential disposal infrastructure.[35]

As noted, we proposed to use MDO as a component of our PSA formulation because it is both bio-sourced and has properties making it suitable as a PSA component, but primarily because of its potential to impact compostability. MDO is a cyclic ketene acetal (CKA) monomer which can be polymerized via radical ring-opening polymerization.[36] Because of its molecular structure, the resulting polymer will have ester groups along its backbone, which should enhance biodegradation relative to strictly carbon-carbon linkages.[37] Recalling the discussion above about the impact on adhesive properties of changing a component in the formulation, we used CNCs to modify the PSA properties so that the final product would continue to align with commercial-

based PSA properties while adhering to principles of sustainability. The impact of CNCs on compostability was also investigated.

1.2 Objectives, hypothesis, and thesis structure

The objective of this thesis was to develop more sustainable adhesives. Our goal was to create a high-performance adhesive produced using a more sustainable technology that contains a considerable percentage of renewable, bio-sourced ingredients and degrades to non-toxic components. We hypothesized that by having ester bonds in the backbone of the polymer and combining this novel chemistry with the unique properties of CNCs, we could produce compostable latex for adhesive applications.

To align with the project's primary goal of enhancing sustainability, we employed water-based (emulsion) polymerization to produce PSAs. By incorporating CNCs, we improved PSA performance properties, replacing traditional, more hazardous additives such as CTAs and crosslinkers. Additionally, the addition of a bio-sourced monomer, MDO, increased the proportion of renewable starting materials, paving the way for the development of a compostable product.

This thesis includes a total of 7 chapters, described below:

Chapter 2 provides an overview of adhesives and adhesion, the emulsion polymerization process, and renewable components, including bio-based monomers and nanomaterials. These components were utilized to enhance PSA properties and support the development of a biodegradable and compostable product.

Chapter 3 was published in Polymer Engineering and Science[38] and focuses on blending cCNCs with commercial latex to enhance PSA properties, including tack, peel strength, and shear adhesion. The study utilized a 2^{5-1} fractional factorial design to evaluate the effects of parameters such as cCNC type, sonication, cCNC loading, blending temperature, and mixing speed on adhesive performance. The work provides both scientific insights and practical guidelines for integrating renewable nanomaterials into commercial adhesive formulations, aligning with the broader goals of sustainability and improved material performance.

Chapter 4 was published in Polymers,[39] focuses on the reactivity of MDO with butyl acrylate (BA) and vinyl acetate (VAc) in the context of bulk free radical terpolymerization. This work provides the first estimation of ternary reactivity ratios for the BA/MDO/VAc system at 50°C, aiming to develop biodegradable PSAs.

Chapter 5 published in ChemSusChem,[40] focuses on the synthesis of poly (MDO/BA/VAc) terpolymers using emulsion polymerization. The inclusion of the bio-based monomer MDO is particularly significant due to its ability to enhance polymer degradability through ring-opening polymerization. While the use of MDO in emulsion polymerization aligns with environmental objectives, it introduces challenges such as MDO hydrolysis, incomplete ring opening, and uneven distribution within the polymer. To further enhance PSA performance, cCNCs were incorporated into the formulations. The resulting terpolymers demonstrated strong potential for application as sustainable PSAs, combining enhanced adhesive properties with environmental degradability.

Chapter 6 submitted to Journal of Applied Polymer Science, focuses on the construction and utilization of a composting facility to evaluate the compostability of poly(BA/MDO/VAc) and poly(BA/MDO/VAc)-cCNC terpolymers. This study investigates the effects of MDO and cCNC on compostability. The compostability was assessed by monitoring CO_2 emissions following guidelines derived from ASTM D5338-15.[41]

Chapter 7 provides a general discussion and summarizes the most important findings in this thesis.

The thesis concludes with several appendices. Appendix I-III contain supporting information related to chapters 3, 5, and 6, respectively. Appendix IV provides a report on health and safety considerations for this project. Appendix V contains a list of publications and conference presentations emanating from this work.

1.3 References

[1] M. A. Dubé, V. A. Gabriel, A. S. Pakdel, Y. Zhang, *Can J Chem Eng* 2021, *99*, 31.

[2] P. T. Anastas, J.C. Warner. Green chemistry: theory and practice. *Oxford University Press*; 1998.p. 2.

[3] M. A. Dubé, S. Salehpour, *Macromol React Eng* 2014, *8*, 7.

[4] R. Jovanović, M. A. Dubé, *Ind Eng Chem Res* 2005, *44*, 6668.

[5] S. Mapari, S. Mestry, S. T. Mhaske, *Polym Bull* 2021, *78*, 4075.

[6] N. M. Chidanand Bilagi, "Pressure Sensitive Adhesives Market Statistics," 2021. www.alliedmarketresearch.com/pressure-sensitive-adhesives-market

[7] N. M. Chidanand Bilagi, “Acrylic Pressure Sensitive Adhesives Market Global Forecast to 2025,” 2020. www.alliedmarketresearch.com/pressure-sensitive-adhesives-market

[8] E. P. Chang, *J Adhes* 1997, Netherlands, *60*, 233.

[9] S. Noppalit, A. Simula, L. Billon, J. M. Asua, *ACS Sustain Chem Eng* 2019, *7*, 17990.

[10] R. J. Young, P. A. Lovell, *Intro to Polym*, CRC Press, 2011.

[11] S. Ren, M. A. Dubé, *Int J Adhes Adhes* 2017, *75*, 132.

[12] L. Qie, M. A. Dubé, *Eur Polym J* 2010, *46*, 1225.

[13] S. D. Tobing, A. Klein, *J Appl Polym Sci* 2001, *79*, 2558.

[14] P. A. Lovell, F. J. Schork, *Biomacromolecules* 2020, *21*, 4396.

[15] C. Wang, F. Chu, C. Graillat, A. Guyot, C. Gauthier, J. P. Chapel, *Polymer (Guildf)* 2005, *46*, 1113.

[16] P. A. Lovell, F. J. Schork, *Biomacromolecules* 2020, 21 (11), 4396.

[17] S. Bunker, C. Staller, N. Willenbacher, R. Wool, *Int J Adhes Adhes* 2003, *23*, 29.

[18] H. Uyama, M. Kuwabara, T. Tsujimoto, M. Nakano, A. Usuki, S. Kobayashi, *Chemistry of Materials* 2003, *15*, 2492.

[19] J. Folini, W. Murad, F. Mehner, W. Meier, J. Gaitzsch, *Eur Polym J* 2020, *134*, 109851.

[20] A. S. Pakdel, E. Niinivaara, E. D. Cranston, R. M. Berry, M. A. Dubé, *Macromol Rapid Commun* 2021, *42*, 2000448.

[21] Y. Zheng, E. K. Yanful, A. S. Bassi, *Crit Rev Biotechnol* 2005, *25*, 243.

[22] A. S. Pakdel, V. Gabriel, R. M. Berry, C. Fraschini, E. D. Cranston, M. A. Dubé, *Cellulose* 2020, *27*, 10837.

[23] V. A. Gabriel, P. Champagne, M. F. Cunningham, M. A. Dubé, *Can J Chem Eng* 2022, *100*, 767.

[24] P. Mali, A. P. Sherje, *Carbohydr Polym* 2022, *275*, 118668.

[25] R. J. Moon, A. Martini, J. Nairn, J. Simonsen, J. Youngblood, *Chem Soc Rev* 2011, *40*, 3941.

[26] V. A. Gabriel, M. N. Tousignant, S. M. W. Wilson, M. D. M. Faure, E. D. Cranston, M. F. Cunningham, B. H. Lessard, M. A. Dubé, *Macromol React Eng* 2022, *16*, 2100051.

[27] E. Lam, U. D. Hemraz, *Nanomaterials* 2021, *11*, 1641.

[28] R. Mohee, G. Unmar, *Waste Management* 2007, *27*, 1486.

[29] S. Nandy, E. Fortunato, R. Martins, *Progress in Natural Science: Materials International* 2022, *32*, 1.

[30] Y. Zheng, E. K. Yanful, A. S. Bassi, *Crit Rev Biotechnol* 2005, *25*, 243.

[31] R.-J. Müller, I. Kleeberg, W.-D. Deckwer, *J Biotechnol* 2001, *86*, 87.

[32] S. Bonhomme, A. Cuer, A.-M. Delort, J. Lemaire, M. Sancelme, G. Scott, *Polym Degrad Stab* 2003, *81*, 441.

[33] M. S. Ayilara, O. S. Olanrewaju, O. O Babalola, O. Odeyemi, *Sustainability* 2020, *12*(11), 4456.

[34] S. Gajalakshmi, S. A. Abbasi, *Crit Rev Environ Sci Technol* 2008, *38*, 311.

[35] J. H. Song, R. J. Murphy, R. Narayan, G. B. H. Davies, *Philos Trans R Soc B Biol Sci* 2009, *364*, 2127.

[36] C. Hardy, M. E. Levere, G. Kociok-Köhn, A. Buchard, *ACS Macro Lett* 2023, *12*, 1443.

[37] F. Wenzel, S. Hamzehlou, L. Pardo, M. Aguirre, J. R. Leiza, *Ind Eng Chem Res* 2021, *60*, 10479.

[38] M. Movafagh, K. M. Meek, P. Bayat, E. D. Cranston, M. Cunningham, P. Champagne, T. Morse, M. Kiriakou, S. George, M. A. Dubé, *Polym Eng Sci* 2024, *64*, 798.

[39] M. Movafagh, K. M. Meek, A. J. Scott, A. Penlidis, M. A. Dubé, *Polymers (Basel)* 2024, *16*, 1330.

[40] M. Movafagh, K. M. Meek, M. A. Dubé, *ChemSusChem* 2025, e202402478.

[41] ASTM D5338-15: Standard Test Method for Determining Aerobic Biodegradation of Plastic Materials Under Controlled Composting Conditions, Conditions, Incorporating Thermophilic Temperatures 2015.

Chapter 2
Background

2.1 Pressure-sensitive adhesives (PSAs)

Adhesives are compounds applied to the surfaces of separate items to keep them firmly joined together.[1] The tendency of dissimilar atoms or molecules to adhere together is known as adhesion, whereas cohesion involves intermolecular interaction between identical materials.[2]

PSAs are polymeric materials that attach to a surface (substrate) instantly with light contact pressure. They can also be removed simply with a light pulling force, leaving no residue on the substrate.[3] Polymers are used in PSA manufacture because of their viscous and elastic properties that allow them to flow and dissipate energy throughout the bonding process through interfacial and interstitial crosslinking and polymer chain entanglement.[3,4] A PSA must be soft and sticky at room temperature; hence its glass transition temperature (T_g) should be low, preferably between -70 and -20 °C.[3] PSA performance is determined by three general adhesive properties: tack, peel strength, and shear strength. Tack force is the energy required to separate the adhesive from a substrate after brief contact and low application pressure; peel adhesion is the capacity of a material to resist removal by peeling; and shear strength is the ability of a material to resist a steady shear force.[3,5–8] Viscoelastic behaviour, T_g, and the polymer molecular weight, among other factors, all significantly impact PSA performance. A proper combination of processability, properties, and additive compatibility is necessary when choosing between different polymer systems, and acrylic PSAs meet this requirement.

In 2018, the worldwide PSA market was estimated at 11.1 billion USD.[9] Concerns about the impact of the polymer industry's primarily petroleum-based feedstocks on the global climate have sparked a movement toward change. Therefore, scientists and producers are looking for ways to create eco-friendly polymeric materials and do so more sustainably.[10] Because it doesn't employ volatile solvents like other polymerization techniques, emulsion (latex- or water-based) polymerization is regarded as a more sustainable method of producing polymers. The creation of PSAs based on latex rather than solvents is becoming more prevalent, just as it did in the paint industry decades ago. In fact, acrylic PSAs made using emulsion polymerization as opposed to solution-based and hot melt technologies, now occupy the largest market share.[11]

Other advantages of latex-based acrylic PSAs include their high solids content, simplicity of application, and the fact that they may be made without the use of tackifiers (another potential source of toxic ingredients) in many cases.[32] Acrylic PSAs are made up of acrylic and methacrylic ester polymers with low T_gs and high molecular weights. Butyl acrylate (BA, T_g = -54°C) and 2-ethylhexyl acrylate (2-EHA, T_g = -65°C) are typical monomers employed in their production. However, increasing the T_g of these "soft" acrylic homopolymers is required to improve their room-temperature performance.[33] Copolymerizing with one or more high polymer T_g components, such as methyl methacrylate (MMA; T_g = 105°C), and acrylic acid (AA; T_g = 106°C), or any of a variety of "hard" monomers, can raise the polymer T_g.[12] Furthermore, adding CTAs[11,13] and crosslinkers[14] to polymers is a common way to change the polymer microstructure. The polymer microstructure, including the molecular weight distribution and degree of crosslinking, directly affect PSA performance properties. In addition to these traditional molecular modification techniques, nanomaterials have shown considerable potential as polymer property modifiers in recent decades.

Thus, due to their renewability and sustainable sourcing, cellulosic nanomaterials have become favoured polymer property modifiers.[15] For example, recent research has demonstrated that the addition of CNCs to emulsion-based acrylic PSAs simultaneously enhanced all three adhesive performance metrics (tack, peel strength and shear strength); this is significant given that typically, increases in shear strength frequently correspond to decreases in tack and peel strength or vice versa.[16–20]

2.2 Emulsion polymerization

Emulsion polymerization is an unparalleled chemical technique for creating aqueous resins with various colloidal and physicochemical properties. Monomer, water, surfactant (aka emulsifier), and a water-soluble initiator make up a classic emulsion polymerization formulation.[21]This heterogeneous free radical polymerization process begins with an oil-in-water emulsifier stabilizing the comparatively hydrophobic monomer in water, followed by the initiating reaction. Water, as the continuous phase, is vital in emulsion polymerization because it keeps the viscosity low, acts as an efficient heat sink, and serves as a conduit for the transfer of monomers.[22,23] Aggregates of surfactants (~100 units), known as micelles, become swollen with monomer and serve as the primary site for the nucleation of polymer particles. The generation of submicron latex particles (0.05 to 1 μm in diameter) results from the capture of free radicals by

micelles, which have a very large oil-water interfacial area. Monomer droplets often cannot effectively compete with micelles in collecting free radicals produced in the aqueous phase due to their relatively modest surface area. Common surfactants are long-chain hydrocarbons with hydrophobic tails and hydrophilic heads and serve to keep the polymer particle dispersion stable. Different surfactant types such as ionic (anionic and cationic) and non-ionic (typically polymeric) may be utilized. Water-soluble initiators, such as potassium persulfate (KPS) and redox systems (for low-temperature polymerization), are extensively employed. Other additives, such as CTAs and crosslinking agents, are employed to manipulate the polymer microstructure.[21]

In this research, the emulsion polymerizations will be conducted in semi-batch mode to ensure better control of the particle size and distribution as well as exploiting the monomer reactivity to control the monomer distribution in the polymer chains. The semi-batch technique is accomplished in two stages: a seed stage and a feed stage. The seed stage governs the total number of particles nucleated, whereas the feed stage determines particle growth rate, heat removal rate, copolymer composition, and particle morphology.[23,24]

Emulsion polymerization proceeds through three discrete intervals: Intervals I, II, and III. In Interval I, the surfactant will stabilize the monomer to create monomer droplets (with 1 to 10 μm in diameter). The particles are nucleated (usually 0-5% monomer conversion). During this interval one observes numerous monomer-swollen micelles, newly nucleated polymer particles and relatively large monomer droplets. First, monomer molecules dissolved in the continuous aqueous phase polymerize with waterborne free radicals to form oligomeric (short-chain) radicals. The oligomeric radicals grow via aqueous phase polymerization until they reach a certain hydrophobicity that results in their absorption into a monomer-swollen micelle (5-10 nm in diameter). This absorption is known as heterogeneous or micellar nucleation and results in the generation of a polymer particle. Typically, one out of every 10^2–10^3 micelles are nucleated into latex particles. The particle nucleation stage (Interval I) ends when all of the monomer-swollen micelles have been nucleated.

Interval II is described as a period of nearly constant polymerization rate. Polymerization within the nucleated particles occurs through the absorption of oligomeric radicals into the particles while monomer diffuses into the growing particles to maintain a constant monomer concentration in the particles. The diffusing monomer emanates from the monomer droplets. The depletion of the monomer droplets marks the transition from Interval II to Interval III.

During Interval III (which usually begins at around 40% conversion), all that remains are monomer-swollen polymer particles, initiator, and trace monomers dissolved in the aqueous phase. The decreasing monomer concentration in the particles, due to polymerization, leads to a decrease in polymerization rate until most or all the remaining monomer is consumed, signifying the end of the polymerization reaction.[24]

2.3 Polymer nanocomposites

Polymer nanocomposites usually incorporate one or more nanoparticle components within a polymer matrix. While hybrid materials have been explored since the 1940s, with a specific focus on rubber tires, this field was revitalized in the 1990s when platelet-like clay particles were exfoliated in various polymers.[26] Polymer nanocomposites have grown into a multibillion-dollar global industry with products ranging from transportation-related reinforcing components to commodity plastics with improved electrical characteristics for shielding and electronics.[27]

In the past, nanocomposite preparation has been employed to improve PSA properties. Different types of nanoparticles, such as hard inorganic[28] or organic nanoparticles,[29] have been employed using various preparation techniques including mechanical mixing,[30,31] and in-situ bulk,[32] solution,[33] suspension,[34] and emulsion polymerization.[18,35,36] In recent years, in our laboratory, CNCs have been used to improve PSA properties in both in-situ polymerization and post-polymerization blending.[16,18,37,38]

2.3.1 Cellulose nanocrystals (CNCs)

Cellulose is a biomaterial that is prevalent throughout the biosphere. It has been used in various industrial applications from paper and textiles to contemporary cellophane films and nutritional fibres. Cellulose is a naturally occurring linear polysaccharide that mostly exists in plants and is most frequently harvested from wood.[39]

Cellulosic research has recently uncovered a paradigm shift from macro- to micro- to nano-scaled cellulose.[42] The rigid rod-like nanoparticles known as cellulose nanocrystals (CNCs), also referred to as cellulose nano-whiskers, have a diameter of 3–50 nm and a length of tens to several mm.[43] The strength-to-weight ratio of CNCs is excellent,[44] and they have been shown to be non-toxic, sustainable, strong, biocompatible, biodegradable, and available at reasonable cost. These qualities have prompted their use in medicine, electronics, building materials, food,

coatings, and cosmetics.[45] CNCs can be easily extracted from wood pulp by hydrolyzing the cellulose with a strong acid (often sulfuric acid), which leaves the highly ordered and regular nanocrystals suspended in an aqueous media.[41] Anomera Inc. creates carboxylated CNCs in a batch method with diluted hydrogen peroxide oxidation to isolate the nanocrystals, resulting in carboxylate groups on the CNC surface. Softwood pulp is used to make the CNCs, which are marketed as DextraCel.[37,46] CNCs are commonly used in polymer composites because they are highly crystalline materials with high tensile strengths (~10 GPa) and high Young's modulus (~150 GPa). Despite having hydrophilic surfaces, CNCs do not swell in water, and they easily form suspensions in water.[47]

It has been projected that by 2025 the market for cellulose nanomaterials will increase from $271.26 million in 2017 to $1076.43 million, with a compound annual growth rate of 18.8 percent.[47]

2.3.2 Latex/CNC nanocomposites

The synthesis of polymer nanocomposites can be roughly categorized into two groups: physical methods and chemical methods, depending on the preparation techniques. In-situ polymerization is a chemical method for manufacturing nanocomposite materials, whereas solution processing, melt mixing techniques, and electrospinning are typical examples of physical methods.[48] In this research, we propose to compare a physical blending method to the use of in-situ polymerization.

A straightforward method for creating polymer nanocomposites is physical blending.[49] By using the blending approach, nanofillers can be dispersed in the base polymer or prepolymer solution. To achieve a homogeneous mixture, nanofillers and polymers can be stirred using physical means such as mechanical stirring, ultrasonic techniques, etc. Nanocomposites can then be created by casting a polymer solution, and the solvent can then be eliminated to leave a solid polymer nanocomposite behind.[50] In the case of CNC as nanofillers, due to the abundance of hydroxyl functionality on the surface, it possesses strong water dispersion properties. As a result, water may be an excellent option as a CNC/polymer composite processing medium.[51] Experience has shown that CNCs must first be dispersed in water at low concentrations before being blended with the latex. Recent industrial CNC production has perfected spray drying[52] of nanoparticles into a powder form. The various buffers, salts, and surfactants in the latex formulation tend to

inhibit redispersing CNCs, and redispersing CNCs directly into the latex from their dry form requires high-energy mixing or ultrasonication, which are likely to degrade the polymer. In other words, creating a homogeneous nanocomposite by mixing CNC powder with latex is difficult. As a result, the addition of a CNC dispersion would inevitably dilute the latex, and this could pose challenges when casting the latex into a film. Nevertheless, this latter approach is necessary to achieve a uniform dispersion of CNCs in the latex, thereby yielding optimal application properties.[49]Dastjerdi et al.[53] blended a CNC dispersion into a poly(BA-co-MMA) emulsion latex for a PSA application. The most significant improvements in adhesive strength were seen at a 1 wt.% CNC loading, where tack, peel strength, and shear resistance were each 2.4, 1.5, and 6.4 times higher than the base case (i.e., without any CNCs). Additionally, the latex viscosity, gel content, and storage and loss moduli increased with increasing CNC loading.

In the in-situ polymerization, the monomer and initiator have been added to a reactor along with CNC suspensions before the reaction. The creation of protocols that allow the reaction to go to completion (i.e., 95-99% conversion) and the latex to remain stable is one of the significant obstacles to be addressed when using CNCs in-situ during polymerization.[16,18] The presence of CNC may also help stabilize the polymer dispersion.[49] Dastjerdi et al., demonstrated how the in-situ method resulted in better PSA performance improvements compared to blending, with increases of up to 3.8x for tack, 6x for peel strength, and 20x for shear strength for the in-situ method compared to 2.4x, 1.5x, and 6.4x for blending. The improved interaction of CNCs with the polymer matrix during both latex synthesis and PSA film casting using the in-situ procedure as opposed to blending was ascribed to be the cause of mechanical performance differences between the two methods.[53] However, in that work, the base-case adhesive properties were not comparable to commercial grade adhesives leading one to wonder whether the adhesive performance enhancements would be as significant if a strong base-case adhesive was prepared. Another point worth noting was that blending was performed under a limited set of conditions that were not optimized for best performance. Thus, there is a need for a more comprehensive study on blending CNCs with a commercial grade adhesive.

Acrylic latexes have shown improvement in mechanical and adhesive properties with the inclusion of CNCs; however, a consensus on the mechanism has not been reached. First, it has been noted that the high crystallinity, high aspect ratio, and capacity of CNCs to form percolating networks within polymer composites improves the cohesive strength of PSAs by raising the

rigidity of the polymer matrix.[54,55] Additionally, CNCs (and all cellulosic materials) contain a high density of surface hydroxyl groups, which may enhance PSA performance through their capacity to establish hydrogen bonds with or graft to more hydrophilic polymers, thereby increasing the PSA's cohesive strength.[16,18,19,53,56] Not surprisingly, the inclusion of the rod-like CNCs in the formulation significantly impacts latex viscosity. Ouzas et al. found that the latex viscosity more than doubled at 1 wt.% CNC loadings, compared to the base case formulations. This increase in viscosity provides some evidence that hydrophilic CNCs do not reside within the latex particles. Additionally, such a sharp rise in viscosity points to strong grafting or, at the very least, hydrogen bonding between the CNCs and the latex particles. Thus, one could surmise that the CNCs lie somewhere near the interface of the continuous aqueous phase and the polymer particles. In that work, tack increased with CNC loading, suggesting that CNCs were not participating in cross-linking reactions even though the apparent latex gel content increased with CNC loading. Due to the increase in viscosity caused by the CNCs, the PSA's ability to form films was enhanced, resulting in the production of a more uniform film. The increased surface contact of the PSA films with the stainless-steel testing panels due to the presence of more hydroxyl groups, which in turn also improved the hydrophilicity of the PSAs, can be used to explain the apparent influence of CNC content on tack. In other words, the CNCs enhanced the PSA's capacity to create better contact (or better wettability) with the testing plates. It's likely that the polar hydroxyl groups on the CNCs aligned with the polar groups on the test panel when they came into contact, improving the adhesion process. A better wettability of the PSA film was also credited with the increase in peel strength. The peel strength was increased by strengthening the initial physical bond that forms between the testing panel and the PSA.[19]

2.4 Composting

2.4.1 Bioplastics

Bioplastics are defined as plastics that are either biobased or biodegradable (2.1).[57,58] The buildup of plastic waste in the environment and the resulting generation of microplastics (5 mm in size) have prompted an international effort to address plastic pollution. This has encouraged the rapid development of bioplastics globally.[59] However, incorrect bioplastic waste disposal can also have a negative impact on ecosystems, particularly when it results in purposeful environmental littering because of false assumptions about the biodegradability of trash and how

landfill sites operate (i.e., landfill sites do not offer much aerobic degradation).[60] Nevertheless, biodegradable bioplastics can play a significant role in advancing sustainability. To create a circular plastics economy, recycling (as in mechanical reprocessing) by itself is ineffective, especially for low-value plastic components such as flexible films or bags, extensively contaminated plastics, or multilayered and multi-component materials. In this regard, replacing problematic plastic parts with compostable bioplastics may provide the possibility of end-of-life management options that adhere to circularity principles, provided that they are compatible with the current infrastructure for the management of organic waste, i.e., they can be treated at the same conditions as organic waste streams.[61] Plastics that can be broken down biologically (by microorganisms such as bacteria or fungi) and decompose into non-toxic compounds (e.g., water, carbon dioxide (CO_2), and biomass) are referred to as biodegradable plastics. Polyhydroxyalkanoate (PHA) is an example of a biodegradable polyester that can be produced through microbial biosynthesis. Other biodegradable polyesters can be chemically synthesized from biobased chemicals, such as polylactic acid (PLA), or can be produced from petrochemicals, such as poly(caprolactam) and polyvinyl alcohol (PVOH). Biobased plastics, such as bio-polyethylene (bio-PE) and bio-polyethylene terephthalate (bio-PET), are made using materials generated from biomass but are not necessarily biodegradable.[58]

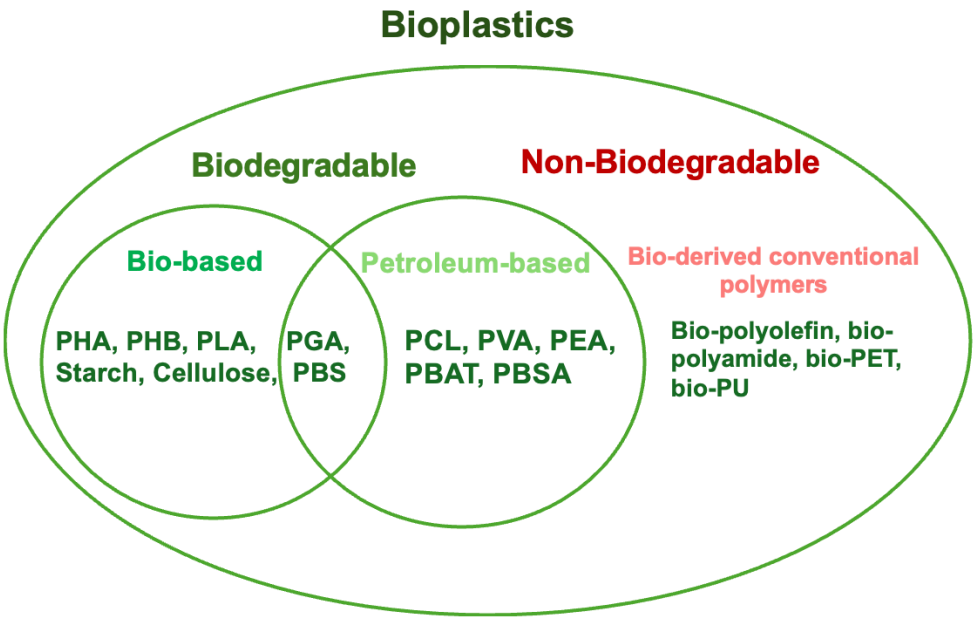

Figure 2.1. Bioplastics categories

The production of bioplastics is expected to increase by about 39% by 2030. To transition to a low-carbon circular economy, we need to better understand the biodegradability of these materials under aerobic and anaerobic conditions, from a molecular design and microphase morphology perspective to external environmental effects.[61]

2.4.2 Biodegradation and compostability

The term "biodegradation" describes the breakdown of organic compounds by bacteria or fungi.[63] A polymer's inherent molecular structure governs how biodegradable it is, and this property can change depending on the degradation environment. For instance, poly-L-lactic acid (PLLA) degrades slowly in landfills, ocean, soil, and home composting environments (37 °C), but quickly in commercial composting facilities (>60 °C).[64] Supporting the sustainable end-of-life management of biodegradable polymers requires an understanding of the distinctions between their biodegradability and compostability.

Composting is the most popular method for managing biodegradable trash in an aerobic environment. Because aerobic composting generates a lot more heat than anaerobic processes, it happens significantly faster and requires less artificial heating. ASTM D6813 states that composting is the controlled aerobic biological decomposition of organic materials into compost, CO_2, water, and heat.[65,66] Composting is often a human-driven process where biodegradation takes place under strict controls with specialized temperature and microbe combinations. Temperature is an important factor in controlling microbial activity. The ideal temperature range for window (pile) composting is 40–65 °C.[67] According to ASTM D6400, ISO 17088, and EN 13432, compostable polymers must satisfy three essential requirements: be intrinsically biodegradable (ASTM D5338); disintegrate in a composting environment without running the risk of ecotoxicity; and fully degrade to CO_2, water, and biomass without leaving any traces of visually detectable residues.[68] It should be emphasized that a biodegradable polymer is not considered compostable if it leaves behind harmful residues. Furthermore, when processed in an industrial composting facility for 180 days, both ASTM D6400 and EN13432 specifications provide a biodegradation rate of >90% of the feedstock.[62] Anaerobic digestion is the dominant process in landfill environments.[69] In an oxygen-free environment, this biodegradation process produces digestate and biogas, a mixture of CH_4 (50–65%) and CO_2 (35–50%) with minor amounts of H_2S and other gases.[61] In our project, we will be using an aerobic composting method to degrade the

polymers. Compared to anaerobic digestion, composting is industrially preferred because it is faster and generates more heat during degradation. Furthermore, there is little if any CH_4 in the by-product, which is a more harmful greenhouse gas than CO_2.

Depolymerization of plastic and mineralization are the two steps of biodegradation. Hydrolysis and oxidation are the two primary processes of depolymerization.[70] Polyesters with hydrolytically labile ester bonds are sensitive to abiotic hydrolysis.[71] The process begins with the hydrolysis of the labile ester bonds, which results in chemical scission and physical erosion, along with biological activity by enzymes or microorganisms, including bacteria, yeast, and fungi. Each MDO repeating unit can be hydrolyzed. The ester group undergoes transesterification (depolymerization) in the presence of water resulting ester bond breakage into carboxyl group end chains and hydroxyl group end chains. Carboxylic acid (by-product) can quicken the hydrolysis by autocatalysis effect. Thus, the goal of hydrolysis is to break down long polymer chains into shorter, functional oligomers that can eventually be consumed by bacteria.[70,72] The mineralization is represented as the second step. Once enough oligomeric fragments have been created, they are carried into cells where the microorganisms bioassimilate and mineralize them. Water, salts, minerals, new biomass, gases (CO_2, CH_4, N_2, H_2), and minerals are all by-products of the mineralization process.[70]

We are very interested in producing biodegradable polymers such as polyesters.[73,74] Ionic ring-opening polymerization, polycondensation, and polyaddition methods are well-known for producing such biodegradable polyesters.[75,76] However, all these approaches have limitations regarding the variety of polymers that may be used or the control of polymerization. In other words, because we are attempting to produce acrylic adhesives, step growth polymerization methods such as polycondensation are not possible. Another method of producing polyesters is via radical ring-opening polymerization, which is a chain-growth polymerization method. Radical ring-opening polymerization is carried out using CKAs.[77,78]

2.5 Ring-opening polymerization

Aliphatic polyesters, made via ring opening polymerization of cyclic monomers (e.g., lactide, glycolide, caprolactone), are the most studied biodegradable polymers. CKAs are cyclic monomers undergo ring-opening polymerization under the right circumstances (as opposed to ring

retaining polymerization) and results to aliphatic polyesters.[79,80] CKAs also align with three green chemistry principles: starting materials such as 1,4-butanediol and diethylene glycol can be bio-sourced (principal #7), no protective groups are utilized in monomer synthesis and polymerization (principle #8), and the polyesters produced are designed for degradation (principle #10).[81]

The disadvantage of CKAs is the conflict between the ring-opening process and the unintended direct vinyl propagation that results in polyacetal. Consequently, the outcome of the majority of CKA monomers is ester and acetal units are randomly combined to form a copolymer. To increase the selectivity of the ring-opening process, two criteria were initially considered while designing a monomer for radical ring-opening polymerization: (i) the ring strain and (ii) the stabilization of the radical when the ring is opened. For instance, it is known that 6-membered ring monomers have challenging ring-opening polymerizations. This is explained by the reduced ring strain of cyclohexane-like monomers (whose ring strain is zero).[82] This situation has led to the predominant use of two cyclic monomers; seven-membered ring CKAs such as MDO and the 5,6-benzo-2-methylene-1,3-dioxepane (BMDO), are both known to undergo complete ring-opening polymerization over a broad range of reaction conditions.[83] MDO can be an excellent candidate for ring opening polymerization because it has (i) an increased steric hindrance of the ring held radical compared to the stability of the ring open radicals, and (ii) a propensity for ring open radicals to undergo backbiting reactions to create more stable radicals.[84]

2.6 MDO polymerization with vinyl monomers

Vinyl polymers have many advantages, including low cost, ease of synthesis, and outstanding mechanical performance. They are used in various applications such as packaging, fibers, films, automotive parts, and general consumer products.[85] However their carbon backbone is resistant to degradation.[86] Furthermore, recycling these materials is both technically and economically difficult and results in a significant amount of trash being dumped in landfills (59% of the 8300 million tonnes of plastic produced since its mass production began in the 1950s were dumped in landfills or the environment), which exacerbates the issue of disposing of municipal waste.[87]

Free radical copolymerization of a CKA with vinyl monomers has been reported as a path to produce backbone degradable polymers.[88,89] In this case, we are seeking to insert MDO monomers along the vinyl polymer backbone. However, the radical copolymerization of MDO

with vinyl monomers is generally difficult due to the comparatively poor incorporation rates of cyclic ketenes in copolymerization with typical vinyl monomers due to unfavourable reactivity ratios.[83] Determining the monomer reactivity ratios is a necessary first step to achieving the appropriate distribution of monomers in the polymer chain and, consequently, a tunable and consistent degradation rate.[90]

Copolymer properties are determined by its composition, sequence distribution, molecular weight, and molecular weight distribution, to name a few. In a batch polymerization, the resulting polymers would not have a uniform distribution of ester groups in the polymer backbones and risk being difficult to biodegrade (Figure 2.2a). To make a (bio)degradable copolymer, it is necessary to include not only the degradable chemical linkages (due to MDO) but also to (i) distribute them evenly within and across the polymer chains and (ii) have enough of these degradable linkages so that relatively short oligomers can be obtained during the degradation process, [84] making them more easily consumed by microorganisms.[91,92] A semi-batch polymerization process, in which acrylates (typically the faster monomer) are partially fed according to a feeding profile determined from the reactivity ratios, could be used to encourage the more regular incorporation of MDO units in acrylate-based polymers (Figure 2.2b). Lena et al., 2020, investigated the effect of different monomer addition profiles on the acrylate copolymerization with MDO. The molecular weight distribution of fragments after alkali degradation suggested that they increased the uniformity of the MDO insertion using a semi-batch technique.[84]

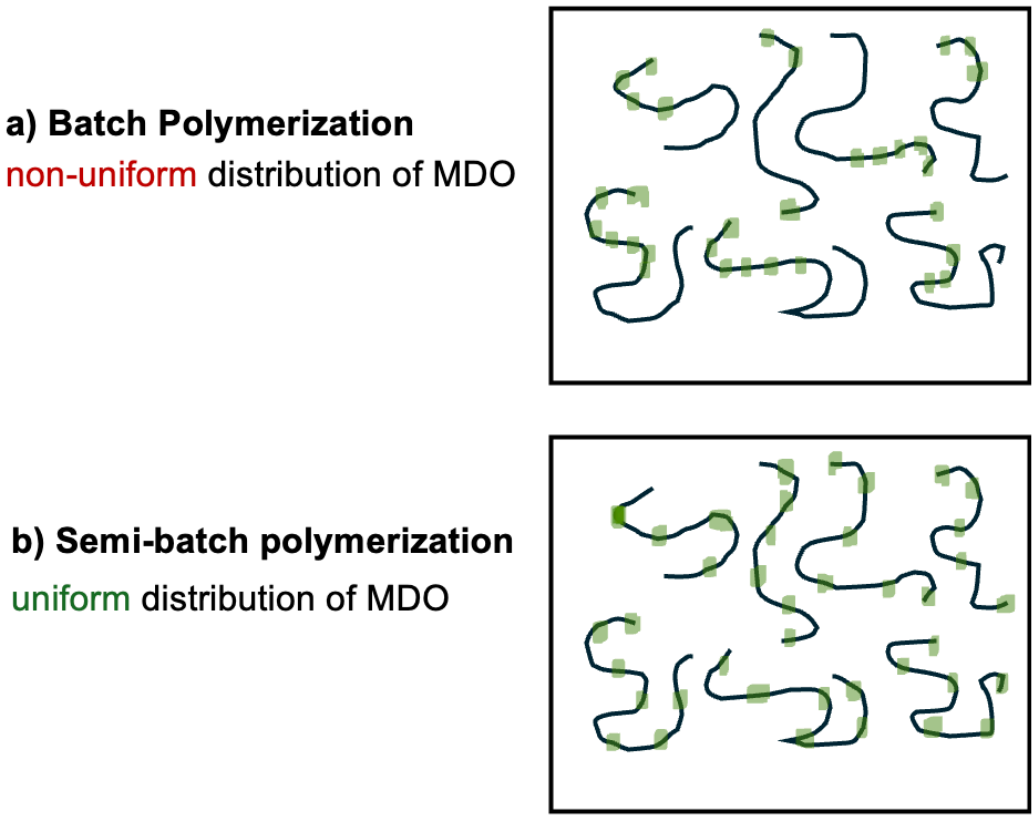

Figure 2.2. Comparing MDO distribution in polymer chains in both a) batch and b) semi- batch polymerization processes

Furthermore, due to the hydrolytic instability of CKA, it is mainly copolymerized in non-nucleophilic organic solvents; there are only a few reports on the polymerization of CKA in water and in emulsion polymerization.[93,94] As noted earlier, to align with green chemistry principles, we seek to avoid the use of solvent-based methods. A successful emulsion copolymerization of MDO could be accomplished by (i) suppressing hydrolysis in the water phase by controlling pH and temperature, and (ii) establishing a process that runs at high instantaneous monomer conversion to promote MDO incorporation.[95] Carter et al., presented a method for making waterborne and biodegradable latex polymers. Because of the presence of backbone ester groups, emulsion polymerization of vinyl acetate (VAc) with MDO yields hydrolytically degradable polymer particles and latex-based coatings, Figure 2.3. If the media was too acidic, the MDO was hydrolyzed, so they kept the pH of the polymerization between 7 and 8. They also used a redox initiation system to decrease the polymerization temperature and time. This new class of latex is well-suited for developing next-generation biodegradable and compostable single-use food service

items and other applications requiring the erosion or degradation of polymer-based films and coatings. Their use in adhesive applications has not been explored.[95]

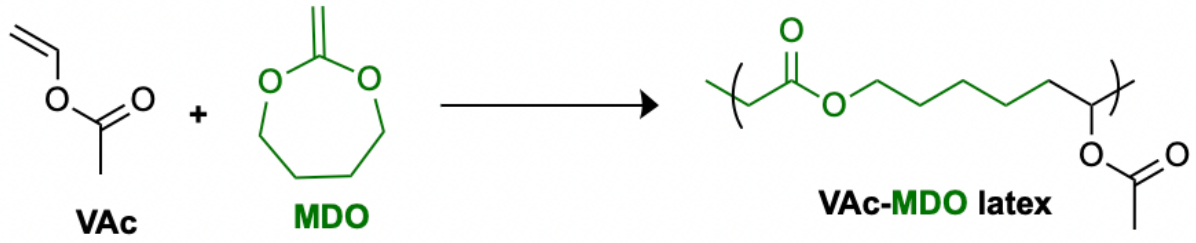

Figure 2.3. A general diagram illustrating the copolymerization of VA and MDO

2.7 Conclusion

This background establishes a comprehensive foundation for the development of sustainable and compostable PSAs. It underscores the pivotal role of emulsion polymerization as a greener alternative to traditional polymerization methods, providing an efficient and environmentally friendly approach to PSA synthesis. By integrating bio-based components such as MDO and cCNCs, this work addresses critical sustainability challenges by enhancing polymer degradability while optimizing adhesive performance.

The research harnesses the unique properties of CNCs to develop PSAs with superior tack, peel strength, and shear strength, meeting both functional and environmental demands. Furthermore, the exploration of radical ring-opening polymerization with MDO highlights its potential to create degradable polymer backbones, aligning industrial performance with environmental sustainability.

2.8 References

[1] S. Ebnesajjad, *Handbook of Adhesives and Surface Preparation*, *Elsevier* 2011, p. 3.

[2] S. J. Marshall, S. C. Bayne, R. Baier, A. P. Tomsia, G. W. Marshall, *Dent Mater* 2010, *26*, 11.

[3] I. Benedek, *Pressure-sensitive adhesives and applications, New York: Marcel Dekker, Inc* 2004, p. 747.

[4] Z. Czech, K. Wilpiszewska, B. Tyliszczak, X. Jiang, Y. Bai, L. Shao, *Int J Adhes Adhes* 2013, *44*, 195.

[5] C. Creton, *MRS Bull* 2003, 434.

[6] ASTM D6195-03. (Reapproved 2011) Standard Test Methods for Loop Tack Published Online, 2003.

[7] ASTM D3330-04. (Reapproved 2018) Standard Test Method for Peel Adhesion of Pressure-Sensitive Tape Published Online, 2004.

[8] ASTM D3654-06. (Reapproved 2011) Standard Test Methods for Shear Adhesion of Pressure-Sensitive Tapes Published Online, 2006.

[9] N. M. Chidanand Bilagi, "Acrylic Pressure Sensitive Adhesives Market Global Forecast to 2025," 2020. www.alliedmarketresearch.com/pressure-sensitive-adhesives-market

[10] T. D. Moshood, G. Nawanir, F. Mahmud, F. Mohamad, M. H. Ahmad, A. AbdulGhani, *Clean Eng Techno* 2022, *6*, 100404.

[11] R. Jovanović, M. A. Dubé, *Ind Eng Chem Res* 2005, *44*, 6668.

[12] M. D. Gower, R. A. Shanks, *J Appl Polym Sci* 2004, *93*, 2909.

[13] G. E. Fonseca, T. F. L. McKenna, M. A. Dubé, *Macromol Symp* 2010, *289*, 72.

[14] S. D. Tobing, A. Klein, *J Appl Polym Sci* 2001, *79*, 2558.

[15] S. J. Eichhorn, A. Etale, J. Wang, L. A. Berglund, Y. Li, Y. Cai, C. Chen, E. D. Cranston, M. A. Johns, Z. Fang, G. Li, L. Hu, M. Khandelwal, K.-Y. Lee, K. Oksman, S. Pinitsoontorn, F. Quero, A. Sebastian, M. M. Titirici, Z. Xu, S. Vignolini, B. Frka-Petesic, *J Mater Sci* 2022, *57*, 5697.

[16] Z. Dastjerdi, E. D. Cranston, M. A. Dubé, *Macromol React Eng* 2017, *11*, 1700013.

[17] A. S. Pakdel, V. Gabriel, R. M. Berry, C. Fraschini, E. D. Cranston, M. A. Dubé, *Cellulose* 2020, *27*, 10837.

[18] A. Ouzas, E. Niinivaara, E. D. Cranston, M. A. Dubé, *Macromol React Eng* 2018, *12*, 1700068.

[19] A. Ouzas, E. Niinivaara, E. D. Cranston, M. A. Dubé, *Polym Compos* 2019, *40*, 1365.

[20] M. V. Kiriakou, A. S. Pakdel, R. M. Berry, T. Hoare, M. A. Dubé, E. D. Cranston, *ACS Materials Au* 2022, *2*, 176.

[21] C. S. Chern, *Prog Polym Sci* 2006, *31*, 443.

[22] E. S. Daniels, E. D. Sudol, M. S. El-Aasser, *Polymer Colloids* 2001, p.1-12.

[23] J. M. Asua, *J Polym Sci A Polym Chem* 2004, *42*, 1025.

[24] P. A. Lovell, F. J. Schork, *Biomacromolecules* 2020, *21*, 4396.

[25] J. Qiu, B. Charleux, K. Matyjaszewski, *Prog Polym Sci* 2001, *26*, 2083.

[26] E. P. Giannelis, R. Krishnamoorti, E. Manias, *Advances in Polymer Science*, *Springer* 1999, 138, 107.

[27] S. K. Kumar, B. C. Benicewicz, R. A. Vaia, K. I. Winey, *Macromolecules* 2017, *50*, 714.

[28] Y. T. Kang, K. S. Hwang, J.-B. Moon, D.-H. Kim, I. Chung, *J Adhes Sci Technol* 2015, *29*, 2345.

[29] A. Bellamine, E. Degrandi, M. Gerst, R. Stark, C. Beyers, C. Creton, *Macromol Mater Eng* 2011, *296*, 31.

[30] S. Fujii, S. Sawada, S. Nakayama, M. Kappl, K. Ueno, K. Shitajima, H.-J. Butt, Y. Nakamura, *Mater Horiz* 2016, *3*, 47.

[31] U. Khan, P. May, H. Porwal, K. Nawaz, J. N. Coleman, *ACS Appl Mater Interfaces* 2013, *5*, 1423.

[32] J. Kajtna, U. Šebenik, M. Krajnc, *Int J Adhes Adhes* 2014, *49*, 18.

[33] S. Patel, A. Bandyopadhyay, A. Ganguly, A. K. Bhowmick, *J Adhes Sci Technol* 2006, *20*, 371.

[34] J. Kajtna, U. Šebenik, *Int J Adhes Adhes* 2009, *29*, 543.

[35] Y. Zhang, M. F. Cunningham, N. M. B. Smeets, M. A. Dubé, *Eur Polym J* 2018, *106*, 128.

[36] J.-K. Oh, C.-H. Park, S.-W. Lee, J.-W. Park, H.-J. Kim, *Int J Adhes Adhes* 2013, *47*, 13.

[37] V. A. Gabriel, M. N. Tousignant, S. M. W. Wilson, M. D. M. Faure, E. D. Cranston, M. F. Cunningham, B. H. Lessard, M. A. Dubé, *Macromol React Eng* 2022, *16*, 2100051.

[38] V. A. Gabriel, E. D. Cranston, M. A. Dubé, *Macromol React Eng* 2020, *14*, 2000027.

[39] T. C. Mokhena, M. J. John, *Cellulose* 2020, *27*, 1149.

[40] E. J. Foster, R. J. Moon, U. P. Agarwal, M. J. Bortner, J. Bras, S. Camarero-Espinosa, K. J. Chan, M. J. D. Clift, E. D. Cranston, S. J. Eichhorn, D. M. Fox, W. Y. Hamad, L. Heux, B. Jean, M. Korey, W. Nieh, K. J. Ong, M. S. Reid, S. Renneckar, R. Roberts, J. A. Shatkin, J. Simonsen, K. Stinson-Bagby, N. Wanasekara, J. Youngblood, *Chem Soc Rev* 2018, *47*, 2609.

[41] D. Klemm, E. D. Cranston, D. Fischer, M. Gama, S. A. Kedzior, D. Kralisch, F. Kramer, T. Kondo, T. Lindström, S. Nietzsche, K. Petzold-Welcke, F. Rauchfuß, *Materials Today* 2018, *21*, 720.

[42] T. C. Mokhena, M. J. John, *Cellulose* 2020, *27*, 1149.

[43] R. J. Moon, A. Martini, J. Nairn, J. Simonsen, J. Youngblood, *Chem Soc Rev* 2011, *40*, 3941.

[44] T. C. Mokhena, M. J. John, *Cellulose* 2020, *27*, 1149.

[45] S. Das, B. Ghosh, K. Sarkar, *Sensors International* 2022, *3*, 100135.

[46] G. Delepierre, O. M. Vanderfleet, E. Niinivaara, B. Zakani, E. D. Cranston, *Langmuir* 2021, *37*, 8393.

[47] J. Shojaeiarani, D. S. Bajwa, S. Chanda, *Compos Part C Open Access* 2021, *5*, 100164.

[48] A. Kamal, M. Ashmawy, A. M. Algazzar, A. H. Elsheikh AH., *Proc Inst Mech Eng Part C* 2021, 236(9), 4843.

[49] S. A. Kedzior, V. A. Gabriel, M. A. Dubé, E. D. Cranston, *Adv Mater* 2021, *33*, 2002404.

[50] N. Yousefi, X. Lin, Q. Zheng, X. Shen, J. R. Pothnis, J. Jia, E. Zussman, J.-K. Kim, *Carbon N Y* 2013, *59*, 406.

[51] S. Mondal, *Polym Plast Technol Eng* 2018, *57*, 1377.

[52] S. Beck, J. Bouchard, R. Berry, *Biomacromolecules* 2012, *13*, 1486.

[53] Z. Dastjerdi, E. D. Cranston, M. A. Dubé, *Int J Adhes Adhes* 2018, *81*, 36.

[54] Z. Dastjerdi, E. D. Cranston, R. Berry, C. Fraschini, M. A. Dubé, *Macromol React Eng* 2019, *13*, 1800050.

[55] V. Favier, G. R. Canova, J. Y. Cavaillé, H. Chanzy, A. Dufresne, C. Gauthier, *Polym Adv Technol* 1995, *6*, 351.

[56] A. S. Pakdel, V. Gabriel, R. M. Berry, C. Fraschini, E. D. Cranston, M. A. Dubé, *Cellulose* 2020, *27*, 10837.

[57] P. K. Samantaray, A. Little, D. M. Haddleton, T. McNally, B. Tan, Z. Sun, W. Huang, Y. Ji, C. Wan, *Green Chemistry* 2020, *22*, 4055.

[58] J. N. Hahladakis, E. Iacovidou, S. Gerassimidou, *Plastic Waste and Recycling*, *Elsevier* 2020, p. 481.

[59] A. Folino, A. Karageorgiou, P. S. Calabrò, D. Komilis, *Sustainability* 2020, *12*, 6030.

[60] P. S. Calabrò, M. Grosso, *Waste Management* 2018, *78*, 800.

[61] P. K. Samantaray, A. Little, A. M. Wemyss, E. Iacovidou, C. Wan, *ACS Sustain Chem Eng* 2021, *9*, 9151.

[62] P. K. Samantaray, A. Little, A. M. Wemyss, E. Iacovidou, C. Wan, *ACS Sustain Chem Eng* 2021, *9*, 9151.

[63] ISO 17088, Specifications for compostable plastics 2012.

[64] J. J. Kolstad, E. T. H. Vink, B. de Wilde, L. Debeer, *Polym Degrad Stab* 2012, *97*, 1131.

[65] M. Pergola, A. Persiani, A. M. Palese, V. di Meo, V. Pastore, C. D'Adamo, G. Celano, *Appl Soil Ecol* 2018, *123*, 744.

[66] M. S. Kim, H. Chang, L. Zheng, Q. Yan, B. F. Pfleger, J. Klier, K. Nelson, E. L.-W. Majumder, G. W. Huber, *Chem Rev* 2023, *123* (16), 9915.

[67] S. Kliem, M. Kreutzbruck, C. Bonten, *Materials* 2020; 13(20):4586.

[68] M. Avella, E. Bonadies, E. Martuscelli, R. Rimedio, *Polym Test* 2001, *20*, 517.

[69] P. S. Calabro', A. Folino, F. Fazzino, D. Komilis, *J Hazard Mater* 2020, *390*, 121653.

[70] S. Grima, V. Bellon-Maurel, P. Feuilloley, F. Silvestre, *J Polym Environ* 2000, *8*, 183.

[71] L. S. Nair, C. T. Laurencin, *Prog Polym Sci* 2007, *32*, 762.

[72] K. de Smit, Y. W. Marien, K. M. van Geem, P. H. M. van Steenberge, D. R. D'hooge, *React Chem Eng* 2020, *5*, 1909.

[73] T. P. Haider, C. Völker, J. Kramm, K. Landfester, F. R. Wurm, *Angew Chem Int Ed* 2019, *58*, 50.

[74] T. Iwata, *Angew Chem Int Ed* 2015, *54*, 3210.

[75] S.-P. Hsu, I.-M. Chu, J.-D. Yang, *J Appl Polym Sci* 2012, *125*, 133.

[76] S. Penczek, J. Pretula, S. Slomkowski, *Chem Teach Int 2021*, *3*, 33.

[77] S. Agarwal, *Polym Chem* 2010, *1*, 953.

[78] A. Tardy, J. Nicolas, D. Gigmes, C. Lefay, Y. Guillaneuf, *Chem Rev* 2017, *117*, 1319.

[79] M. R. Hill, E. Guégain, J. Tran, C. A. Figg, A. C. Turner, J. Nicolas, B. S. Sumerlin, *ACS Macro Lett* 2017, *6*, 1071.

[80] O. Nuyken, S. Pask, *Polymers (Basel)* 2013, *5*, 361.

[81] J. Folini, W. Murad, F. Mehner, W. Meier, J. Gaitzsch, *Eur Polym J* 2020, *134*, 109851.

[82] A. Tardy, N. Gil, C. M. Plummer, D. Siri, D. Gigmes, C. Le-Fay, Y. Guillaneuf, *ACS Mac Lett* 2023*,* 12 (11), 1443.

[83] A. Tardy, J. Nicolas, D. Gigmes, C. Lefay, Y. Guillaneuf, *Chem Rev* 2017, *117*, 1319.

[84] J.-B. Lena, A. W. Jackson, L. R. Chennamaneni, C. T. Wong, F. Lim, Y. Andriani, P. Thoniyot, A. M. van Herk, *Macromolecules* 2020, *53*, 3994.

[85] V. Siracusa, P. Rocculi, S. Romani, M. D. Rosa, *Trends Food Sci Technol* 2008, *19*, 634.

[86] R. A. Gross, B. Kalra, *Science (1979)* 2002, *297*, 803.

[87] F. Wenzel, S. Hamzehlou, L. Pardo, M. Aguirre, J. R. Leiza, *Ind Eng Chem Res* 2021, *60*, 10479.

[88] T. Pesenti, J. Nicolas, *ACS Macro Lett* 2020, *9*, 1812.

[89] S. Agarwal, *Polym Chem* 2010, *1*, 953.

[90] S. Cummings, Y. Zhang, N. Kazemi, A. Penlidis, M. A. Dubé, *J Appl Polym Sci* 2016, *133*.

[91] F. Kawai, *Appl Microbiol Biotechnol* 1993, *39*.

[92] S. Weidner, G. Kuehn, B. Werthmann, H. Schroeder, U. Just, R. Borowski, R. Decker, B. Schwarz, I. Schmuecking, I. Seifert, *J Polym Sci A Polym Chem* 1997, *35*, 2183.

[93] P. Galanopoulo, N. Gil, D. Gigmes, C. Lefay, Y. Guillaneuf, M. Lages, J. Nicolas, M. Lansalot, F. D'Agosto, *Angewandte Chemie International Edition* 2022, *61*.

[94] J. M. Siebert, D. Baumann, A. Zeller, V. Mailänder, K. Landfester, *Macromol Biosci* 2012, *12*, 165.

[95] M. C. D. Carter, A. Hejl, S. Woodfin, B. Einsla, M. Janco, J. DeFelippis, R. J. Cooper, R. C. Even, *ACS Macro Lett* 2021, *10*, 591.

Chapter 3
Improved Pressure-Sensitive Adhesive Performance Using Carboxylated Cellulose Nanocrystals via Blending

Maryam Movafagh[1], Kelly M. Meek[1], Parisa Bayat[1], Emily D. Cranston[2], Michael Cunningham[3], Pascale Champagne[4], Timothy Morse[5], Michael Kiriakou[5], Sean George[6], Marc A. Dubé[1]

[1]Department of Chemical and Biological Engineering, University of Ottawa, Ottawa, ON, Canada
[2]Department of Wood Science and Department of Chemical and Biological Engineering, University of British Columbia, Vancouver, BC, Canada
[3]Department of Chemical Engineering, Queen's University, Kingston, ON, Canada
[4]Energy Mining & Environment Research Centre, National Research Council, Montreal, QC, Canada
[5]Anomera Inc., Montreal, QC, Canada
[6]BASF Corp., Charlotte, NC, United States

This chapter is a manuscript published in Polymer Engineering and Science (2024; 64(2): 798-816).
DOI: 10.1002/pen.26585

3.1 Abstract

Carboxylated cellulose nanocrystals (cCNCs) were blended with high-quality commercial latex to enhance key pressure-sensitive adhesive (PSA) properties: tack, peel strength, and shear adhesion. Initially, a 2^{5-1} fractional factorial design was used to evaluate the effect of five factors: cCNC type (never-dried vs. dried re-dispersed), the use of sonication to disperse the cCNC, cCNC loading, blend temperature, and mixing speed. The regression analysis identified optimal blend conditions and the three most significant factors. It was found that increasing mixing speed had the strongest positive impact on all three PSA properties. A subsequent design of experiments looked at using a different mixing system – a homogenizer – and the data was viewed relative to the mixing power. Further increases in mixing beyond the original design framework led to increases in shear adhesion but decreased tack and peel strength. Nevertheless, in all cases, the PSA properties of the blended latexes exceeded that of the base-case latex without cCNCs. The second factor of importance was the cCNC loading. The blending of cCNCs at levels beginning at 0.5 phm (parts per hundred parts monomer) led to the simultaneous improvement in all three PSA properties compared to the base-case latex. The 1 phm level appeared to provide the best impact on the PSA properties. Finally, the need to sonicate the cCNCs dispersions before blending was

significant. The results were further supported by rheological measurements, which demonstrated significant increases in viscosity with cCNC addition. This study clearly demonstrates the effectiveness of cCNC blending to improve all PSA properties simultaneously and provides practical insights for industrial-scale application.

3.2 Introduction

Adhesives are compounds applied to the surfaces of separate items to keep them firmly joined together.[1] Pressure-sensitive adhesives (PSAs) are polymeric materials that instantly attach to a surface (substrate) with light contact pressure and often can be removed with a light pulling force, leaving no residue on the substrate.[2] They are used for labels, tapes, films, and other specialized applications, making them vital in everyday life.[3] The worldwide demand for PSAs continues to grow.[4] The global market for PSAs was evaluated at $9.8 billion in 2020 and is predicted to reach $17.6 billion by 2030. A compound annual growth rate of 6.1% from 2021 to 2030 is predicted.[5]

Historically, PSAs have been produced using solution polymerization, posing evident hazardous conditions at the synthesis stage and during product application. Several decades ago, increased environmental concerns on the management of volatile organic compounds resulted in the growth of emulsion polymerization to produce latexes for water-borne coating applications as alternatives to solvent-borne coatings.[6] Similarly, commercial PSA production has shifted to emulsion polymerization in recent decades.[7] The transition from solution-based technology to emulsion polymerization leads to an inevitable impact on PSA performance.[8] Typically, PSA performance is determined by: tack, peel strength, and shear adhesion. Tack force is the energy required to separate the adhesive from a substrate after brief contact and low application pressure. Peel strength is the capacity of a material to resist removal by peeling. Tack and peel strength reflect the adhesion of the PSA to a substrate. Shear adhesion is the ability of a material to resist a steady shear force and reflects the internal, cohesive strength of the PSA.[2,9–12]

Several factors impact the adhesive and cohesive properties of PSAs. For example, the ability of the PSA to flow and wet the substrate leads to improved tack.[13] The flowability is directly influenced by the polymer glass transition temperature (T_g), molecular weight and distribution, and microstructure. Thus, the choice of monomers in the PSA formulation and the reaction conditions are critical to achieving good adhesion. Surface forces largely influence

wettability, but the polymer molecular weight and microstructure also play a role. The formation of a network within the adhesive polymer matrix influences cohesion. Thus, the polymer molecular weight and the cross-link density of the dried PSA films play an important role. It is noted that many factors influence tack and peel strength similarly. In contrast, shear adhesion tends to be affected oppositely, e.g., cross-linking raises the elastic modulus, which has a negative effect on tack and peel strength but will increase shear adhesion as it strengthens the polymer network's cohesion. Thus, improving tack, peel strength and shear adhesion simultaneously remains a significant challenge in latex-based PSA production.[14,15]

The compartmentalized character of polymer latexes (i.e., discrete polymer particles suspended in water) typically results in PSA films with poorer PSA properties, specifically, lower shear adhesion than their solution-polymerized counterparts. Additives such as chain transfer agents (CTAs) and cross-linkers are often used to modify the polymer microstructure and compensate for the property changes emanating from the change in production methods.[16,17] Another approach is using nanomaterials (e.g., inorganic[18] or organic[19]) leading to PSA nanocomposites.[20] The synthesis of PSA nanocomposites can be categorized into two groups depending on the preparation techniques (i.e., physical or chemical methods). In situ polymerization is a chemical method, whereas blending, melt mixing, and electrospinning are typical examples of physical methods.[21] For in situ polymerization, a nanoparticle suspension is added to the reactor along with the monomer, initiator, and surfactant before the reaction.[22] In the blending approach, nanoparticle suspensions are dispersed in the base latex using mechanical stirring, ultrasonic techniques, etc.[23]

The nanoparticles' unique structure and surface characteristics (e.g., high surface area and often abundant functional groups) can efficiently and positively influence PSA properties.[24–27] However, using nanoparticles poses numerous potential risks to human health and the environment.[28] Cellulose nanocrystals (CNCs) have attracted much attention for nanocomposite production due to their non-toxicity, renewability and availability.[29] CNCs can be extracted from wood pulp by hydrolyzing the cellulose with a strong acid (often sulfuric acid), which leaves the highly ordered nanocrystals suspended in aqueous media.[30] In recent years, CNCs have been shown to improve PSA properties.[31–34] The strength-to-weight ratio of these rod-like nanoparticles is excellent due to their highly crystalline structure.[35] CNCs are hydrophilic and easily dispersed in aqueous media, which makes them eminently compatible with emulsion

polymerization.[29] Their high aspect ratio affects PSA properties, allowing them to form a network at an interface or in the continuous phase of a matrix rather than the typical close-packed monolayer seen when using spherical nanoparticles.[29] CNC-based nanocomposites for PSA applications showed simultaneous improvement in tack, peel strength and shear adhesion using both in situ[36,37] and blending[34,36] approaches up to a concentration of 1.0 wt.% (based on solids). The initial base case formulations (i.e., those without CNCs) in the referenced studies had relatively poor PSA properties compared to commercially available formulations. Nonetheless, they were used to demonstrate advances in adhesive properties and describe how the CNCs affected performance. It was also noted that, for the most part, CNC concentrations greater than 1.0–2.0 wt.% resulted in instability during emulsion polymerization.[34] It was consistently demonstrated that the in situ method resulted in better PSA performance improvements compared to blending due to the improved interactions of the CNCs with the polymer matrix during latex synthesis and PSA film casting.[38] In any case, the addition of CNCs increased the hydrophilicity of the PSAs and, consequently, their ability to adhere, which improved tack and, to some extent, peel strength. Greater cohesive forces due to potential polymer-nanoparticle entanglement or hydrogen bonding were attributed to the increased shear adhesion and improved elasticity.[38]

Recently, Gabriel et al. used carboxylated CNCs (cCNCs) to prepare nanocomposite PSAs using both in situ and blending approaches. Unlike typical sulfated CNCs extracted by sulfuric acid hydrolysis, Anomera Inc. produces cCNCs using a batch method with dilute hydrogen peroxide oxidation to isolate the nanocrystals, resulting in carboxylate groups on the CNC surface as opposed to the sulfate half-esters found on sulfated CNCs.[39,40] Thus, the milder process was one of the motivations to use cCNCs. An attractive feature for the use of CNCs in general is the ability to modify and functionalize the surfaces. Thus, another motivating factor is the difference in the CNC surfaces both in terms of the existing functional groups (i.e., carboxylate vs. sulfate half-esters) and their surface charge densities. The cCNCs generally have a lower surface charge density than the sulfated CNCs.[41]Thus, we are interested in discovering the impact of the surface differences on CNC-nanocomposite latex adhesive performance.

At 0.5–1.0 wt.% loadings, both preparation methods improved peel strength, tack, and shear adhesion.[31] They also blended at two different temperatures (room temperature and the latex polymerization temperature, 60 °C) to measure CNC-nanocomposite PSA performance. Both heated and unheated blends performed slightly better than the base case formulation (i.e., without

CNCs). There was no significant difference in peel strength comparing the heated and unheated blend. However, the heated blend showed higher shear adhesion.[33]

Despite the poorer performance of the blending approach compared to the in-situ technique in the previous studies, we note that the base case latex did not always result in an adhesive with commercial-level performance. In addition, the blending approach was usually performed without optimizing the blend conditions; hence, a direct comparison of performance would be difficult. In this work, we used a physical blending method to produce nanocomposite PSAs using cCNCs. This study aimed to optimize blending conditions for a commercial emulsion-based PSA. Initially, a two-level fractional factorial (2^{5-1}) design was used to determine the optimal blending conditions in a reactor. Subsequently, we examined the PSA properties at different cCNC concentrations under these optimal blending conditions. Finally, we blended the latex with cCNCs using a homogenizer to further explore the impact of mixing on PSA performance.

3.3 Materials and Methods

3.3.1 Materials

DextraCel (i.e., carboxylated CNCs or cCNCs) was obtained from Anomera Inc. (Montreal, QC) in two forms: a "never-dried" form (4.5 wt.% suspension in water) and a "dried" form (spray-dried re-dispersible powder). The carboxylate groups on the cCNC surface were in the sodium-salt form for both forms. The "apparent" cCNC size via dynamic light scattering (DLS) was 102 ±0.4 nm, and the carboxylate group content via conductimetric titration was 141 ±10 mmol.[39] CNCs are reported to have a hydroxyl content of 2–3 mmol g^{-1}.[42] Atomic force microscopy (AFM) images revealed that the cCNCs were 206 ±36 nm long and 4.6 ±1.4 nm in cross-section.[39] Details of the DLS and AFM procedures are found in the citation mentioned above. A commercial-grade emulsion-based PSA was supplied by BASF Inc. (Mississauga, Canada). The latex consisted of an aqueous acrylate copolymer emulsion containing carboxylic acid groups (0.5 wt.%) for PSA applications. The dried latex film exhibits adhesive performance over a wide temperature range, with a bulk density of 1.04 $g.cm^{-3}$ and a T_g of -58 ^oC. The wet latex dispersion had a solids content of 64 wt.%, and a density of 1.01 $g.cm^{-3}$. Distilled deionized water (DDW) with a resistivity of 18.02 ±0.2 MΩ-cm was used for all experiments and characterization.

3.3.2 Fractional Factorial Design

The blending of the commercial-grade emulsion-based latex with cCNCs was evaluated using a 2^{5-1} fractional factorial design (Tables 3.1 and 3.2). In the first design stage, 16 blends or runs, along with 3 replicate runs (runs 17, 18 and 19) and 1 additional run (run 20), were tested (Table 3.2). The experiments were run in random order, and the data were analyzed using Minitab™ software to generate empirical models for the various measured responses (tack, peel strength and shear adhesion). The design factors included: cCNC type: never-dried (4.5 wt.% cCNC suspension in water) vs. dried (dried cCNC powder redispersed in water); cCNC loading: 0.5 and 1 phm (parts per hundred parts monomer by mass); the use of sonication; the mixing temperature; and the mixing rate (Table 3.1).

Table 3.1. Different factors and levels for blending the BASF latex with cCNC

Factors	Low level (-1)	High level (+1)
cCNC type (X_1)	Never-dried	Dried redispersed
cCNC loading (X_2)	0.5 phm	1 phm
Sonication (X_3)	Non-sonicated	Sonicated
Mixing temperature (X_4)	Cold blending (25 °C)	Hot blending (80 °C)
Mixing speed (X_5)	250 rpm	300 rpm

Blending was accomplished in batches of about 250 mL in a jacketed 1 L stainless steel LabMax™ (Mettler Toledo) reactor. The reactor was equipped with an anchor stirrer. The blend temperature and stirring speed were controlled by iControl™ LabMax software. The latex (~250 mL) was added to the reactor and heated to the desired temperature (25 or 80 °C) while mixing (250 or 300 rpm). Blending at 25 °C was chosen to evaluate the possibility of blending at ambient temperatures while blending at 80 °C served to mimic the temperature conditions commonly used during polymerization. Once the blending temperature was reached, the cCNC suspension was poured slowly into the reactor via a top head port. The blending time started with the addition of the cCNCs and was carried out for 30 minutes. After the blending period, the latex was cooled to 25 °C, if necessary. The blends were characterized for latex viscosity using a rheometer and for particle size using dynamic light scattering (DLS). Films were cast from the latex for PSA testing.

Table 3.2. 2^{5-1} Fractional factorial design for blending a commercial latex with cCNC

Run #	X_1 cCNC type	X_2 cCNC loading	X_3 Sonication	X_4 Mixing Temperature	X_5 Mixing Speed
1	-1	-1	-1	-1	+1
2	+1	-1	-1	-1	-1
3	-1	+1	-1	-1	-1
4	+1	+1	-1	-1	+1
5	-1	-1	+1	-1	-1
6	+1	-1	+1	-1	+1
7	-1	+1	+1	-1	+1
8	+1	+1	+1	-1	-1
9	-1	-1	-1	+1	-1
10	+1	-1	-1	+1	+1
11	-1	+1	-1	+1	+1
12	+1	+1	-1	+1	-1
13	-1	-1	+1	+1	+1
14	+1	-1	+1	+1	-1
15	-1	+1	+1	+1	-1
16	+1	+1	+1	+1	+1
*17	-1	+1	+1	-1	+1
*18	+1	-1	+1	-1	+1
*19	+1	-1	-1	-1	-1
*20	+1	-1	-1	-1	-1

*Replicate experiments: 17 replicates 7, 18 replicates 6, and 19 replicates 2; and additional run 20.

In a subsequent design, the commercial latex was blended in the reactor at the optimal conditions emanating from the first design, with cCNC at six different loadings (0.3, 0.4, 0.5, 0.6, 0.7, 1 phm). In a final set of runs, the commercial latex was blended with the never-dried, sonicated cCNCs using a Silverson mixer (henceforth referred to as a homogenizer) at three different rotor speeds of 2000, 2500 and 3000 rpm. The latex was added to a beaker and placed in an ice bath to

maintain a temperature of 20 ± 5 ºC, and the mixer was started. The cCNC suspension was added in ~20 mL aliquots to the latex over a period of 2 min; the total mixing time was 10 min. For these blends, the cCNC concentration was fixed at 1 phm. Additional runs were completed at 3000 rpm with cCNC concentrations of 1.5 and 2 phm.

Finally, the cCNCs were added to the emulsion-based latex to study the effect of the type of CNCs (dry re-dispersed versus never-dried form) and their dispersion method on the final latex properties.

In all cases, before blending, cCNCs were filtered through glass microfiber filter paper with a 2.7 µm pore size to ensure the removal of larger particles and aggregates. This filtration step aimed to enhance the dispersion quality and promote uniform particle size distribution within the adhesive matrix. Also, to monitor the particle size and assess the efficacy of the filtration process, DLS measurements were performed on the cCNCs before each use. These measurements allowed for detecting any aggregation or potential issues with the cCNC dispersions. CNC preparation depended on the cCNC type and whether ultrasonication was used and is described below:

Never-dried cCNCs. Never-dried cCNCs (4.5 wt.% dispersion, as received) were diluted in DDW to 1 wt.% and mixed for about 5 min with a magnetic stir bar before adding to the commercial latex.

Never-dried ultrasonicated cCNCs. Never-dried cCNCs (4.5 wt.% dispersion, as received) were diluted to 1 wt.% in DDW, mixed for about 5 min with a magnetic stir bar, then ultrasonicated. Probe ultrasonication was performed in an ice bath using a Fisher Scientific 550 sonic dismembrator at 75% amplitude for three intervals of 5 min, with 5 min of rest in between. The volumes of cCNC suspensions ultrasonicated in this work ranged from 200 to 500 mL, and the energy input by ultrasonication was always above the recommended 10-20 $kJ.g^{-1}$ of CNC necessary to achieve well-dispersed samples.[43]

Dried re-dispersed cCNCs. Dried cCNCs were added to DDW to formulate a 1 wt.% cCNC dispersion and mixed using a magnetic stir bar overnight.

Dried re-dispersed ultrasonicated cCNCs. Dried cCNCs were dispersed in the same way as in the "dried re-dispersed" method, followed by three cycles of probe ultrasonication as described above.

Additional tests were conducted to compare the dispersion of cCNCs in water using a sonicator versus a Silverson high-shear mixer.

3.3.3 Rheological Measurement

Flow curve tests were conducted with an Anton Paar MCR 301 rotational rheometer. The rheometer was configured with a concentric cylinder geometry. A general-purpose disintegrating head was used. The gap between the inner and outer cylinder was 1.15 mm, and the temperature of the outer cylinder was maintained at 25 ±1.0 ºC. Viscosities were recorded under a linearly increased shear rate from 1 to 20 s^{-1} in 200 s. The rheometer was used to measure the viscosity of the wet dispersions: the cCNC/latex blends and the base-case latex. Additional rheological testing was performed on selected samples to measure the viscoelastic properties (i.e., loss modulus (G'), storage modulus (G")). The oscillation frequency was varied from 0.01 to 30 $rad.s^{-1}$ at a constant shear strain rate of 0.5%.

3.3.4 Dynamic Mechanical Analysis (DMA)

Dynamic mechanical analysis (DMA) was performed using an RDA III rheometer (TA Instruments). The geometry used was a pair of 25 mm parallel plates, and the sample thickness was 1.80 ± 0.2 mm. The PSA samples were prepared as follows: initially, a specific volume of latex was placed into a silicon mold. The latex underwent a drying process at room temperature in a fumehood lasting approximately 10 days until a consistent weight was achieved. Subsequently, the latex was cut to create disk-shaped specimens. Frequency sweep tests were performed at 23 °C, covering a range of oscillation frequencies (ω) from 0.01 to 80 Hz; measured values had 10% uncertainty.

3.3.5 Particle Size and Distribution

DLS was used to measure the size and distribution of the polymer particles and cCNCs with a Malvern NanoS Zetasizer 2000 at an angle of 176°. The polymer latex or cCNC suspensions were diluted to 0.025 wt.% in DDW and were placed in a polystyrene cuvette to full. The viscosity of the sample was the same as that of DDW. Three measurements of 10-14 scans were performed for each sample, and the results were reported as the z-average particle size. In general, DLS is better suited for characterizing spherical particles; thus, measurements for rod-like particles, such as cCNCs, are not an exact measure. Rather, DLS provides an apparent diameter and can be used as a point of comparison between the samples within our study.

3.3.6 Latex Film Preparation and PSA Testing

Pressure Sensitive Tape Council standards (PSTC), including PSTC16 for tack, PSTC101 for peel strength, and PSTC107A for shear adhesion, were followed for specimen preparation and testing procedures for measuring PSA properties. The blended and base-case PSA latexes were cast on 30 μm corona-treated Mylar sheets using Meyer rods #20 and #30 to produce films of approximately 20 $g.m^{-2}$, which were dried at controlled conditions (temperature: 23 ±1 °C, and relative humidity: 50 ±5%) for 48 h before testing (2 films per sample) to produce films of approximately 20 $g.m^{-2}$. An Instron 3000 Universal Tester, together with Bluehill 2 Materials Testing software, was used to measure the tack and peel strength as the force per unit width required for removing the PSA strip from the substrate. Each test was repeated six times for each latex film (three samples per film for each test), and the average results and standard deviations were reported.

Tack. Strips of 1″ × 6″ (2.54 cm × 15.24 cm) were cut, and a drop loop was formed by taping 1″ (2.54 cm) of each end of the strip, which was secured in the upper grip of the Instron tester. The upper grip was moved downward at a rate of 2 $mm.s^{-1}$ until an area of 1″ × 1″ (2.54 cm × 2.54 cm) of a stainless-steel substrate mounted on the lower grip was covered. The upper grip was then pulled up at a 5 $mm.s^{-1}$ rate, and the maximum force ($N.m^{-1}$) required for removal was recorded as tack.

Peel strength. Peel strength was measured by separating the adhesive from the substrate at a 180° angle with respect to the substrate. Strips of 1″ × 5″ (2.54 cm × 12.7 cm) were cut and adhered to a stainless-steel substrate via the application of a 2040 g roll coater (twice front-to-back movement along the length of the strip) at a rate of 10 $mm.s^{-1}$. Subsequently, the substrate and the PSA strip were fixed in the lower and upper grips, respectively. The upper grip was then pulled upward at a rate of 5 $mm.s^{-1}$, and the average force required for peeling ($N.m^{-1}$) was reported as peel strength.

Shear adhesion. A homemade shear tester was used to record the time a PSA strip could hold against a constant vertical force. Strips of 0.5″ × 5″ (1.27 cm × 12.7 cm) were cut, and one end of the strip was laminated on a stainless-steel substrate to cover a 0.5″ × 0.5″ area using the roll coater (2040 g) in a similar way to specimen preparation for peel strength testing (four passes at a rate of 10 $mm.s^{-1}$). A C-clamp was used to hang a 500 g weight to the other end of the strip.

The time (h) elapsed until the covered area was removed and the hung weight dropped was reported as shear adhesion.

3.4 Results and Discussion

3.4.1 Initial Factorial Design

A regression analysis of the 2^{5-1} fractional factorial design experiments was conducted using Minitab™ software to examine the relationships between the factors (cCNC type, cCNC loading, sonication, mixing temperature, and mixing speed) and the response variables (tack, peel strength and shear adhesion). The data shown in Table 3.3 include PSA test results for the base-case commercial latex as received; the base-case results were not used in the regression analysis. A backward elimination procedure was employed, with a significance level (α) of 0.05. The resulting regression equations for the PSA properties are found in Table 3.4. It is noted that non-significant main effects (X_i) were included in the models if those main effects were included in two-factor interaction terms (X_iX_j) that were statistically significant, according to standard practice. The model summary shows R-squared values of 84.18% for tack, 74.58% for peel strength and 95.62% for shear adhesion. The adjusted R-squared values, a better measure of goodness-of-fit, account for the number of predictors in the model; the values were 69.94, 62.85 and 91.67% for the tack, peel strength and shear adhesion models, respectively. These values suggest a reasonably good fit of the model to the data for the purposes of this first stage in the investigation. Inspection of the residuals revealed no suspicious patterns in the data (see Appendix I, Figure I.1). The lack-of-fit tests for the regression models are shown in the Appendix I, Table I.1. There is no significant lack-of-fit for the tack (p-value = 0.257) or shear adhesion models (p-value = 0.56). On the other hand, the lack-of-fit for peel strength is statistically significant (p-value = 0.006). In summary, the tack and shear adhesion models provide a reliable means to predict the performance of the blends, while the peel strength model does not. Nevertheless, for the purposes of this first step in the investigation, we used the regression analysis results from all three to direct further study and identify important experimental factors.

The analysis of variance (ANOVA) (Table 3.5) demonstrates the overall significance of the regression model parameters. Among the individual terms, several factors significantly affected the adhesive properties. Rather than verifying each model in turn, it is better to look at all three simultaneously.

In all cases, the most important factor was X_5 (mixing speed); this is evident because, in each model, X_5 had the largest positive coefficient (Table 3.4) and largest F-value (Table 3.5). In the first place, as was observed in multiple studies in the past and as discussed in the introduction, the addition of CNCs to an adhesive formulation has a positive impact on both adhesion and cohesion.[31,36,37,44,45] The observed increase in both adhesive and cohesive properties with higher mixing speed is attributed to the improved cCNC dispersion in the latex. More intense mixing, therefore, facilitated the intermingling of the cCNCs with the latex polymer particles, favouring a more uniform distribution of cCNCs in the final adhesive film. This led to more effective contact of cCNCs with the substrate during adhesion and more efficient entanglement with diffusing polymers during the film drying process, leading to better cohesive strength. The significance of mixing speed led to further investigation of mixing, discussed later.

Not surprisingly, cCNC loading (X_2) also played an important role in all three regression models: second-most important for tack and shear adhesion, and third-most for peel strength. Notably, the X_2 coefficients are negative, which suggests using a 0.5 phm is better than a 1.0 phm cCNC loading. These results imply that a maximum effect on PSA performance may be achieved with a lower cCNC loading, which is consistent with previous studies.[31,44,45] On the other hand, in the tack and peel strength models, the two-factor interactions, including X_2, were significant and positive (Table 3.4). Thus, these results indicated a requirement for further study of cCNC loading, which followed this initial experimental design and is discussed later.

While sonication (factor X_3) was significant only for the shear adhesion model, it was included in all models because of its significance as a factor for two two-factor interactions in each model. Considering the magnitude and signs of the coefficients in the models, the use of sonication of the initial cCNC dispersion is recommended. Particle size analysis of the never-dried cCNCs yielded an average particle size of 102 nm, which decreased to 74.5 nm after sonication.

Mixing temperature (factor X_4) was not significant as a main effect except in the peel strength model. It was included in all the models as there were significant two-factor interactions involving X_4. For the most part, all models point to using room temperature instead of the higher temperature associated with the typical emulsion polymerization (80 ^{o}C). Finally, X_1 (cCNC type) was not significant as a main effect in any of the models and appeared only twice as a significant two-factor interaction. This suggests that using dried re-dispersed cCNCs vs. never-dried cCNCs does not affect PSA performance.

Table 3.3. PSA properties of base-case commercial latex and blends with cCNCs. Run conditions are found in Tables 1 and 2.

Run#	PSA Properties		
	Tack ($N.m^{-1}$)	**Peel strength ($N.m^{-1}$)**	**Shear adhesion (h)**
Base-case	485 ±41	245 ±16	13.3 ±2
1	490 ±40	230 ±14	16.5 ±3
2	350 ±25	120 ±8	2.7 ±1
3	110 ±7	41 ±4	5.0 ±1
4	230 ±15	104 ±7	10.2 ±2
5	250 ±15	101 ±6	5.9 ±3
6	430 ±32	248 ±20	34.0 ±7
7	650 ±100	312 ±26	27.5 ±6
8	250 ±25	166 ±10	3.3 ±1
9	345 ±28	271 ±20	9.1 ±2
10	440 ±25	389 ±29	16.4 ±3
11	280 ±17	189 ±12	10.4 ±2
12	340 ±22	169 ±11	9.7 ±2
13	410 ±20	228 ±18	8.8 ±2
14	340 ±24	224 ±15	9.6 ±3
15	270 ±16	102 ±7	7.8 ±1
16	290 ±19	311 ±22	8.2 ±3
17	550 ±50	313 ±22	32.0 ±7
18	480 ±38	260 ±21	29.0 ±6
19	320 ±22	140 ±10	4.5 ±2
20	380 ±21	250 ±22	10.4 ±2

Table 3.4. Regression models for responses.

Response	Regression model
Tack	$= 341.6 - 2.2\ X_1 - 35.9\ X_2 + 23.1\ X_3 - 2.2\ X_4 + 57.3\ X_5 - 42.9\ X_1X_5 + 36.9\ X_2X_3 - 35.0\ X_3X_4 - 41.6\ X_4X_5$
Peel strength	$= 206.3 - 16.7\ X_2 + 8.6\ X_3 + 29.0\ X_4 + 56.1\ X_5 + 30.4\ X_2X_3 - 27.7\ X_3X_4$
Shear adhesion	$= 11.244 + 0.173\ X_1 - 1.148\ X_2 + 1.930\ X_3 - 1.244\ X_4 + 4.617\ X_5 - 2.419\ X_1X_2 - 3.330\ X_3X_4 + 1.906\ X_3X_5 - 3.667\ X_4X_5$

Table 3.5. Analysis of variance (ANOVA) results.*

Source	Tack		Peel strength		Shear adhesion	
	F-value	*p-value*	*F-value*	*p-value*	*F-value*	*p-value*
X_1	0.02	0.88	-	-	0.07	0.794
X_2	5.54	0.04	1.84	0.198	3.15	0.106
X_3	2.3	0.16	0.47	0.504	0.014	0.014
X_4	0.02	0.88	5.4	0.037	0.087	0.087
X_5	13.77	0.004	20	0.001	49.88	0.000
X_1X_2	-	-	-	-	13.65	0.004
X_1X_5	7.89	0.019	-	-	-	-
X_2X_3	6.03	0.034	6.13	0.028	-	-
X_3X_4	5.28	0.044	4.92	0.045	26.47	0.000
X_3X_5	-	-	-	-	8.7	0.015
X_4X_5	7.28	0.022	-	-	31.46	0.000

*Terms that were non-significant were not included in the final regression and have no value. Terms that were non-significant in all three models are not shown.

The optimal combination of factors that maximize the PSA properties was determined using the response optimization function in Minitab™. The optimization goals were set to maximize the values of tack, peel strength and shear adhesion. The weights and importance values for each response variable were assigned equally to ensure a balanced optimization approach. Details of the optimization approach are found in the Appendix I (Tables I.2 and I.3, and Figure

I.2). Regardless of whether all three models or only the tack and shear adhesion models were used, the optimization results remained the same. The optimization suggests the optimal conditions X_1 = -1, X_2 = 1, X_3 = 1, X_4 = -1, X_5 = 1, which coincides with the conditions of run 7 (Tables 3.2 and 3.3). In other words, the suggested optimal conditions are to blend the latex with never-dried cCNC at 1 phm loading using sonication to disperse the cCNC before blending, followed by blending at room temperature at a high mixing speed. The results of the optimal conditions (run 7) showed significant and simultaneous increases in all three PSA properties compared to the base-case latex; i.e., tack increased by 34%, peel strength increased by 23%, and shear adhesion increased by 107%. The simultaneous improvement in all three PSA properties is a remarkable observation. Normally, as noted earlier in the introduction, one expects tack and peel strength to trend opposite to shear adhesion.[15]

From the replicate data, the experimental error was calculated as 12% for tack, 7% for peel strength, and 28% for shear adhesion. The experimental errors in these instances include the analytical errors from the measurement methods. As is typical for PSA measurements, the analytical errors tend to be the largest contributors to the overall error and vary from sample to sample. Thus, in all figures where error bars are shown, the error bars were calculated as plus/minus two standard deviations based only on the sample measurement errors.

Earlier, there was some indication that the lower cCNC loading (0.5 phm) would be preferred. However, the optimization results suggested otherwise. Regardless, the above study led to further exploration of the impact of the two most important factors: mixing and cCNC loading.

3.4.2 Mixing Power

Because of the significance of mixing, blending was also conducted using a Silverson high-shear mixer. The Silverson high-shear mixer was utilized at different mixing speeds (2500, 3000, and 3500 rpm) at a mixing time of 10 min, at room temperature. The same sample volumes were used in both cases. Because of the differing mixing vessel geometries in the LabMax reactor (1.25 L reactor with anchor impeller) and the homogenizer (1 L glass beaker with a general-purpose integrated head), a more reasonable means of comparison is the mixing power. The power provides a representation of the energy input during blending. To convert the mixing speed in the reactor and homogenizer to power, one uses:

$$P = N^3 D^5 \rho P_0 \qquad (3.1)$$

where P is power (W), P_0 is the power number, N is the rotational speed (s^{-1}), D is the impeller diameter (m), and ρ is the density of the fluid being mixed ($kg.m^{-3}$). Given the specific values for the impeller diameter (90 mm) and the homogenizer head diameter (28 mm), as well as the power numbers for the impeller type anchor (0.6) and the head of the homogenizer (2), one can calculate the corresponding power for each mixing system from eq. (3.1) (Table 3.6).

Table 3.6. Converting mixing speed to mixing power

Blending system	Speed (rpm)	Power (W)
Reactor	250	0.26
Reactor	300	0.46
Homogenizer	2000	1.4
Homogenizer	2500	2.7
Homogenizer	3000	4.7

Earlier results indicated that increasing the mixing power from 0.26 to 0.46 W in the reactor (i.e., variable X_5, mixing speed) had a significant positive impact on all PSA properties, including tack, peel, and shear adhesion (see Table 3.4). Subsequent increases in mixing power up to 4.7 W by using the homogenizer led to a significant enhancement in shear adhesion with decreases in tack and peel strength (Figure 3.1). The increased quality of cCNC dispersion led to a greater number of cCNC-latex particle interactions. These interactions had as a primary effect, a significant increase in shear strength due to the formation of CNC-particle networks via entanglements. This increase in stiffness due to the formation of networks resulted in a drop in adhesion, affecting tack and peel strength negatively. This is the typical trade-off one would expect between adhesion and cohesion.[22,34,46] Nonetheless, all three PSA performance properties remained well above that of the base-case latex. These results confirm that PSA performance is sensitive to mixing. Following these favourable results using the homogenizer, further blends at cCNC loadings of 1.5 and 2 phm were tested. However, it was observed that increasing the cCNC concentration to 1.5 phm or higher led to a decrease in PSA performance (Table 3.7). Additionally, at these higher cCNC loadings, the PSAs exhibited cohesive failure; a residue was left on the substrate during the peel strength tests.

Table 3.7. PSA Properties of never-dried sonicated cCNCs blended with commercial latex using the homogenizer at 3,000 rpm and room temperature.

cCNC loading (phm)	Tack ($N.m^{-1}$)	Peel strength* ($N.m^{-1}$)	Shear adhesion (h)
1.5	290 ±14	200 ±8.3	23 ±6
2	205 ±8	151.5 ±12	8.8 ±3

*Cohesive failure.

The presence of a single peak in the DLS analysis when comparing the commercial latex as received, the latex without cCNC after mixing in the homogenizer at 3,000 rpm for 10 min, and the latex-cCNC blends in the reactor (300 rpm) and homogenizer (3,000 rpm) using the optimal conditions (1 phm never-dried, sonicated cCNCs at room temperature) indicates a homogeneous dispersion of cCNCs throughout the polymer latex (see Appendix I, Figure I.3). The average particle sizes for the samples of as-received commercial latex and that mixed without cCNC in the homogenizer were the same (307 nm). This suggests that the homogenizer did not in any way cause colloidal instability in the latex. After blending the cCNCs with the latex in the reactor at 300 rpm, the latex particle size increased to 398 nm. This implies that a potential interaction between the polymer particles and cCNCs possibly contributed to the creation of larger particle aggregates or complexes. On the other hand, the blend of cCNCs with the homogenizer yielded a particle size of 383 nm. One could suppose that some breakdown of aggregates occurred. This outcome reflects the homogenizer's influence on promoting more effective dispersion and particle size reduction in the blended composition. The difference in particle sizes between the blends in the reactor and those in the homogenizer further supports the impact of mixing. Not surprisingly, therefore, the choice of blending equipment and the power (and mixing speed) play critical roles in determining PSA performance when blending cCNCs or any other nanoparticle. The suggested interaction between the cCNCs and the polymer particles can be attributed to various factors, such as hydrogen bonding, electrostatic interactions, or physical entanglements.

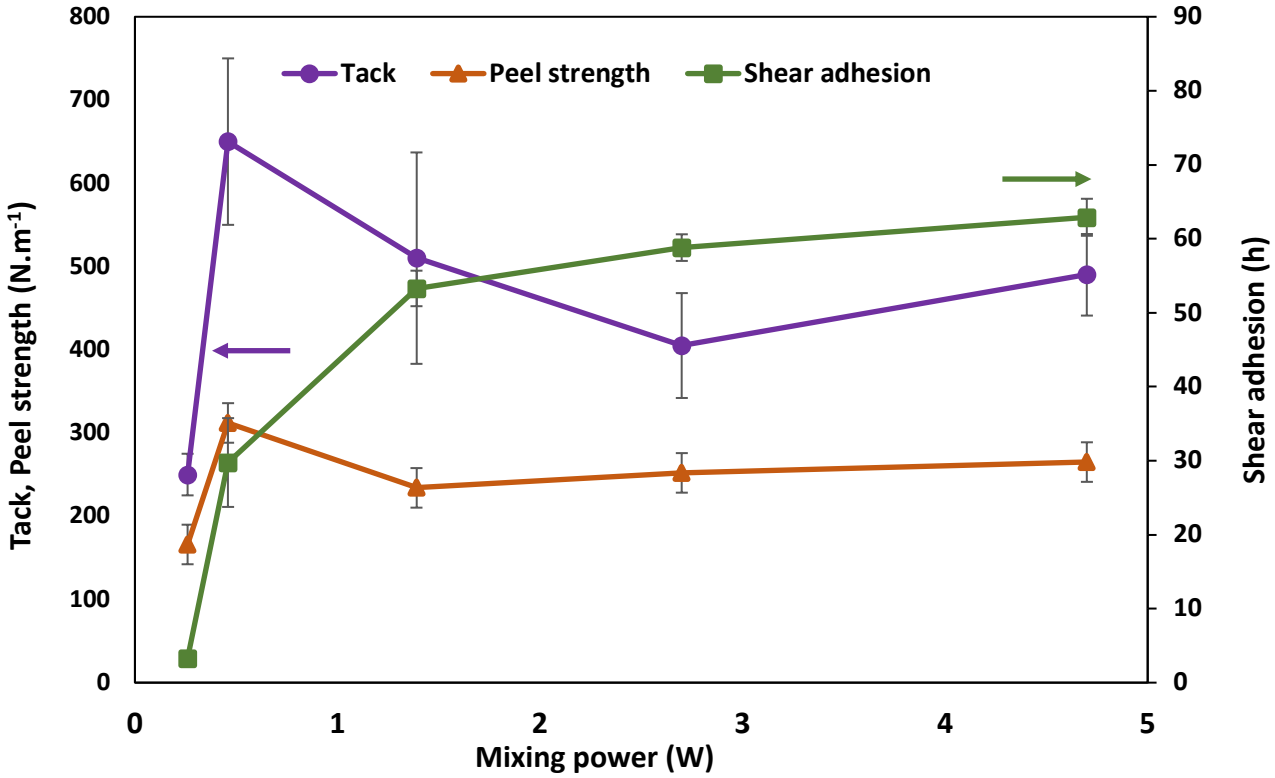

Figure 3.1. PSA properties vs. power for latex blends at optimal conditions (1 phm never-dried sonicated cCNCs at room temperature). To convert power to rpm, see Table 3.6. The lines in the figure are for improved visualization only. As noted earlier, error bars represent plus/minus two standard deviations of the measurement error only.

3.4.3 cCNC Loading

Recall that the second most important factor in the regression analysis from the first experimental design was cCNC loading. Thus, another designed experiment was conducted wherein the commercial latex was blended at the optimal blending conditions obtained from the first design, except that the cCNC loading was varied: 0.3, 0.4, 0.5, 0.6, 0.7, and 1 phm (Figure 3.2). A control sample (no cCNCs) was generated by subjecting the commercial latex to the optimal blend conditions. As shown in Figure 3.2, tack increased from 484 to 650 $N.m^{-1}$ or 34% after increasing the cCNC loading from 0 to 1 phm. The effect of cCNC loading was only observed beyond 0.4 phm cCNC. Shear adhesion showed a remarkable increase after increasing cCNC loading from 0 to 1 phm, as indicated by the time required for the PSA samples to drop from the test unit; times ranged from 12.7 to 27.5 h or a 117% increase. The effect of cCNC loading on peel

strength was less significant, increasing from 255 to 312 $N.m^{-1}$ or a 22% increase.[47] These results demonstrate the remarkable and simultaneous improvement in all three PSA properties as observed in the initial factorial experiments and in other studies. [15]

It is useful to consider the results above compared to previous studies (Table 3.8). Most of those studies were conducted with in situ addition of the cCNCs to the polymer formulation with occasional simple, non-optimized blend tests. Furthermore, sulfated CNCs were employed in most of those studies, and the PSA base-case formulations were of a different composition and were not optimized for PSA performance. In the first place, one notices that the simultaneous improvement in tack, peel strength and shear adhesion was achieved whenever CNCs were added to the formulation, whether via in situ polymerization or by blending. The data in Table 3.8 reflect the best PSA performance for each case. In line with prior research, our results show that the most pronounced increase in PSA properties occurred following adding 1 phm CNCs, as was the case for most of the other investigations. This finding underscores the significance of CNC loading in influencing adhesive performance and suggests a critical threshold for optimal enhancement. As noted earlier, for many of the studies shown in Table 3.8, the base-case PSA formulations were not optimal regarding their PSA performance. None of them compared well with the commercial latex used in this study regarding tack and peel strength. It should be noted that the shear adhesion test strips used in those studies were 1” x 0.5” compared to that in the current study, which was 0.5” x 0.5”. Thus, the commercial base-case latex used in this study already exhibited high tack, peel strength, and shear adhesion yet still saw further improvement in PSA performance with CNC incorporation. This suggests that the enhancements achieved through the addition of CNCs to the latex are not confined to weaker adhesive formulations but can also complement and amplify the inherent properties of already strong adhesives.

As noted, increasing CNC content demonstrates a noticeable enhancement in all three key PSA performance properties. Various factors influence these simultaneous enhancements. Shear adhesion is normally affected by molecular weight and crosslinking of the latex polymer. The increased shear adhesion has been attributed to possible hydrogen bond formation between the CNCs and the polymer particles, and entanglement of the CNCs with diffusing polymers during PSA film formation.[34,37,45,48] Moreover, the crystalline nature of CNCs provided mechanical strength, while their high aspect ratio facilitated the formation of percolating networks within the polymer matrix.[49,50] These networks enhance the polymer matrix's rigidity, consequently

improving cohesive forces while preserving the polymer's microstructure, including its glass transition temperature.[22,34] Tack is predominantly determined by the PSA's ability to wet the substrate effectively, signifying its rapid adhesion during brief contact. Peel strength gauges the adhesive bond's potency between the PSA and substrate after applying the required pressure to achieve substrate wetting. The surface groups on the cCNCs, particularly the hydroxy and carboxylate moieties, improve adhesion via hydrogen bonding with the substrate.[33,45] The physical and chemical properties of cCNCs, including their hydrophilicity and carboxylate groups, contributed synergistically to these improvements. The hydrophilic nature of the cCNCs facilitated their dispersion in water, while the carboxylate groups improved film wettability and adhesion through surface interactions.

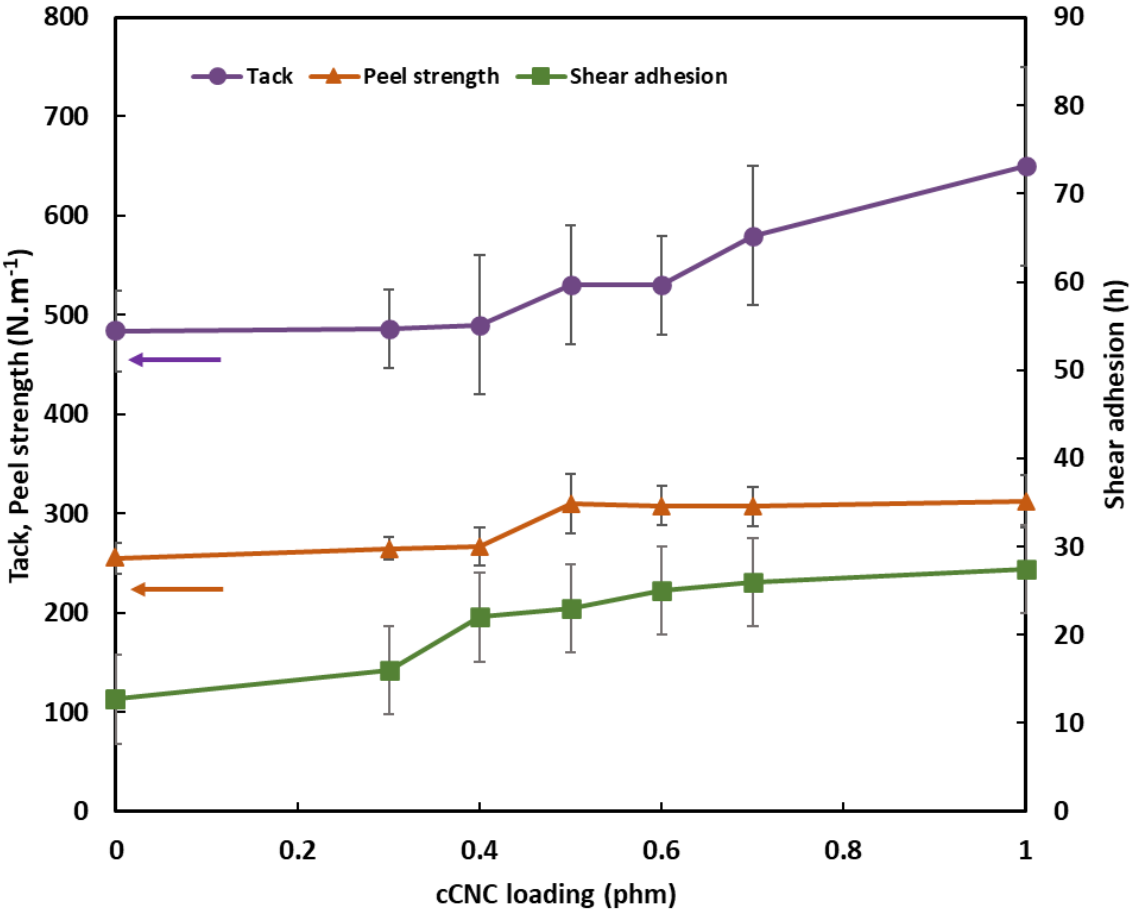

Figure 3.2. PSA properties of the commercial latex-cCNC blends vs. cCNC loading at optimal conditions.

Table 3.8. Studies on emulsion-based latex-CNC nanocomposites – best results reported for each. (BA: n-butyl acrylate, MMA: methyl methacrylate, VA: vinyl acetate, AA: acrylic acid, sCNC: sulfated CNC; cold blending = room temperature, hot blending = 60 ºC)

Ref. #	Monomer system (wt.% composition)	Base-case latex properties			Latex-CNC nanocomposite properties			% increase in latex-CNC nanocomposite properties			Comment
		Tack ($N.m^{-1}$)	Peel strength ($N.m^{-1}$)	Shear adhesion* (h)	Tack ($N.m^{-1}$)	Peel strength ($N.m^{-1}$)	Shear adhesion* (h)	Tack (%)	Peel strength (%)	Shear adhesion (%)	
[38]	BA/MMA (90/10)	50	17	5	170	50	60	240	194	1,100	In situ at 1 phm sCNC
					110	22	17	120	29	240	Cold blending at 1 phm sCNC
[33]	EHA/BA/MMA (39/41/20)	75	10 1	10	135	16	39	80	60	290	In situ at 1 phm sCNC
					181	34	18	141	240	80	Cold blending at 1 phm sCNC
[44]	BA/VA/AA (90/6/4)	200	10	20	422	125	112	111	1150	460	In situ at 0.75 phm sCNC
[31]	BA/MMA (90/10)	100	10	2	450	240	2.2	350	2300	12	In situ at 0.5 cCNC
					370	15	8	270	50	300	Cold blending at 0.5 phm cCNC
					280	100	4.2	180	900	110	Cold blending at 1 phm cCNC
					215	30	6.5	115	200	225	Hot blending at 0.5 phm cCNC
					260	100	4	160	900	100	Hot blending at 1 phm cCNC
This study	Commercial acrylate-based PSA	485	245	13*	650	311	27	34	27	106	Cold blending at 1 phm cCNC

*Shear adhesion test strips for all references were 1” x 0.5”; the current study used 0.5” x 0.5” strips due to the significantly higher shear adhesion of the commercial base-case latex. Testing of the commercial PSA in this study using a 1” x 0.5” test area resulted in >150 h; the test was prematurely aborted.

3.4.4 cCNC Sonication

To evaluate the effectiveness of the dispersion of the never-dried cCNCs in water, their apparent particle diameter was determined using DLS. Three distinct dispersion methods were compared: ultrasonication, a high-shear homogenizer, and one-minute mixing using a magnetic stir bar (referred to henceforth as non-sonicated). Sonication exhibited superior dispersibility compared to the other methods tested. Sonication yielded an apparent average particle diameter of never-dried cCNCs of 74.5 ±1 nm, in contrast to the non-sonicated cCNCs, which exhibited a particle diameter of 102 ±1 nm. The homogenizer was employed at two distinct speeds (5,000 and 10,000 rpm) over varied durations, ranging from 15 to 45 min; the particle sizes ranged from 92.7 ±2 to 86.7 ±1 nm. This is consistent with studies that showed sonication plays a crucial role in achieving a more uniform and effective dispersion of cCNC particles in water.[51,52] The improved dispersion achieved through sonication can be attributed to the mechanical forces generated by high-frequency ultrasound waves. These forces effectively break down the agglomerates and promote the separation of individual cCNC particles, yielding a more homogeneous distribution in water.[53,54] In contrast, the high shear provided by the homogenizer alone was not as effective in achieving a comparable level of dispersion. Therefore, throughout this investigation, sonication was used to disperse the cCNCs unless a non-sonication condition was required via the experimental design.

The impact of sonication on cCNC dispersion was also examined for its influence on the PSA properties of latex-cCNC blends (Table 3.9). The runs were conducted at the optimal blend conditions noted earlier. Clearly, and as corroborated by the initial designed experiment, the sonication of the cCNCs is vital to improving PSA performance. Lower energy alternatives to disperse the cCNCs are not adequate (Table 3.9).

Table 3.9. Effect of cCNC dispersion method on PSA properties of room temperature blends using 1 phm never-dried cCNCs at a mixing speed of 300 rpm. Plus-minus errors represent one standard deviation.

cCNC dispersion method	Tack ($N.m^{-1}$)	Peel strength ($N.m^{-1}$)	Shear adhesion (h)
Sonicated	650 ±100	312 ±26	27.5 ±6
Homogenizer	220 ±35	150 ±15	8.0 ±1
Non-sonicated	190 ±30	125 ±12	6.5 ±1

3.4.5 Rheological Analysis

The viscosity of the 16 blends from the original 2^{5-1} factorial design, along with one additional replicate run, and the base-case latex, the latter run at 40 and 50% solids, was measured using a rheometer (Table 3.10). Similar to the PSA performance analysis, the viscosity data were regressed using the Minitab™ software with a backward elimination method at $\alpha = 0.5$. The regression model is:

$$\text{Viscosity} = 251.47 - 22.20\,X_1 + 96.92\,X_2 - 13.13\,X_3 + 23.70\,X_4 - 17.13\,X_5 + 44.20\,X_1X_3 - 27.98\,X_1X_4 - 53.35\,X_1X_5 - 70.73\,X_2X_3 + 39.15\,X_2X_4 + 60.97\,X_2X_5 - 44.55\,X_3X_4 - 64.73\,X_3X_5 \quad (3.2)$$

It is noted that the non-significant main effect (X_3) was included in the model because several two-factor interactions which included X_3 were statistically significant, according to standard practice. R-squared was 99.88% and the adjusted R-squared was 99.01%, indicating an excellent fit of the model to the data. Inspection of the residuals revealed no suspicious patterns in the data (see Appendix I, Figure I.4). The lack-of-fit test for the regression model showed no significant lack-of-fit (p-value = 0.11). The ANOVA results are shown in Table 3.11.

Based on the regression analysis, while most of the factors were statistically significant in the model, the cCNC loading (X_2) had the most significant effect on viscosity (Table 3.11). This is consistent with numerous previous reports of the effect of cCNCs on latex viscosity.[45,55] Increasing the cCNC loading led to increased viscosity because cCNCs are rigid, elongated particles with a high aspect ratio. When cCNCs are dispersed in a latex, they can act as physical barriers to flow and create entanglements with diffusing polymer chains, further hindering flow. The strong two-factor interaction effect due to X_2X_3 (cCNC loading-sonication) suggests that increasing cCNC loading without sonication can increase viscosity. It may be attributed to the formation of cCNC agglomerates within the latex. This factor can contribute to higher resistance to flow and restrict the mobility of the polymer chains, resulting in an increase in viscosity.[56,57]

Table 3.10. Final latex viscosity. Recall that conditions for each run vary according to Tables 3.1 and 3.2. Viscosity reported at shear rate of 1 s^{-1}.

Run #	cCNC loading (phm)	Viscosity (mPa.s)
Base-case (40% solids)	-	4.0
Base-case (50% solids)	-	15.0
1	0.5	40.2
2	0.5	202.2
3	1	307.4
4	1	235.6
5	0.5	403.0
6	0.5	34.6
7	1	137.3
8	1	461.8
9	0.5	74.4
10	0.5	71.0
11	1	902.0
12	1	284.0
13	0.5	160.0
14	0.5	251.0
15	1	165.0
16	1	294.0

Table 3.11. Analysis of variance (ANOVA) results.*

Source	Viscosity	
	F-value	*p-value*
X_1	18.88	0.049
X_2	359.97	0.003
X_3	6.61	0.124
X_4	21.53	0.043
X_5	11.24	0.079
X_1X_3	74.88	0.013
X_1X_4	30.00	0.032
X_1X_5	109.00	0.009
X_2X_3	191.71	0.005
X_2X_4	58.75	0.017
X_2X_5	142.45	0.007
X_3X_4	76.04	0.013
X_3X_5	160.56	0.006

*Terms that were non-significant are not shown.

Further rheological analysis of the blended latex with cCNCs was done using an Anton-Paar rheometer. The blended latexes displayed non-Newtonian behaviour in contrast to the linear behaviour observed in the latex without cCNC (see Appendix I, Figure I.5). This suggests that adding cCNC introduces significant changes in the rheological properties of the latex. The increased viscosity of the cCNC-latex blends, approximately 15 times higher than that of the latex without cCNC, greatly enhanced the flow characteristics during the film casting process. The higher viscosity provided improved control over the coating thickness and reduced the likelihood of uneven coverage on the Mylar backing. Furthermore, the non-Newtonian behaviour exhibited by the latex-cCNC blends showed shear-thinning or pseudoplastic properties. Shear-thinning behaviour implies that the viscosity of the latex decreases as the shear rate or applied stress increases, facilitating easier flow and levelling. This property is particularly advantageous for achieving a smooth and uniform coating, even on complex surfaces. Additionally, the pseudoplastic nature of the latex enables improved flow during application while maintaining higher viscosity at rest. This characteristic ensures effective adhesion to the substrate without excessive dripping or sagging. Consequently, the combination of increased viscosity and non-

Newtonian behaviour in the cCNC-blended latex contributed to improved film castability compared to the base-case latex. These rheological changes provide enhanced control over the film-forming process, enabling the production of adhesive films with superior uniformity and precise thickness control.

The storage modulus (G') and loss modulus (G'') are rheological parameters that describe the viscoelastic behaviour of a material. PSA properties are strongly dependent on their viscoelastic properties. Figure 3.3 shows the plots of G' and G'' as a function of oscillatory angular frequency (ω) for the base-case latex and latex-cCNC blends for runs 3 and 7 (Table 3.2). Runs 3 and 7 were selected because run 3 had the lowest PSA performance while run 7 had the best PSA performance (Table 3.3); recall that run 7 coincides with the optimal blend conditions. These moduli provide information about the material's ability to store and dissipate elastic energy under deformation. The viscoelastic properties of the base-case latex were compared to latex-cCNC blends under different blending conditions while maintaining the same concentration of cCNC. Despite the variations in blending conditions, such as mixing speed, temperature, or shear rate, the dominance of G' over G'' remained consistent. This suggests that the presence of cCNC significantly increased the material's elastic behaviour, reinforcing the adhesive and improving its stiffness. The cCNC particles can act as reinforcing fillers, increasing the overall stiffness and strength of the adhesive. This confirms that the latex displayed viscoelastic behaviour with a solid-like nature, regardless of the specific blending conditions. This is possible when the material contains a type of yield stress. When the stress applied in the oscillatory measurement is below the yield stress, the measured properties are that of the network, and the storage modulus is larger than the loss modulus; hence the material behaves similarly to a solid. Adding 1 phm cCNC led to an increase in both G' and G'', indicating enhanced stiffness and elastic behaviour of the latex.[58] In run 3, adding cCNC to the commercial latex resulted in a lower increase in G' compared to Run 7. The observed difference in the increase in G' between the runs is attributed to the dispersion quality of the CNC within the adhesive matrix. Run 3 used non-sonicated cCNCs and was blended at the lowest speed (250 rpm), whereas run 7 used sonicated cCNCs and was blended at the highest mixing speed (300 rpm). Achieving a uniform and well-dispersed distribution of CNC particles is crucial for maximizing their reinforcing effects and enhancing the stiffness of the adhesive.[59] These results, therefore, align with the earlier conclusions about the effect of mixing speed (and power).

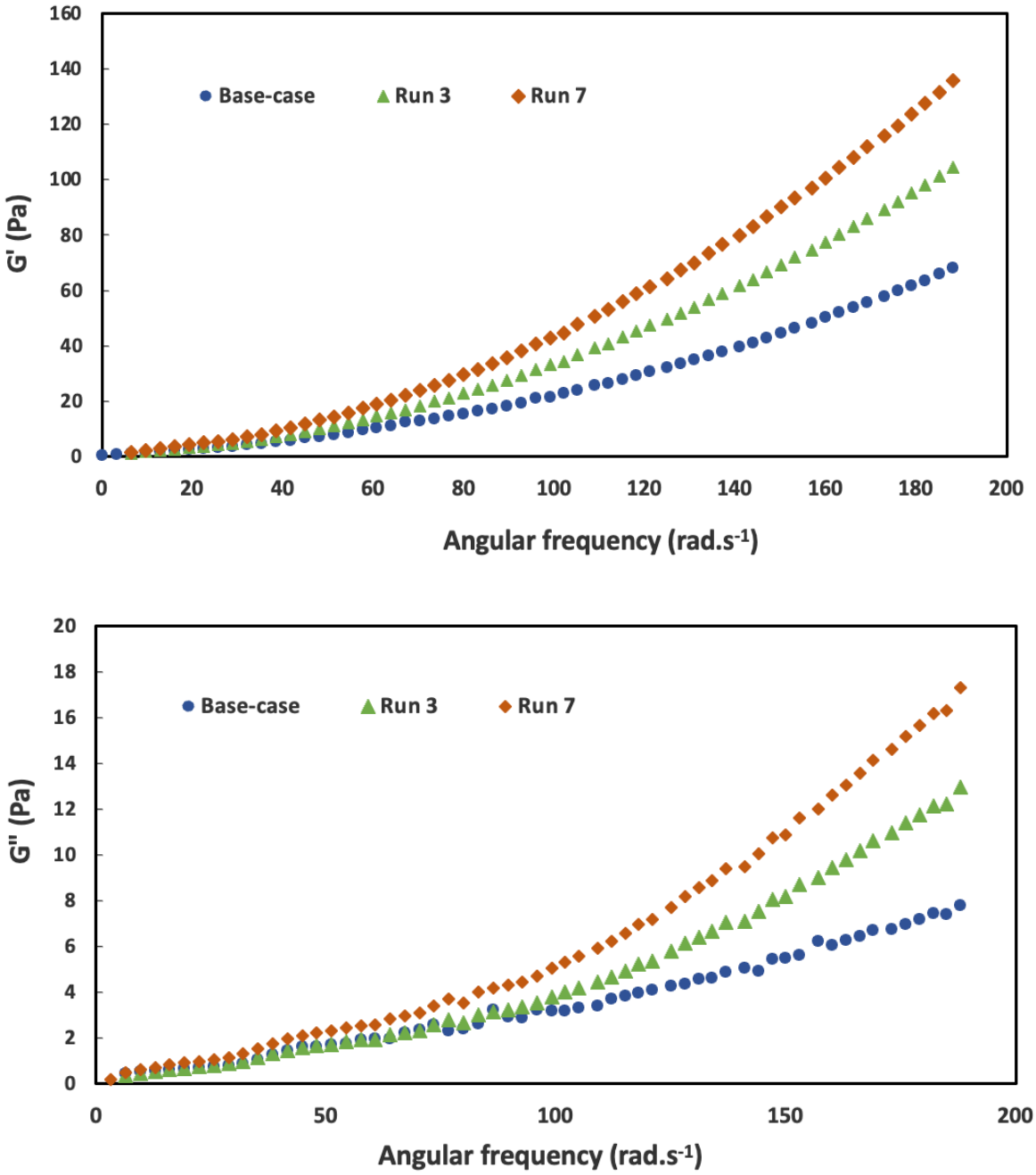

Figure 3.3. Effects of angular frequency on the storage and loss modulus of the base-case latex, run 3 and run 7. Run 3 used non-sonicated cCNCs blended at 250 rpm, whereas run 7 used sonicated cCNCs blended at 300 rpm (Table 3.2).

In addition to the rheological analysis of the wet latex, the viscoelastic behaviour of dried PSA-cCNC films was determined using DMA (Figure 3.4). The analysis was run on the base-case sample and runs 6 and 7 to compare the effect of cCNC loading on the loss and storage moduli. Adding cCNCs to the PSA films led to a notable increase in film elasticity (G'). This can be

attributed to the reduced chain mobility within the PSA matrix imposed by the presence of cCNCs. The observed increase in elasticity suggests entanglements of the polymer with the cCNCs and thus, aligns with the increased shear adhesion measured for runs 6 and 7 compared to the base-case (Table 3.3). The G″ also significantly rose with increased cCNC loading. This suggests an enhancement in the internal damping properties of the material, likely linked to the interactions between the CNCs and the polymer matrix.[45,60] Finally, G' surpassed G″, indicating that the polymer's elasticity dominated viscous flow behaviour. G' remained below 0.3 MPa for all three samples. The viscoelastic measurements viewed through the lens of the Dahlquist criterion align with the observation that the PSA–cCNC nanocomposites maintained high tack adhesion properties.[38,61]

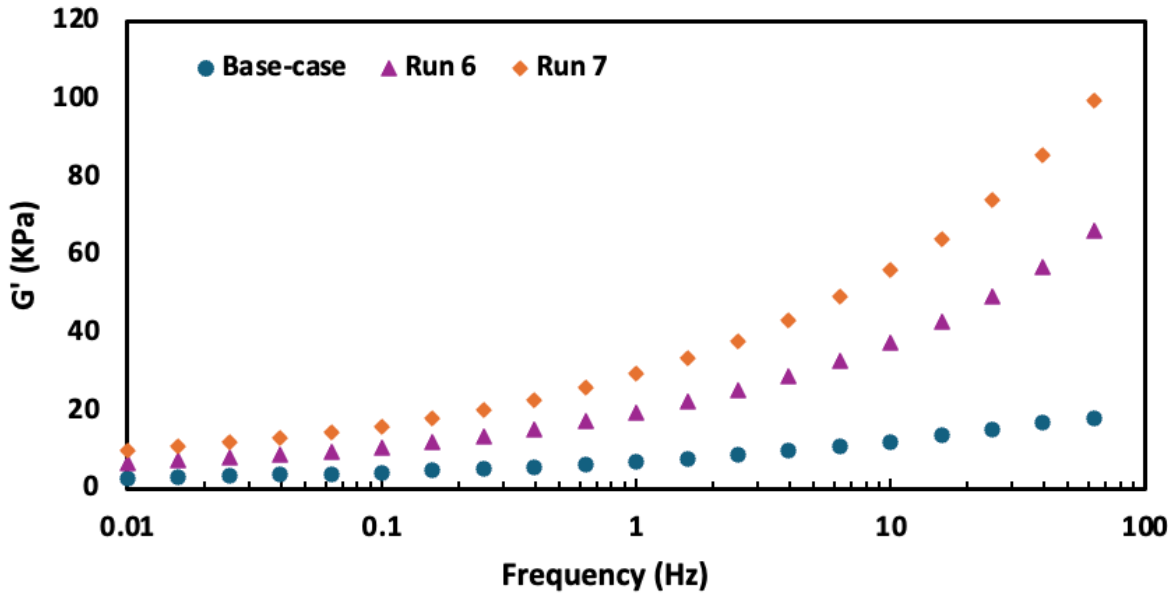

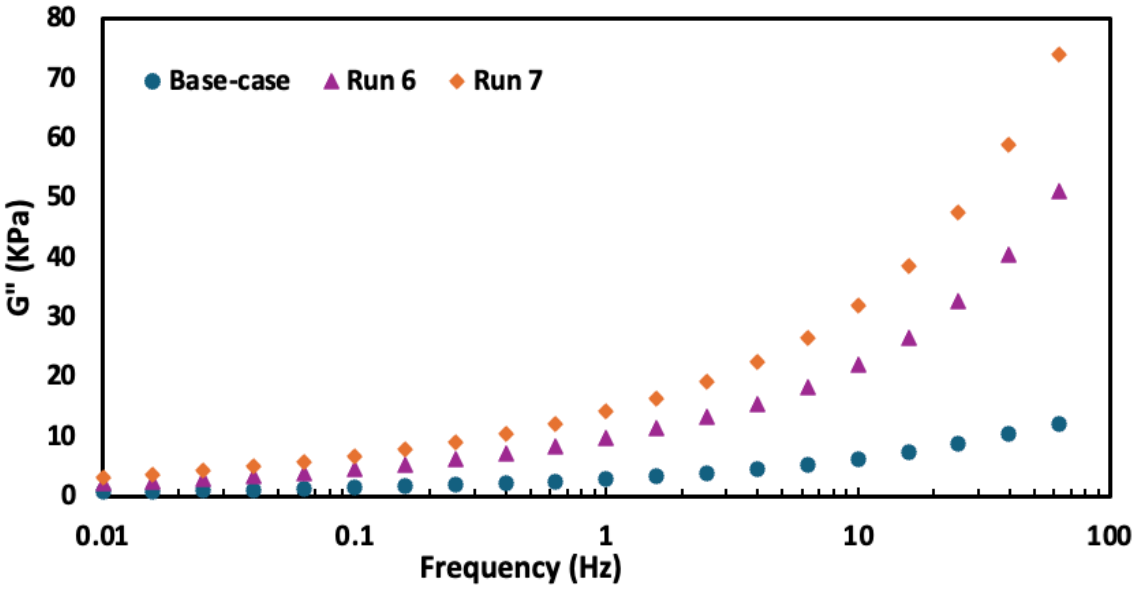

Figure 3.4. Storage and loss modulus vs. frequency for the base-case latex, run 6 and run 7 dried films. Runs 6 and 7 contained 0.5 and 1 phm cCNC, respectively (Table 3.2).

3.5 Conclusion

This investigation has shown how blending cCNCs with commercial-grade, high-quality latex improves adhesive properties. Guided by a factorial design approach, we demonstrated how adding cCNCs simultaneously improves tack, peel strength and shear adhesion. The regression analysis on the 2^{5-1} factorially-designed experiments clearly demonstrated the importance of mixing speed, or rather, power, to increase PSA performance. Additional experiments to increase the power using a homogenizer showed further improvements in shear adhesion but a decrease in tack and peel strength. Still, the tack and peel strength remained above the levels of the base-case latex. Ultimately, the homogenizer led to a substantial increase (370%) in shear adhesion compared to the base-case latex. This outcome reinforces the pivotal role of mixing speed and its influence on cohesion.

In the next step in the study, increased cCNC loading was also shown to improve all three PSA performance indicators significantly and simultaneously. For the most part, a 1 phm cCNC loading was preferred. Finally, the pronounced effect of sonication emerged as a significant facet, attributed to the discernible improvement in cCNC dispersion, a conclusion substantiated by DLS

results. This underscores the critical role of sonication in achieving uniform distribution, leading to enhanced adhesive performance.

Rheological measurements were consistent with the findings above. The blended latex-cCNC formulations showcased a shift from linear behaviour to non-Newtonian characteristics, fostering viscoelastic attributes essential for optimal adhesive performance. The heightened viscosity observed, approximately 15 times higher than that of the cCNC-free latex, improved the film casting process, enabling a degree of thickness control and more uniform coverage of the adhesive backing. Moreover, the non-Newtonian behaviour exhibited shear-thinning properties, enhancing flow and levelling during film casting.

There were several motivating factors in the pursuit of this investigation. Firstly, we sought to answer the question of whether the addition of CNCs to an already high-performing adhesive would result in performance improvements. This study unequivocally showed improved PSA performance. Secondly, there is continued interest in whether an in situ approach (i.e., adding the CNC to the latex formulation before polymerization) is better than post-polymerization blending. This study was not intending to answer that question fully, but we have laid out a protocol to at least give blending a fair evaluation. Now, armed with these results, we can proceed to improved comparisons with in situ approaches. Lastly, the practical industrial-scale application of CNCs in adhesive formulations is important. The question is: "What is feasible in an industrial setting?". Revisiting the optimal blending conditions: our analysis suggested using never-dried cCNCs at 1 phm loading using sonication to disperse the cCNCs before blending, followed by blending with the latex at room temperature at a high mixing speed. Recall that the cCNC type was not shown to be significant; thus, using a dried cCNC and re-dispersing it on-site would be a practical alternative to avoid shipping the much heavier cCNC dispersions. The use of room temperature blending would clearly not be inconvenient, and in any case, blend temperature was not a significant factor. The significance of the mixing speed (or power) points to considering what mixing equipment will be used in the industrial setting. Given the results of this investigation, mixing energy is something that can be easily addressed commercially. Finally, the use of sonication appears to be important for preparing the cCNC dispersions. Sonication is not typically welcomed in industrial processes. It is possible that one could choose not to sonicate the cCNC dispersions before blending, and while the property improvements may not be optimal, there would

still be significant PSA performance improvement. This points to our future investigations of whether an in-situ addition of cCNC might preclude the need for sonication.

3.6 References

[1] S. Ebnesajjad, *Handbook of Adhesives and Surface Preparation*, Elsevier 2011, p. 3.

[2] I. Benedek, *Pressure-Sensitive Adhesives and Applications*, 2004.

[3] S. Mapari, S. Mestry, S. T. Mhaske, *Polymer Bulletin* 2021, *78*, 4075.

[4] S. Bunker, C. Staller, N. Willenbacher, R. Wool, *Int J Adhes Adhes* 2003, *23*, 29.

[5] N. M. E. P. Chidanand Bilagi, "Pressure Sensitive Adhesives Market Statistics-2030," 2021.

[6] P. A. Lovell, F. J. Schork, *Biomacromolecules* 2020, *21*, 4396.

[7] T. D. Moshood, G. Nawanir, F. Mahmud, F. Mohamad, M. H. Ahmad, A. AbdulGhani, *Clean Eng Technol* 2022, *6*, 100404.

[8] R. Jovanović, M. A. Dubé, *Journal of Macromolecular Science, Part C: Polymer Reviews* 2004, *44*, 1.

[9] C. Creton, *MRS Bull* 2003, 434.

[10] ASTM D6195-03 (Reapproved 2011) Standard Test Methods for Loop Tack 2003.

[11] ASTM D3654-06. (Reapproved 2011) Standard Test Methods for Shear Adhesion of Pressure-Sensitive Tapes Published Online, 2006

[12] ASTM D3654-06 (Reapproved 2011) Standard Test Methods for Shear Adhesion of Pressure-Sensitive Tapes 2006.

[13] S. Ren, M. A. Dubé, *Int J Adhes Adhes* 2017, *75*, 132.

[14] J. Hamlin, M. Nuruddin, V. Tarabara, C. Szczepanski, *AIChE Journal* 2022, *68*.

[15] I. Benedek, L. J. Heymans, *Pressure-Sensitive Adhesives Technology*, Marcel Dekker Inc., New York, 1997.

[16] L. Qie, M. A. Dubé, *Macromol React Eng* 2011, *5*, 117.

[17] L. Qie, M. A. Dubé, *Eur Polym J* 2010, *46*, 1225.

[18] Y. T. Kang, K. S. Hwang, J.-B. Moon, D.-H. Kim, I. Chung, *J Adhes Sci Technol* 2015, *29*, 2345.

[19] A. Bellamine, E. Degrandi, M. Gerst, R. Stark, C. Beyers, C. Creton, *Macromol Mater Eng* 2011, *296*, 31.

[20] D. M., E. Guillaume, C. Chivas-Joly, *Properties of Nanofillers in Polymer: Nanocomposites and Polymers with Analytical Methods*, InTech 2011, p.263.

[21] N. Hamadneh, W. Khan, W. S. Khan, *Science and applications of Tailored Nanostructures Publisher* 2016.

[22] S. A. Kedzior, V. A. Gabriel, M. A. Dubé, E. D. Cranston, *Advanced Materials* 2021, *33*, 2002404.

[23] N. Yousefi, X. Lin, Q. Zheng, X. Shen, J. R. Pothnis, J. Jia, E. Zussman, J.-K. Kim, *Carbon N Y* 2013, *59*, 406.

[24] Y. Yamamoto, S. Fujii, K. Shitajima, K. Fujiwara, S. Hikasa, Y. Nakamura, *Polymer (Guildf)* 2015, *70*, 77.

[25] J. Kajtna, U. Šebenik, *Int J Adhes Adhes* 2009, *29*, 543.

[26] T. Wang, P. J. Colver, S. A. F. Bon, J. L. Keddie, *Soft Matter* 2009, *5*, 3842.

[27] T. Wang, C. -H. Lei, A. B. Dalton, C. Creton, Y. Lin, K. A. S. Fernando, Y. -P. Sun, M. Manea, J. M. Asua, J. L. Keddie, *Advanced Materials* 2006, *18*, 2730.

[28] W. Najahi-Missaoui, R. D. Arnold, B. S. Cummings, *Int J Mol Sci* 2020, *22*, 385.

[29] R. J. Moon, A. Martini, J. Nairn, J. Simonsen, J. Youngblood, *Chem Soc Rev* 2011, *40*, 3941.

[30] D. Klemm, E. D. Cranston, D. Fischer, M. Gama, S. A. Kedzior, D. Kralisch, F. Kramer, T. Kondo, T. Lindström, S. Nietzsche, K. Petzold-Welcke, F. Rauchfuß, *Materials Today* 2018, *21*, 720.

[31] V. A. Gabriel, M. N. Tousignant, S. M. W. Wilson, M. D. M. Faure, E. D. Cranston, M. F. Cunningham, B. H. Lessard, M. A. Dubé, *Macromol React Eng* 2022, *16*, 2100051.

[32] V. A. Gabriel, E. D. Cranston, M. A. Dubé, *Macromol React Eng* 2020, *14*, 2000027.

[33] A. Ouzas, E. Niinivaara, E. D. Cranston, M. A. Dubé, *Macromol React Eng* 2018, *12*, 1700068.

[34] Z. Dastjerdi, E. D. Cranston, M. A. Dubé, *Macromol React Eng* 2017, *11*, 1700013.

[35] T. C. Mokhena, M. J. John, *Cellulose* 2020, *27*, 1149.

[36] A. Ouzas, E. Niinivaara, E. D. Cranston, M. A. Dubé, *Polym Compos* 2019, *40*, 1365.

[37] A. S. Pakdel, V. Gabriel, R. M. Berry, C. Fraschini, E. D. Cranston, M. A. Dubé, *Cellulose* 2020, *27*, 10837.

[38] Z. Dastjerdi, E. D. Cranston, M. A. Dubé, *Int J Adhes Adhes* 2018, *81*, 36.

[39] G. Delepierre, O. M. Vanderfleet, E. Niinivaara, B. Zakani, E. D. Cranston, *Langmuir* 2021, *37*, 8393.

[40] M. P. Andrews, T. Morse, *Method for producing functionalized nanocrystalline cellulose and functionalized nanocrystalline cellulose thereby produced*, Published online 2017.

[41] V. A. Gabriel, P. Champagne, M. F. Cunningham, M. A. Dubé, *Can J Chem Eng* 2022, *100*, 767.

[42] S. Eyley, W. Thielemans, *Chemical Communications* 2011, *47*, 4177.

[43] M. Girard, D. Vidal, F. Bertrand, J. R. Tavares, M.-C. Heuzey, *Ultrason Sonochem* 2021, *71*, 105378.

[44] A. S. Pakdel, E. D. Cranston, M. A. Dubé, *Macromol React Eng* 2021, *15*, 2100023.

[45] A. S. Pakdel, E. Niinivaara, E. D. Cranston, R. M. Berry, M. A. Dubé, *Macromol Rapid Commun* 2021, *42*, 2000448.

[46] E. Limousin, I. Rafaniello, T. Schäfer, N. Ballard, J. M. Asua, *Langmuir* 2020, *36*, 2052.

[47] P. Hajji, J. Y. Cavaillé, V. Favier, C. Gauthier, G. Vigier, *Polym Compos* 1996, *17*, 612.

[48] B. Demirbay, *Polym Eng Sci* 2023.

[49] D. Trache, A. F. Tarchoun, M. Derradji, T. S. Hamidon, N. Masruchin, N. Brosse, M. H. Hussin, *Front Chem* 2020, *8*.

[50] S. Mondal, *Polym Plast Technol Eng* 2018, *57*, 1377.

[51] X. Yang, E. Bakaic, T. Hoare, E. D. Cranston, *Biomacromolecules* 2013, *14*, 4447.

[52] S. A. Kedzior, J. O. Zoppe, R. M. Berry, E. D. Cranston, *Curr Opin Solid State Mater Sci* 2019, *23*, 74.

[53] C. Miao, M. Zhao, W. Y. Hamad, *Colloids Surf a Physicochem Eng Asp* 2023, *675*, 131929.

[54] M. A. Johns, C. Lam, B. Zakani, L. Melo, E. R. Grant, E. D. Cranston, *Cellulose* 2023.

[55] H. J. Kim, J. H. Jeong, Y. H. Choi, Y. Eom, *Korea-Australia Rheology Journal* 2021, *33*, 165.

[56] M. R. Kamal, V. Khoshkava, *Carbohydr Polym* 2015, *123*, 105.

[57] E. Gicquel, J. Bras, C. Rey, J.-L. Putaux, F. Pignon, B. Jean, C. Martin, *Cellulose* 2019, *26*, 7619.

[58] D. Bagheriasl, P. J. Carreau, B. Riedl, C. Dubois, *Polym Compos* 2018, *39*, 2685.

[59] O. Oguz, N. Candau, A. Demongeot, M. K. Citak, F. N. Cetin, G. Stoclet, V. Michaud, Y. Z. Menceloglu, *Polym Eng Sci* 2021, *61*, 1028.

[60] E. Fortunati, F. Luzi, A. Janke, L. Häußler, J. Pionteck, J. M. Kenny, L. Torre, *Polym Eng Sci* 2017, *57*, 521.

[61] C. A. Dahlquist, "Adhesion and Cleavage Stress at Interfaces Between Solids and a Pressure-Sensitive Adhesive," *Adhesion*, ASTM International, 100 Barr Harbor Drive, PO Box C700, West Conshohocken, PA 19428-2959 1964, p. 46.

Chapter 4
Bulk Free Radical Terpolymerization of Butyl Acrylate, 2-Methylene-1,3-Dioxepane and Vinyl Acetate: Terpolymer Reactivity Ratio Estimation

Maryam Movafagh[1], Kelly M. Meek[2], Alison J. Scott[3], Alexander Penlidis[4], Marc A. Dubé[1]

[1]Department of Chemical and Biological Engineering, University of Ottawa, Ottawa, Canada
[2]Department of Chemical and Materials Engineering, Concordia University, Montreal, Canada
[3]Department of Process Engineering and Applied Science, Dalhousie University, Halifax, Canada
[4]Institute for Polymer Research (IPR), Department of Chemical Engineering, University of Waterloo, Waterloo, Canada

This chapter is a manuscript published in Polymers (2024; 16(10):133).

DOI: 10.3390/polym16101330.

4.1 Abstract

This investigation introduces the first estimation of ternary reactivity ratios for a butyl acrylate (BA), 2-methylene-1,3-dioxepane (MDO), and vinyl acetate (VAc) system at 50°C, with an aim to develop biodegradable pressure-sensitive adhesives (PSAs). In this study, we applied the Error-in-Variables Model (EVM) to estimate reactivity ratios. The ternary reactivity ratios were found to be r_{12} = 0.417, r_{21} = 0.071, r_{13} = 4.459, r_{31} = 0.198, r_{23} = 0.260, and r_{32} = 55.339 (BA/MDO/VAc 1/2/3), contrasting with their binary counterparts, which are significantly different, indicating the critical need for ternary system analysis to accurately model multicomponent polymerization systems. Through the application of a recast Alfrey-Goldfinger model, this investigation predicts the terpolymer's instantaneous and cumulative compositions at various conversion levels, based on the ternary reactivity ratios. These predictions not only provide crucial insights into the incorporation of MDO across different initial feed compositions but also offer estimates of the final terpolymer compositions and distributions, underscoring their potential in designing compostable or degradable polymers.

4.2 Introduction

Since the early 1970s, there has been a growing awareness of the environmental challenges posed by plastic disposal, prompting discussions and initiatives to find viable solutions. In recent years, this issue has gained heightened urgency, extending beyond the realm of polymer science, and becoming a topic of widespread interest and debate.[1] Polymers, regarded as a fundamental human necessity, are prized for their lightweight nature, cost-effectiveness, and stability under diverse environmental conditions.[2] Although plastics play an integral role in modern industries, the majority are petroleum-derived and non-degradable, leading to indefinite lifetimes in landfills and elsewhere.[3,4] A key objective of the sustainable polymer community is to develop feedstocks and polymeric materials from renewable resources that can be easily degraded or chemically recycled.[5,6]

A considerable portion of widely used polymers is derived from vinyl monomers, manufactured through free radical polymerization or other methods.[7,8] However, they often result in polymers with entirely carbon-based backbones, impeding efforts towards facile degradation. Radical ring-opening polymerization (rROP) has emerged as a valuable strategy, leveraging radical chemistry to induce the opening of cyclic monomers, thereby facilitating the introduction of degradable linkages into polymer backbones.[9,10] When combined with the radical polymerization of common olefinic comonomers, rROP permits the integration of degradable linkages into carbon-carbon backbones that would otherwise be nondegradable. The application of rROP copolymerization has predominantly centered around cyclic ketene acetals (CKAs).[11–14] with vinyl monomers.

The free radical polymerization of 2-methylene-1,3-dioxepane (MDO), a seven-membered CKA, enables the quantitative opening of its ring to yield an aliphatic polyester resembling poly(3-caprolactone) (PCL),[15,16] traditionally synthesized through metal-catalyzed ring-opening polymerization (ROP). Distinctions between PCL obtained via radical initiation and metal catalyst systems manifest in branching, crystallinity, and mechanical properties. Notably, the seven-membered CKAs exhibit greater steric hindrance of the non-ring-opened radicals and enhanced stability of the ring-opened radicals, collectively promoting a predominantly ring-opened structure in the final polymer. MDO can also be considered as a bio-sourced monomer as it is produced from diols such as 1,4-butanediol and diethylene glycol, which are themselves bio-sourced.[17]

Copolymerization stands as a pivotal process in tailoring the properties of polymer products, allowing for a meticulous adjustment of material characteristics through the manipulation of comonomer types and their incorporation in the resulting copolymer chains. The resulting tailored materials find applications in specific contexts, with the copolymer's composition, composition distribution, molecular weight, and molecular weight distribution playing crucial roles in defining its properties.[18] When aiming to create (bio)degradable copolymers, it becomes imperative not only to incorporate sufficient degradable chemical linkages to produce short oligomers after degradation but also to ensure their regular distribution within and across chains.[18–20] Addressing the challenge of incorporating MDO units in acrylate-based polymers,[20,21] specifically focusing on achieving a uniform distribution, a proposed solution entails estimating the reactivity ratios of the monomer system before initiating deeper studies in copolymerization and copolymer properties.

Reactivity ratios play a pivotal role in the kinetics of multicomponent polymerization systems. Despite the widespread use of terpolymerization in both industrial and academic settings, there remains a notable lack of studies dedicated to estimating reactivity ratios for such intricate systems. To effectively control copolymer or terpolymer composition, key parameters such as copolymer reactivity ratios (r_{ij}) come into play. These ratios, expressing the ratio of the propagation rate constant of homopropagation to that of cross-propagation, allow predictions of polymerization rate, composition, sequence length, molecular weight, and, consequently, the performance characteristics of the final product. The Mayo–Lewis equation serves as a tool to calculate instantaneous polymer composition using these reactivity ratios.[22] A commonly accepted analogy exists between copolymerization and terpolymerization mechanisms, enabling researchers to apply reactivity ratios derived from binary pairs (obtained through copolymerization experiments) in models addressing terpolymerizations. Nevertheless, the direct application of binary reactivity ratios to terpolymerization systems is not universally applicable. Utilizing the binary-ternary analogy, even as an approximation, necessitates making significant assumptions about the system. When binary reactivity ratios are employed to characterize ternary systems, the potential outcomes encompass suboptimal performance in predicting terpolymer composition (not to mention molecular weight, polymerization rate, etc.), and inaccuracies in determining the characteristics of the resulting terpolymer product. In previous studies, the suggestion emerged that the direct estimation of ternary reactivity ratios from terpolymer composition data is preferable over the use

of binary copolymer reactivity ratios.[23,24] Discrepancies in the prediction of terpolymer composition using binary reactivity ratios have been noted and are due to the presence of the third monomer [23] (More explanations on this are given later, below Equation 4.17.).

In this study, we focus on pressure-sensitive adhesives (PSAs), a class of polymers that exhibit adhesive properties with minimal pressure application. These adhesives form bonds upon contact with a surface and are extensively employed in applications where material adhesion and residue-free removal are paramount. The adhesive's ability to balance elasticity and strength depends on factors such as the polymer's glass transition temperature (T_g). The T_g characterizes the transition from a glassy ('hard', 'solid-like') to a 'liquid-like' (rubbery, flexible) state and is a critical determinant of adhesive performance. Achieving the desired T_g, often below the application temperature, necessitates a precise combination of monomers with varying T_g values.[25] Monomers such as n-butyl acrylate (BA), 2-ethylhexyl acrylate (EHA), and methyl methacrylate (MMA) are frequently employed in PSA formulations (with homopolymer T_g values of −54, −50, and 105°C, respectively). Consequently, adhesive properties can be precisely controlled by manipulating the polymer composition through the combination of low T_g monomers (i.e., BA and EHA) with the higher T_g monomer (i.e., MMA).[26]

In this study, vinyl acetate (VAc) was chosen as the high T_g monomer due to its well-documented favorable reactivity ratios with MDO, leading to random copolymerization, high conversion, and the generation of the ring-opened (ester) form of MDO.[20,27–31] Furthermore, for PSA applications, we specifically chose BA as the low T_g monomer, as previously mentioned. MDO is a bio-sourced monomer, and it should be noted that while BA and VAc utilized in this study are petroleum-based, they can also be bio-sourced.[32–34] This work introduces an estimation of bulk terpolymer reactivity ratios for BA/MDO/VAc at 50°C. To our knowledge, this investigation represents the first attempt to estimate ternary reactivity ratios for the BA/MDO/VAc system.

4.3 Materials and methods

4.3.1 Materials

n-BA (≥ 99% purity), VAc (≥ 99% purity) and azobisisobutyronitrile (AIBN, 98% purity) were purchased from Sigma Aldrich. MDO was obtained from Wacker Chemie (München,

Germany) and was used as received. Deuterated chloroform (Fisher, 99.8%) was used for characterization. Reagent grade solvents (Fisher) for sample workup (e.g., acetone, methanol) were used as packaged. BA and VAc monomers underwent a rigorous purification process, passing through inhibitor removal columns acquired from Sigma Aldrich. This process effectively eliminated any traces of inhibitors, such as hydroquinone or monomethyl ether hydroquinone.

4.3.2 Experimental method

The experimental setup included terpolymerizations of BA/MDO/VAc conducted in glass ampoules at a constant temperature of 50°C. Three separate monomer compositions were used: ~80/10/10, 10/80/10 and 10/10/80 (w/w/w) BA/MDO/VAc. Approximately 5 grams of each monomer mixture, containing 0.1 wt.% AIBN, were carefully transferred into glass ampoules with dimensions of 150-180 mm in length, a tube diameter of 10 mm, thickness of ~1 mm, and a volume of approximately 12 mL.

The reaction mixtures underwent degassing through three or more cycles of a freeze-pump-thaw procedure. Subsequently, the ampoules were flame-sealed and then immersed in a temperature-controlled water bath maintained at 50°C. The ampoules were removed from the water bath at various times to ensure a range of conversions. The reactions were terminated by quenching the ampoules in an ice bath. All the samples were characterized for conversion using standard gravimetric techniques. After adequate cooling, the ampoules and their contents were weighed, and the contents were poured into pre-weighed dishes containing acetone. The monomer was soluble in acetone, whereas the polymer precipitated. The monomer-acetone-polymer mixtures were allowed to soak for 12 hours and subsequently agitated in a wrist-action shaker for 30 minutes. The liquid was decanted, and the resulting polymers were left to dry in a vacuum oven at 50°C overnight. For higher conversion (solid) samples, a freezing and breaking method was employed to extract the samples. Each ampoule was submerged in liquid nitrogen to rapidly freeze its contents. Once frozen, the ampoules were cautiously removed from the liquid nitrogen and safely fractured, granting access to the polymer samples contained within. Each sample was placed in toluene until fully dissolved, followed by the addition of methanol to induce polymer precipitation. The resulting solvent mixture was decanted, and the polymer samples were dried as above. For all samples, the dried polymers were weighed to calculate the conversion. Each dried sample was analyzed for composition using ^{1}H-NMR spectroscopy.

4.3.3 Characterization

^{1}H-NMR peak assignments were established with references to copolymers of BA/VAc,[35] VAc/MDO,[36] and BA/MDO.[18] To enhance precision in the ^{1}H-NMR peak assignments for the BA/MDO/VAc terpolymer, poly(MDO) and BA/VAc copolymers were synthesized. Subsequently, these polymers were characterized using ^{1}H-NMR spectroscopy.

As previously mentioned, gravimetry was used to determine the monomer conversion based on the weight of the dry polymer relative to the weight of the starting reaction mixture. A Bruker 400 MHz ^{1}H-NMR spectrometer was used to measure the compositions of the terpolymer. Samples were dissolved in deuterated chloroform ($CDCl_3$) at a ratio of 0.02 g polymer to 1.5 g solvent. The spectrometer was configured for 1D analysis, generating 32 scans per minute. Figure 4.1 depicts ^{1}H-NMR spectra for a typical BA/MDO/VAc terpolymer, along with peak assignments. The BA/MDO/VAc terpolymer compositions were calculated using:

$$A_1 = z \tag{4.1}$$

$$A_2 = 2x + 2y \tag{4.2}$$

$$A_3 = 7x + 8y + 5z \tag{4.3}$$

$$A_4 = 3x \tag{4.4}$$

$$F_{BA} = x / (x + y + z) \tag{4.5}$$

$$F_{MDO} = y / (x + y + z) \tag{4.6}$$

$$F_{VAc} = z / (x + y + z) \tag{4.7}$$

Where x, y and z relate to the BA, MDO and VAc protons, respectively, found in areas A_1, A_2, A_3 and A_4. Area A_1 represents the −CH protons of VAc (“m” in Figure 4.1) ($\delta = 4.7 – 4.9$ ppm), A_2 represents the $-CH_2O$ protons of BA and MDO (“c” and “h” in Figure 4.1) ($\delta = 3.1 – 4.2$ ppm), area A_4 represents the $-CH_3$ of BA (“f” in Figure 4.1) ($\delta = 0.7 – 1$ ppm), whereas area A_3 represents the remaining 20 protons of BA, MDO and VAc ($\delta = 1.1 – 2.9$ ppm). After solving for x, y, and z (Equations 4.1, 4.2, 4.3, and 4.4), the terpolymer composition was calculated using Equations 4.5, 4.6, and 4.7. This composition analysis was conducted for all the BA/MDO/VAc terpolymers.

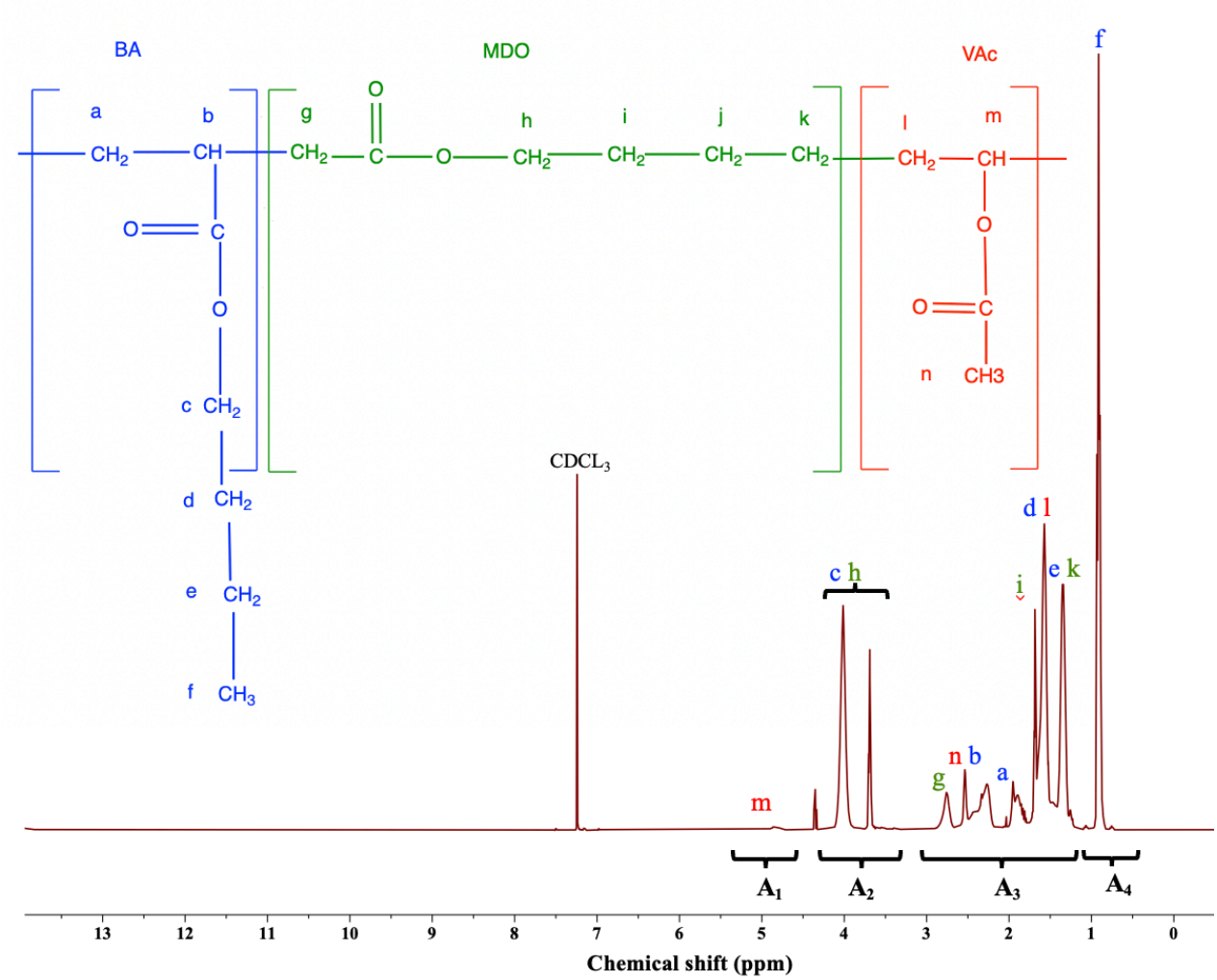

Figure 4.1. [1]H-NMR spectrum of a BA/MDO/VAc terpolymer with the feed composition of ~ 84/9/7 (mol%/mol%/mol%), respectively, at 82 wt.% conversion (F_{BA} = 74 mol%, F_{MDO} 20mol%, F_{VAc} = 6 mol%).

4.3.4 Reactivity ratio estimation in terpolymerization

Terpolymerization systems, which involve the polymerization of three different monomers, indeed present a complex and rich area for research in polymer science. These systems are more complex than copolymerization, where only two monomers are involved, due to the larger number of possible interactions and resulting polymer structures. The increased complexity in terpolymerization arises from the various combinations in which the monomers can react, leading to a wide variety of polymer properties and applications.

The kinetics of terpolymerization systems, as first described by Alfrey and Goldfinger,[37] consider the various possible interactions between the monomers. In a terpolymerization system, three different monomers can act as the terminal monomer on the growing polymer chain (Reaction scheme 4.1). Thus, the growing polymer radical chain ending in monomer *i* (designated as $\sim\sim M_i^{\cdot}$) can react with any of the three monomers (M_i) in the reaction mixture, leading to nine different propagation reaction (k_{ij}) steps according to the terminal model:[37]

$$\begin{aligned}
\sim\sim\sim M_1^{\cdot} + M_1 &\xrightarrow{k_{11}} \sim\sim\sim M_1 - M_1 \\
\sim\sim\sim M_1^{\cdot} + M_2 &\xrightarrow{k_{12}} \sim\sim\sim M_1 - M_2 \\
\sim\sim\sim M_1^{\cdot} + M_3 &\xrightarrow{k_{13}} \sim\sim\sim M_1 - M_3 \\
\sim\sim\sim M_2^{\cdot} + M_1 &\xrightarrow{k_{21}} \sim\sim\sim M_2 - M_1 \\
\sim\sim\sim M_2^{\cdot} + M_2 &\xrightarrow{k_{22}} \sim\sim\sim M_2 - M_2 \\
\sim\sim\sim M_2^{\cdot} + M_3 &\xrightarrow{k_{23}} \sim\sim\sim M_2 - M_3 \\
\sim\sim\sim M_3^{\cdot} + M_1 &\xrightarrow{k_{31}} \sim\sim\sim M_3 - M_1 \\
\sim\sim\sim M_3^{\cdot} + M_2 &\xrightarrow{k_{32}} \sim\sim\sim M_3 - M_2 \\
\sim\sim\sim M_3^{\cdot} + M_3 &\xrightarrow{k_{33}} \sim\sim\sim M_3 - M_3
\end{aligned}$$

Reaction scheme 4.1: Terminal model for terpolymer propagation reactions.

The propagation rate parameters, k_{ij}, represent the rate of addition of monomer *j* to a growing radical chain ending in monomer *i*. To predict the terpolymer composition, one uses the reactivity ratios, denoted as $r_{ij} = \frac{k_{ii}}{k_{ij}}$, which indicates the propensity of a monomer to homopropagate (k_{ii}), rather than cross-propagate (k_{ij}). Thus, for a terpolymer system, six reactivity ratios can be defined:[24,37]

$$\begin{aligned}
r_{12} &= \frac{k_{11}}{k_{12}} \qquad r_{13} = \frac{k_{11}}{k_{13}} \qquad r_{23} = \frac{k_{22}}{k_{23}} \\
r_{21} &= \frac{k_{22}}{k_{21}} \qquad r_{31} = \frac{k_{33}}{k_{31}} \qquad r_{32} = \frac{k_{33}}{k_{32}}
\end{aligned} \tag{4.8}$$

The Alfrey–Goldfinger (AG) equations conventionally employ ratios of the instantaneous mole fractions within the terpolymer as the response variables (note: by instantaneous we mean the terpolymer composition of the polymer chains generated at a single moment, as opposed to the cumulative composition, which is what is measured via ^{1}H-NMR spectroscopy). However, in practice, experimental data often consist of individual mole fractions rather than their ratios. This leads to a loss of information (when using ratios) and alters the error structure when applying these ratios directly to experimental findings.[24] To address these limitations, the AG model was re-derived to allow each terpolymer mole fraction to be presented as a single response.[24] This re-derivation aligns with the need for a more accurate and practical approach to model terpolymerization kinetics, as it preserves the integrity of the experimental data and facilitates a more straightforward interpretation of results. The revised equations (Equations 4.9–4.11) are designed to provide a more accurate representation of the terpolymer composition without the complications introduced by using ratio-based responses.[24] Therein, F_i represents the instantaneous mole fraction of monomer i bound in the terpolymer, f_i represents the mole fraction of unreacted monomer i in the polymerizing mixture, and the reactivity ratios (r_{ij}) from Equation 4.8 are included.

$$F_1 - \frac{f_1\left(\frac{f_1}{r_{21}r_{31}}+\frac{f_2}{r_{21}r_{32}}+\frac{f_3}{r_{31}r_{23}}\right)\left(f_1+\frac{f_2}{r_{12}}+\frac{f_3}{r_{13}}\right)}{\left(\begin{array}{l} f_1\left(\frac{f_1}{r_{21}r_{31}}+\frac{f_2}{r_{21}r_{32}}+\frac{f_3}{r_{31}r_{23}}\right)\left(f_1+\frac{f_2}{r_{12}}+\frac{f_3}{r_{13}}\right) \\ +f_2\left(\frac{f_1}{r_{12}r_{31}}+\frac{f_2}{r_{12}r_{32}}+\frac{f_3}{r_{13}r_{32}}\right)\left(f_2+\frac{f_1}{r_{21}}+\frac{f_3}{r_{23}}\right) \\ +f_3\left(\frac{f_1}{r_{13}r_{21}}+\frac{f_2}{r_{23}r_{12}}+\frac{f_3}{r_{13}r_{23}}\right)\left(f_3+\frac{f_1}{r_{31}}+\frac{f_2}{r_{32}}\right) \end{array}\right)} = 0 \tag{4.9}$$

$$F_2 - \frac{f_2\left(\frac{f_1}{r_{12}r_{31}}+\frac{f_2}{r_{12}r_{32}}+\frac{f_3}{r_{13}r_{32}}\right)\left(f_2+\frac{f_1}{r_{21}}+\frac{f_3}{r_{23}}\right)}{\left(\begin{array}{l} f_1\left(\frac{f_1}{r_{21}r_{31}}+\frac{f_2}{r_{21}r_{32}}+\frac{f_3}{r_{31}r_{23}}\right)\left(f_1+\frac{f_2}{r_{12}}+\frac{f_3}{r_{13}}\right) \\ +f_2\left(\frac{f_1}{r_{12}r_{31}}+\frac{f_2}{r_{12}r_{32}}+\frac{f_3}{r_{13}r_{32}}\right)\left(f_2+\frac{f_1}{r_{21}}+\frac{f_3}{r_{23}}\right) \\ +f_3\left(\frac{f_1}{r_{13}r_{21}}+\frac{f_2}{r_{23}r_{12}}+\frac{f_3}{r_{13}r_{23}}\right)\left(f_3+\frac{f_1}{r_{31}}+\frac{f_2}{r_{32}}\right) \end{array}\right)} = 0 \tag{4.10}$$

$$F_3 - \frac{f_3\left(\frac{f_1}{r_{13}r_{21}}+\frac{f_2}{r_{23}r_{12}}+\frac{f_3}{r_{13}r_{23}}\right)\left(f_3+\frac{f_1}{r_{31}}+\frac{f_2}{r_{32}}\right)}{\left(\begin{array}{l} f_1\left(\frac{f_1}{r_{21}r_{31}}+\frac{f_2}{r_{21}r_{32}}+\frac{f_3}{r_{31}r_{23}}\right)\left(f_1+\frac{f_2}{r_{12}}+\frac{f_3}{r_{13}}\right) \\ +f_2\left(\frac{f_1}{r_{12}r_{31}}+\frac{f_2}{r_{12}r_{32}}+\frac{f_3}{r_{13}r_{32}}\right)\left(f_2+\frac{f_1}{r_{21}}+\frac{f_3}{r_{23}}\right) \\ +f_3\left(\frac{f_1}{r_{13}r_{21}}+\frac{f_2}{r_{23}r_{12}}+\frac{f_3}{r_{13}r_{23}}\right)\left(f_3+\frac{f_1}{r_{31}}+\frac{f_2}{r_{32}}\right) \end{array}\right)} = 0 \tag{4.11}$$

These equations were developed strictly for instantaneous composition measures. By utilizing data from low conversion processes, one assumes that changes in the composition of the terpolymer over time are minimal, meaning the overall cumulative composition measured can be closely equated to its instantaneous state at low conversions. Nonetheless, this limiting condition leads to potential errors for fast polymerizations and from composition drift from systems with widely differing reactivity ratios (e.g., BA/VAc [38]).

To address these challenges, a cumulative ternary composition model that considers the full conversion trajectory of the polymerization process was introduced.[39] This model, detailed in Equations 4.12–4.14, connects the cumulative composition of each comonomer in the terpolymer ($\overline{F_i}$) with the initial feed's monomer mole fraction ($f_{i,0}$), the mole fraction of unreacted monomer within the polymerizing mixture (f_i), and the total molar conversion (X_n).[39]

$$\overline{F_1} = \frac{f_{1,0} - f_1(1-X_n)}{X_n} \tag{4.12}$$

$$\overline{F_2} = \frac{f_{2,0} - f_2(1-X_n)}{X_n} \tag{4.13}$$

$$\overline{F_3} = \frac{f_{3,0} - f_3(1-X_n)}{X_n} \tag{4.14}$$

When a constant composition cannot be presumed, i.e., when composition drift becomes significant, f_i needs to be assessed with respect to the conversion trajectory, as depicted in Eqs. (15)–(17).

$$\frac{df_1}{dX_n} = \frac{f_1 - F_1}{1-X_n} \tag{4.15}$$

$$\frac{df_2}{dX_n} = \frac{f_2 - F_2}{1-X_n} \tag{4.16}$$

$$\frac{df_3}{dX_n} = \frac{f_3 - F_3}{1-X_n} \tag{4.17}$$

This approach allows for a more accurate accounting of composition changes over time, particularly in systems where composition drift cannot be ignored.[23] The complexity of terpolymerization is underscored by the fact that the ternary reactivity ratios are not independent of each other and must be estimated simultaneously from the terpolymerization data, as their values can influence one another. For instance, despite the reactivity ratio between comonomers 1 and 2, $r_{12} = \frac{k_{11}}{k_{12}}$, which primarily reflects the propagation relation between comonomers 1 and 2, the presence of monomer 3 in the polymerization mixture can still exert an influence on it. Unlike copolymer systems, which involve two monomers, the addition of a third monomer can affect the polymerization behaviour and the incorporation rates of all three monomers. Therefore, it is crucial to study and model terpolymerization processes on their own terms, rather than trying to extrapolate from simpler copolymer systems.[39] That way one also avoids error propagation via binary copolymer reactivity ratios into the terpolymer composition. From a parameter estimation point of view, one obtains much richer information content due to the inclusion of conversion and cumulative terpolymer composition data. Last but not least, properly estimating binary copolymer reactivity ratios would require a minimum of twelve copolymerizations (with appropriate replication, which is often ignored), compared to only three terpolymerization runs, as long as the terpolymerization feed fractions are optimally located (hence, even with full independent replication, which is a very good feature to have, the number of trials is reduced by 50%).

Challenges associated with reactivity ratio estimation and experimental design in copolymer and terpolymer systems have largely been addressed through the implementation of the error-in-variables model (EVM), extensively discussed by Kazemi et al. .[24] The EVM technique stands out as a robust non-linear regression approach, encompassing all sources of experimental error in both the independent and dependent variables[22,23,40] When utilizing EVM, the experimenter must carefully account for all sources of error, and the EVM procedure yields estimates of the true values of the independent variables within the model, alongside parameter estimates.[23] An additional advantage of employing EVM lies in its compatibility with the cumulative composition model for medium-high conversion data in terpolymer systems. This alternative offers several advantages over the standard instantaneous model, particularly in eliminating the assumption of negligible composition drift (required for the instantaneous model) and retaining more information content, i.e., more data points across the conversion trajectory, from a single experiment. Consequently, EVM emerges as the most statistically sound and

comprehensive approach for reactivity ratio estimation [41]. The versatility of the EVM algorithm extends to its direct application to terpolymerization data, obviating the need for relying on binary reactivity ratios in ternary systems. Detailed procedures for this application have been previously clarified by Kazemi et al.[24] The Direct Numerical Integration (DNI) method described therein can be applied to the ternary cumulative composition model, enabling the use of data up to medium-high conversion levels.

4.4 Results and Discussion

This investigation utilized the EVM method to determine the reactivity ratios for BA/MDO/VAc terpolymerization (BA/MDO/VAc 1/2/3). Using a MATLAB-based EVM program [22,24], we analyzed the data, which included monomer feed composition (the manipulated variable), conversion (measured by gravimetry), and cumulative copolymer composition (measured by ^{1}H-NMR spectroscopy). Table 4.1 shows the ternary reactivity ratios along with the copolymer reactivity ratios used as starting values in the EVM procedure (and related computer program). The quality of the ternary reactivity ratio estimates was supported by clearly defined joint confidence regions (JCRs), shown in Figure 4.2. A direct comparison between the binary reactivity ratios, reported from three separate copolymer data sets in the literature, and the ternary reactivity ratios, obtained from a singular experimental data set, highlights substantial disparities (Table 4.1).

Table 4.1. Binary reactivity ratios (from literature) and ternary reactivity ratio estimates (BA/MDO/VAc designated as monomers 1/2/3).

Reactivity ratios	r_{12}	r_{21}	r_{13}	r_{31}	r_{23}	r_{32}
Binary[18,38]	1.761	0.044	5.938	0.026	0.950	1.710
Ternary	0.417	0.071	4.459	0.198	0.260	55.339

Figure 4.2 presents the ternary reactivity ratio point estimates within their 95% JCRs derived for each monomer pair. The JCRs serve as a quantitative measure of the uncertainty associated with the point estimates, offering insight into their reliability. The area encompassed by a JCR is inversely related to the precision of the corresponding point estimate: a smaller JCR area signifies lower variance and, consequently, higher reliability of the estimates. Based on our analysis, two interesting remarks can be made from the outset. First, the three JCRs of Figure 4.2

do not encompass the estimates from the binary reactivity ratios (this will be discussed further below). Secondly, almost all JCRs are parallel to one of the axes, thus indicating minimum covariance (correlation) between the respective parameters, which is a good feature, offering more confidence in the design of experiments.

a)

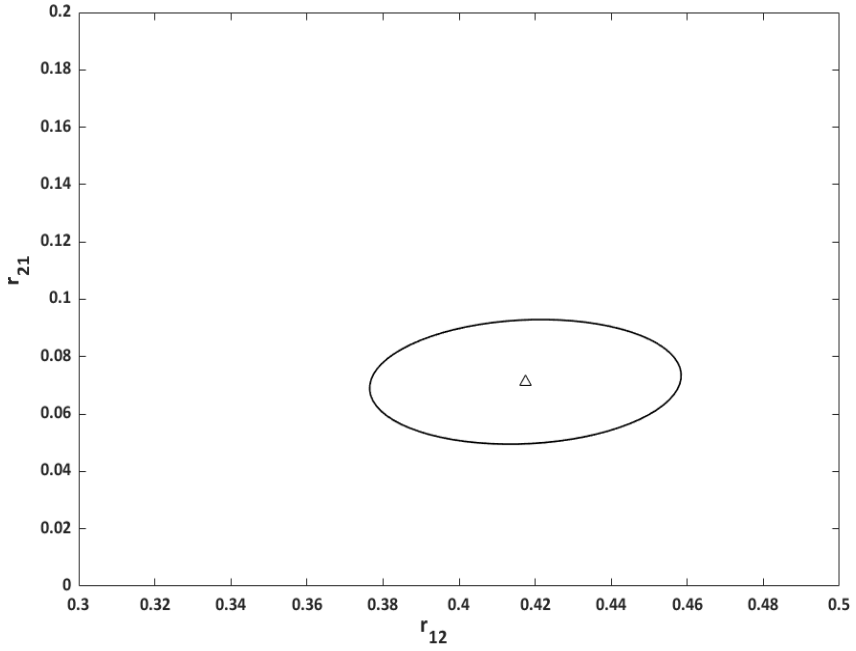

b)

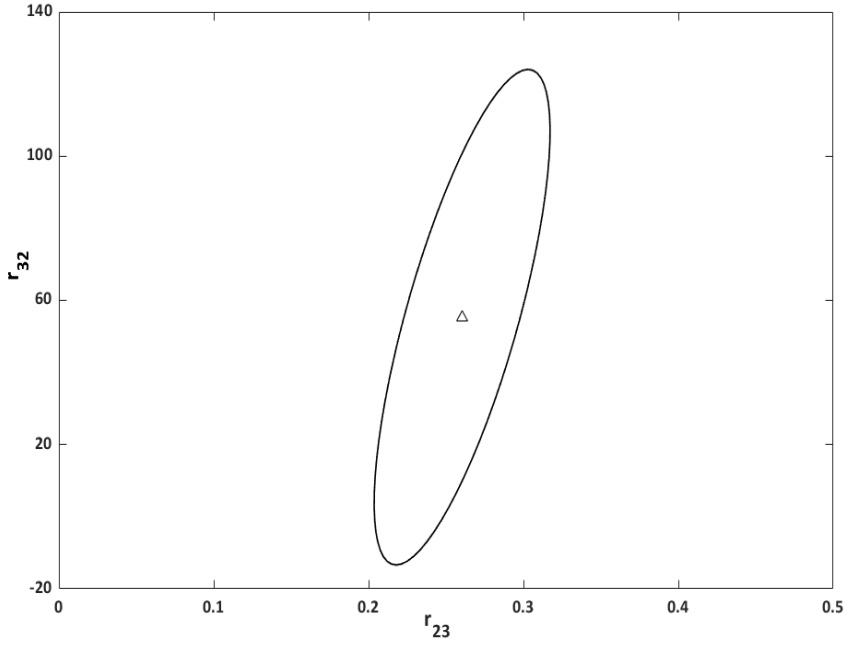

c)

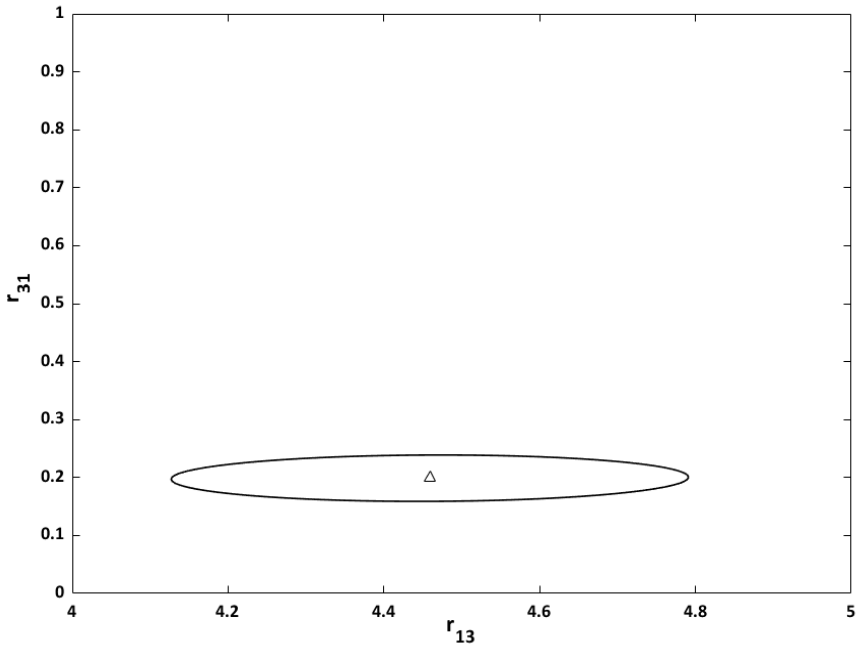

Figure 4.2. 95% Joint Confidence Regions (JCRs) of the BA/MDO/VAc ternary reactivity ratio estimates (BA/MDO/VAc designated as monomers 1/2/3). Thus, Figure 4.2a represents the BA/MDO reactivity ratios, Figure 4.2b shows the MDO/VAc reactivity ratios, and Figure 4.2c the BA/VAc reactivity ratios. JCRs are shown as lines, whereas point estimates as triangles.

For the BA/MDO pair (Figure 4.2a), the reactivity ratio point estimates $r_{12} = 0.417$ and $r_{21} = 0.071$ are both below 1, indicating that both BA and MDO tend to cross-propagate rather than homopolymerize. In other words, a BA-ended radical will more likely add MDO monomer than BA monomer. This tendency is much higher, however, for the MDO-ended radicals signifying that the generation of uninterrupted series of MDO units in a chain is highly unlikely. The JCR in Figure 4.2a, shows a relatively equal degree of low uncertainty in each of the reactivity ratios. For the BA/VAc pair (Figure 4.2c), the reactivity ratio point estimates of $r_{13} = 4.459$ and $r_{31} = 0.198$ indicate the propensity of both BA- and VAc-ended radicals to add BA monomer rather than VAc monomer. This suggests a tendency to generate relatively longer series of BA units in the terpolymer, i.e., BA "blockiness". As was the case in Figure 4.2a, the JCR in Figure 4.2c shows again a relatively equal degree of low uncertainty in each of the reactivity ratios. Finally, for the MDO/VAc pair (Figure 4.2b), the reactivity ratio point estimates of $r_{23} = 0.260$ and $r_{32} = 55.339$ indicated the strong tendency for both MDO- and VAc-ended radicals to add VAc monomer rather than MDO monomer. While these reactivity ratios suggest that long sequences of VAc monomer

units in the polymer chains would be likely, one cannot take these reactivity ratios in isolation from those of the other pairs. In other words, the presence of BA in the system and the BA/VAc reactivity ratios indicate the low likelihood of a series of VAc monomer units in the polymer chain. The JCR in Figure 4.2b shows a much higher uncertainty in r_{32} with relatively higher confidence in r_{23}.

In Figure 4.3, the agreement between the experimental data and the model predictions for the cumulative and instantaneous compositions of BA/MDO/VAc terpolymerizations using the ternary reactivity ratios is shown for the three compositions studied. Overall, the experimental data align well with the model predictions for cumulative compositions. Arguably, the predictions for the BA/MDO/VAc = 84/9/7 molar feed composition (Figure 4.3a) for BA and MDO are not perfect. The same holds for some of the low conversion data for BA and VAc for the BA/MDO/VAc = 14/12/74 molar feed composition (Figure 4.3c). However, these predictions are vastly better than those using the copolymer reactivity ratios (Figure 4.4). In general, the ternary composition predictions are consistent with the measured cumulative terpolymer compositions.

a)

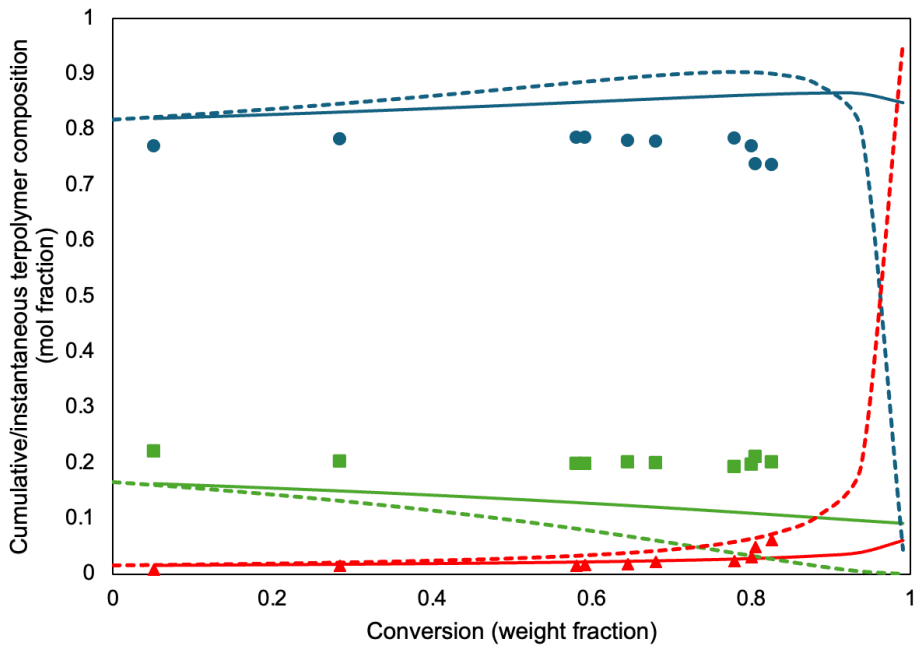

b)

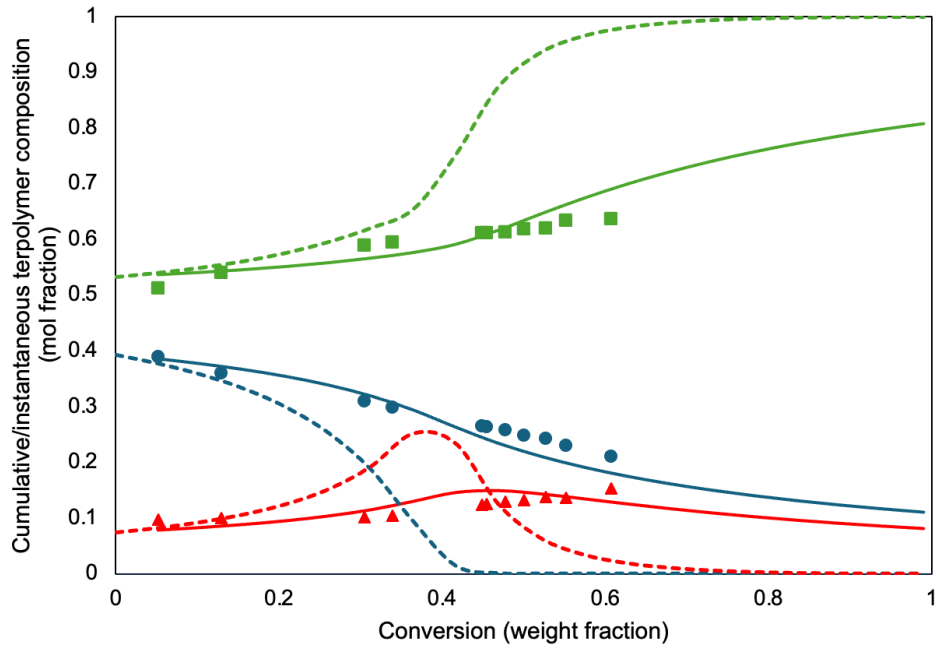

c)

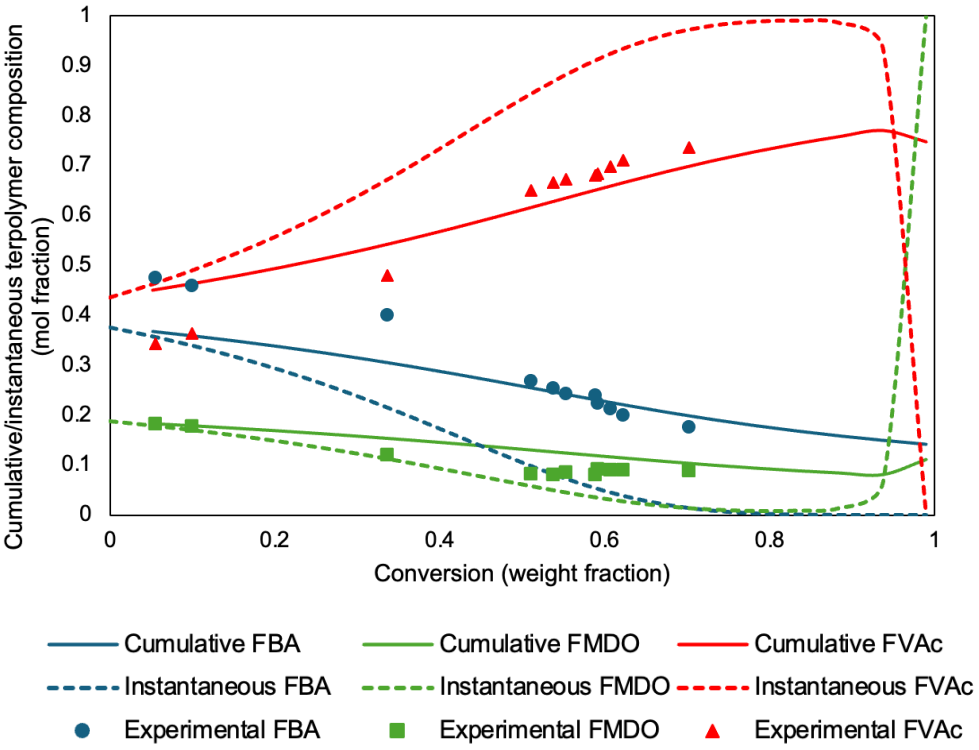

Figure 4.3. Comparison of model predictions of cumulative and instantaneous terpolymer compositions using ternary reactivity ratios and experimental data for BA/MDO/VAc terpolymerizations at various feed compositions (BA/MDO/VAc (mol%/mol%/mol%) a) 84/9/7, b) 11/81/8, and c) 14/12/74). Experimental data are shown as symbols for BA (blue circles), MDO (green squares) and VAc (red triangles), colors of dashed and solid lines correspond to the same monomers.

Recall that the motivation for this study was to produce adhesives with a reasonable distribution of MDO to ensure better degradability (or compostability). This compels us to consider how the instantaneous terpolymer composition behaves. The instantaneous terpolymer compositions shown in Figure 4.3 (an added benefit from mathematical modelling) all suggest significant composition drift for the BA/MDO/VAc system, particularly at higher conversions in Figure 4.3a, but even at fairly low conversions in Figures 4.3b and 4.3c. Thus, the composition drift was most notable for the MDO- and VAc-rich systems. For example, the significant composition drift in the MDO-rich system (Figure 4.3b), as noted through the instantaneous composition, shows that the production of polymer chains beyond 70% conversion would be dominated by MDO. The VAc-rich system (Figure 4.3c) exhibits a temporary halt in MDO incorporation between 75 and 85% conversion, followed by a resumed increase in MDO incorporation into the polymer. These two cases contrast with the BA-rich system (Figure 4.3a), where MDO continues to be incorporated into the polymer up to 95% conversion, suggesting a more uniform distribution of MDO throughout the polymerization process. In terms of compostability or degradability, one desires a uniform distribution of MDO and thus, the terpolymer composition in Figure 4.3a would be desirable.

The question remains: how much MDO is required in the formulation and how much composition drift can be tolerated? Even a minimal addition of 1 mol% MDO to the polymer backbone has been shown to initiate degradation, underscoring MDO's role in enhancing degradability.[30] However, this alone does not ensure degradability. Overall degradation and degradation rate are influenced by many factors such as polymer structure, environmental conditions (pH, temperature, humidity), and polymer molecular weight[42,43]. The research literature suggests that adding 5-10 mol% MDO to the polymer backbone is a practical starting point for achieving biodegradation.[30,31,44] At the very least, a 5 mol% MDO addition appears to be a reliable threshold for developing degradable (or compostable) polymers because their insertion at that frequency would mean the presence of an MDO moiety to enable the breakup of high molecular weight polymer chains into lower molecular weight segments, which are more easily degraded. Thus, the terpolymer composition in Figure 4.3a satisfies this condition. Finally, for applications as a PSA, the BA-rich system also satisfies the need for a low T_g, with a theoretical value of -47°C calculated based on the Fox equation.[45–48] Thus, the low composition drift,

favorable MDO incorporation and applicability as a PSA makes the system in Figure 4.3a an obvious choice for our future work.

A detailed examination of the binary reactivity ratio predictions (Figure 4.4) reveals that the compositions in the BA-rich (Figure 4.4a) and MDO-rich (Figure 4.4b) systems were not accurately predicted, particularly when contrasted with the predictions made using ternary reactivity ratios for the same formulations. The prediction of the cumulative compositions of all three components in all three cases clearly illustrate the discrepancy between the use of binary and ternary reactivity ratios. As anticipated from previous discussions (herein and in the references), this outcome supports the use of reactivity ratios derived from ternary data rather than using the reactivity ratios derived from copolymerization experiments.

For the BA/MDO pair, the binary reactivity ratio r_{12} (1.761) was significantly higher than its ternary counterpart (0.417). This suggests an increased propensity for BA to add to a growing MDO chain in the presence of VAc, contrary to the binary system where BA had a higher tendency to propagate with itself. This shift indicates a stronger interaction between BA and MDO in the ternary system, possibly leading to a polymer with a more balanced incorporation of BA and MDO units. For the BA/VAc interaction, the observed decrease in the r_{13} value from 5.938 in the binary system to 4.459 in the ternary system indicates a small shift in BA's behaviour. Despite both values being significantly greater than 1, indicating a predominant preference of BA for self-addition, the decrease in the ternary system reactivity ratio suggests that BA's relative tendency to add to VAc has increased in the presence of MDO. Simultaneously, the increase in the r_{31} value from 0.026 to 0.198, although still below 1, indicates a stronger, yet still limited, tendency for VAc to add to BA in the ternary system compared to the binary system. The most striking changes were observed in the MDO/VAc pair, where the r_{23} value dramatically decreased from 0.950 (binary) to 0.260 (ternary), whereas the r_{32} value surged from 1.71 (binary) to 55.339 (ternary). The observed decrease in the r_{23} value from 0.950 in the binary system to 0.260 in the ternary system does indeed suggest a significant shift in MDO's behaviour towards VAc. Initially, with an r_{23} value close to 1 in the binary system, MDO showed a nearly equal preference for adding to VAc as to itself, indicating a balanced reactivity between homo- and cross-propagation. However, the substantial reduction in this value in the ternary system suggests that MDO's preference for adding to VAc over itself has increased markedly. This shift could lead to a terpolymer with more frequent sequences of VAc units directly linked to MDO. The dramatic increase in the r_{32} signifies a

substantial change in VAc's affinity towards MDO in the ternary system. All of the above comments suggest that, generally, the addition of a third monomer to a copolymer can have unexpected impacts in several directions, depending on the application.

a)

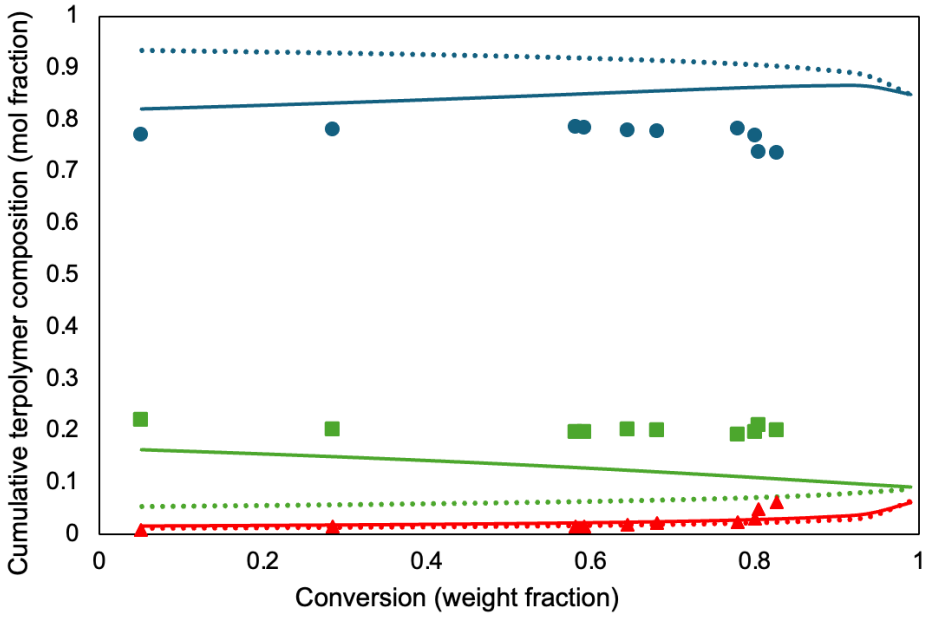

b)

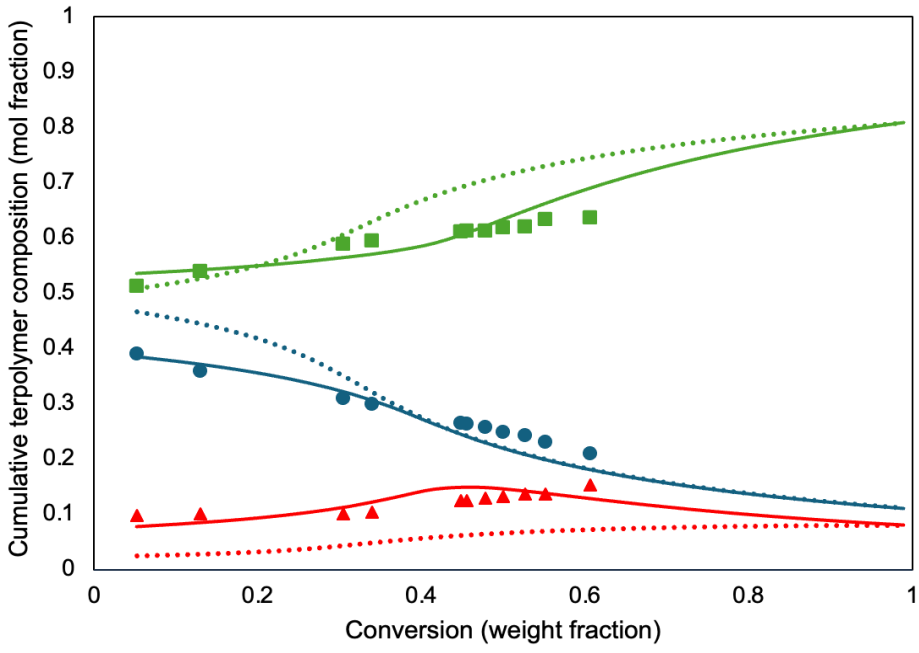

c)

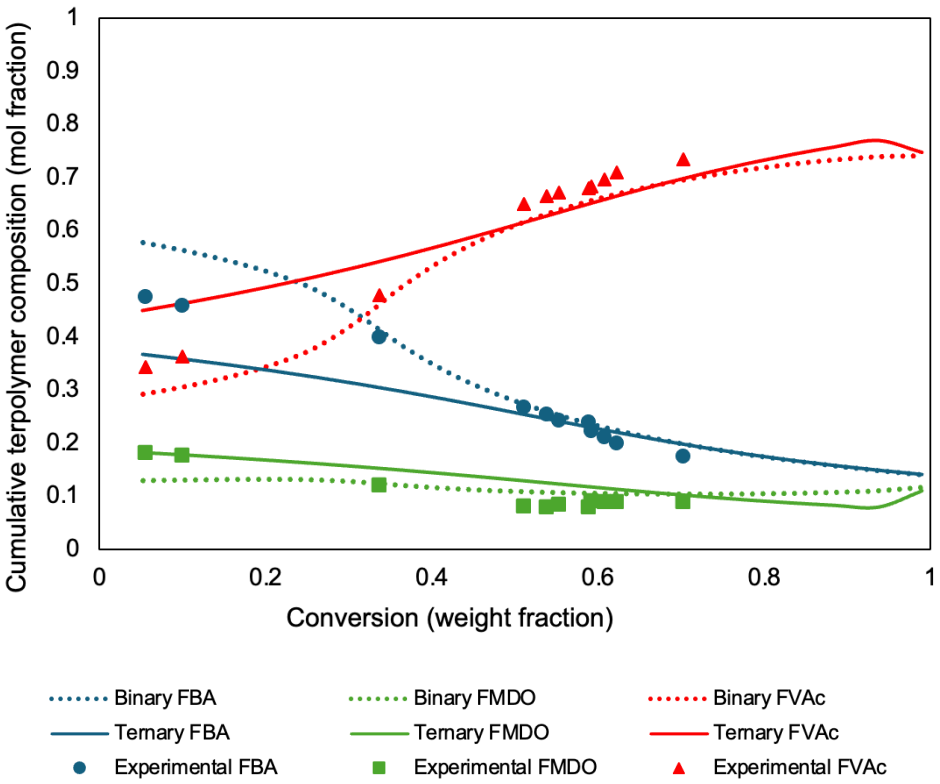

Figure 4.4. Comparison of model predictions of cumulative terpolymer composition using binary reactivity ratios (dotted lines) vs. using ternary reactivity ratios (solid lines) for BA/MDO/VAc terpolymerizations at various feed compositions (BA/MDO/VAc (mol%/mol%/mol%) a) 84/9/7, b) 11/81/8, and c) 14/12/74). Experimental data are shown as symbols for BA (blue circles), MDO (green squares) and VAc (red triangles), colors of dashed and solid lines correspond to the same monomers.

The monomer conversion versus time data for all three feed compositions are shown in Figure 4.5. It can be seen that the BA-rich and VAc-rich systems had faster rates of polymerization than the MDO-rich system. The ternary reactivity ratios, indicating MDO's preference for cross-propagation with BA and VAc over homopropagation, align with the observed reaction rates.

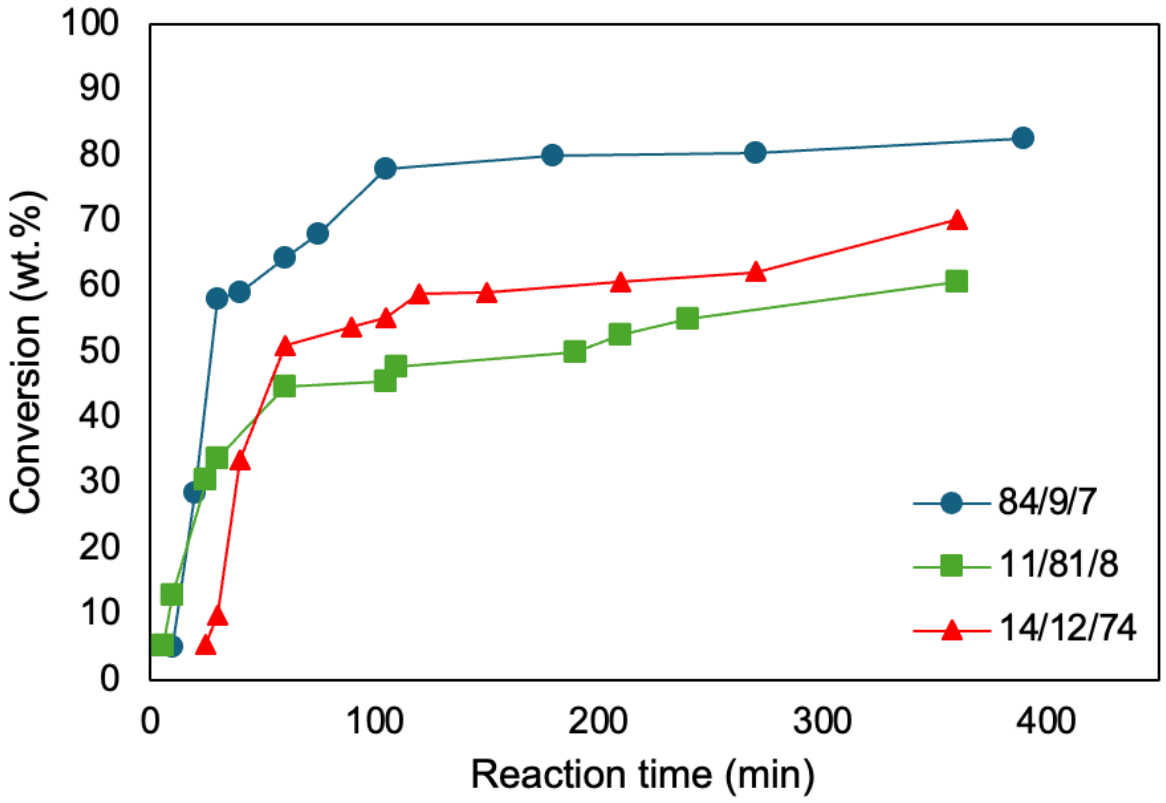

Figure 4.5. Conversion versus time for bulk BA/MDO/VAc terpolymerization at various feed compositions (BA/MDO/VAc (mol%/mol%/mol%) 84/9/7 (circles), 11/81/8 (squares), 14/12/74 (triangles))

4.5 Conclusion

This study marks a significant advancement in the understanding of terpolymerization kinetics for the BA/MDO/VAc system, particularly through the accurate estimation of ternary reactivity ratios using EVM. Our findings reveal ternary reactivity ratios as $r_{12} = 0.417$, $r_{21} = 0.071$, $r_{13} = 4.459$, $r_{31} = 0.198$, $r_{23} = 0.260$, and $r_{32} = 55.339$ (BA/MDO/VAc as monomers 1/2/3), which contrast significantly with binary reactivity ratios, underscoring the complex nature of terpolymer systems and the necessity for ternary analysis. The application of a modified Alfrey-Goldfinger model enabled proper prediction of both instantaneous and cumulative terpolymer compositions, providing deep insight into the polymerization process and the specific incorporation behaviour of MDO in varying feed compositions, in order to optimize formulations of degradable (compostable) polymer backbones.

These composition predictions are crucial for designing polymers with desired properties, particularly in the realm of biodegradable PSAs, where the precise control over polymer composition and distribution is paramount. The study's comprehensive approach offers a robust framework for accurately describing complex polymerization systems, paving the way for future innovations in sustainable polymer design.

4.6 References

[1] J. M. Millican, S. Agarwal, *Macromolecules* 2021, *54*, 4455.

[2] A. Chamas, H. Moon, J. Zheng, Y. Qiu, T. Tabassum, J. H. Jang, M. Abu-Omar, S. L. Scott, S. Suh, *ACS Sustain Chem Eng* 2020, *8*, 3494.

[3] D. K. Schneiderman, M. A. Hillmyer, *Macromolecules* 2017, *50*, 3733.

[4] R. Geyer, J. R. Jambeck, K. L. Law, *Sci Adv* 2017, *3*.

[5] M. A. Dubé, S. Salehpour, *Macromol React Eng* 2014, *8*, 7.

[6] M. A. Dubé, V. A. Gabriel, A. S. Pakdel, Y. Zhang, *Can J Chem Eng* 2021, *99*, 31.

[7] D. Wan, K. Satoh, M. Kamigaito, Y. Okamoto, *Macromolecules* 2005, *38*, 10397.

[8] T. Öztürk, B. Savaş, E. Meyvacı, A. Kılıçlıoğlu, B. Hazer, *J of Poly Research* 2020, *27*, 76.

[9] J. Folini, W. Murad, F. Mehner, W. Meier, J. Gaitzsch, *Eur Polym J* 2020, *134*, 109851.

[10] S. Reddy Mothe, J. S. J. Tan, L. R. Chennamaneni, F. Aidil, Y. Su, H. C. Kang, F. C. H. Lim, P. Thoniyot, *J of Polym Sci* 2020, *58*, 1728.

[11] S. Agarwal, *Polym Chem* 2010, *1*, 953.

[12] S. Jin, K. E. Gonsalves, *Macromolecules* 1997, *30*, 3104.

[13] T. Endo, "Radical Ring-Opening Polymerization," *Poly Sci: A Comprehensive Reference*, Elsevier 2012, p. 507.

[14] A. Tardy, J. Nicolas, D. Gigmes, C. Lefay, Y. Guillaneuf, *Chem Rev* 2017, *117*, 1319.

[15] W. J. Bailey, Z. Ni, S. Wu, *J of Polym Sci: Polym Chem Ed* 1982, *20*, 3021.

[16] S. Jin, K. E. Gonsalves, *Macromolecules* 1997, *30*, 3104.

[17] J. Folini, W. Murad, F. Mehner, W. Meier, J. Gaitzsch, *Eur Polym J* 2020, *134*, 109851.

[18] J.-B. Lena, A. W. Jackson, L. R. Chennamaneni, C. T. Wong, F. Lim, Y. Andriani, P. Thoniyot, A. M. van Herk, *Macromolecules* 2020, *53*, 3994.

[19] S. Weidner, G. Kuehn, B. Werthmann, H. Schroeder, U. Just, R. Borowski, R. Decker, B. Schwarz, I. Schmuecking, I. Seifert, *J Polym Sci a Polym Chem* 1997, *35*, 2183.

[20] J.-B. Lena, A. M. Van Herk, *Ind Eng Chem Res* 2019, *58*, 20923.

[21] M. R. Hill, E. Guégain, J. Tran, C. A. Figg, A. C. Turner, J. Nicolas, B. S. Sumerlin, *ACS Macro Lett* 2017, *6*, 1071.

[22] A. L. Polic, T. A. Duever, A. Penlidis, *J Polym Sci A Polym Chem* 1998, *36*, 813.

[23] A. J. Scott, A. Penlidis, *Eur Polym J* 2018, *105*, 442.

[24] N. Kazemi, T. A. Duever, A. Penlidis, *AIChE Journal* 2014, *60*, 1752.

[25] I. Benedek, *Pressure-Sensitive Adhesives and Applications*, CRC Press, 2004.

[26] S. Srivastava, *Des Monomers Polym* 2009, *12*, 1.

[27] F. Wenzel, S. Hamzehlou, L. Pardo, M. Aguirre, J. R. Leiza, *Ind Eng Chem Res* 2021, *60*, 10479.

[28] G. Hedir, C. Stubbs, P. Aston, A. P. Dove, M. I. Gibson, *ACS Macro Lett* 2017, *6*, 1404.

[29] C. A. Bell, G. G. Hedir, R. K. O'Reilly, A. P. Dove, *Polym Chem* 2015, *6*, 7447.

[30] J. Undin, T. Illanes, A. Finne-Wistrand, A.-C. Albertsson, *Polym Chem* 2012, *3*, 1260.

[31] S. Agarwal, R. Kumar, T. Kissel, R. Reul, *Polym J* 2009, *41*, 650.

[32] R. O. Dunn, M. W. Shockley, M. O. Bagby, *J Am Oil Chem Soc* 1996, *73*, 1719.

[33] D. S. Shrestha, J. Van Gerpen, J. Thompson, *Trans ASABE* 2008, *51*, 1365.

[34] A. Niesbach, P. Lutze, A. Górak, *Comp Aid Chem Eng* 2013, 32, 223.

[35] M. Abdollahi, B. Massoumi, M. R. Yousefi, F. Ziaee, *J Appl Polym Sci* 2012, *123*, 543.

[36] D. Ding, X. Pan, Z. Zhang, N. Li, J. Zhu, X. Zhu, *Polym. Chem.* 2016, *7*, 5258.

[37] T. Alfrey, G. Goldfinger, *J Chem Phys* 1944, *12*, 322.

[38] M. A. Dubé, A. Penlidis, *Polymer (Guildf)* 1995, *36*, 587.

[39] A. J. Scott, V. A. Gabriel, M. A. Dubé, A. Penlidis, *Processes* 2019, *7*, 444.

[40] M. Dubé, R. A. Sanayei, A. Penlidis, K. F. O'Driscoll, P. M. Reilly, *J Polym Sci A Polym Chem* 1991, *29*, 703.

[41] A. J. Scott, A. Penlidis, *Processes* 2018, *6*, 8.

[42] B. Ghanbarzadeh, H. Almasi, "Biodegradable Polymers," *Biodegradation - Life of Science*, InTech 2013.

[43] A. Samir, F. H. Ashour, A. A. A. Hakim, M. Bassyouni, *Npj Mater Degrad* 2022, *6*, 68.

[44] C. Lefay, Y. Guillaneuf, *Prog Polym Sci* 2023, *147*, 101764.

[45] D. Ding, X. Pan, Z. Zhang, N. Li, J. Zhu, X. Zhu, *Polym. Chem.* 2016, *7*, 5258.

[46] C. Hagiopol, “Copolymers,” *Encyclopedia of Condensed Matter Physics*, Elsevier 2005, p. 235.

[47] M. Fernandez-Garcia, R. Cuervo-Rodriguez, E. L. Madruga, *J Polym Sci B Polym Phys* 1999, *37*, 2512.

[48] E. Browne, Z. A. Worku, A. M. Healy, *Pharmaceutics* 2020, *12*, 43.

Chapter 5
Butyl Acrylate/2-Methylene-1,3-Dioxepane/Vinyl Acetate Emulsion Terpolymerization: Incorporating Backbone Degradable Linkages into Adhesive Applications

Maryam Movafagh[1], Kelly M. Meek[1,2], Marc A. Dubé[1]

[1]Department of Chemical and Biological Engineering, University of Ottawa, Ottawa, ON
[2]Department of Chemical and Materials Engineering, Concordia University, Montreal, QC

This chapter is a manuscript published in ChemSusChem (2025).
DOI: 10.1002/cssc.202402478

5.1 Abstract

The ring-opening polymerization of bio-based monomer 2-methylene-1,3-dioxepane (MDO) can reportedly enhance polymer degradability. Butyl acrylate (BA)/MDO/vinyl acetate (VAc) terpolymers were synthesized via emulsion polymerization for their eventual application as pressure-sensitive adhesives (PSAs). While using MDO in emulsion polymerization leads to a more sustainable process, it also presents challenges such as MDO hydrolysis, MDO ring retention, and inadequate MDO distribution. By carefully selecting reaction conditions such as pH and temperature, MDO hydrolysis and MDO ring retention were mitigated, and a uniform distribution of MDO throughout the terpolymer was confirmed. In addition, carboxylated cellulose nanocrystals (cCNCs) were incorporated into the final formulation to enhance the PSA properties.

5.2 Introduction

Polymer materials offer unrivalled benefits to humanity, meeting a variety of needs over a range of applications. However, due to their widespread use and existing production and disposal methods, polymers present substantial environmental issues by contributing to climate change, air pollution, waste generation, and water pollution.[1] This motivates high interest in producing biodegradable polymers such as polyesters.[2,3] Aliphatic polyesters are prominent in the category of biodegradable polymers because of their hydrolyzable ester bonds and comparatively short aliphatic chains within the macromolecules, making them significant examples of polymers which align with the principles of environmental sustainability.[4] Ionic ring-opening polymerization,

polycondensation, and polyaddition methods are well-known for producing such biodegradable polyesters.[5,6] However, all these approaches have limitations, including heightened sensitivity to impurities, increased operational costs, and restricted monomer applicability, which must be carefully navigated to exploit their full potential.[7]

Another method of producing polyesters is via radical ring-opening polymerization, a chain-growth polymerization method. One example of radical ring-opening polymerization uses cyclic ketene acetals (CKAs).[8,9] Aliphatic polyesters, made via ring-opening polymerization of CKAs, are the most studied biodegradable polymers. Because of the molecular structure of CKAs, the resulting polymers will have ester groups along their backbone, which should enhance biodegradation compared to polymers possessing backbones solely consisting of carbon-carbon linkages. The disadvantage of CKAs is the conflict between the ring-opening process and the unintended direct vinyl propagation that results in polyacetals (aka ring retention). To increase the selectivity of the ring-opening process, two criteria were initially considered while designing a monomer for radical ring-opening polymerization: (i) the ring strain and (ii) the stabilization of the radical when the ring is opened. For instance, it is known that 6-membered ring monomers have challenging ring-opening polymerizations. This is explained by the reduced ring strain of cyclohexane-like monomers for which the ring strain is zero.[10] This situation has led to the predominant use of two cyclic monomers: seven-membered ring CKAs such as MDO and the 5,6-benzo-2-methylene-1,3-dioxepane (BMDO). Both MDO and BMDO are known to undergo complete ring-opening polymerization over a broad range of reaction conditions. MDO can be an excellent candidate for ring-opening polymerization because it has (i) an increased steric hindrance of the ring-held radical compared to the stability of the ring-open radicals and (ii) a propensity for ring-open radicals to undergo backbiting reactions to create more stable radicals.[11] In addition, MDO is a bio-based monomer because it is produced from starting materials such as 1,4-butanediol and diethylene glycol, which are themselves bio-sourced materials.[12]

Free radical copolymerization involving CKA with vinyl monomers has been previously established to create polymers with degradable backbones.[9,13] In our current work, we aim to incorporate MDO monomer into the backbone of a vinyl terpolymer. Historically, achieving high incorporation rates of cyclic ketenes such as MDO in copolymerization with common vinyl monomers has been challenging, partly attributed to unfavorable reactivity ratios that limit their compatibility.[8] Despite these difficulties, our recent findings demonstrate successful bulk

terpolymerization of butyl acrylate (BA), MDO, and vinyl acetate (VAc), achieving substantial MDO incorporation within a BA-rich terpolymer backbone.[14]

Due to their hydrolytic instability, CKAs are mainly copolymerized in non-nucleophilic organic solvents; there are only a few reports on the polymerization of CKA in water and in emulsion polymerization.[15,16] To align with green chemistry principles,[17] which advocate for the minimization of solvent use, there is a significant interest in exploring solvent-free methods such as emulsion polymerization. This technique is distinguished for its ability to produce aqueous resins with diverse colloidal and physicochemical properties. Monomer, water, surfactant (i.e., emulsifier), and a water-soluble initiator make up a classic emulsion polymerization formulation. This heterogeneous free radical polymerization process begins with an oil-in-water emulsifier stabilizing the comparatively hydrophobic monomer in water, followed by the initiation reaction, ultimately leading to the nucleation of polymer particles. Water, as the continuous phase, is vital in emulsion polymerization because it keeps the viscosity low, acts as an efficient heat sink, and serves as a conduit for the transfer of monomers. Common surfactants are long-chain hydrocarbons with hydrophobic tails and hydrophilic heads and serve to keep the polymer particle dispersion stable. Different surfactant types, such as ionic (anionic and cationic) and non-ionic (typically polymeric), may be utilized. Water-soluble initiators, such as potassium persulfate (KPS) and redox systems (for low-temperature polymerization), are extensively employed.[18,19]

Carter et al. presented a method for making waterborne and biodegradable latex polymers using MDO.[20] Because of the presence of backbone ester groups, emulsion polymerization of vinyl acetate (VAc) with MDO yielded hydrolytically degradable polymer particles and latex-based coatings. They found that a successful emulsion copolymerization of MDO could be accomplished by (i) suppressing MDO hydrolysis in the water phase by controlling pH and temperature, and (ii) establishing a process that runs at high instantaneous monomer conversions to promote MDO incorporation.[20] To avoid MDO hydrolysis, it is important to run the polymerization at a low temperature (e.g., 40 °C) and under mildly basic conditions (e.g., pH = 8). On the other hand, under alkaline conditions, VAc monomer can hydrolyze. They also used a redox initiation system to allow for a reduced polymerization temperature and reaction time. This new class of latex was well-suited for developing next-generation biodegradable and compostable single-use food service items and other applications requiring the degradation of polymer-based films and coatings.[20]

Kordes et al., in a study on the copolymerization of MDO and VAc, cited the challenges of producing MDO-based polymers in both batch and semi-batch emulsion polymerization.[21] However, there is evidence that semi-batch emulsion polymerization can result in reduced MDO hydrolysis by minimizing MDO-water contact.[20,22,23] Beyond controlling MDO hydrolysis, achieving a uniform distribution of MDO within the polymer backbone is crucial for producing a degradable polymer. In our terpolymer system, which comprises BA, VAc, and MDO, each monomer pair exhibits unique reactivity ratios and distinct tendencies for homo-propagation versus cross-propagation with the other monomers. In a previous study of the terpolymer reactivity ratios for this system, we demonstrated that batch polymerization was indeed sufficient to generate polymer chains with significant and uniform levels of MDO.[14] This has opened the door to the use of batch polymerization while controlling MDO hydrolysis and achieving significant MDO incorporation into the BA/MDO/VAc terpolymer.[11,24]

One class of polymeric materials of interest in this research is pressure sensitive adhesives (PSAs). PSAs can quickly adhere to solid surfaces under low pressure (i.e., finger pressure) and are viscoelastic polymeric materials with a low glass transition temperature (T_g) ranging from -70 to -20 ^{o}C.[25] They are used for labels, tapes, films, and other specialized applications, making them vital in everyday life.[26] The adhesive and cohesive properties of PSAs are closely tied to their viscoelastic properties.[27] Firstly, the wetting of the substrate and the Van der Waals and polar forces between the PSA and the substrate give rise to adhesion. On the other hand, intermolecular forces, and covalent interactions, such as polymer crosslinks, influence the cohesion of a PSA. Often, these forces are impacted by various production factors in opposing ways, making the control of their properties challenging. To adjust adhesive characteristics in PSA formulations, a "hard monomer" (i.e., high polymer T_g), such as methyl methacrylate (MMA), can be copolymerized with a "softer" monomer (i.e., low polymer T_g) such as 2-ethyl hexyl acrylate (EHA).[28,29] The worldwide demand for PSAs continues to grow.[30] The PSA market is dominated by polyacrylates made by free radical polymerization. Acrylic adhesives have the benefits of transparency, outstanding cohesive strength, adequate tack and peel strength, and good heat and aging resistance. The "soft" monomers typically provide the required flowability and wettability to give the PSA film adequate tack and peel strength. The PSA gains hardness and internal strength from the "hard" monomers.[31]

Historically, PSAs have been produced using solution polymerization, which presents evident hazards both at the synthesis stage and during product application. As mentioned, increased environmental concerns on the management of volatile organic compounds (VOCs) have resulted in tremendous growth in the use of emulsion polymerization to make latexes for water-borne adhesive applications as alternatives to solvent-borne adhesives.[32] In previous work, we successfully developed PSAs containing BA and/or VAc via emulsion polymerization. Because of our desire to make compostable PSAs, the use of MDO in the formulation makes sense. Not only would MDO enhance compostability, as discussed above, but its low homopolymer T_g (-59 °C),[33] makes it an ideal replacement for petroleum-based monomers in PSA formulations. Moreover, the potential for MDO to be used in an emulsion polymerization allows us to align with several important sustainability principles. Thus, we propose to displace some of the petroleum-based, non-biodegradable components in a PSA formulation with MDO.[34]

In this work, we demonstrate the synthesis, characterization, and application of BA/MDO/VAc emulsion terpolymers, focusing on the innovative use of MDO in emulsion polymerization to develop next-generation, environmentally friendly PSAs.

5.3 Materials and Methods

5.3.1 Materials

BA (≥99%) and VAc (≥99%) were purchased from Sigma-Aldrich (Oakville ON, Canada). BA and VAc monomers were passed through inhibitor removal columns acquired from Sigma-Aldrich. This process effectively eliminated any traces of inhibitors, such as hydroquinone or monomethyl ether hydroquinone. MDO was obtained from Wacker Chemie (München, Germany). TERGITOL™ 15-S40 surfactant (70 wt.% in water), 2-acrylamido-2-methyl-1-propanesulfonic acid sodium salt solution (Na-AMPS, 50 wt.% in water), ammonium persulfate (APS, 98%), tert-butyl hydroperoxide (t-BHP, 70 wt.% in water), iron (II) sulfate heptahydrate (≥99%), ethylenediaminetetraacetic acid (EDTA, >98.5%), tetrahydrofuran (THF, ≥99.9%), deuterated chloroform ($CDCl_3$, ≥ 99.9%), and ammonium hydroxide (28.0-30.0 wt.%) were obtained from Sigma-Aldrich. Bruggolite FF6 M reducing agent was obtained from Brüggemann (Newtown Square PA, USA). DextraCel™ (i.e., carboxylated CNCs or cCNCs) was obtained from Anomera Inc. (Montreal, QC) in a "never-dried" form (6.6 wt.% suspension in water). The carboxylate groups on the cCNCs' surface were in the sodium-salt form. The "apparent" cCNC diameter via

dynamic light scattering (DLS) was 102 ±0.4 nm, and the carboxylate group content via conductimetric titration was 141 ±10 mmol.[35] Deuterated water (D_2O, ≥99.96%) was obtained from Cambridge Isotopes Labs (Tewksbury MA, USA). The wetting agent, bis(2-ethylhexyl) sulfosuccinate sodium salt (≥95%), was obtained from TCI America (Portland OR, USA). Distilled de-ionized water (DDW) with a resistivity of 18.0 ± 0.2 MΩ cm was used for synthesis and characterization purposes. All reagents and chemicals were used as received unless otherwise specified.

5.3.2 Methods

Emulsion Terpolymerization of BA/MDO/VAc. The emulsion terpolymerization formulation (Table 5.1) was developed by combining ideas from our previous work with PSAs,[36–38] and that from Carter et al.[20] PSAs were synthesized using a batch emulsion polymerization process conducted under a nitrogen atmosphere in a 1.25 L stainless steel reactor (Mettler Toledo LabMax Automatic Lab Reactor). The reactor contents were mixed at 200 rpm and maintained at a constant temperature of 40°C. A surfactant mixture was initially prepared by combining TERGITOL™ 15-S40 (16 wt.% in DDW) and Na-AMPS with DDW. Na-AMPS was added to provide colloidal stability. According to Mothe et al.,[23] neutral surfactants such as TERGITOL™ 15-S40 are also effective in promoting latex stability. The surfactant mixture was stirred for approximately 30 minutes. Following this, the surfactant mixture and additional DDW were added to the reactor under a nitrogen blanket at the process conditions. Subsequently, an iron (II) sulfate heptahydrate solution (0.15 wt.% in DDW) and an EDTA solution (1 wt.% in DDW) were added to the mixture at 40ºC. Due to the poor solubility of EDTA in water, a few drops of ammonium hydroxide were added to enhance its solubility. A redox system comprising solutions of t-BHP, APS (6.3 wt.% in DDW), and Bruggolite FF6 M (8 wt.% in DDW), a sulfinic acid-based reductant, was charged to the reactor. The pH of the reactor contents was then adjusted to between 7.8 and 9 using ammonium hydroxide and stabilized for 2 minutes at 40°C before introducing the monomer mixture. For all runs, the BA/VAc ratio in the monomer mixture was 9:1 (w/w), with MDO concentrations varying from 0 to 20 wt.%. After 70 minutes of polymerization, an additional shot of the redox system was administered to ensure complete monomer conversion and to accelerate the polymerization process. The reactor process conditions were maintained for an additional 20 minutes at 40°C before being cooled to room temperature. Throughout the 90-minute polymerization process, the

pH was kept within a range of 7.8 to 8.8 by periodic adjustments with ammonium hydroxide. [21,23] It was important to maintain the pH in this range to suppress the hydrolysis of MDO as well as the other monomers. MDO hydrolysis is significantly reduced under alkaline conditions compared to neutral or acidic environments.[21,22,39]

A dual-channel pH meter (Fisher Scientific/Accumet Research, model AR50) was utilized to monitor the pH of samples collected throughout the reaction process and of the final latex. Offline pH measurement was used instead of a direct probe because measurement inaccuracies could arise due to the formation of a thin latex film on the probe.[21] During the reaction, samples were taken periodically to monitor pH, particle size and distribution, monomer conversion, and terpolymer composition. There was no visible coagulum in all samples and the final latex; therefore, the samples were not filtered. The final latex was further characterized for gel content, degree of ring-opening/retaining, degree of MDO hydrolysis, T_g, and PSA performance (tack, peel strength, shear adhesion). After dilution in THF, the dried polymer was unfilterable (0.4 μm filter), and molecular weight analysis was impossible.

Table 5.1. Emulsion polymerization formulation

Component	Amount[a]
Monomer mixture:	
BA/MDO/VAc	~218 g
Surfactant mixture:	
TERGITOL™ 15-S40	3.50
Na-AMPS (surfmer)	0.64
Initiators:	
t-BHP/APS	0.31/0.75
Bruggolite FF6 M	1.44
Initiator shot:	
t-BHP/APS	0.04/0.09
Bruggolite FF6 M	0.18
Reducing agent:	
iron (II) sulfate heptahydrate	0.01
EDTA	0.01
Buffer:	
ammonium hydroxide[b]	~1
DDW (total)[c]	379 g

[a] All amounts in phm (parts per hundred parts monomer) unless otherwise indicated.
[b] Ammonium hydroxide quantity varied to keep the pH between 7.8 and 8.8.
[c] DDW distributed in various solutions as per details in the procedure.

5.3.3 Characterization

Solids content and monomer conversion: Samples were collected throughout the reaction, and a few drops of hydroquinone solution (~0.1 g of 0.8 wt.% aqueous solution) were added to quench the reaction. To calculate the solids content, about 2 g of latex was weighed in an aluminum dish and dried at ambient temperature in a fume hood until a constant weight was achieved (~3-4 days). The solids content was calculated as:

$$\boldsymbol{Solids\ content}\ (\%) = \boldsymbol{W_{dried\ sample}} / \boldsymbol{W_{latex}} \qquad (5.1)$$

The instantaneous monomer conversion was then calculated based on the amount of monomer and other ingredients charged to the reactor:

$$X = \frac{\textbf{Solid content} - w_I - w_{surf}}{w_m} \quad (5.2)$$

where w_I, w_{surf}, and w_{m} represent the weight fraction of initiator, surfactant, and monomer respectively, introduced to the reaction mixture by that time in the process. Overall conversion was calculated via equation (5.2) by replacing the weight fractions with the total weight fractions of the ingredients added over the course of the entire reaction.

MDO Hydrolysis Residue and Volatile Content: Thermogravimetric analysis (TGA) was conducted to detect MDO hydrolysis products and any remaining volatile compounds, such as unreacted monomers, which may persist after the drying process. As explained above, polymer samples were prepared at ambient temperature under the fume hood. TGA platinum pans were torched and tared using the TGA 550 (TA Instruments), and samples were subsequently placed on the prepared pans for testing.

Particle size and distribution: Dynamic light scattering (DLS) by Malvern NanoS Zetasizer 2000 at an angle of 176° was used to measure the size and size distribution (PDI) of the polymer particles. Samples were prepared by diluting a drop of latex in approximately 5 mL DDW. Each measurement was taken as an average of 3 measurements.

Polymer composition: A Bruker 400 MHz ^{1}H-NMR spectrometer was used to measure the terpolymer composition. Dried polymer samples were dissolved in $CDCl_3$ at a ratio of 0.02 g polymer per 1.5 g solvent. The spectrometer was configured for 1D analysis, generating 32 scans.

Degree of ring-opening/retaining: Quantitative ^{13}C-NMR spectroscopy experiments were performed to assess the degree of ring-opening versus ring retention in the final dried latex samples. The experiments were performed at 600 MHz using a 90° pulse with inverse gated proton decoupling, a 60-second recycle delay while collecting 472 transients. The samples were dissolved in $CDCl_3$. The ^{13}C-NMR experiment was repeated on a single sample with a 120-second recycle delay, and the results suggested that the spin system was fully relaxed after 60 seconds.

MDO hydrolysis: The analysis of MDO hydrolysis was performed on final latex samples using ^{1}H-NMR spectroscopy on an Avance IIIHD 600 MHz NMR spectrometer equipped with a

cryoprobe. D_2O was used as the solvent to facilitate the suppression of proton signals from water. A modified Watergate pulse sequence with gradients was used to suppress the ^1H signals from water using an 8 ms ^1H 90° pulse, collecting 64 transients with a 1-second recycle delay and a 1.70 s acquisition time.[40,41]

Glass transition temperature: Dried polymer (5-10 mg) was weighed and sealed in an aluminum pan. An empty sealed pan was used as a reference. A differential scanning calorimeter (DSC) (Model Q1000 from TA Instruments) was used to measure the polymer T_g. The T_g was calculated from the inflection point in the reverse heat flow curve using the software provided. DSC was performed over a temperature range of T = -100 to 100 °C at a heating rate of 10 °C/min under a nitrogen atmosphere. The thermal history of each sample was erased in the first cycle by cooling to -100 °C, followed by heating to 100 °C, and then cooling to -100 °C. All thermal transitions were assigned from the second heating cycle.

Gel content: Approximately 0.03 g of dried polymer was weighed and heat-sealed in a poly(vinylidene fluoride) Durapore-coated membrane pouch. The membrane pouch was then soaked in 80 mL THF in a 100 mL capped glass vial for 14 h. The glass vial was then shaken for 24 h using a mechanical shaker. The membrane pouch was then removed and dried in a fume hood until it reached a constant weight. The remaining dry gel was weighed, and the gel content calculated as:

$$\boldsymbol{Gel\ content}\ (\%) = \frac{\boldsymbol{W_{dried\ gel\ and\ pouch} - W_{dry\ pouch}}}{\boldsymbol{W_{dry\ polymer\ and\ pouch} - W_{dry\ pouch}}} \quad (5.3)$$

PSA performance: Pressure Sensitive Tape Council standards (PSTC) including PSTC16 for tack, PSTC101 for peel strength, and PSTC107A for shear adhesion were followed for specimen preparation and testing procedures for measurement of PSA properties. Final PSA latexes were cast on 30 μm corona-treated Mylar sheets using a Meyer rod and dried at controlled conditions (temperature: 23±1 °C, and relative humidity: 50±5 %) for 48 hours before the test (2 films per sample). To enhance the film-casting process, a wetting agent, bis(2-ethylhexyl) sulfosuccinate sodium salt, was added to the latex formulation at a concentration of 0.2 wt.% of the total latex. The latex mixture was stirred overnight. The final dried film thicknesses, expressed as a weight per unit area, were measured and found to be uniform, with a film weight of approximately 20 g/m^2.

The dried cast films were tested for tack and peel strength using an Instron 3000 Universal Tester, together with Bluehill 2 Materials Testing Software. Strips of 1″ × 6″ were cut for tack, and a drop loop was formed by taping 1″ of each end of the strip, which was secured in the upper grip of the Instron. The upper grip was moved downward at a rate of 2 mm/s until an area of 1″ × 1″ of a stainless-steel substrate mounted on the lower grip was covered. The upper grip was then pulled up at a 5 mm/s rate, and the maximum force (N/m) required for removal was recorded as tack.

Peel strength was measured by separating an adhesive from a substrate at a 180° angle with respect to the substrate. Strips of 1″ × 5″ were cut and adhered to a stainless-steel substrate via application of a 2040 g roll coater (twice front-to-back movement along the length of the strip) at a rate of 10 mm/s. Subsequently, the substrate and the PSA strip were fixed in the lower and upper grips, respectively. The upper grip was then pulled upward at a rate of 5 mm/s, and the average force required for peeling (N/m) was reported as peel strength.

An in-house built shear tester was used to record the time a PSA strip could hold against a constant vertical force. Strips of 1″ × 5″ were cut, and one end of the strip was laminated on a stainless-steel substrate to cover a 1″ × 0.5″ area using the roll coater (2040 g) in a similar way to specimen preparation for the peel strength (four passes at a rate of 10 mm/s). A C-clamp was used to hang a 500 g weight to the other end of the strip. The time (h) that passed until the covered area was removed and the hung weight dropped was reported as shear adhesion.

Each PSA test was repeated six times for each latex cast to film (three samples per film for each test), and the average results and standard deviations were recorded.

5.4 Results and Discussions

Using the formulation in Table 5.1, five polymerizations were conducted at BA/VAc ratios of 9:1 (w:w) with MDO concentrations varying from 0 to 20 wt.%. Overall monomer conversion versus time exhibited similar trends for all runs, culminating in final conversions exceeding 97 wt.% (Figure 5.1, Table 5.2). The solids content ranged from 37 to 39 wt.%, with a target of 38 wt.% based on literature recommendations,[20,21] which suggested reducing water content to minimize MDO hydrolysis. TGA analysis of the dried polymer samples was conducted to evaluate the presence of any residual small molecules, particularly MDO hydrolysis products. The thermogram showed no weight loss up to 350°C (see Appendix II, Figure II.1), indicating no residual small molecules or volatile compounds in the dried polymer. Attempts to find direct

evidence of MDO hydrolysis products, i.e., 4-hydroxybutyl acetate (4-HBA), were also made via water-suppression ^{1}H-NMR spectroscopy on the final latex for each run. Unfortunately, the carbonyl groups for BA polymer and MDO polymer appear in the same range (3.5 to 4 ppm) as expected for 4-HBA.[21] Thus, the NMR results were inconclusive. However, due to the high monomer conversion levels, the TGA results, and the high MDO content in the polymer (see Table 5.2), we can conclude that hydrolysis was minimal if it did occur (see Appendix II, Figure II.2, for additional details).

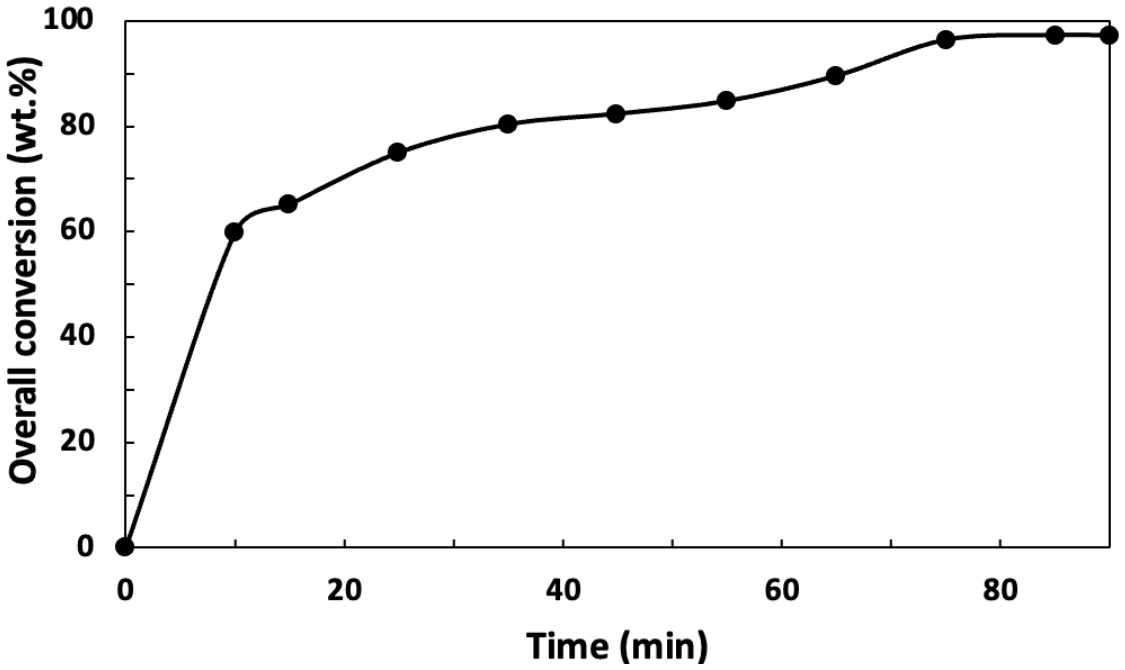

Figure 5.1. Typical overall monomer conversion versus time (BMV20 is shown as an example).

The average particle size of the final latexes decreased after adding MDO but did not vary much with MDO content (Table 5.2). The final particle size distributions were narrow for all runs, exhibiting a low polydispersity index (PDI) of approximately 0.02. Data on the z-average particle size versus time are shown in the Appendix II. The polymer gel content also did not vary significantly, with an average value of 55 wt.%. As noted, it was impossible to filter the dissolved polymer (in THF) for molecular weight analysis. This was not surprising due to the high levels of BA in the formulation.[25]

Table 5.2. Summary of final latex properties

	Formulation		Final latex			
Latex ID[a]	**BA/MDO/VAc monomer content (wt.%)**	**MDO monomer content (mol%)**	**Final conversion (wt.%)**	**MDO content[b] (mol%)**	**Z-average particle diameter (nm)**	***T_g* (°C)**
BV	90/0/10	-	98.0 ± 1	-	170.0 ± 1.2	-50.24
BMV5	85.5/5.0/9.5	5.3	97.5 ± 1	4.85	147.0 ± 0.9	-49.79
BMV10	81.0/10.0/9.0	10.6	97.0 ± 0.9	9.98	152.0 ± 1.0	-47.25
BMV15	76.5/15.0/8.5	15.9	97.0 ± 0.5	14.10	151.0 ± 0.8	-37.45
BMV20	72.0/20.0/8.0	21.1	97.0 ± 0.5	20.36	159.0 ± 1.2	-34.49

[a] Latex ID indicates monomer included in formulation (B = BA, M = MDO, V = VAc) and number refers to wt.% MDO.
[b] MDO content represents the combined contribution of both ring-opened and ring-retained MDO.

The MDO content in the final latex was calculated from ^{1}H-NMR spectroscopy (Figure 5.2) and ranged from 4.45 to 20.36 mol% (Table 5.2). The analysis was like that used previously.[14] The composition was calculated from four regions, A_1, A_2, A_3 and A_4, shown in Figure 5.2. Area A_1 represents the −CH protons of VAc (δ = 4.7 – 4.9 ppm), area A_2 represents the $-CH_2O$ protons of BA and MDO (δ = 3.3 – 4.2 ppm), area A_4 represents the $-CH_3$ of BA (δ = 0.7 – 1 ppm) and area A_3 encompasses the remaining protons for BA, MDO, and VAc (δ = 1 – 2.5 ppm). It should be noted that there were some overlapping peaks for peak assignments “a, k” and “k, d’, d”. In those runs conducted at 40°C, the percentage of MDO retained in its ring structure was approximately 27 mol% for BMV5, 26 mol% for BMV10, 30 mol% for BMV15, and 30 mol% for BMV20. The calculation method, along with detailed peak assignments and the ^{1}H-NMR spectra for the other runs, are provided in the Appendix II (Figures II.4-II.8).

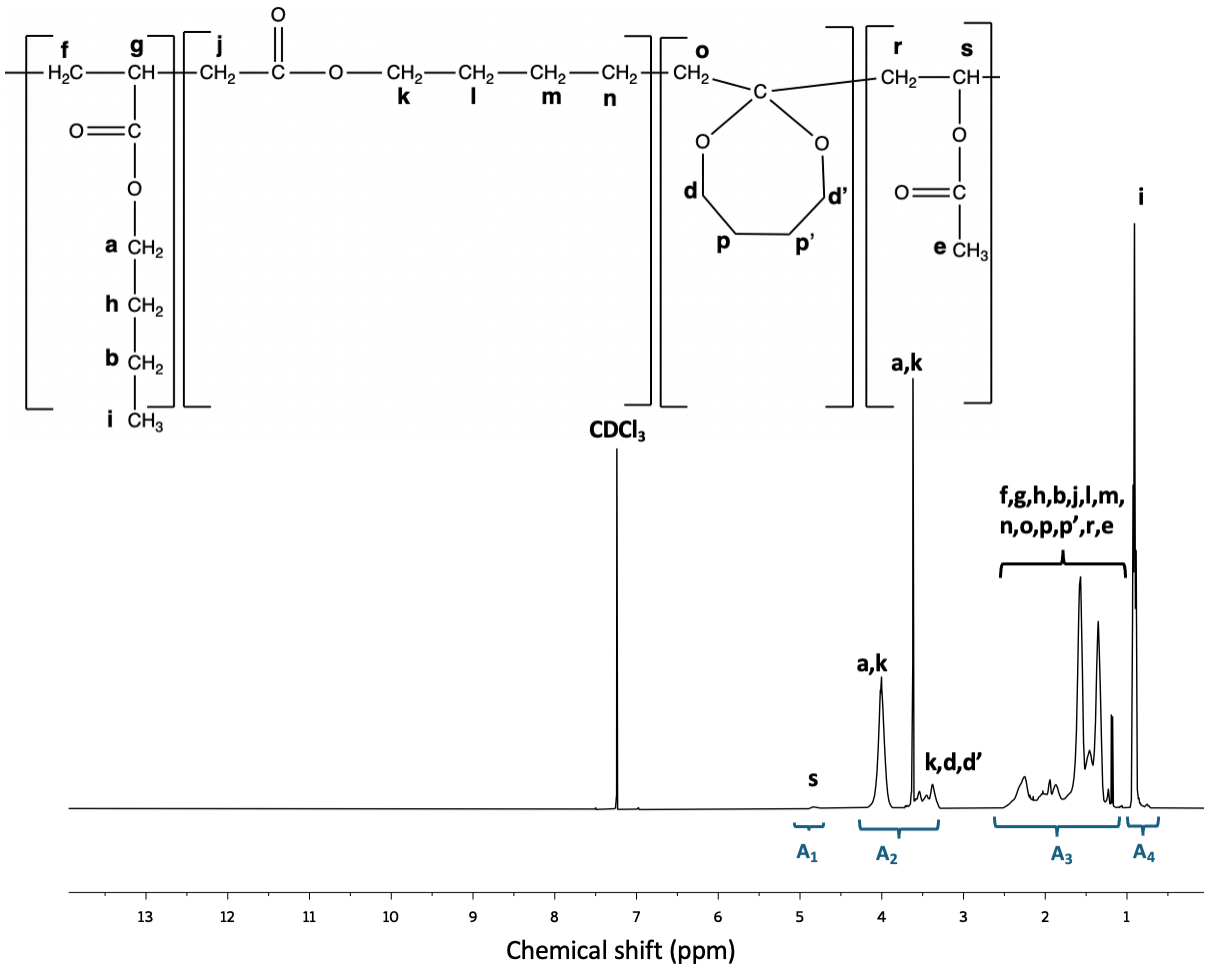

Figure 5.2. ^{1}H-NMR spectrum for BMV20 in $CDCl_3$. Detailed peak assignments are shown in the Appendix II (Figure II.5).

Analysis of the terpolymer composition versus conversion revealed a homogeneous distribution of MDO throughout the polymer backbone, which is crucial for enhancing the final product's degradation properties (Figure 5.3 and Appendix II).[11] The nearly constant amount of MDO throughout the polymerization indicates a uniform distribution of MDO in each composition. The ternary reactivity ratios for the system (BA/MDO/VAc, 1/2/3) were previously determined using an integrated error-in-variables method to be $r_{12} = 0.417$, $r_{21} = 0.071$, $r_{13} = 4.459$, $r_{31} = 0.198$, $r_{23} = 0.260$, and $r_{32} = 55.339$,[14] and predict a uniform distribution of MDO for all feed compositions studied (Figure 5.4). It should be noted that the model predictions are for bulk polymerization, and no correction for partitioning of monomer in the water phase was accounted for. Nevertheless, the model predictions of the terpolymer composition are excellent (Figure 5.3 and Appendix II). The reactivity ratios suggest a preferential reaction of MDO with

BA and VAc, supporting the observed compositional homogeneity. Furthermore, the DSC results of all compositions (see Appendix II) showed a single inflection point, which points to the formation of random terpolymers with a uniform distribution of MDO units. This random distribution of MDO within the terpolymer matrix has significant implications for the properties of the dried latex, particularly its degradability and compostability. A uniform distribution of MDO ensures that the degradable linkages are evenly dispersed throughout the polymer, promoting consistent and efficient degradation when exposed to environmental conditions conducive to composting. However, due to the presence of ring-retained MDO in the terpolymers, these four runs (Table 5.2) would not necessarily have uniformly distributed MDO ester groups in the terpolymer backbone.

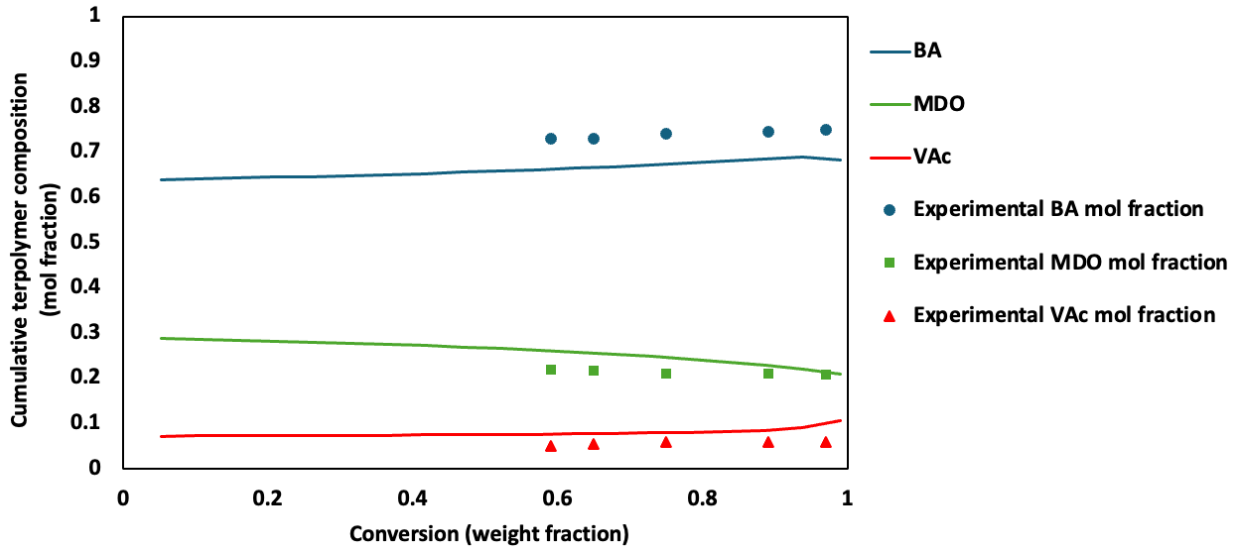

Figure 5.3. Model predictions of cumulative terpolymer composition using ternary reactivity ratios (solid lines) for BMV20. Experimental data are shown as symbols for BA (blue circles), MDO (green squares) and VAc (red triangles). Additional figures for other feed compositions are shown in the Appendix II.

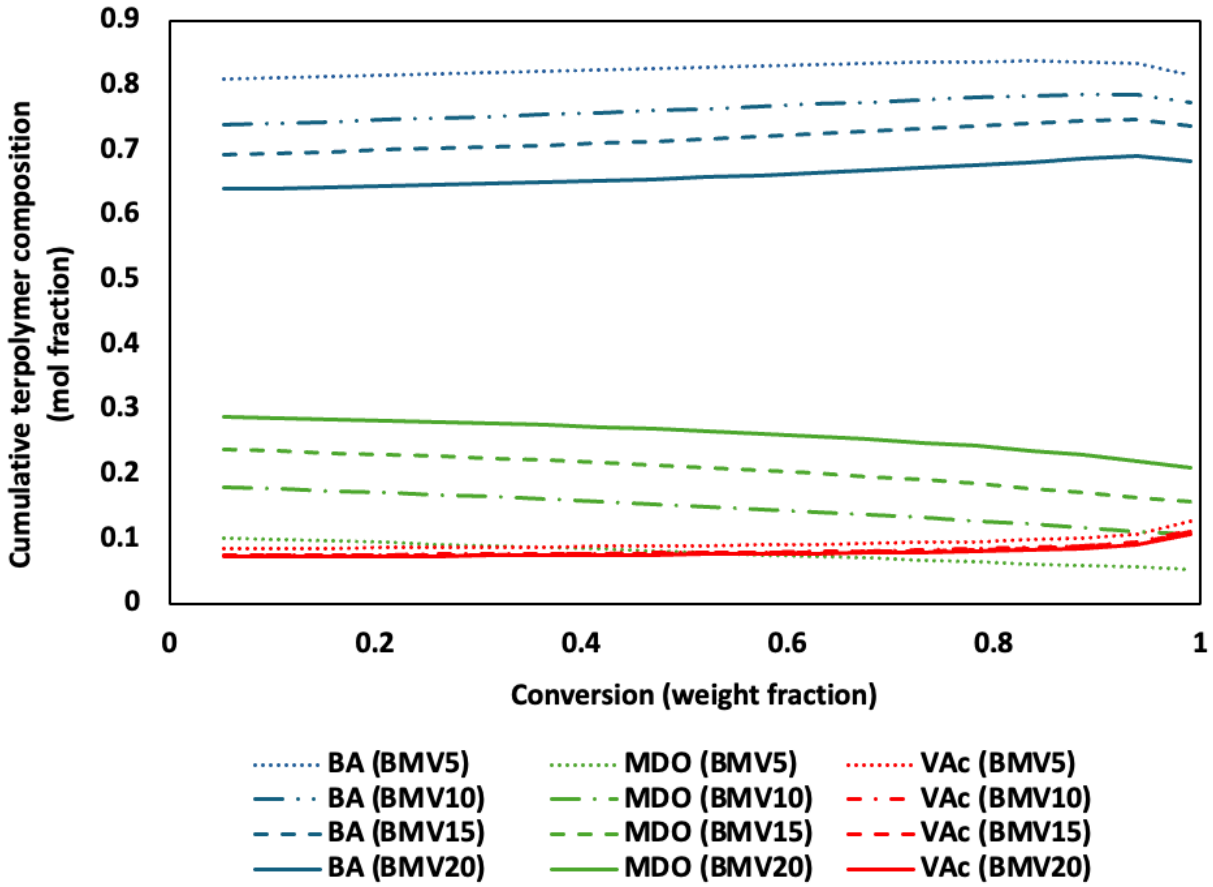

Figure 5.4. Model predictions of cumulative terpolymer composition vs conversion using ternary reactivity ratios for all terpolymers (BMV5, BMV10, BMV15, and BMV20).

It is well known that the free-radical polymerization of MDO can result in various products.[42] These possibilities include complete ring-opening leading to polyester formation, a mix of ring-opening and polyacetal formation (i.e., due to ring retaining polymerization), or complete polyacetal formation (Scheme 5.1). The specific outcome depends on factors such as the comonomer, initiator type, and polymerization temperature.[42,43] As noted earlier, results from ^{1}H-NMR spectra raised doubts in determining the precise amount of ring-retained MDO due to peak overlap. Quantitative ^{13}C-NMR spectra were then used to determine the proportion of ring-retained MDO units in the terpolymer. In Figure 5.2, the ^{13}C-NMR results for BMV20 show peaks at approximately 167.5, 172, and 173 ppm, related to the −COO groups of VAc (“e”), BA (“a”), and MDO ring-opened polymerization (“b”), respectively. The peak at ~100 ppm, indicates the cyclic structure of ring-retained MDO polymerization (shown as “d”). The analysis suggested that the ring-retained MDO content in the terpolymer ranged from 15 to 50 mol% of

the MDO polymerized; however, due to the low signal-to-noise ratio typical of ^{13}C-NMR spectra, the reliability of the quantities is in question compared to the values calculated via ^{1}H-NMR shown earlier. Nevertheless, a visible peak at 100 ppm (peak "d", Figure 5.4) suggests significant ring-retained MDO in the terpolymers. Spectra and calculations for the other three runs are shown in the Appendix II (Figures II.11-II.13).

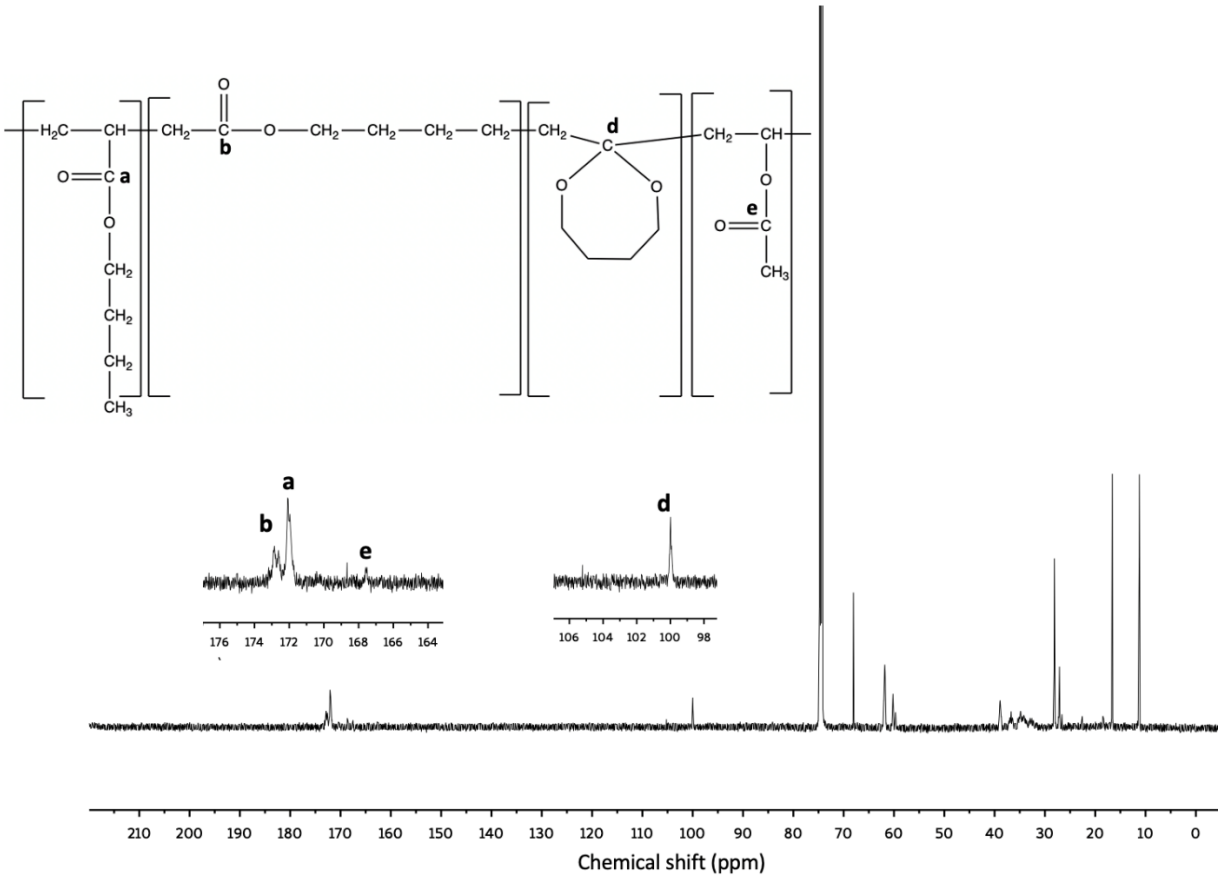

Figure 5.5. ^{13}C-NMR spectrum for BMV20 in $CDCl_3$. The peak at 105 ppm is a narrow artifact observed in our ^{13}C-NMR results using the AVIII600 NMR instrument.

Scheme 5.1. Free radical polymerization of MDO leads to ring-retained MDO (polyacetal) or ring-opened MDO (polyester).

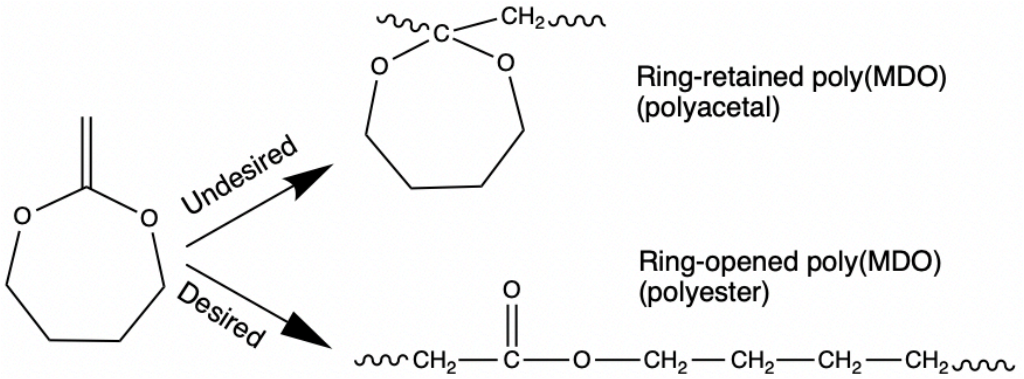

Attempts to measure the proportion of ring-retained MDO via DSC gave results ranging from 3 to 15 wt.%. Literature suggests that ring-opened MDO homopolymer typically exhibits a T_g of approximately -59°C, lower than BA homopolymer at -54°C. Consequently, it was anticipated that incorporating ring-opened MDO would reduce the terpolymer's T_g. However, our experimental data showed a contrasting trend (Table 5.2). Analysis suggested that the formation of polyacetal structures (i.e., ring-retained MDO) rather than polyester plays a critical role in the observed T_g behaviour. Polyacetal chains are known for their rigidity due to their cyclic nature, leading to reduced segmental mobility and higher T_g. To further investigate the T_g behaviour, the Fox equation was employed to calculate the theoretical weight fraction of ring-retained MDO in the terpolymer:

$$\frac{1}{T_{g_{total}}} = \frac{w_{BA}}{T_{g_{BA}}} + \frac{w_{VAc}}{T_{g_{VAc}}} + \frac{w_{MDO(ring-opened)}}{T_{g_{MDO\ (ring-opened)}}} + \frac{w_{MDO(ring-retained)}}{T_{g_{MDO\ (ring-retained)}}}$$

where w_{BA}, w_{VAc}, $w_{MDO(ring\text{-}opened)}$, $w_{MDO(ring\text{-}retained)}$ are the weight fractions of BA, VAc, ring-opened MDO, and ring-retained MDO, respectively. The T_g values used in the equation were $T_{g_{BA}}$ = -54 °C, $T_{g_{VAc}}$ = 30 °C, $T_{g_{MDO\ (ring-opened)}}$ = -59 °C, and $T_{g_{MDO\ (ring-retained)}}$≈183 °C. The weight fractions of BA, VAc, and total MDO (including both ring-opened and ring-retained forms) were employed from the ^{1}H-NMR peak assignments, while the overall T_g*s* were obtained from DSC results. Although widely used, the Fox equation is not entirely reliable for copolymer or terpolymer T_g estimation.[44] The calculated ring-retained MDO content using the Fox equation ranged from 3 to

15 wt.%. However, these values were significantly lower than the ~40 wt.% ring-retained MDO calculated from the quantitative ^{13}C-NMR.

Given the uncertainty in the T_g for ring-retained MDO, the unreliability of the Fox equation, and the low signal-to-noise ratio of the ^{13}C-NMR spectra, providing a reliable measure of the amount of ring-retained MDO is not possible. However, as noted earlier, there is no doubt from both the DSC and ^{13}C-NMR results that significant ring-retained MDO is present in the terpolymers.

Table 5.3 presents the comparative results of PSAs with varying MDO content. Based on commercial PSAs[38,45] and our previous lab-made adhesives[38,46] the tack and shear adhesion values were within an acceptable range; however, the peel strength was low. The initial castability of our PSA was low due to the low solids content in the latexes, necessitating the addition of a wetting agent to improve film formation (see Appendix II). Without the wetting agent, it was challenging to form a uniform film. Once the wetting agent was added, uniform films were produced. The addition of a wetting agent, however, can lead to poorer PSA performance.[25] The inclusion of 5.5 and 10 wt.% MDO did not significantly alter the tack and peel strength, indicating a threshold effect on the influence of MDO. However, when the concentration was increased to 15 and 20 wt.%, there was a decrease in tack and peel strength. Shear adhesion was found to decrease with the addition of MDO at 5 wt.% initially but increased with further increases in MDO concentration. The decline in tack and peel strength with higher MDO content can be attributed to the increased stiffness of the adhesive film, which diminished its ability to effectively wet and bond to surfaces.[25] Thus, the effect was due to the increase in T_g (Table 5.2) at higher MDO levels, reflecting the augmented rigidity of the polymer matrix. The increased T_g also contributed to the increased shear adhesion.

Table 5.3. PSA properties of dried cast films

Latex ID	Tack (N/m)	Peel strength (N/m)	Shear adhesion (h)
BV	210 ± 15	49 ± 7	3 ± 1
BMV5	208 ± 11	49 ± 6	2.2 ± 0.5
BMV10	210 ± 10	47 ± 7	2.8 ± 1
BMV15	190 ± 10	25 ± 5	3.2 ± 1
BMV20	175 ± 9	25 ± 5	4 ± 1.2

To mitigate MDO ring retention and enhance PSA properties without causing MDO hydrolysis, an additional run was conducted by increasing the polymerization temperature to 50 °C. The solids content was increased to 45 wt.% to decrease the possibility of MDO hydrolysis.[21] Finally, a cCNC suspension was added to the final latex via blending to improve the PSA properties.[38,45,46] For the additional run, the polymer composition of terpolymer BMV10 was used. The research literature suggests that adding 5–10 mol% MDO to the polymer backbone is a practical starting point for achieving biodegradation.[14] The new BMV10 terpolymer latex (i.e., BMV10-NEW) had a solids content of ~45 wt.% before adding the cCNC suspension, while it decreased to ~38 wt.% after the cCNC suspension was added. Monomer conversion was almost 97 wt.%. However, due to the increased solids content, the polymer particle size increased by ~130 nm to 280 nm (see Appendix II for more details). Based on the ^{1}H-NMR results (see Appendix II), the MDO content was 8.5 mol%, and our ^{1}H-NMR calculations indicated approximately 9 mol% of the MDO was retained in its ring structure. However, the ^{13}C-NMR results did not show any peak at 100 ppm. As shown in the ^{13}C-NMR spectrum in Figure 5.6, there was no peak at 100 ppm, indicating that no MDO ring retention was detectable. Additionally, DSC results showed a decreased terpolymer T_g from -47.25 °C (for the original BMV10) to -52.6 °C, which aligns with the MDO predominantly undergoing ring-opening polymerization.

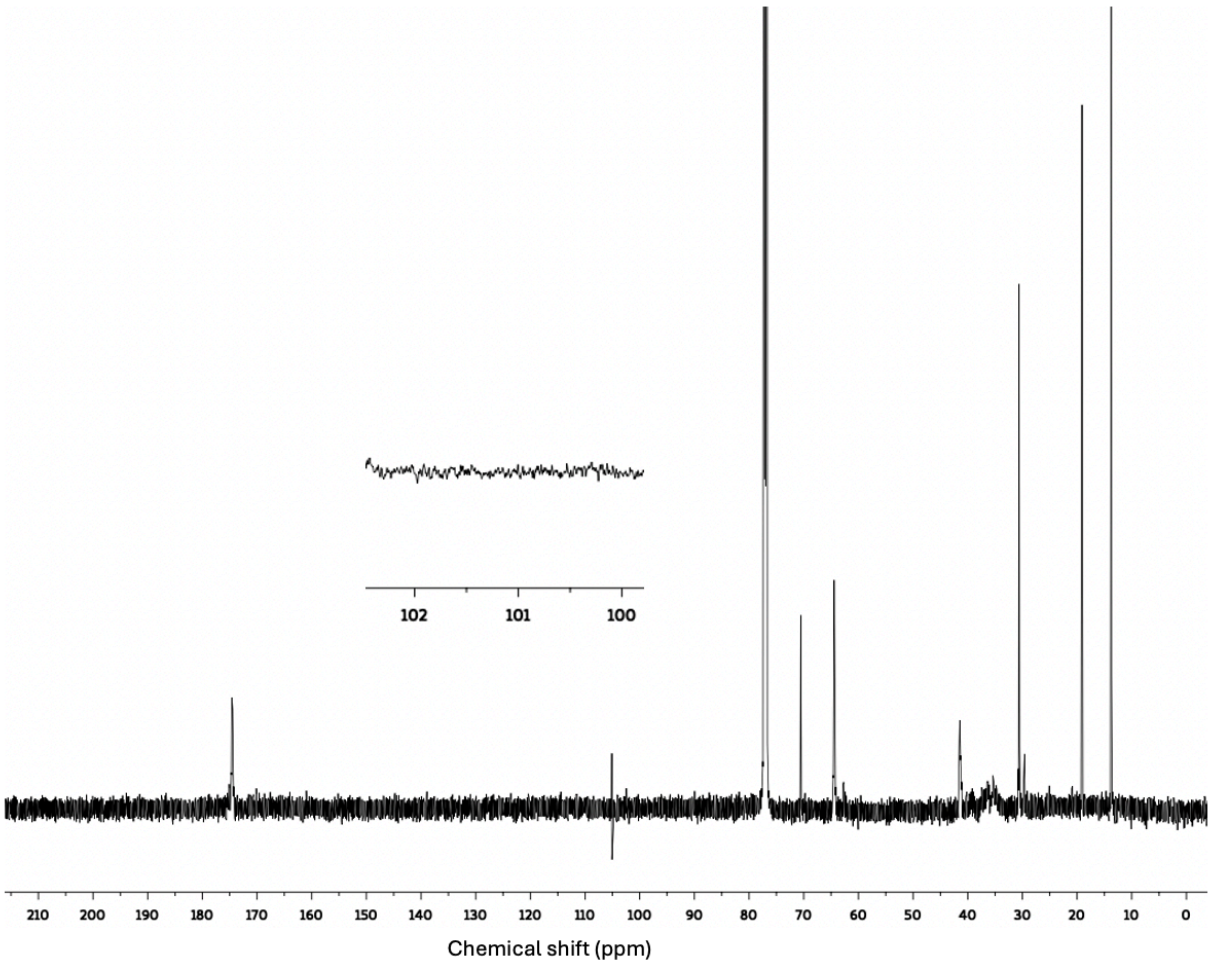

Figure 5.6. ^{13}C-NMR spectrum for BMV10-NEW in $CDCl_3$. This result is without the addition of cCNCs. The peak at 105 ppm is a narrow artifact observed in our ^{13}C-NMR results using the AVIII600 NMR instrument.

As noted above, 2.5 wt.% of a never-dried cCNC suspension in water was added to the latex at the end of the polymerization via blending to further enhance the PSA properties. The never-dried cCNC suspension (6.6 wt.%) was diluted in DDW to 2.5 wt.%, mixed for about 5 minutes with a magnetic stir bar, and then ultrasonicated before being added to the BMV10-NEW latex. Probe ultrasonication of the cCNC suspension was performed in an ice bath using a Fisher Scientific 550 sonic dismembrator at 75% amplitude for three intervals of 5 minutes, with 5-minute rest periods in between. The cCNC suspension was blended into the latex in the reactor at the polymerization temperature (50°C) at a reactor mixing speed of 300 rpm. According to our previous work, these blending conditions are optimal for simultaneously enhancing all PSA

properties.[45] Because of the addition of the water from the cCNC suspension, the final solids content prior to film casting was comparable to the previous runs; the dried film thicknesses were measured and shown to be the same. The BMV10-NEW-cCNC dried latex films showed no deficiencies, were smooth and free of holes, and no wetting agent was needed (see Appendix II). Table 5.4 presents the PSA properties after adding the cCNCs. All PSA properties increased simultaneously after polymerizing at 50ºC and adding the cCNCs, with peel strength and shear adhesion increasing by a factor of almost 2 compared to the original BMV10 latex films.

Table 5.4. PSA properties of the cast films

Latex ID	Tack (N/m)	Peel strength (N/m)	Shear adhesion (h)
BMV10	210 ± 10	47 ± 7	2.8 ± 1
BMV10-NEW-cCNC[a]	280 ± 15	120 ± 10	6.2 ± 1.5

[a] BMV10-NEW-cCNC represents the new BMV10 run incorporating cCNC.

5.5 Conclusions

The synthesis and characterization of BA/MDO/VAc emulsion terpolymers, focusing on the innovative use of MDO in emulsion polymerization for PSA applications, has been demonstrated. By increasing the polymerization temperature to 50 °C and optimizing the solids content, we effectively promoted MDO ring-opening while controlling hydrolysis. Water suppression, ^{1}H-NMR spectroscopy, high monomer conversion levels, and the polymer composition led us to conclude that MDO hydrolysis was minimized if it was present. In addition, the DSC and ^{13}C-NMR spectroscopy confirmed the successful incorporation of MDO with no ring retention. The ^{1}H-NMR spectroscopy of samples throughout each run showed that a batch polymerization approach was sufficient to enable the even distribution of MDO in the polymer chains. This was not surprising, given the reactivity ratios for this system. The key to controlling MDO hydrolysis was maintaining a pH above neutral in the reaction mixture, minimizing the exposure to water, and using a relatively low reaction temperature. On the other hand, hydrolysis of VAc was a concern (at higher pH), and a sufficiently elevated reaction temperature was necessary to minimize MDO ring retention. The addition of cCNCs enabled the production of PSA films with significantly improved properties, particularly peel strength and shear adhesion. This

study underscores the potential of using bio-based monomers and green chemistry principles to create degradable, high-performance adhesive materials for PSA applications.

5.6 References

[1] M. A. Dubé, V. A. Gabriel, A. S. Pakdel, Y. Zhang, *Can J Chem Eng* 2021, *99*, 31.

[2] T. P. Haider, C. Völker, J. Kramm, K. Landfester, F. R. Wurm, *Ang Chemie Int Ed* 2019, *58*, 50.

[3] T. Iwata, *Ang Chemie Int Ed* 2015, *54*, 3210.

[4] M. Vert, *Biomacromolecules* 2005, *6*, 538.

[5] O. Nuyken, S. Pask, *Polymers (Basel)* 2013, *5*, 361.

[6] S.-P. Hsu, I.-M. Chu, J.-D. Yang, *J Appl Polym Sci* 2012, *125*, 133.

[7] V. Delplace, J. Nicolas, *Nat Chem* 2015, *7*, 771.

[8] A. Tardy, J. Nicolas, D. Gigmes, C. Lefay, Y. Guillaneuf, *Chem Rev* 2017, *117*, 1319.

[9] S. Agarwal, *Polym Chem* 2010, *1*, 953.

[10] C. Hardy, M. E. Levere, G. Kociok-Köhn, A. Buchard, *ACS Macro Lett* 2023, *12*, 1443.

[11] J.-B. Lena, A. W. Jackson, L. R. Chennamaneni, C. T. Wong, F. Lim, Y. Andriani, P. Thoniyot, A. M. Van Herk, *Macromolecules* 2020, *53*, 3994.

[12] F. Wenzel, S. Hamzehlou, L. Pardo, M. Aguirre, J. R. Leiza, *Ind Eng Chem Res* 2021, *60*, 10479.

[13] T. Pesenti, J. Nicolas, *ACS Macro Lett* 2020, *9*, 1812.

[14] M. Movafagh, K. M. Meek, A. J. Scott, A. Penlidis, M. A. Dubé, *Polymers (Basel)* 2024, *16*, 1330.

[15] J. M. Siebert, D. Baumann, A. Zeller, V. Mailänder, K. Landfester, *Macromol Biosci* 2012, *12*, 165.

[16] P. Galanopoulo, N. Gil, D. Gigmes, C. Lefay, Y. Guillaneuf, M. Lages, J. Nicolas, M. Lansalot, F. D'Agosto, *Ang Chemie Int Ed* 2022, *61*.

[17] M. A. Dubé, S. Salehpour, *Macromol React Eng* 2014, *8*, 7.

[18] J. M. Asua, *J Polym Sci A Polym Chem* 2004, *42*, 1025.

[19] C. S. Chern, *Prog Polym Sci* 2006, *31*, 443.

[20] M. C. D. Carter, A. Hejl, S. Woodfin, B. Einsla, M. Janco, J. DeFelippis, R. J. Cooper, R. C. Even, *ACS Macro Lett* 2021, *10*, 591.

[21] B. R. Kordes, L. Ascherl, C. Rüdinger, T. Melchin, S. Agarwal, *Macromolecules* 2023, *56*, 1033.

[22] M. C. D. Carter, A. Hejl, M. Janco, J. DeFelippis, P. Yang, M. Gallagher, Y. Liang, *Macromolecules* 2023, *56*, 5718.

[23] S. R. Mothe, W. Zhao, A. M. van Herk, P. Thoniyot, *Macromolecules* 2024, *57*, 2937.

[24] M. A. Dubé, J. B. P. Soares, A. Penlidis, A. E. Hamielec, *Ind Eng Chem Res* 1997, *36*, 966.

[25] R. Jovanović, M. A. Dubé, *J of Macro Sci, Part C: Polymer Reviews* 2004, *44*, 1.

[26] S. Mapari, S. Mestry, S. T. Mhaske, *Polym Bulletin* 2021, *78*, 4075.

[27] E. P. Chang, *J Adhes* 1997, *60*, 233.

[28] R. J. Young, P. A. Lovell, *Introduction to Polymers*, CRC Press, 2011.

[29] S. Noppalit, A. Simula, L. Billon, J. M. Asua, *ACS Sustain Chem Eng* 2019, *7*, 17990.

[30] S. Bunker, C. Staller, N. Willenbacher, R. Wool, *Int J Adhes Adhes* 2003, *23*, 29.

[31] S. Ren, M. A. Dubé, *Int J Adhes Adhes* 2017, *75*, 132.

[32] P. A. Lovell, F. J. Schork, *Biomacromolecules* 2020, *21*, 4396.

[33] J. Undin, T. Illanes, A. Finne-Wistrand, A.-C. Albertsson, *Polym Chem* 2012, *3*, 1260.

[34] J. Folini, W. Murad, F. Mehner, W. Meier, J. Gaitzsch, *Eur Polym J* 2020, *134*, 109851.

[35] G. Delepierre, O. M. Vanderfleet, E. Niinivaara, B. Zakani, E. D. Cranston, *Langmuir* 2021, *37*, 8393.

[36] G. E. Fonseca, T. F. McKenna, M. A. Dubé, *Chem Eng Sci* 2010, *65*, 2797.

[37] R. Jovanovic, M. A. Dubé, *Can J Chem Eng* 2007, *85*, 341.

[38] P. Bayat, K. M. Meek, M. Movafagh, E. D. Cranston, M. F. Cunningham, P. Champagne, T. Morse, M. V. Kiriakou, S. R. George, M. A. Dubé, *Biomacromolecules* 2024.

[39] S. R. Mothe, L. R. Chennamaneni, J. Tan, F. C. H. Lim, W. Zhao, P. Thoniyot, *Macromol Chem Phys* 2023, *224*.

[40] M. Liu, X. Mao, C. Ye, H. Huang, J. K. Nicholson, J. C. Lindon, *J of Mag Res* 1998, *132*, 125.

[41] M. Piotto, V. Saudek, V. Sklenář, *J Biomol NMR* 1992, *2*, 661.

[42] S. Maji, M. Zheng, S. Agarwal, *Macromol Chem Phys* 2011, *212*, 2573.

[43] Y. Shi, S. Agarwal, *e-Polymers* 2015, *15*, 217.

[44] J. Gao, A. Penlidis, *J of Macro Sci, Part C: Polymer Reviews* 1998, *38*, 651.

[45] M. Movafagh, K. M. Meek, P. Bayat, E. D. Cranston, M. Cunningham, P. Champagne, T. Morse, M. V. Kiriakou, S. George, M. A. Dubé, *Polym Eng Sci* 2024, *64*, 798.
[46] V. A. Gabriel, M. N. Tousignant, S. M. W. Wilson, M. D. M. Faure, E. D. Cranston, M. F. Cunningham, B. H. Lessard, M. A. Dubé, *Macromol React Eng* 2022, *16*, 2100051.

Chapter 6
Assessing the Biodegradability of 2-Methylene-1,3-Dioxepane (MDO)-Based Multicomponent Polymers Under Aerobic Composting Conditions

Maryam Movafagh[1], Vida A. Gabriel[1], Marc A. Dubé[1], Kelly M. Meek[1,2]

[1]Department of Chemical and Biological Engineering, University of Ottawa, Ottawa, ON
[2]Department of Chemical and Materials Engineering, Concordia University, Montreal, QC

This chapter is a manuscript to be submitted to Journal of Applied Polymer Science.

6.1 Abstract

The increasing accumulation of plastic waste in the environment has spurred the development of compostable polymers. Butyl acrylate/vinyl acetate (BA/VAc) copolymer formulations incorporating varying amounts of 2-methylene-1,3-dioxepane (MDO) monomer were subjected to a 60-day composting process, with their biodegradation monitored via CO_2 emissions. The MDO was added to the formulation to provide ester bonds in the polymer backbone to promote their hydrolysis and facilitate the breakdown of the polymer into smaller fragments. A lab-made composting setup based on the ASTM D5338 standard was used to provide continuous monitoring of environmental conditions and CO_2 emissions to track biodegradation. The highest 60-day biodegradation observed was 12.49% for a sample containing ~9 mol% MDO. This contrasted with BA/VAc samples without MDO, which had zero biodegradation. Biodegradation was influenced by the amount of ester groups (i.e., ring-opened MDO content), as well as the polymer gel content. An additional experiment with carboxylated cellulose nanocrystals (cCNCs) in the BA/MDO/VAc formulation was shown to promote even greater biodegradation due to the increased hydrophilicity and improved microbial access provided by the cCNCs. Overall, this study demonstrates that MDO-based formulations, especially those incorporating cCNCs, show promise as environmentally friendly, compostable products in support of a more sustainable polymer industry.

6.2 Introduction

The buildup of plastic waste in the environment has prompted an international effort to address plastic pollution. This has encouraged the rapid development of bio-based and biodegradable polymers.[1] Polymers are described as “bio-based” when their formulation comprises materials from biological sources. Biodegradable polymers are so-named because they can be broken down biologically (i.e., by microorganisms such as bacteria or fungi) and decompose into non-toxic compounds (e.g., water, carbon dioxide (CO_2) and biomass). It should be noted that biodegradable polymers are not necessarily bio-based, nor are bio-based polymers necessarily biodegradable. In addition, it is worth noting that landfill sites function primarily as anaerobic digestion sites, which are not conducive to the aerobic degradation required for many biodegradable polymers.[2] Moreover, while polymer recycling has been effective for many polymer materials, many products, such as flexible films or bags, extensively contaminated plastics, or multilayered and multi-component materials, are not recyclable. Thus, revising the formulations of these materials to incorporate biodegradable moieties and disposing of them through industrial composting is an interesting pathway to more sustainable polymer reaction engineering practice.[3]

Some well-known biodegradable polyesters can be synthesized from biobased chemicals, such as polylactic acid (PLA), or can be produced from petrochemicals, such as poly(caprolactam) and polyvinyl alcohol (PVOH). As noted above, "biodegradation" describes the breakdown of organic compounds by bacteria or fungi.[4] A polymer's inherent molecular structure governs how biodegradable it is. For example, polymers with carbon-based backbones (e.g., poly(ethylene)) are difficult to biodegrade. On the other hand, many polyesters containing oxygen or ester groups in their backbone are easier to biodegrade. Polymer depolymerization and mineralization are the two steps in biodegradation. Depolymerization consists of hydrolysis and oxidation.[5] Hydrolysis results in the breakdown of long polymer chains into shorter, functional oligomers that can eventually be consumed by bacteria.[5,6] Once enough oligomeric fragments have been generated, they are carried into the microorganisms’ cells where they are bio-assimilated and mineralized. Water, salts, new biomass, gases (e.g., CO_2, CH_4, N_2, H_2), and minerals are all by-products of the mineralization process.[5]

Polyesters with hydrolytically labile ester bonds are sensitive to abiotic hydrolysis.[7] The process begins with the hydrolysis of the labile ester bonds, which results in chemical scission and

physical erosion, along with biological activity by enzymes or microorganisms, including bacteria, yeast, and fungi.[8] A class of ringed polymers, cyclic ketene acetals (CKAs), have attracted attention for their possible inclusion in chain-growth polymer formulations, thereby inserting ester groups along the polymer backbone to promote biodegradation.[9,10] For example, the copolymerization of methyl methacrylate (MMA) with 2-methylene-1,3-dioxepane (MDO) yielded polymers with improved hydrolytic degradability.[11] The ester group was reported to undergo transesterification (depolymerization) in the presence of water, resulting in ester bond breakage into carboxyl and hydroxyl group chain ends. The carboxylic acid by-product was shown to quicken the hydrolysis by autocatalysis.[12] Thus, incorporating ester groups into the polymer backbone may lead to increased biodegradation.

Composting is the most popular method for managing biodegradable waste in an aerobic environment. Because aerobic composting generates significantly more heat than anaerobic processes, it is a faster process and requires less supplementary heating. In an oxygen-free environment, the biodegradation process produces digestate and biogas, a mixture of CH_4 (50–65%) and CO_2 (35–50%) with minor amounts of H_2S and other gases.[3] In comparison, in the aerobic process, there is little if any CH_4 in the by-product, which is a more harmful greenhouse gas than CO_2. ASTM D6813 defines composting as the controlled aerobic biological decomposition of organic materials into compost, CO_2, water, and heat.[13,14] Industrial composting is a process where biodegradation occurs under strict controls with specialized temperature and microbe combinations.[15] Temperature is an important factor in controlling microbial activity. The ideal temperature range for window (pile) composting is 40–65°C.[16] For instance, poly-L-lactic acid (PLLA) degrades slowly in landfills, ocean, soil, and home composting environments but does degrade quickly in commercial composting facilities (>60°C).[17] According to ASTM D6400, ISO 17088, and EN 13432, compostable polymers must satisfy three essential requirements: be intrinsically biodegradable; disintegrate in a composting environment without running the risk of ecotoxicity; and fully degrade to CO_2, water, and biomass without leaving any traces of visually detectable residues.[18] It should be emphasized that a biodegradable polymer is not considered compostable if it leaves behind harmful residues. Furthermore, when processed in an industrial composting facility for 180 days, both ASTM D6400 and EN13432 specifications provide a biodegradation rate of >90% of the feedstock.[19] As mentioned earlier, anaerobic digestion is the

dominant process in landfill environments.[20] In this project, we will use an aerobic composting method to degrade the polymers.

Butyl acrylate (BA) and vinyl acetate (VAc) are widely used in water-based adhesive and coating formulations.[21] In adhesive applications, BA imparts flexibility and good wetting properties, enhancing adhesion. VAc, being a high T_g monomer, enhances the cohesive properties of the adhesive, improving its internal strength and resistance to mechanical stress.[21,22] In this work, we are interested in the use of an emulsion polymerization formulation to prepare BA/VAc pressure-sensitive adhesives (PSAs), commonly found in products like sticky notes, labels, and stickers[23] – such as price labels applied to fruit peels. While fruit peels are compostable, their labels can end up in composting bins and contaminate composting systems, as they are not biodegradable. To address the general issue of compostable adhesives, we sought to enhance their biodegradability by incorporating MDO into the formulation. We tested the compostability of BA/MDO/VAc terpolymers with varying MDO content, synthesized in our recent work.[24] We hypothesized that the polymer samples could undergo hydrolysis, starting with the cleavage of the MDO ester bonds, which would break them down into smaller oligomers that could be bioassimilated and mineralized by the microorganisms in the compost. The biodegradability of these terpolymers was assessed in a lab-made composting setup using a design adapted from Aguirre.[25] For the composting method, a modified version of the ASTM D5338[26] standard was used.

6.3 Materials and Methods

6.3.1 Materials

The BA/MDO/VAc polymer samples tested in this study were synthesized via emulsion polymerization in previous work (Table 6.1).[24] The organic compost (aka inoculum) was commercially sourced from Miracle-Gro, a supplier of natural compost derived from decomposed plant matter, food scraps, and yard waste. The compost had a dark, crumbly texture and a rich, earthy aroma. The moisture content of the compost was measured at 65% relative humidity, and the pH was approximately 6.8, determined using a dual-channel pH meter (Fisher Scientific/Accumet Research, model AR50). The pH measurement was conducted by preparing a slurry of the compost, mixing one part compost with two parts distilled, de-ionized water. For the control materials, starch powder (purchased from Sigma Aldrich) was used as the positive control,

while moisture-resistant HDPE pellets from McMaster-Carr served as the negative control. Compressed gas cylinders were purchased from Messer and included one CO_2-free air cylinder and one containing air with 400 ppm CO_2.

Table 6.1. Composition of Polymer Samples

Sample	Terpolymer Composition (BA/MDO/VAc) (mol%)	Terpolymer Composition (BA/MDO/VAc) (wt.%)	Ring-opened MDO in terpolymer (mol%)
BV	93.12/00.00/6.88	95.27/00.00/4.72	-
BMV5	87.05/4.85/6.10	91.18/4.2/4.29	3.54
BMV10	84.22/9.98/5.80	86.82/9.16/4.01	7.39
BMV15	80.51/14.10/5.39	83.26/12.98/3.74	9.87
BMV20	74.88/20.36/4.76	77.89/18.52/3.57	14.25
BMV10-NEW-cCNC*	84.98/8.90/6.12	87.93/7.82/4.23	8.09

*BMV10-NEW-cCNC contains 0.75 parts per hundred parts monomer (phm) cCNCs. In addition, this sample was produced under conditions that promoted more ring-opening polymerization.[24]

6.3.2 Methods

6.3.2.1 Composting Set-up

A series of 15 bioreactors was designed and built to simulate the enclosed aerated static pile commonly used in municipal composting facilities to measure aerobic degradation based on the ASTM D5338 standard (Figure 6.1). The design was adapted from Aguirre[25] and a detailed layout and description are provided in the Appendix III. The apparatus includes sensors, a temperature control bath, and a ventilation system. A multi-part lid was added to the water bath to minimize water evaporation, ensuring stable thermal conditions and reducing the need for frequent refilling. A water tap was included for easy filling and draining. Thermophilic conditions (60 ± 2°C) were maintained using a Thermo Scientific™ SC100 Immersion Circulator, which provided precise temperature control across all 15 bioreactors, which were immersed in the water bath (Figure 6.1). A LabVIEW-based data acquisition system was developed to automate sensor communication, measuring temperature, relative humidity, and CO_2 concentrations (measured in

ppm) throughout the experiments using Sensirion SCD30 sensors. This system ensured accurate and consistent data collection to infer the degree and rate of aerobic degradation via CO_2 emissions.

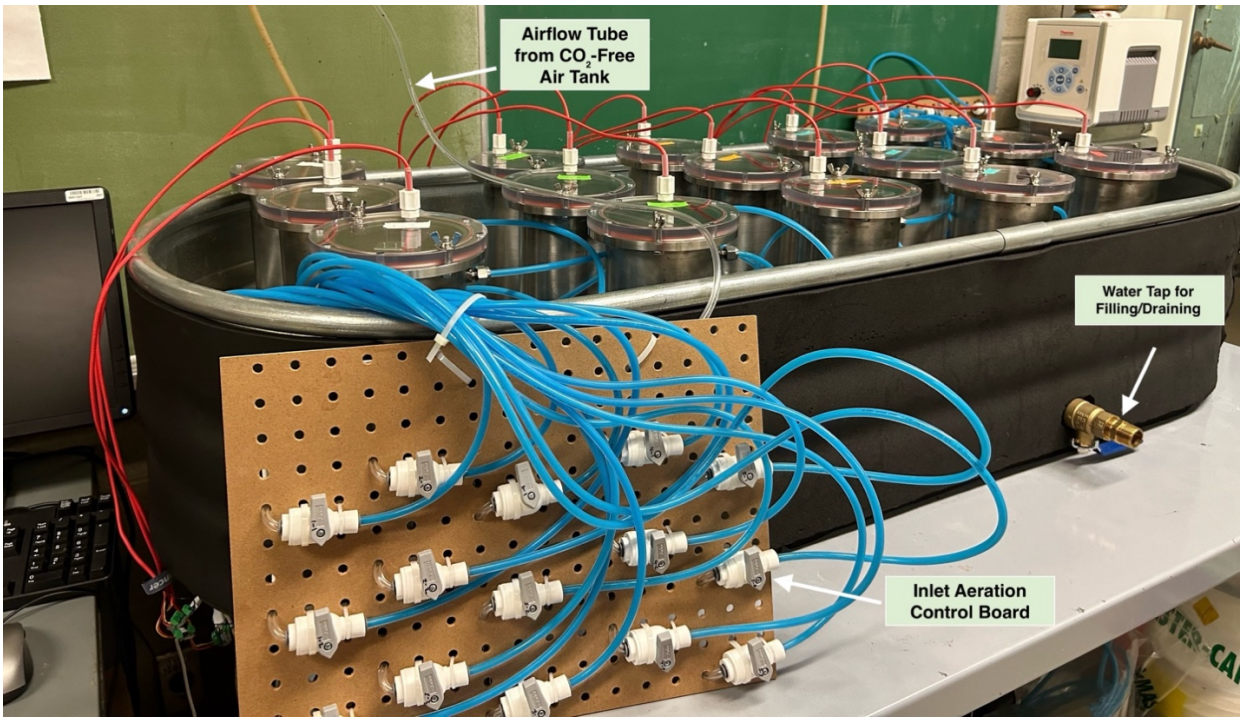

Figure 6.1. Composting setup with 15 bioreactors submerged in a water bath controlled by an immersion circulator to maintain a consistent temperature. Airflow is regulated via an aeration control board with 15 valves connected to polyethylene tubes, either CO_2-free air or standard 400 ppm CO_2 air (for calibration) to each bioreactor.

The CO_2 sensors were calibrated using a certified 400 ppm CO_2-air tank (Messer) through a 10-minute CO_2 purging process to ensure accurate and reliable measurements throughout the study. The sensors were connected to an Arduino microcontroller, enabling real-time monitoring and adjustment of sensor outputs. Using Arduino code, the sensor readings were compared to the reference concentration, and necessary adjustments were made to correct for any sensor drift or inaccuracies. This calibration process was performed before each experiment and periodically throughout the study to ensure consistency in CO_2 measurements.

Test samples, consisting of latex polymers (Table 6.1), were poured into silicone molds to create granules matching the shape of polyethylene granules used as the negative control. The samples were dried for two weeks under a fume hood to ensure they were free of residual water before testing.

6.3.2.2 Experimental Conditions Using Adapted ASTM D5338-15

This study followed ASTM D5338-15 to evaluate the aerobic biodegradability of plastic materials under thermophilic conditions. The method measures the percentage of carbon converted to CO_2 and monitors biodegradation rates, applicable to various plastic types for industrial composting. The 15 bioreactors were allocated as three blanks (i.e., containing inoculum only), three positive controls (i.e., containing inoculum and starch), three negative controls (i.e., containing inoculum and polyethylene), and the remaining reactors containing inoculum and samples in triplicate. Averages of each set of three bioreactors were used in the calculations. The inoculum was sieved through a 10 mm mesh, added in equal amounts (~700 g) to each bioreactor, and mixed with 25 g of dried sample or starch or polyethylene, except the blank. The bioreactors were run for approximately 60 days. Continuous O_2 purging was applied to support microbial activity and ensure optimal conditions for biodegradation. The bioreactor temperatures were maintained at 58 ±2°C and 70% relative humidity. This study incorporated two key modifications to ASTM D5338-15: (1) CO_2 measurement using SCD30 sensors instead of $Ba(OH)_2$ titration for real-time monitoring, and (2) omission of bioreactor mass measurements due to the high weight of the bioreactors relative to the samples.

6.3.2.3 Biodegradation Analysis

The degree of biodegradation was calculated by measuring CO_2 emissions from the bioreactors in ppm using a Sensirion SCD30 sensor, and was converted to moles of CO_2 (n_{CO_2}) using the ideal gas law:

$$n_{CO_2} = PV_{CO_2}/RT \quad (6.1)$$

where P is the pressure (assumed to be atmospheric, 1 atm), V_{CO2} is the CO_2 volume, n_{CO2} is the number of moles of CO_2, R is the universal gas constant, and T is the absolute temperature in Kelvin. For this study, the temperature was maintained at 58 ±2°C (333 K). For the given conditions and a gas mixture dominated by N_2, O_2, and CO_2, the compressibility factor (z) is 1.00, confirming ideal gas behaviour. The measured CO_2 concentration (ppm) was converted to volume using the following relationship:

$$V_{CO_2} = CO_2 \text{ Concentration (ppm)} \times V_{gas}/10^6 \quad (6.2)$$

where the CO_2 concentration was measured by the sensor, and V_{gas} is the headspace volume. The headspace volume of the bioreactor was calculated as the difference between the total reactor

volume (3.1 L) and the inoculum volume (1.0 L), resulting in a headspace volume of 2.1 L. The moles of CO_2 (Equation 1) were converted to mass (m_{CO_2}) using the molar mass of CO_2 (44 g/mol) and further converted to the mass of carbon (m_C) using the fraction of carbon in CO_2:

$$m_C = m_{CO_2} \times 12/44 \quad (6.3)$$

To isolate the contribution of the polymer ($m_{C,polymer}$) to the total CO_2 emissions (m_C, Equation 3) the CO_2 mass from the blank ($m_{C,inoculum}$) was subtracted from the measured values:

$$m_{C,polymer} = m_C - m_{C,inoculum} \quad (6.4)$$

The biodegradation percentage of the polymer was calculated by relating the carbon in the polymer-derived CO_2 emissions to the total theoretical carbon content ($m_{C,theor}$) in the polymer sample:

$$\text{Biodegradation (\%)} = (m_{C,polymer}/m_{C,theor}) \times 100 \quad (6.5)$$

The carbon content of the BA/MDO/VAc terpolymer samples and the starch positive control is shown in Table 6.2. The terpolymer compositions measured by ^{1}H-NMR spectroscopy were shown earlier in Table 6.1. For each bioreactor, a 25 g sample was added for treatment.

Table 6.2. Theoretical carbon ($m_{C,theor}$) content for 25 g composting samples

Sample	Carbon Content (g)
BV	16.75
BMV5	16.71
BMV10	16.67
BMV15	16.64
BMV20	16.58
BMV10-NEW-cCNC*	16.76
Starch	11.01

*There was 0.75 phm cCNC in this sample. In this sample, 0.0825 g of carbon was attributed to the cCNC component.

6.3.2.4 Thermogravimetric Analysis (TGA)

Thermogravimetric analysis (TGA) coupled with Fourier Transform Infrared Spectroscopy (FTIR) was conducted to examine the thermal degradation behaviour of BMV10-NEW-cCNC and BMV20 before and after composting. Initially, the samples were completely dried at 50°C in an

oven. TGA platinum pans were torched and tared using the TGA 550 (TA Instruments), and the samples were placed on the prepared pans for testing. The TGA system was coupled with an FTIR spectrometer (Thermo Fisher Scientific, Nicolet iS50 FTIR), which was directly connected to the TGA unit to analyze the evolved gases in real time during the thermal degradation process. The off-gases generated during sample degradation were carried through a gas flow system to the FTIR spectrometer, where they were monitored and analyzed. The FTIR spectrometer was equipped with a heated gas cell, enabling accurate detection of evolved gaseous components such as CO_2, H_2O, and other volatile organic compounds.

6.3.2.5 Attenuated Total Reflectance Fourier Transform Infrared (ATR-FTIR) Spectroscopy

The Agilent Cary 630 FTIR spectrometer (Agilent Technologies, Santa Clara CA, USA), equipped with an ATR diamond crystal interface, was used to determine the molecular structure of BMV10-NEW-cCNC and BMV20 before and after composting. The analysis was performed at a resolution of 16 cm^{-1} over a range of wavenumbers from 650 to 4000 cm^{-1}, using MicroLab Expert software.

6.4 Results and Discussion

During the composting experiments, the CO_2 emissions were continuously monitored using LabVIEW software, which recorded CO_2 concentrations in the bioreactors' headspace every 25 seconds via SCD30 sensors. The data for each bioreactor were saved daily as separate Excel files, generating large datasets. To facilitate analysis, the data were processed, and cumulative CO_2 emissions were calculated for 5-day intervals (i.e., a total of 12 data points per bioreactor). Table 6.3 illustrates the cumulative CO_2 emissions and biodegradation percentage for the positive (starch) and negative (HDPE) controls and each polymer sample. The CO_2 emissions for the inoculum (blank) were subtracted from each measurement. The experimental setup followed the adapted ASTM D5338-15 noted earlier, which recommends calculating average CO_2 emissions across three bioreactors for each sample type. However, in certain cases (i.e., for BV, BMV10, BMV15, BMV20, and the positive control), the results were based on two bioreactors due to sensor calibration issues for the third bioreactor. For the inoculum and starch, high CO_2 emissions were measured, as expected, due to a high level of biodegradation. Based on the average CO_2 emissions,

83.69% of the starch positive control biodegraded over the 60-day period. The negative control and the BV copolymer had essentially zero biodegradation.

Table 6.3. Cumulative net CO_2 emissions and final biodegradation percentages after the 60-day composting period.

Sample ID	Cumulative CO_2 Emissions ($\times 10^6$ ppm)	Final Biodegradation (%)
Positive Control (Starch)	10.0500	83.69
Negative Control (HDPE)	0.0012	~ 0
BMV10-NEW-cCNC	2.2800	12.49
BMV20	1.9650	10.83
BMV15	1.5980	8.85
BMV10	0.2100	1.16
BMV5	0.0030	~ 0
BV	0.0018	~ 0

*Blank (inoculum only) generated 11.12 x 10^6 ppm cumulative CO_2 emissions. These were subtracted from each sample.

Figure 6.2 shows the cumulative CO_2 emissions over the 60-day composting period, where all BMV samples exhibited a significant lag in biodegradation. This delay can be attributed to several factors, including microbial adaptation[27] and crosslinking[28] in the polymer samples. In the early stages of composting, the microbial community requires time to acclimatize to the polymer material. This adaptation phase involves microbial colonization, enzyme production for degradation, and the establishment of a robust microbial biomass.[29] The polymer samples had similar high gel contents (~55 wt%). The crosslinked structure of the polymers indicates that a significant fraction of the polymer network was chemically restricted from undergoing hydrolytic cleavage or microbial assimilation. This structural rigidity reduced the mobility of the polymer chains and restricted enzymatic access, further hindering biodegradation. This, combined with the microbial adaptation phase, slowed down the overall degradation process. Consequently, measurable CO_2 emissions were delayed, resulting in the initial lag phase. For most of the BMV samples, inflection points were observed where CO_2 emissions began to increase after a certain time period. BMV20, BMV10-NEW-cCNC, and BMV15 showed an inflection point around 15 days, while BMV10 showed an inflection point around 20 days, and BMV5 showed minimal CO_2

emissions throughout the composting period. In contrast, the starch positive control did not exhibit this lag phase, and its biodegradation rate was significantly higher. Starch's simpler molecular structure, composed of glucose units linked by easily hydrolyzable glycosidic bonds, makes it more readily accessible to microbial enzymes, promoting faster biodegradation compared to the more complex synthetic BMV samples, which require longer microbial adaptation and enzymatic breakdown.

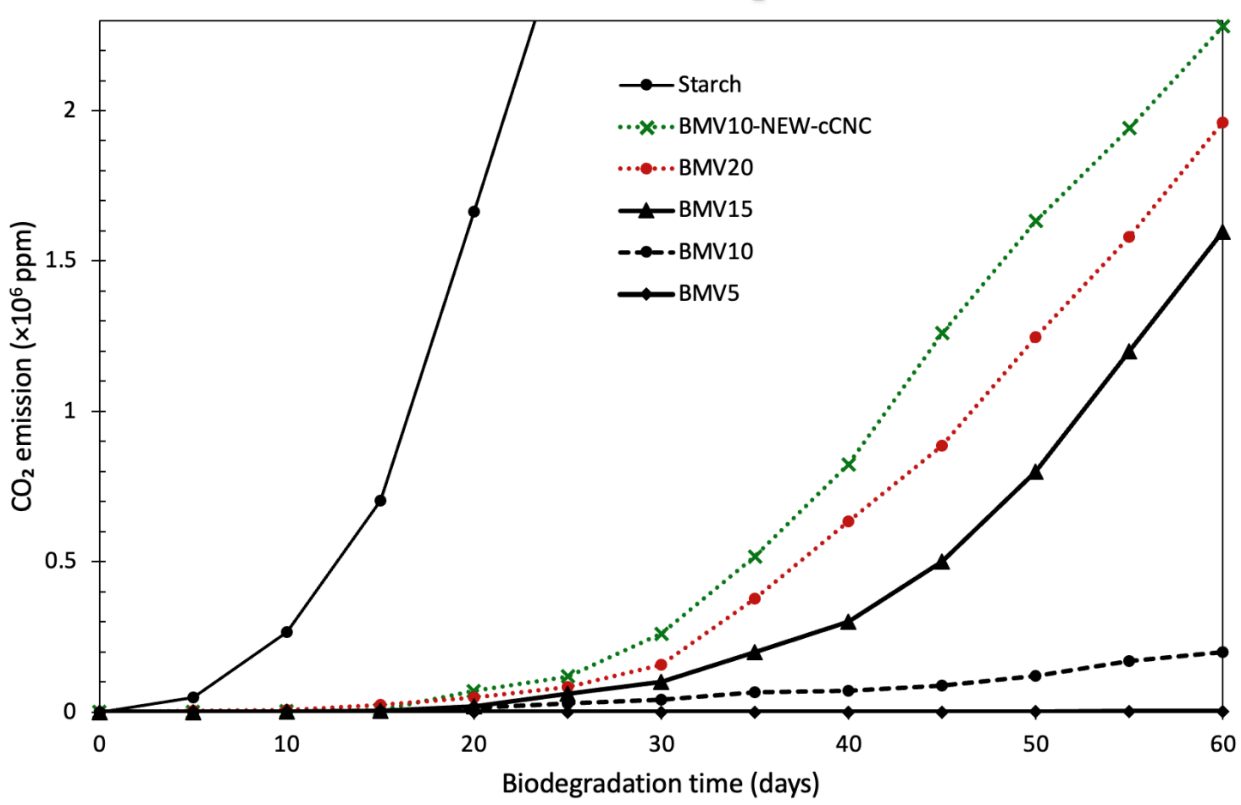

Figure 6.2. Cumulative CO_2 emissions over 60 days.

With increasing MDO content (from BMV5 to BMV20), increasing amounts of biodegradation were measured (Table 6.3, Figure 6.2). This supports the hypothesis that more oxygen in the polymer backbone will lead to greater levels of biodegradation. However, BMV10-NEW-cCNC demonstrated the highest amount of biodegradation. As noted earlier (Table 6.1), BMV10-NEW-cCNC was produced at conditions promoting significantly greater ring-opening polymerization of the MDO monomer.[24] As shown in our previous work, BMV10-NEW-cCNC had roughly 8.09 mol% ring-opened MDO in the terpolymer with very low ring-retained MDO present (see also Table 6.1). All other samples (i.e., BMV5 through BMV20) were considered to

have significant levels of ring-retained MDO. Thus, based solely on the amount of ring-opened MDO in the terpolymers, BMV10-NEW-cCNC would be expected to biodegrade in amounts somewhere between BMV10 and BMV15. However, there was another factor potentially contributing to the biodegradation: the addition of cCNCs. While the amount of cCNCs in the formulation was low, the biodegradation of the cCNCs themselves would not be expected to contribute to the additional amounts of CO_2 generated. It is likely that the dispersion of the nanomaterials throughout the terpolymer matrix enabled greater permeation of the sample by the microorganisms, thereby enhancing the level of biodegradation. In addition, the hydrophilicity of the cCNCs encouraged hydrolysis of the polymer, consistent with findings elsewhere.[30–33] The lower CO_2 emissions, particularly for BV and BMV5, suggest that a minimum amount of ring-opened MDO would be necessary to initiate biodegradation.[24]

Figure 6.3 presents the TGA results for BMV10-NEW-cCNC and BMV20 before and after composting. The trends for both samples were similar. Before composting, both exhibited thermal degradation at lower temperatures, between 260 and 360°C, due to the presence of unstable ester bonds in the MDO components. After composting, the small transition peak between 260 and 360°C was absent, indicating the degradation of these unstable bonds during composting. Additionally, both samples showed higher weight loss after composting (~4%), suggesting that the composting process led to a decrease in the molecular weight of the polymers by breaking down the polymer backbone. There was no significant difference in thermal degradation behaviour between BMV10-NEW-cCNC and BMV20, although, after composting, the BMV20 sample showed a degradation peak transition at a slightly higher temperature (approximately 2°C higher), consistent with the slight difference in biodegradation (Table 6.3).

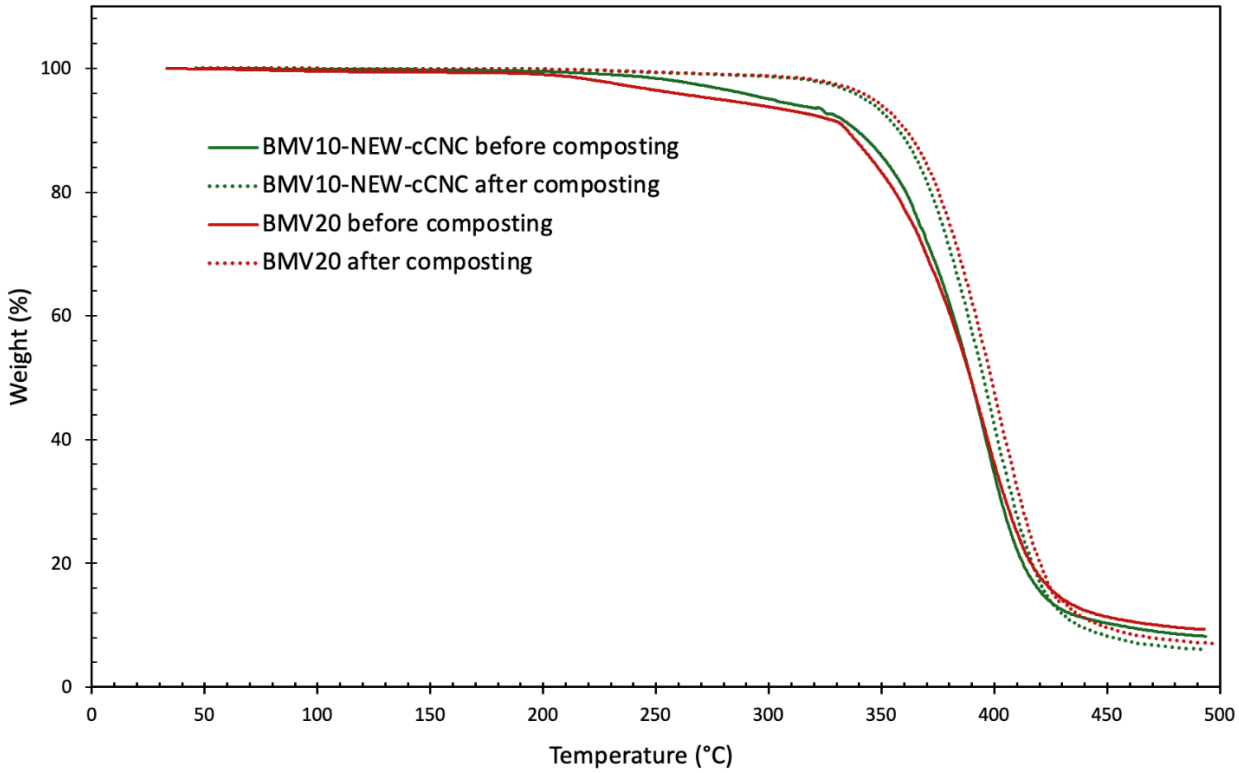

Figure 6.3. TGA curves showing the weight loss as a function of temperature for BMV10-NEW-cCNC (green) and BMV20 (red), before (solid lines) and after (dashed lines) composting.

The ATR-FTIR spectra of BMV10-NEW-cCNC and BMV20 before and after composting were similar, with the main difference occurring in the OH stretch region (between 3000 and 3500 cm^{-1}), which is indicative of the formation of hydroxyl groups due to the hydrolysis of ester bonds (Figure 6.4).[35] For BMV20 before composting, the ATR-FTIR spectrum in the 3000–3500 cm^{-1} region appeared as a straight line, suggesting no hydroxyl group formation. In contrast, for BMV10-NEW-cCNC, there was a slight curve in this region before composting, which can be attributed to the presence of hydroxyl groups, primarily due to the cCNC component. After composting, both BMV10-NEW-cCNC and BMV20 exhibited a more distinct curve in the 3000–3500 cm^{-1} region, reflecting an increase in hydroxyl group formation due to ester bond hydrolysis during the composting process.

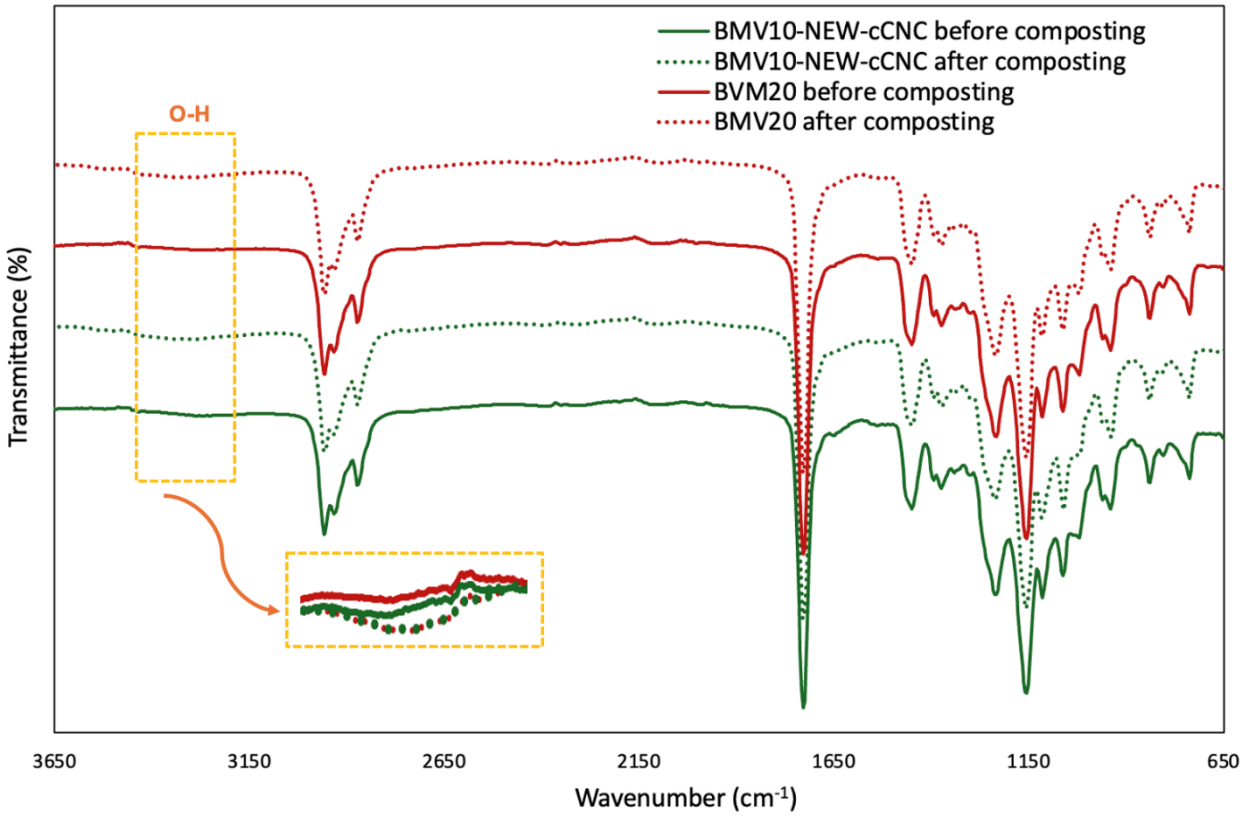

Figure 6.4. ATR-FTIR spectra of BMV10-NEW-cCNC (green) and BMV20 (red) before (solid lines) and after (dashed lines) composting, highlighting the O-H group in all four samples. Inset shows curves in the range of interest overlapped for comparison.

During the 60-day composting process, the samples exhibited reduced flexibility, diminished ductility, and a noticeable whitening (Figure 6.5). These changes were due to the hydrolysis of ester bonds in the MDO units, resulting in shorter polymer chains and a disrupted network, which reduced elasticity. The whitening was attributed to water absorption during composting, altering the material's surface and facilitating hydrolysis. These physical changes, coupled with CO_2 emissions data, confirm the material's degradation under composting conditions, supporting its promise for compostable applications.

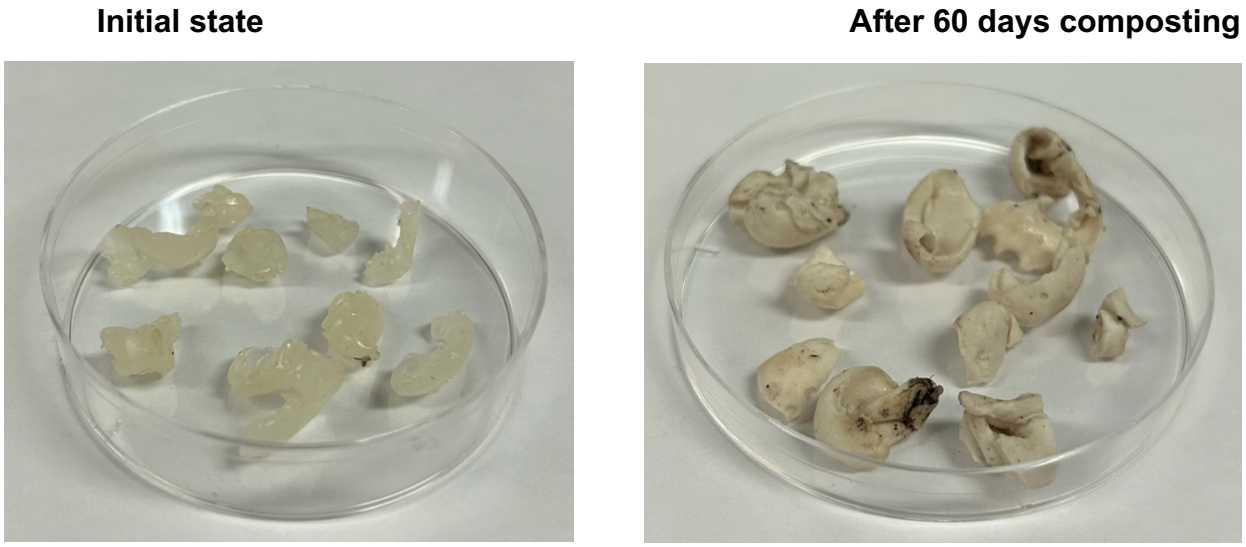

Figure 6.5. Visual comparison of BMV10-NEW-CNC before and after 60 days of composting

6.5 Conclusion

This study assessed the biodegradability of MDO-based multicomponent polymers under aerobic composting conditions. The experimental setup, which included a lab-made composting system based on the ASTM D5338 standard, allowed for precise and continuous monitoring of CO_2 emissions, providing a clear measure of biodegradation. This setup ensured that environmental conditions, such as temperature, humidity, and CO_2 concentrations, were optimal for evaluating biodegradation.

The results indicate that incorporating MDO into the polymer matrix enhances biodegradability by promoting the hydrolysis of ester bonds, which leads to the formation of oligomeric byproducts that can be assimilated by microorganisms. The highest biodegradation observed among the polymer samples was for BMV10-NEW-cCNC (12.49%) over a 60-day period. This study highlights the important role of ester groups in promoting biodegradation. The importance of incorporating the MDO through a ring-opening polymerization as opposed to ring-retained was also demonstrated. In addition, the incorporation of cCNCs into the formulation significantly improved biodegradation. The presence of cCNCs increased the polymer's hydrophilicity, providing greater accessibility for microbial degradation and enhancing the overall hydrolysis of the polymer chains. While biodegradation was observed in most samples, the presence of high gel content and crosslinking hindered degradation.

Overall, the incorporation of MDO into polymer formulations proved beneficial for enhancing biodegradation under aerobic composting conditions. Moreover, the inclusion of cCNCs could further enhance biodegradation by improving microbial access and promoting hydrolysis. These findings support the potential of MDO-based formulations, especially those containing cCNCs, as environmentally friendly, compostable polymer products for various applications.

6.6 References

[1] A. Folino, A. Karageorgiou, P. S. Calabrò, D. Komilis, *Sustainability* 2020, *12*, 6030.

[2] P. S. Calabrò, M. Grosso, *Waste Manag* 2018, *78*, 800.

[3] P. K. Samantaray, A. Little, A. M. Wemyss, E. Iacovidou, C. Wan, *ACS Sustain Chem Eng* 2021, *9*, 9151.

[4] ISO 17088, Specifications for compostable plastics 2012.

[5] S. Grima, V. Bellon-Maurel, P. Feuilloley, F. Silvestre, *J Polym Environ* 2000, *8*, 183.

[6] K. de Smit, Y. W. Marien, K. M. van Geem, P. H. M. van Steenberge, D. R. D'hooge, *React Chem Eng* 2020, *5*, 1909.

[7] L. S. Nair, C. T. Laurencin, *Prog Polym Sci* 2007, *32*, 762.

[8] A. Bher, P. C. Mayekar, R. A. Auras, C. E. Schvezov, *Int J Mol Sci* 2022, *23*, 12165.

[9] A. Calderón-Díaz, A. C. Boggiano, W. Xiong, N. Kaiser, W. R. Gutekunst, *ACS Macro Lett* 2024, *13*, 1390.

[10] M. Movafagh, K. M. Meek, A. J. Scott, A. Penlidis, M. A. Dubé, *Polymers (Basel)* 2024, *16*, 1330.

[11] J. Undin, A. Finne-Wistrand, A.-C. Albertsson, *Biomacromolecules* 2013, *14*, 2095.

[12] B. R. Kordes, L. Ascherl, C. Rüdinger, T. Melchin, S. Agarwal, *Macromolecules* 2023, *56*, 1033.

[13] M. Pergola, A. Persiani, A. M. Palese, V. Di Meo, V. Pastore, C. D'Adamo, G. Celano, *Applied Soil Eco* 2018, *123*, 744.

[14] M. S. Kim, H. Chang, L. Zheng, Q. Yan, B. F. Pfleger, J. Klier, K. Nelson, E. L.-W. Majumder, G. W. Huber, *Chem Reviews* 2023 *123* (16), 9915.

[15] S. Gajalakshmi, S. A. Abbasi, *Crit Rev Environ Sci Technol* 2008, *38*, 311.

[16] B. G. Hermann, L. Debeer, B. De Wilde, K. Blok, M. K. Patel, *Polym Degrad Stab* 2011, 96, 1159.

[17] J. J. Kolstad, E. T. H. Vink, B. de Wilde, L. Debeer, *Polym Degrad Stab* 2012, *97*, 1131.

[18] M. Avella, E. Bonadies, E. Martuscelli, R. Rimedio, *Polym Test* 2001, *20*, 517.

[19] P. K. Samantaray, A. Little, A. M. Wemyss, E. Iacovidou, C. Wan, *ACS Sustain Chem Eng* 2021, *9*, 9151.

[20] P. S. Calabro', A. Folino, F. Fazzino, D. Komilis, *J Hazard Mater* 2020, *390*, 121653.

[21] R. Jovanović, M. A. Dubé, *Ind Eng Chem Res* 2005, *44*, 6668.

[22] R. Jovanović, M. A. Dubé, *J of Macro Sci, Part C: Polymer Reviews* 2004, *44*, 1.

[23] I. Benedek, L. J. Heymans, *Pressure-Sensitive Adhesives Technology*, Marcel Dekker Inc., New York, 1997.

[24] M. Movafagh, K. M. Meek, M. A. Dubé, *ChemSusChem* 2025, e202402478.

[25] E. Castro Aguirre, *Design and Construction of a Medium-scale Automated Direct Measurement Respirometric System to Assess Aerobic Biodegradation of Polymers*, Master's Thesis, *Michigan State University*, 2013.

[26] ASTM D5338-15: Standard Test Method for Determining Aerobic Biodegradation of Plastic Materials Under Controlled Composting Conditions, Conditions, Incorporating Thermophilic Temperatures 2015.

[27] N. Mohanan, Z. Montazer, P. K. Sharma, D. B. Levin, *Front Microbiol* 2020, *11*.

[28] M. Żenkiewicz, R. Malinowski, P. Rytlewski, A. Richert, W. Sikorska, K. Krasowska, *Polym Test* 2012, *31*, 83.

[29] F. Degli-Innocenti, M. Barbale, S. Chinaglia, E. Esposito, M. Pecchiari, F. Razza, M. Tosin, *Polym Degrad Stab* 2022, *199*, 109934.

[30] P. Bayat, K. M. Meek, M. Movafagh, E. D. Cranston, M. F. Cunningham, P. Champagne, T. Morse, M. V. Kiriakou, S. R. George, M. A. Dubé, *Biomacromolecules* 2024.

[31] I. Seoane, L. Manfredi, V. Cyras, L. Torre, E. Fortunati, D. Puglia, *Polymers (Basel)* 2017, *9*, 561.

[32] S. Parajuli, O. Alazzam, M. Wang, L. C. Mota, S. Adhikari, D. Wicks, E. E. Ureña-Benavides, *Colloids Surf A Physicochem Eng Asp* 2020, *596*, 124705.

[33] M. Movafagh, K. M. Meek, P. Bayat, E. D. Cranston, M. Cunningham, P. Champagne, T. Morse, M. Kiriakou, S. George, M. A. Dubé, *Polym Eng Sci* 2024, *64*, 798.

[34] M. Ghorbani, E. Prince, *Biomacromolecules* 2025, *26*, 118.

[35] A. Leroy, S. Ribeiro, C. Grossiord, A. Alves, R. H. Vestberg, V. Salles, C. Brunon, K. Gritsch, B. Grosgogeat, Y. Bayon, *J Mater Sci Mater Med* 2017, *28*, 87.

Chapter 7
General Discussion and Conclusion

7.1 General discussion

The primary objective of this research was to develop sustainable pressure-sensitive adhesives (PSAs) by incorporating bio-based monomers and additives using emulsion (water-based) polymerization. By optimizing monomer selection and reaction conditions, and using bio-based nanoparticle incorporation, this study achieved a balance between adhesive performance and environmental sustainability while ensuring favourable end-of-life characteristics and industrial feasibility.

7.2 Sustainability and Performance Considerations in PSAs

PSAs play a crucial role in applications spanning packaging, medical devices, automotive, and industrial tapes. Their ability to form an instant bond under light pressure while enabling clean removability makes them indispensable across industries.[1] PSA performance is defined by three key properties: tack, which determines the adhesive's ability to create an immediate bond; peel strength, which measures resistance to peeling forces; and shear adhesion, which indicates the ability to endure sustained stress. These properties are intrinsically linked to the polymer's microstructure, particularly molecular weight, glass transition temperature (T_g), and viscoelasticity.[2]

To achieve an optimal balance between adhesion and cohesion, PSAs typically require a T_g between -70°C and -20°C, ensuring sufficient softness for adhesion while maintaining structural integrity under stress.[1] However, despite their versatility, most commercial PSAs rely on petroleum-based monomers and additives and solution-based polymerization, raising concerns about their environmental impact. In response, research efforts have increasingly focused on bio-based and degradable PSAs, leading to advancements in polymer composition, synthesis techniques, and end-of-life solutions.[3]

7.2.1 Emulsion-Based PSAs

Emulsion polymerization is a widely used technique for producing PSAs due to its environmental benefits, including low volatile organic compound (VOC) emissions, water-based processing, and ease of scalability. Unlike solution polymerization, where monomers are dissolved in an organic solvent and polymerized in a homogeneous phase, emulsion polymerization occurs in a dispersed system, where monomer droplets are stabilized by surfactants in water.[4] This compartmentalization of radicals leads to the formation of high molecular weight polymers, resulting in enhanced mechanical strength and tunable adhesion properties. Additionally, emulsion-based PSAs offer superior film formation, lower toxicity, and improved stability, making them an attractive choice for environmentally friendly adhesive applications.[5]

Despite these advantages, shear adhesion can be a limiting factor in emulsion-based PSAs, particularly for applications requiring high cohesive strength. In Chapter 3, I investigated a commercial emulsion-based PSA that exhibited low shear strength.[6] To address this, I applied a design of experiments (DOE) approach, specifically a $2^{(n-1)}$ fractional factorial design, to systematically evaluate the impact of incorporating a green nanoparticle (cCNCs) through blending. By optimizing the formulation and processing conditions, I was able to simultaneously improve all three key PSA performance indicators, achieving a balance between adhesion and cohesion in a manner feasible for industrial implementation.

7.2.2 MDO emulsion polymerization for Sustainability and Degradability

The integration of 2-methylene-1,3-dioxepane (MDO) into butyl acrylate (BA)/vinyl acetate (VAc) terpolymers via emulsion polymerization offers a promising pathway toward sustainable and degradable pressure-sensitive adhesives (PSAs). The primary goal of this work was to incorporate backbone-degradable ester linkages within an aqueous polymerization system while addressing key challenges such as monomer distribution, hydrolysis, and ring retention.

Chapter 4 explored the reactivity ratios of BA, VAc, and MDO using the Error-in-Variables Model (EVM), demonstrating that batch polymerization could achieve a uniform distribution of MDO throughout the polymer backbone for the formulation compositions required for adhesive applications.[7] A crucial aspect of this study was the determination of ternary reactivity ratios, as binary reactivity ratios alone did not provide an accurate prediction of terpolymer composition. The ternary reactivity ratios differed significantly from previously reported binary values,

underscoring the necessity of directly measuring the ternary system's parameters. The estimated reactivity ratios were: r_{12}=0.417, r_{12}=0.417, r_{21}=0.071, r_{13}=4.459r, r_{31}=0.198, r_{23}=0.26, and r_{32}=55.339, r_{32}=55.339. These values indicate that MDO preferentially reacts with BA and VAc rather than undergoing homopolymerization. This preferential cross-propagation of MDO with BA and VAc ensures the formation of a random terpolymer structure rather than block or gradient copolymers, which is crucial for achieving a uniform distribution of MDO along the polymer backbone and providing consistent degradation properties across the polymer matrix.

The successful incorporation of MDO into emulsion terpolymers was influenced by three primary challenges: hydrolysis sensitivity, ring retention, and monomer conversion efficiency. Addressing these issues was crucial to ensuring the formation of a well-defined, degradable polymer matrix suitable for sustainable PSAs.

Building on these findings, Chapter 5 focused on implementing MDO in emulsion polymerization, where batch polymerization was used to produce BA/MDO/VAc terpolymers.[8] One of the most significant challenges was hydrolysis sensitivity, as MDO is hydrolytically unstable in aqueous systems, leading to premature degradation before successful incorporation into the polymer backbone. To mitigate this, polymerization was conducted under a carefully controlled pH range of 7.8–8.8 and at a low reaction temperature of 40°C. These conditions were optimized to minimize hydrolysis, ensuring that MDO remained reactive throughout the polymerization process. Additionally, maintaining this pH balance was critical in preventing unwanted side reactions, such as the alkaline hydrolysis of VAc, which could compromise the stability and performance of the resulting terpolymer. Another major challenge was ring retention, which led to the formation of polyacetal linkages instead of the desired degradable polyester bonds. The extent of ring retention in MDO polymerization varied across formulations, with ^{1}H-NMR and ^{13}C-NMR analyses confirming that 15–50 mol% of MDO remained in its cyclic form. To minimize this effect, the polymerization temperature was increased to 50°C, which was successful in significantly enhancing ring opening, as evidenced by ^{13}C-NMR results, where peaks corresponding to cyclic MDO disappeared. Furthermore, DSC analysis revealed a decrease in the glass transition temperature (T_g), indicating a higher proportion of polyester linkages and improved polymer flexibility, a key property for adhesive applications. To further enhance the performance of MDO-based latex PSAs, CNCs were incorporated into the formulation to improve adhesive

properties, reinforcing the polymer matrix and optimizing mechanical stability while maintaining the degradability potential of the system.

7.2.3 cCNC-Based PSA Nanocomposites

Cellulose nanocrystals (CNCs) have emerged as a promising class of bio-based nanomaterials with unique mechanical, chemical, and rheological properties. Their high crystallinity and excellent strength-to-weight ratio make them highly suitable for reinforcing polymeric systems. Among these, PSAs have particularly benefited from CNC incorporation, as these nanostructures enhance mechanical stability, cohesive strength, and adhesion performance.[9]

The integration of CNCs into PSA formulations has been explored through different processing techniques, including in-situ polymerization and post-polymerization blending.[10] While in-situ polymerization ensures uniform nanoparticle dispersion during polymerization, blending remains a practical and scalable approach for modifying commercial PSA formulations. The addition of CNCs has been shown to improve PSA properties by reinforcing the polymer matrix, promoting hydrogen bonding, and modifying viscosity to enhance film formation and adhesive application.

In Chapter 3, the incorporation of carboxylated CNCs (cCNCs) into a commercial latex-based PSA demonstrated significant improvements in adhesive performance. We optimized key processing parameters, identifying high-speed mixing and sonication as critical factors in enhancing tack, peel strength, and shear adhesion. Homogenization increased shear adhesion by 370% while maintaining strong tack and peel strength, confirming the effectiveness of controlled cCNC dispersion. Additionally, rheological analysis revealed improved film uniformity and adhesive application.

Following these findings, in Chapter 5 I further validated the impact of optimal blending conditions, where cCNCs were incorporated into the PSA formulation and again demonstrated simultaneous improvements in PSA properties.

7.2.4 Biodegradability Under Controlled Composting Conditions

The increasing accumulation of plastic waste has driven research toward biodegradable alternatives that can decompose into non-toxic compounds under controlled environmental conditions. Composting provides an effective means of managing biodegradable polymers, utilizing microbial activity in aerobic conditions to convert materials into CO_2, water, and biomass.

The biodegradability of polymers largely depends on their molecular structure, with ester-containing backbones being more susceptible to hydrolysis and microbial assimilation.[11,12]

In Chapter 6, the biodegradability of BA/MDO/VAc terpolymers was evaluated under controlled composting conditions using a lab-made composting setup following ASTM D5338 standards. The incorporation of MDO into the polymer backbone aimed to enhance hydrolytic degradation, facilitating microbial assimilation and mineralization. Among the tested samples, BMV10-NEW-cCNC, which contained 10 wt% MDO and CNC, exhibited the highest degradation over a 60-day composting period, with CO_2 emissions indicating a biodegradation rate of approximately 12.49%. These findings confirm the potential of MDO-based PSAs for compostable adhesive applications, supporting sustainable material development.

7.3 Novelty of this research

This research presents a novel approach to the development of PSAs by integrating the bio-based monomer MDO and bio-based nanoparticles, cCNCs, through emulsion polymerization. This method provides a water-based, low-VOC alternative to conventional solution or bulk polymerization, aligning with green chemistry principles and significantly reducing environmental impact while maintaining high adhesive performance.

In this work, ternary reactivity ratios for the BA/MDO/VAc system are reported for the first time, providing a more precise understanding of monomer distribution within the polymer backbone, which is critical for achieving uniform MDO distribution and consistent degradation properties. Additionally, this research addresses significant challenges in both the aqueous polymerization of MDO and the ring retention issue, which can reduce the degradability of the resulting polymers. To overcome these challenges, the study optimized pH and temperature conditions to minimize ring retention and promote the formation of degradable polyester bonds, ensuring efficient MDO incorporation and improved polymer flexibility.

Furthermore, the integration of cCNCs via blending, a straightforward and scalable approach, significantly improved the tack, peel strength, and shear adhesion of the resulting PSAs, demonstrating that bio-based nanocomposites can effectively enhance the mechanical performance of degradable adhesives.

Finally, this work provides real-world biodegradation data for MDO-based PSAs using a custom ASTM D5338-compliant composting setup. This is a critical step toward demonstrating

the end-of-life benefits of these materials and supporting their commercialization as sustainable alternatives to traditional PSAs.

Overall, this thesis integrates chemistry, material science, and process engineering to develop a comprehensive and scalable approach to produce biodegradable PSAs, addressing both performance and sustainability challenges.

7.4 Future Work

Building on the findings of this study, future research should focus on optimizing the formulation and processing of cCNC-based PSAs for industrial applications. One key area of investigation is the scalability of these formulations, particularly in identifying alternative dispersion techniques that reduce reliance on high-energy sonication while ensuring uniform cCNC distribution. This will help facilitate industrial adoption and improve cost-effectiveness while maintaining performance consistency.

Another important direction is exploring the potential of in-situ polymerization as an alternative to post-polymerization blending. By incorporating cCNCs directly into the polymerization process, improved nanoparticle-polymer interactions may be achieved, leading to enhanced adhesion stability and mechanical performance over time. This approach could also result in a more significant increase in PSA properties compared to post-polymerization blending.

A crucial avenue for further investigation is the increase in MDO content in emulsion polymerization formulations to assess its impact on biodegradability. The current study demonstrated that even with 20 wt% MDO at 40°C, the PSA was not fully compostable. Therefore, further studies should explore higher MDO loadings and alternative polymerization conditions that may promote degradation. Additionally, performing polymerization at higher temperatures could provide insights into the stability of the MDO ring structure under elevated conditions. This would help determine whether ring retention is feasible and how it affects degradation properties. Understanding the relationship between polymerization temperature and ring retention could be key in optimizing the degradation behaviour of these materials.

Further studies on biodegradability and compostability are also necessary. While the current research demonstrated partial degradation over a 60-day period, longer-term studies should be conducted to assess the full biodegradation pathway, microbial interactions, and any potential ecotoxicity concerns. Extending composting trials to industrial-scale facilities would provide

valuable insights into the real-world performance of these adhesives and help develop strategies for large-scale implementation.

By addressing these challenges, future research can advance the development of high-performance, biodegradable PSAs that align with both industrial needs and sustainability goals.

7.5 References

[1] I. Benedek, *Pressure-Sensitive Adhesives and Applications*, CRC Press, 2004.

[2] I. Benedek, L. J. Heymans, *Pressure-Sensitive Adhesives Technology*, Marcel Dekker Inc., New York, 1997.

[3] R. Jovanović, M. A. Dubé, *J of Macro Sci, Part C: Polymer Reviews* 2004, *44*, 1.

[4] C. S. Chern, *Prog Polym Sci* 2006, *31*, 443.

[5] P. A. Lovell, F. J. Schork, *Biomacromolecules* 2020, *21*, 4396.

[6] M. Movafagh, K. M. Meek, P. Bayat, E. D. Cranston, M. Cunningham, P. Champagne, T. Morse, M. Kiriakou, S. George, M. A. Dubé, *Polym Eng Sci* 2024, *64*, 798.

[7] M. Movafagh, K. M. Meek, A. J. Scott, A. Penlidis, M. A. Dubé, *Polymers (Basel)* 2024, *16*, 1330.

[8] M. Movafagh, K. M. Meek, M. A. Dubé, *ChemSusChem* 2025, e202402478.

[9] A. S. Pakdel, E. Niinivaara, E. D. Cranston, R. M. Berry, M. A. Dubé, *Macromol Rapid Commun* 2021, *42*, 2000448.

[10] S. A. Kedzior, V. A. Gabriel, M. A. Dubé, E. D. Cranston, *Advanced Materials* 2021, *33*, 2002404.

[11] P. K. Samantaray, A. Little, A. M. Wemyss, E. Iacovidou, C. Wan, *ACS Sustain Chem Eng* 2021, *9*, 9151.

[12] M. Pergola, A. Persiani, A. M. Palese, V. Di Meo, V. Pastore, C. D'Adamo, G. Celano, *Applied Soil Ecology* 2018, *123*, 744.

Appendix I
Supporting Information for "Chapter 3: Improved Pressure-Sensitive Adhesive Performance Using Carboxylated Cellulose Nanocrystals via Blending"

Maryam Movafagh[1], Kelly M. Meek[1], Parisa Bayat[1], Emily D. Cranston[2], Michael Cunningham[3], Pascale Champagne[4], Timothy Morse[5], Michael Kiriakou[5], Sean George[6], Marc A. Dubé[1]

[1]Department of Chemical and Biological Engineering, University of Ottawa, Ottawa, ON, Canada
[2]Department of Wood Science and Department of Chemical and Biological Engineering, University of British Columbia, Vancouver, BC, Canada
[3]Department of Chemical Engineering, Queen's University, Kingston, ON, Canada
[4]Energy Mining & Environment Research Centre, National Research Council, Montreal, QC, Canada
[5]Anomera Inc., Montreal, QC, Canada
[6]BASF Corp., Charlotte, NC, United States

This chapter is a manuscript published in Polymer Engineering and Science (2024; 64(2): 798-816). DOI: 10.1002/pen.26585.

A crucial step in model assessment is the scrutiny of residuals. We rigorously analyzed the residuals of our regression models, seeking any discernible patterns that might indicate deficiencies in the models. The results of this analysis were reassuring; we found no discernible pattern in the residuals across all response variables.

a)

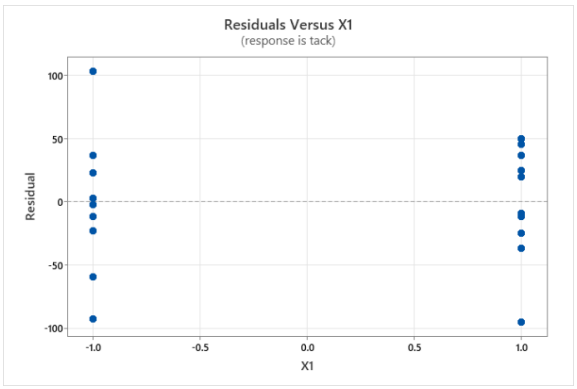
Residuals Versus X1
(response is tack)
Residual
X1

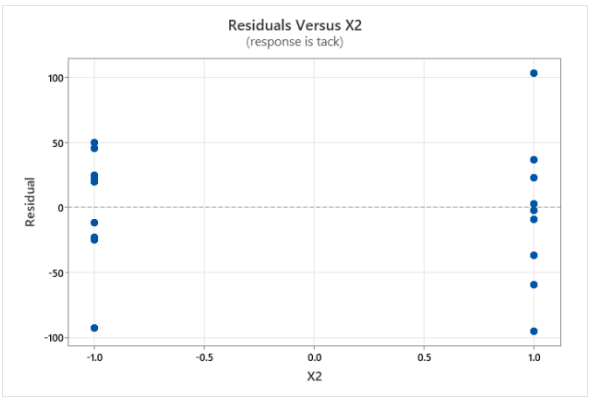
Residuals Versus X2
(response is tack)
Residual
X2

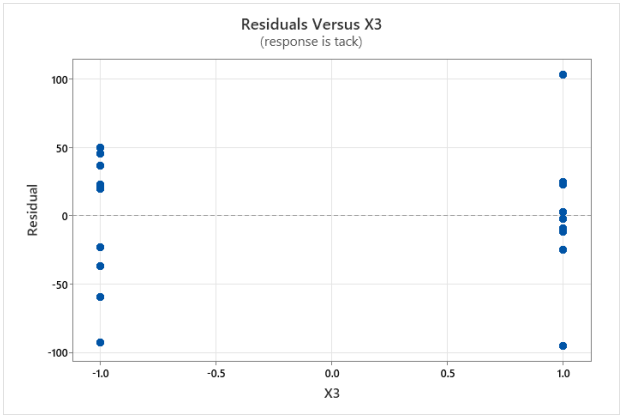
Residuals Versus X3
(response is tack)
Residual
X3

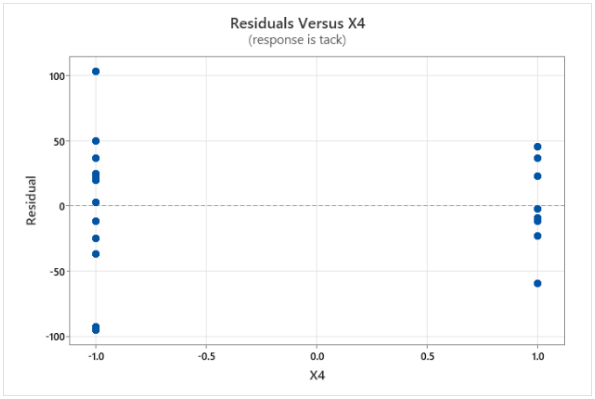
Residuals Versus X4
(response is tack)
Residual
X4

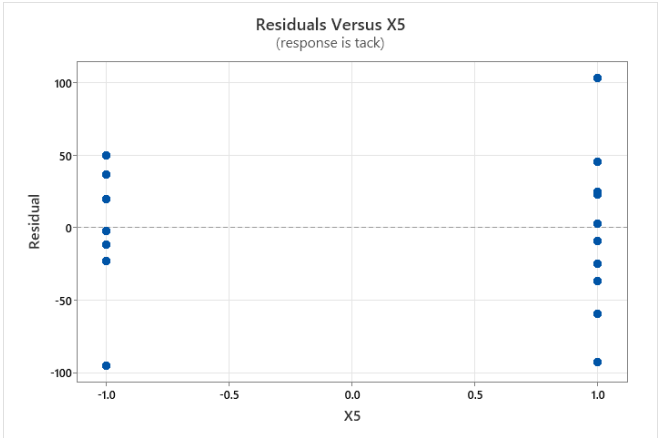
Residuals Versus X5
(response is tack)
Residual
X5

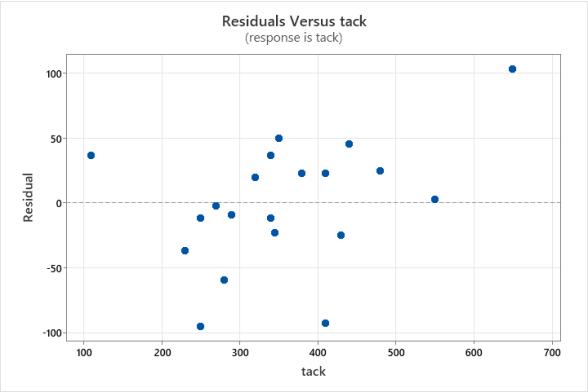
Residuals Versus tack
(response is tack)
Residual
tack
100
50
0
-50
-100
100
200
300
400
500
600
700

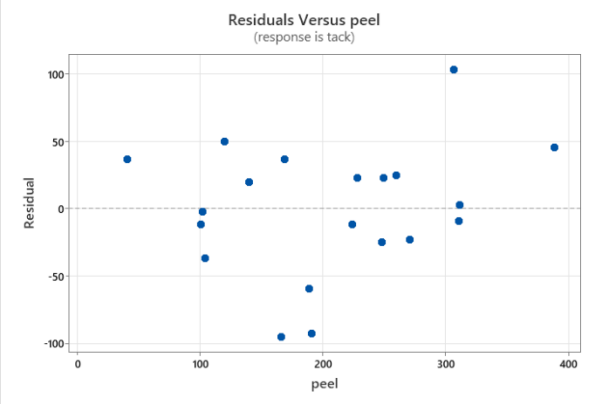
Residuals Versus peel
(response is tack)
Residual
peel
100
50
0
-50
-100
0
100
200
300
400

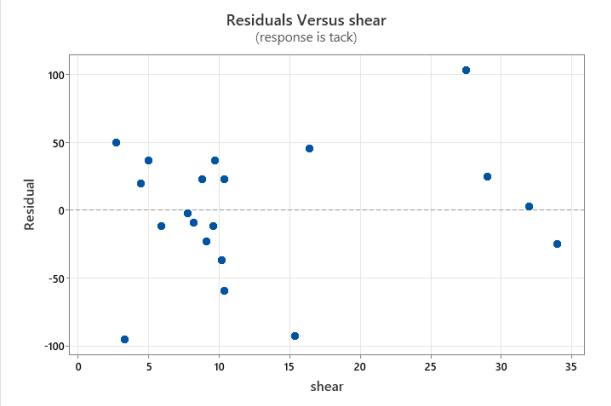
Residuals Versus shear
(response is tack)
Residual
shear
100
50
0
-50
-100
0
5
10
15
20
25
30
35

b)

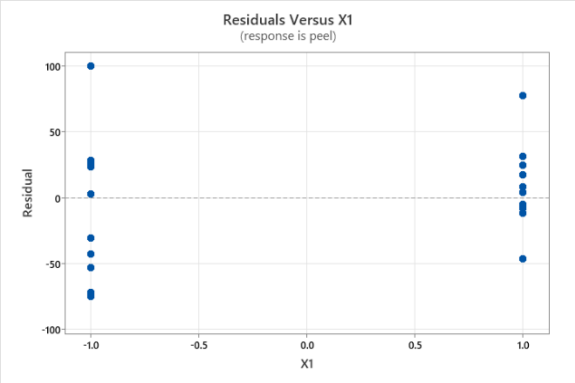
Residuals Versus X1
(response is peel)
Residual
X1

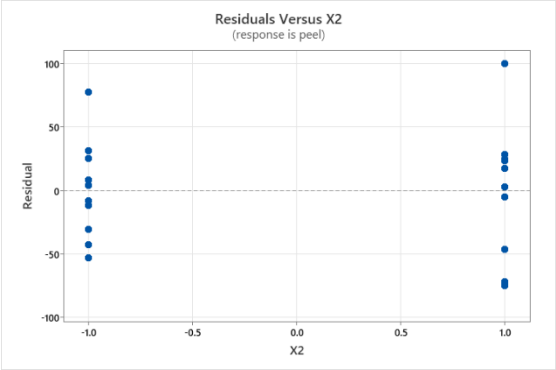
Residuals Versus X2
(response is peel)
Residual
X2

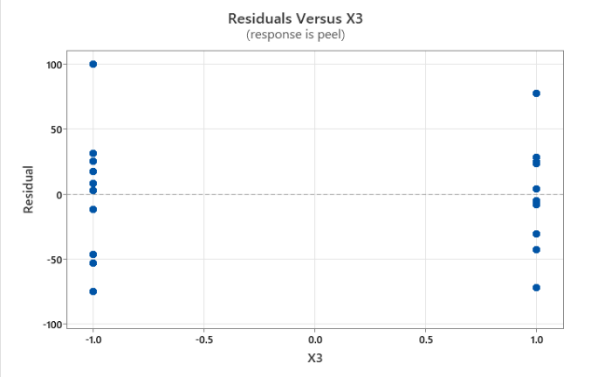
Residuals Versus X3
(response is peel)
Residual
X3

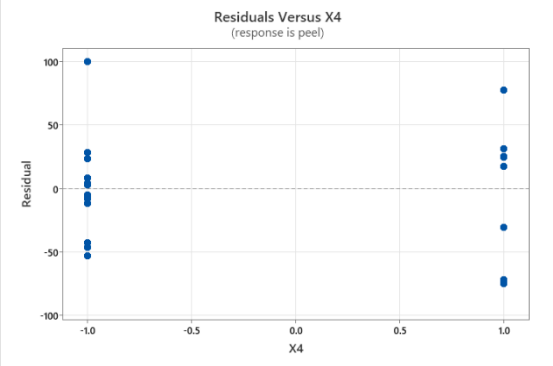
Residuals Versus X4
(response is peel)
Residual
X4

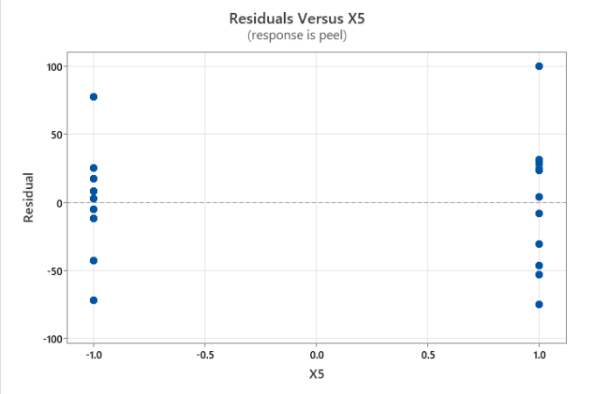
Residuals Versus X5
(response is peel)
Residual
X5

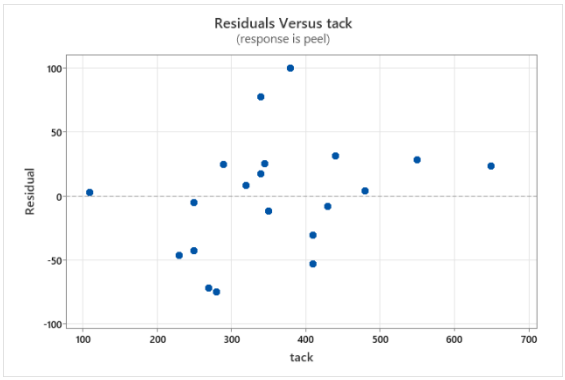
Residuals Versus tack
(response is peel)
Residual
tack
100
50
0
-50
-100
100
200
300
400
500
600
700

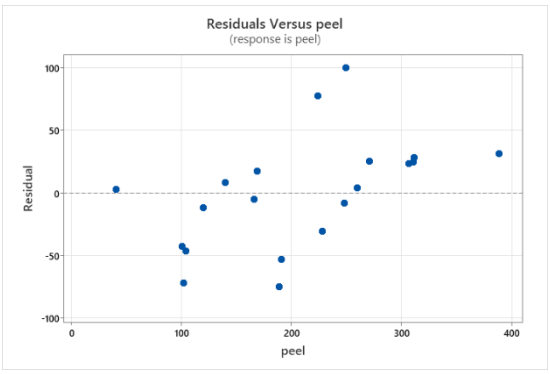
Residuals Versus peel
(response is peel)
Residual
peel
100
50
0
-50
-100
0
100
200
300
400

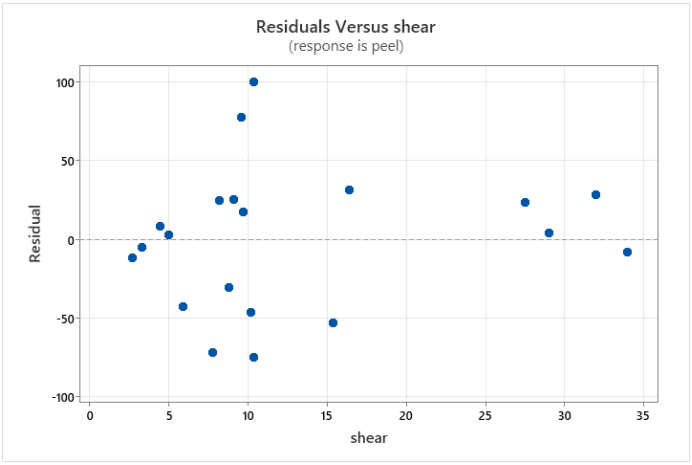
Residuals Versus shear
(response is peel)
Residual
shear
100
50
0
-50
-100
0
5
10
15
20
25
30
35

c)

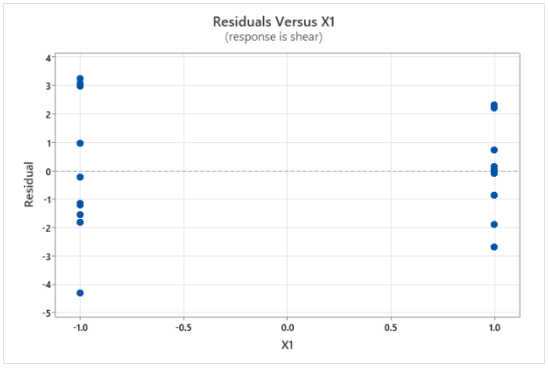
Residuals Versus X1
(response is shear)
Residual
X1

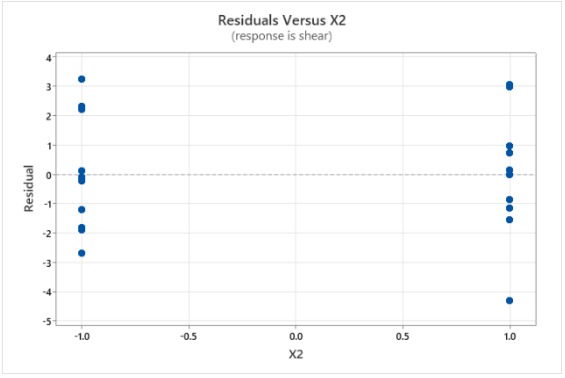
Residuals Versus X2
(response is shear)
Residual
X2

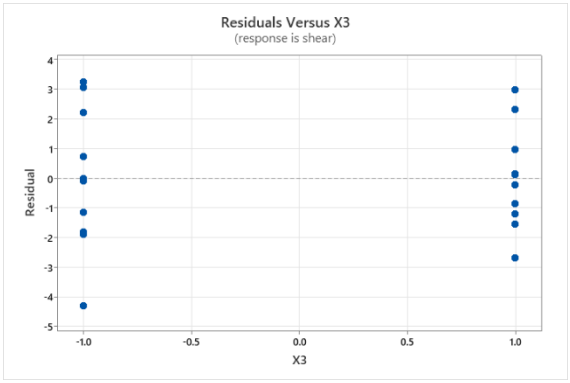
Residuals Versus X3
(response is shear)
Residual
X3

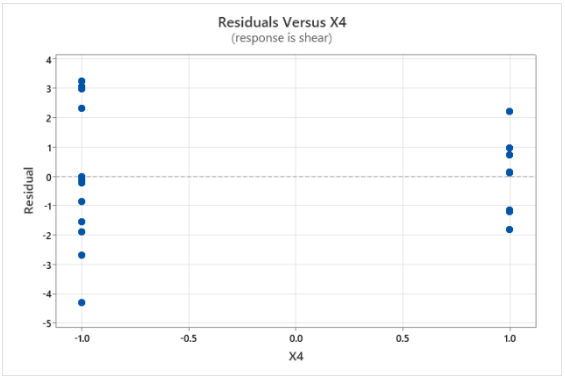
Residuals Versus X4
(response is shear)
Residual
X4

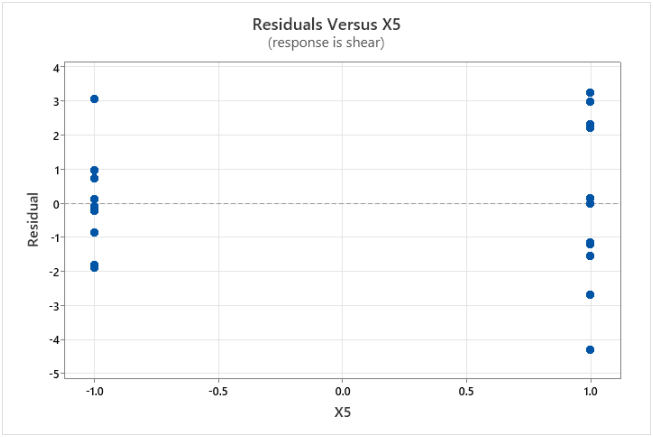
Residuals Versus X5
(response is shear)
Residual
X5

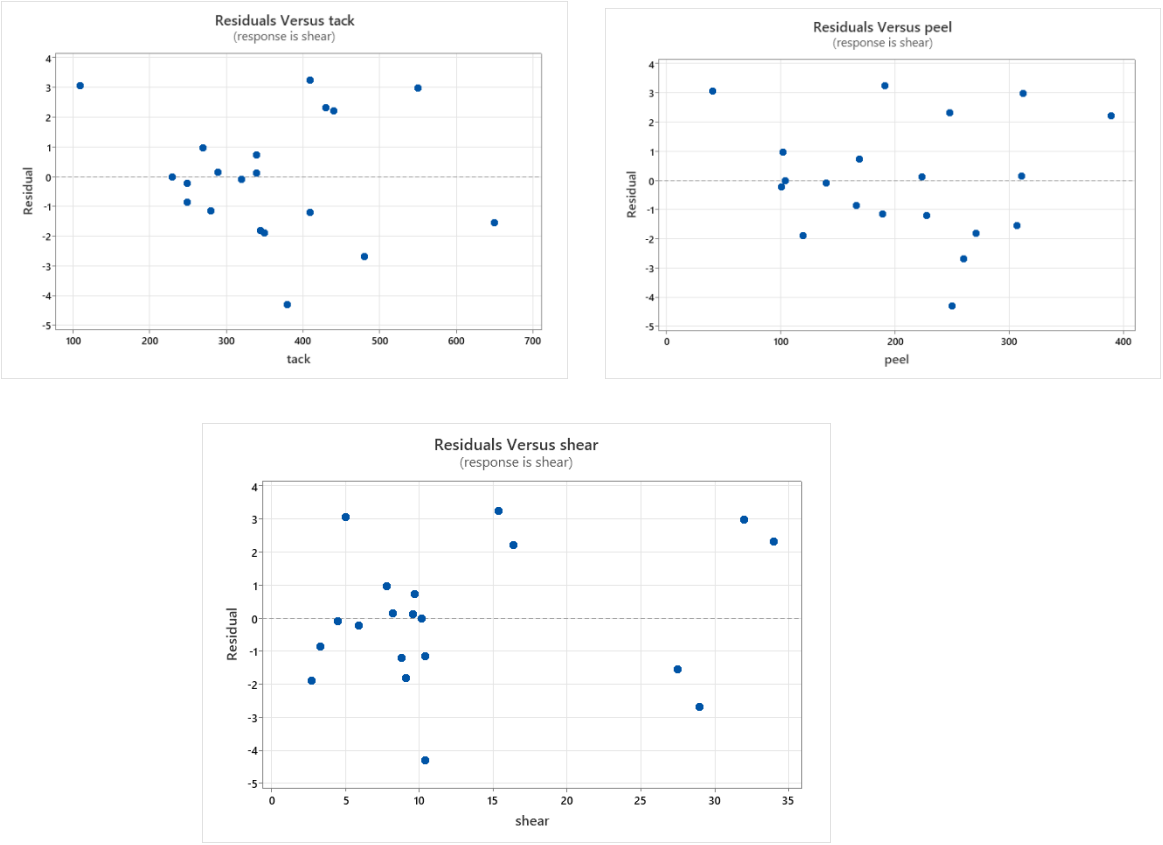

Figure I.1. Residual plots for a) tack, b) peel strength and c) shear strength

Table I.1. Error tables for PSA regression models

Source	Tack				
	F-value	*p-value*	*DF*	*Adj SS*	*Adj MS*
Lack-of-Fit	2.37	0.257	7	37078	5296.8
Error	*	*	10	43778	4377.8
Pure error	*	*	3	6700	2233.3
Total	*	*	19	276744	*

Source	Peel strength				
	F-value	*p-value*	*DF*	*Adj SS*	*Adj MS*
Lack-of-Fit	40.52	0.006	10	38426	3842.6
Error	*	*	13	38710	2977.7
rePure error	*	*	3	285	94.8
Total	*	*	19	152305	*

Source	Shear strength				
	F-value	*p-value*	*DF*	*Adj SS*	*Adj MS*
Lack-of-Fit	0.97	0.566	7	54.62	7.803
Error	*	*	10	78.8	7.803
Pure error	*	*	3	24.24	8.082
Total	*	*	19	1799.15	*

Table I.2. Optimization parameters

Response goal	goal	lower	target	upper	weight	importance
Tack	maximum	2.7	34	34	1	1
Peel strength	maximum	41	389	389	1	1
Shear strength	maximum	110	650	650	1	1

Table I.3. Solution based on selected optimization parameters.

solution	X_1	X_2	X_3	X_4	X_5	Shear fit	Peel fit	Tack fit	Composite desirability
1	-1	1	1	-1	1	29.03	283.42	547.02	0.78

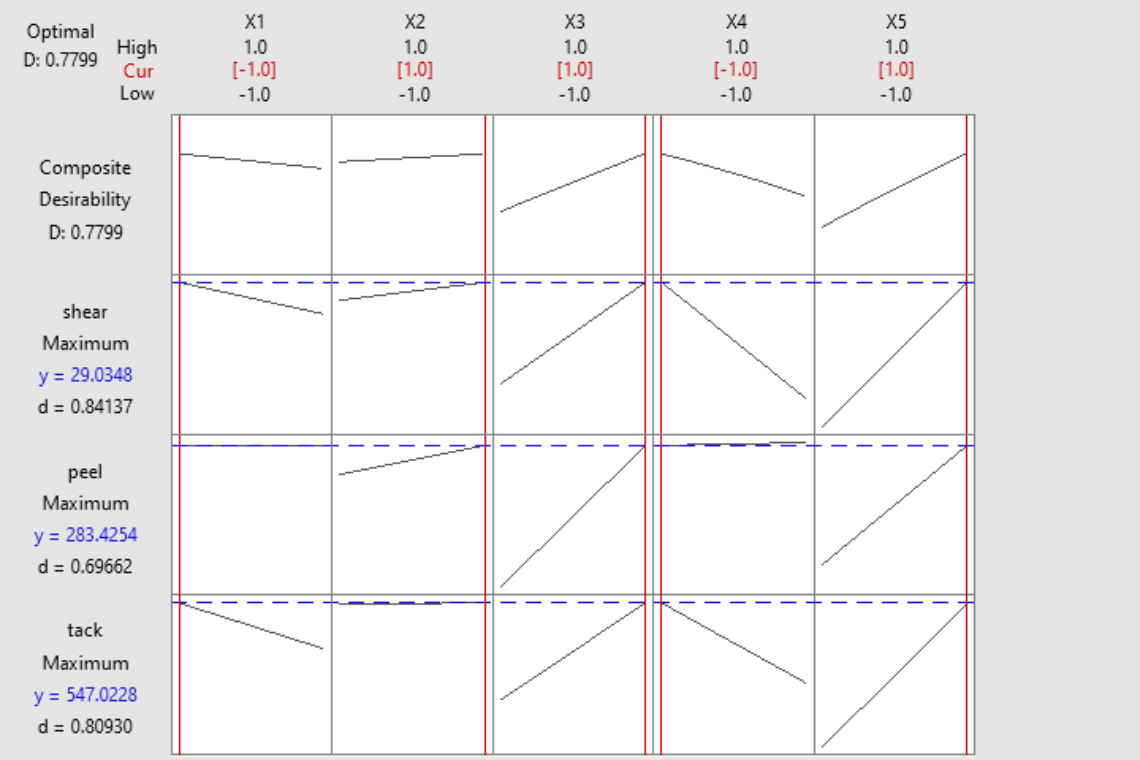

Figure I.2. Response optimizer plot

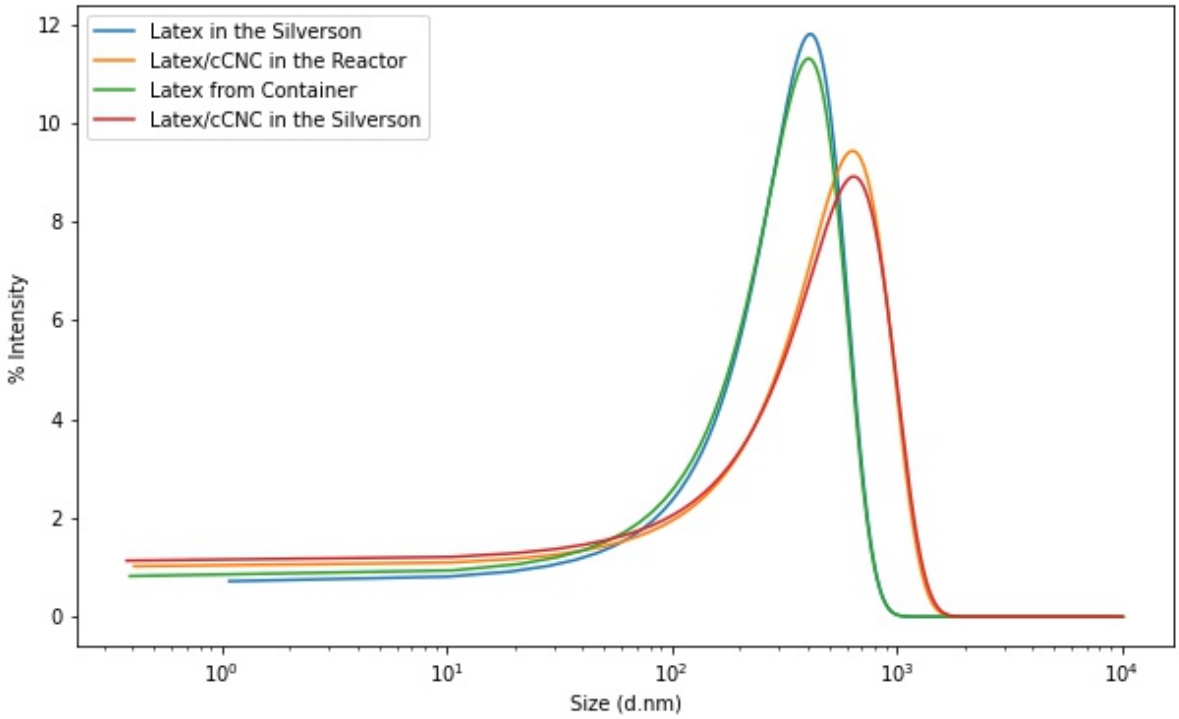

Figure I.3. Comparing the particle size distribution of latex from the container, latex putting into Silverson mixer without cCNC, and latex-cCNC blends in the reactor and Silverson mixer using 1 phm never-dried, sonicated cCNC. The mixing speeds of the reactor and Silverson mixer were 300, and 3,000 rpm respectively.

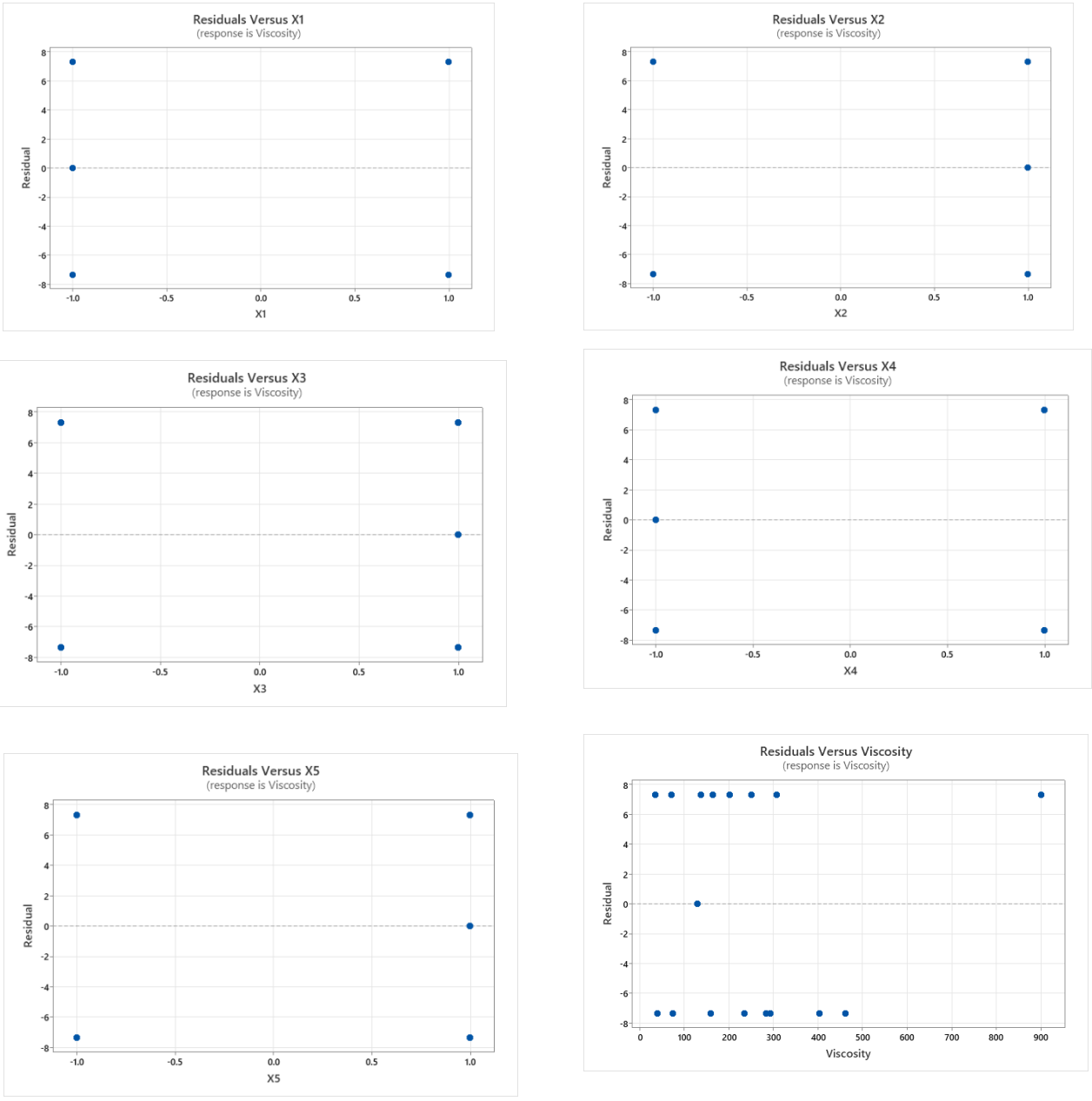

Figure I.4. Residual plots for viscosity

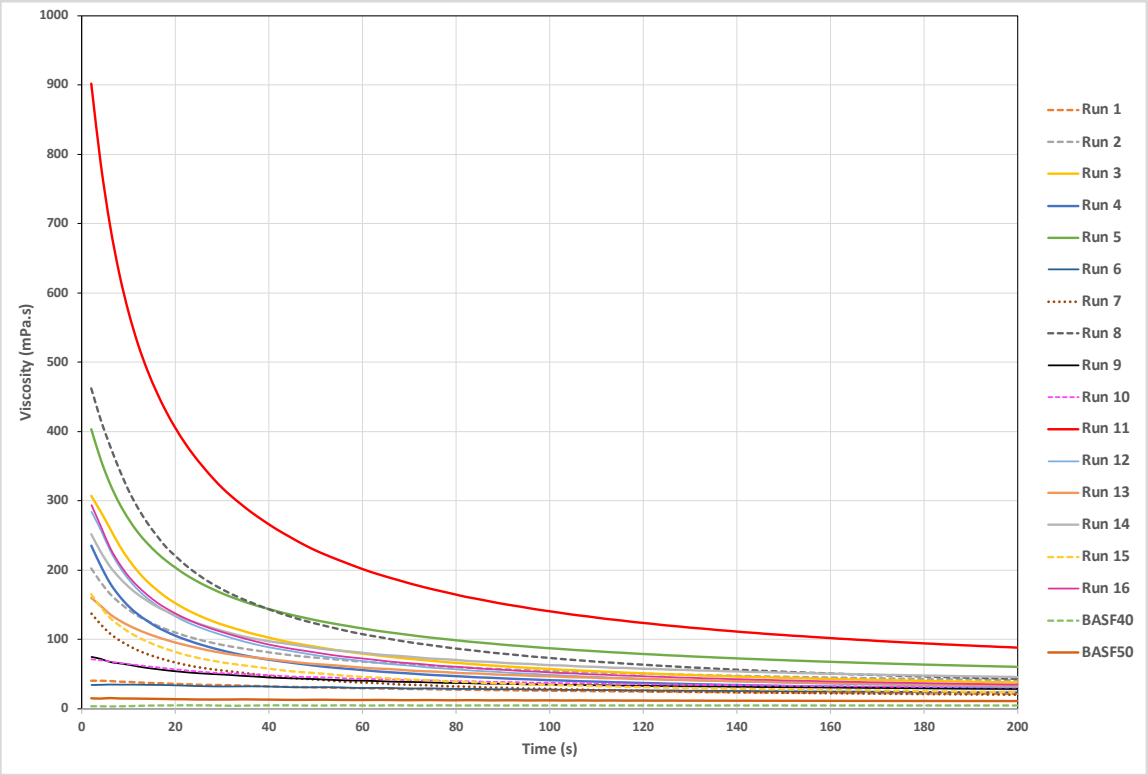

Figure I.5. Latex viscosity vs. time for factorial design and base case runs

Appendix II
Supporting information for "chapter 5: Butyl Acrylate/2-Methylene-1,3-Dioxepane/Vinyl Acetate Emulsion Terpolymerization: Incorporating Backbone Degradable Linkages into Adhesive Applications"

Maryam Movafagh[1], Kelly M. Meek[1,2], Marc A. Dubé[1]

[1]Department of Chemical and Biological Engineering, University of Ottawa, Ottawa, ON
[2]Department of Chemical and Materials Engineering, Concordia University, Montreal, QC

This chapter is a manuscript published in ChemSusChem (2025).
DOI: 10.1002/cssc.202402478

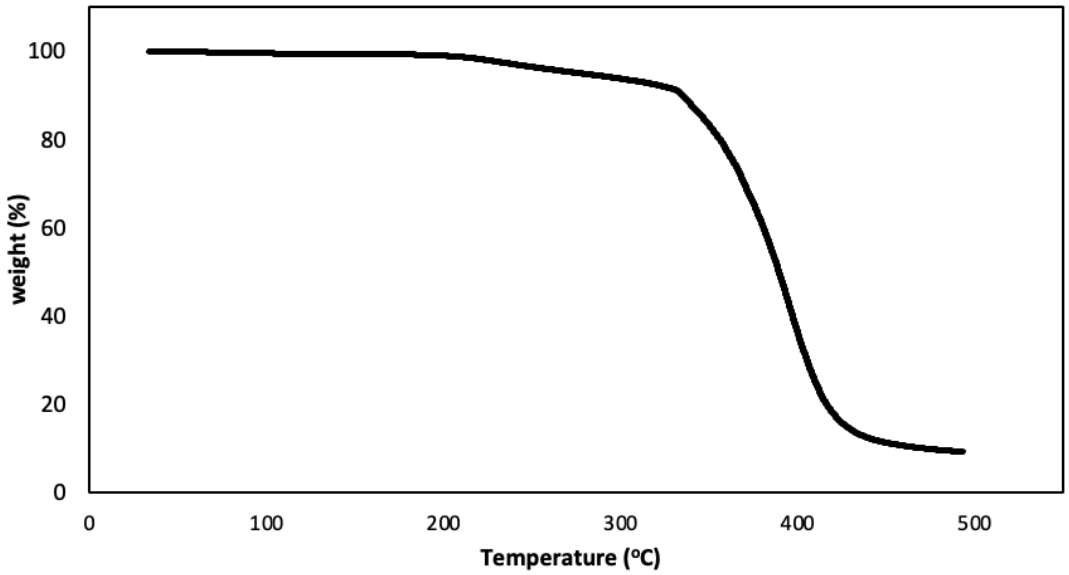

Figure II.1. TGA results of BMV20 after drying for solids content measurement

Scheme II.1. General scheme of MDO hydrolysis to 4-hydroxybutyl acetate (4-HBA)

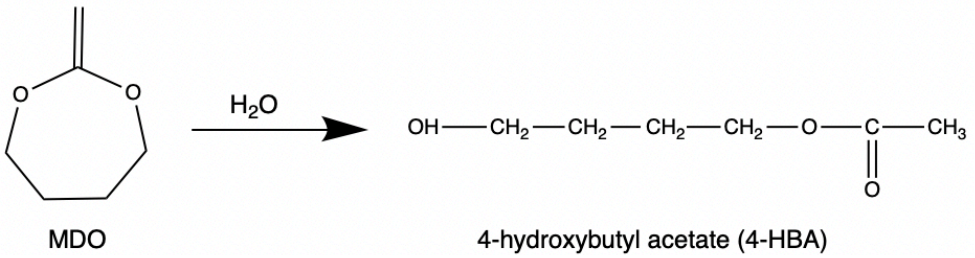

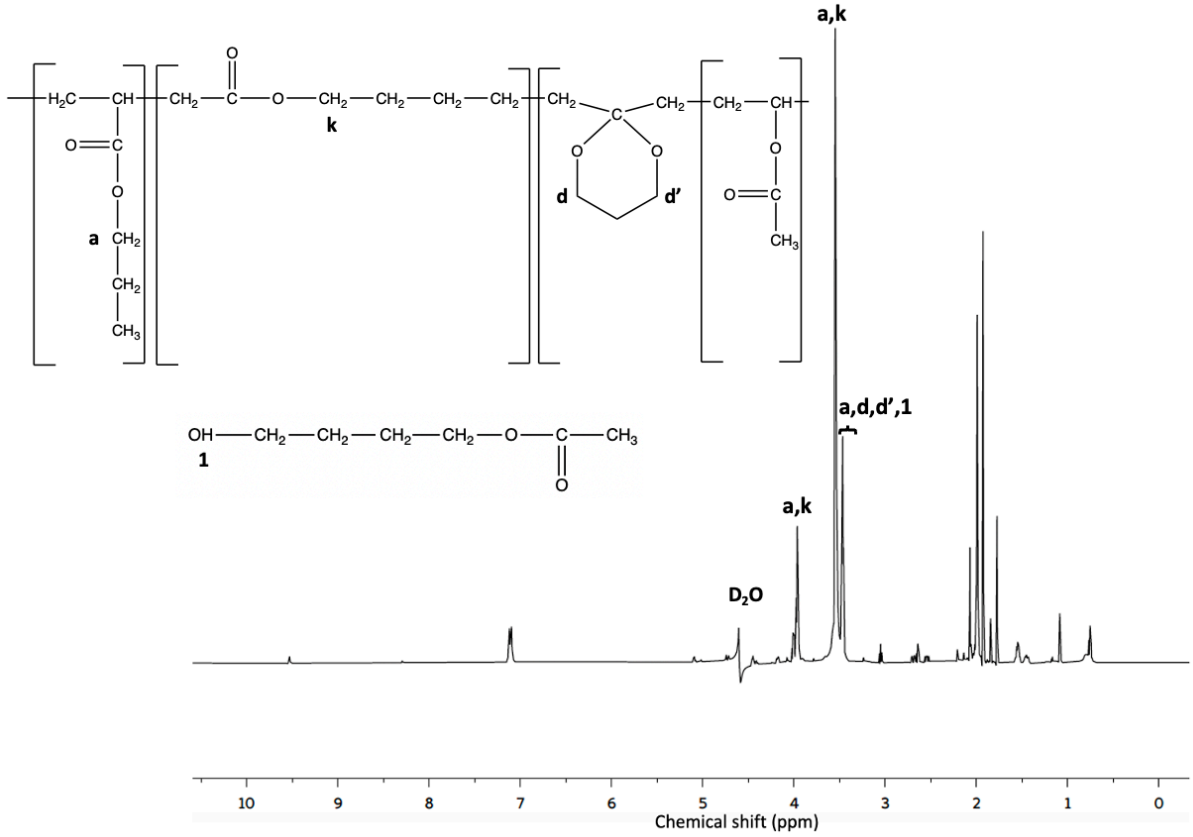

Figure II.2. ^{1}H-NMR Watergate spectrum of BMV20 latex in D_2O.

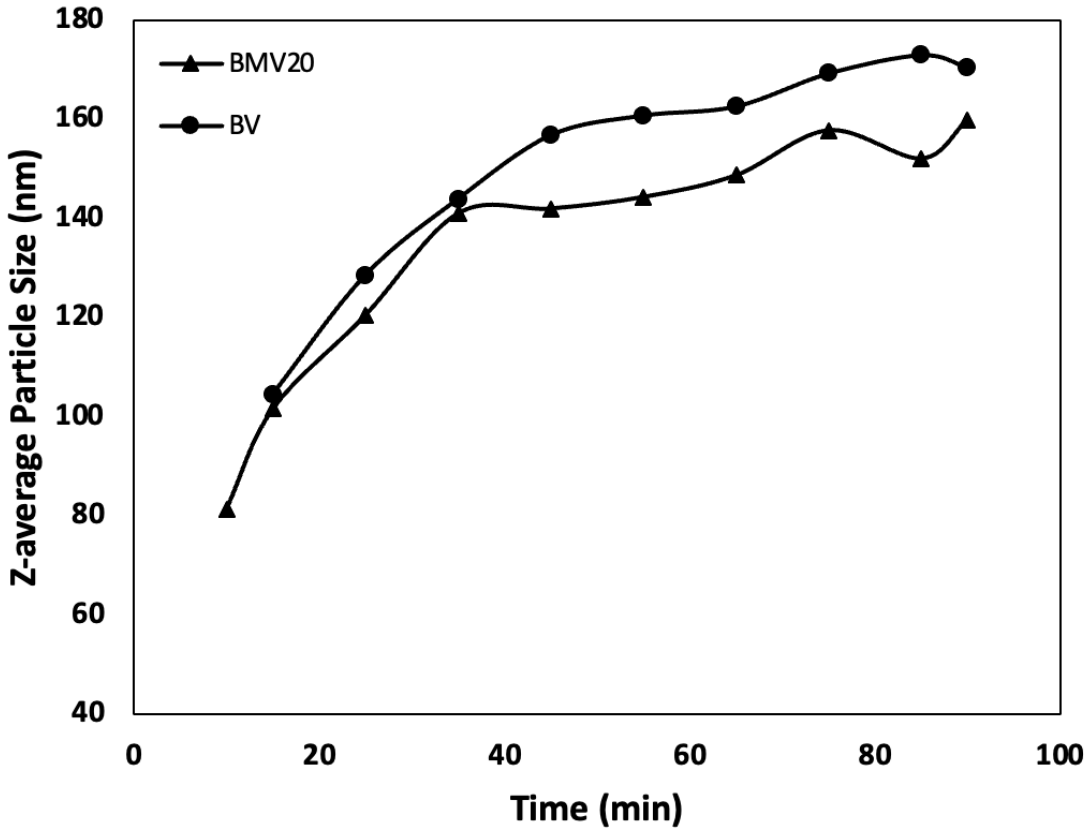

Figure II.3. Z-average particle size versus time for BV and BMV20. All terpolymers—BMV5, BMV10, BMV15, and BMV20—exhibit similar particle sizes and follow the same trend. BMV20 is used here as a representative example for comparison with BV.

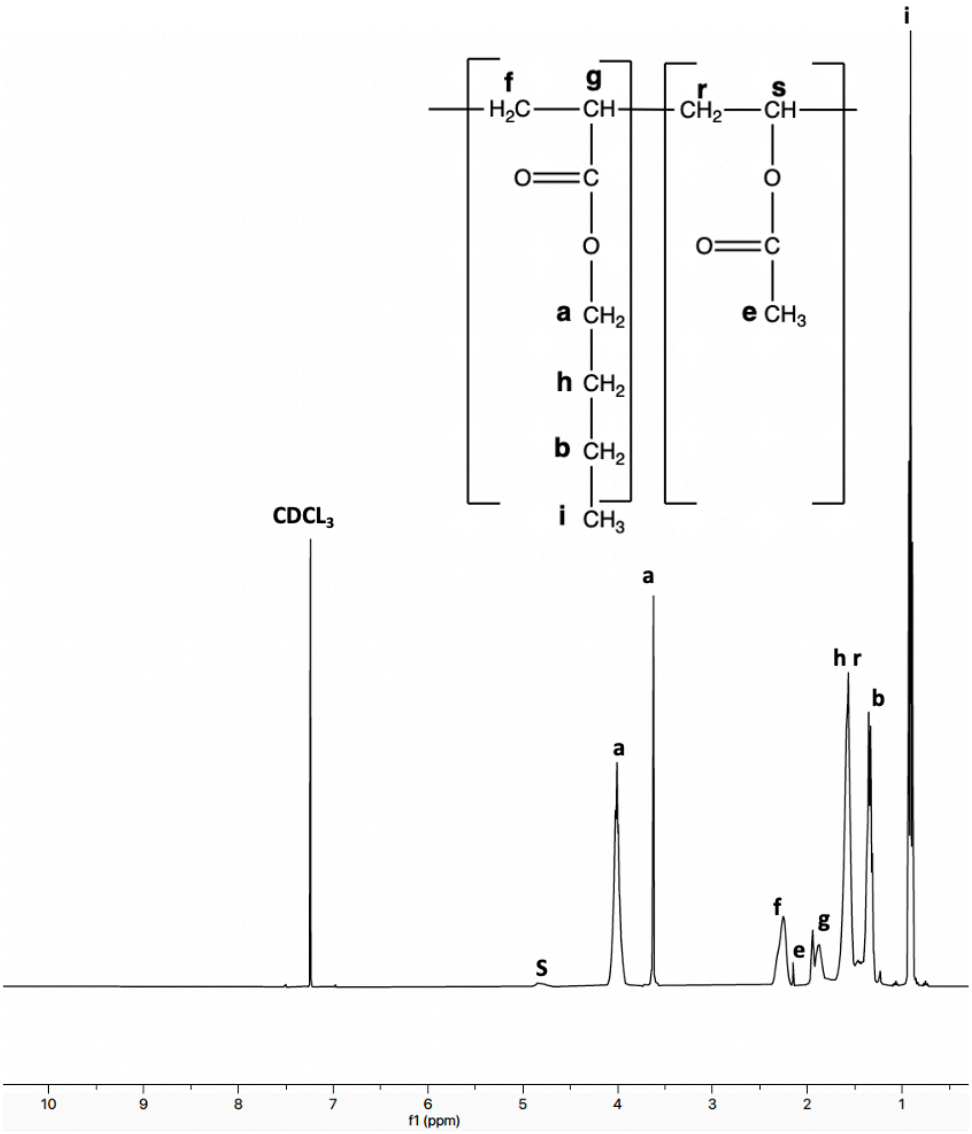

Figure II.4. ^{1}H-NMR spectrum for BV in $CDCl_3$.

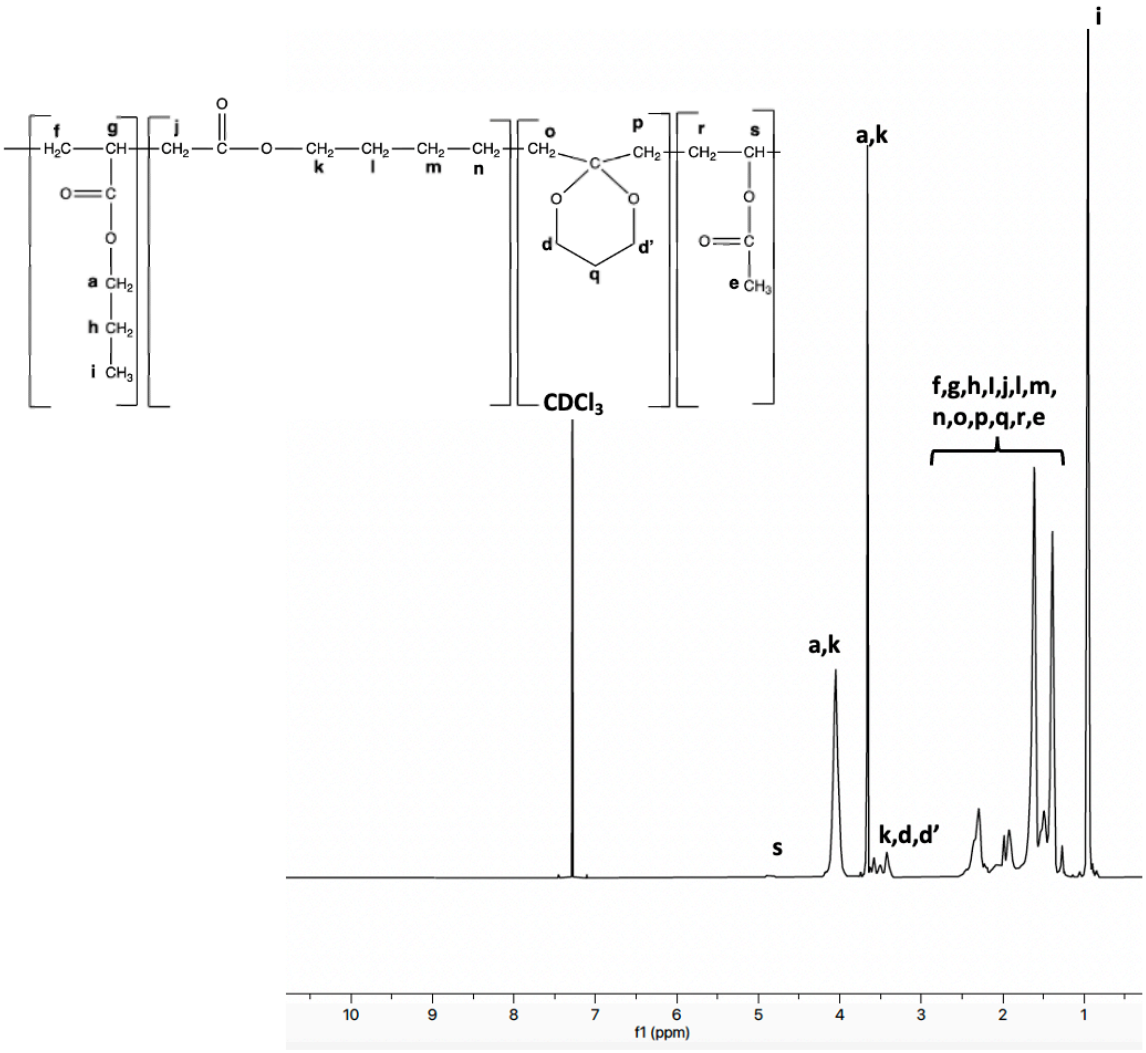

Figure II.5. ^{1}H-NMR spectrum for BMV5 in $CDCl_3$.

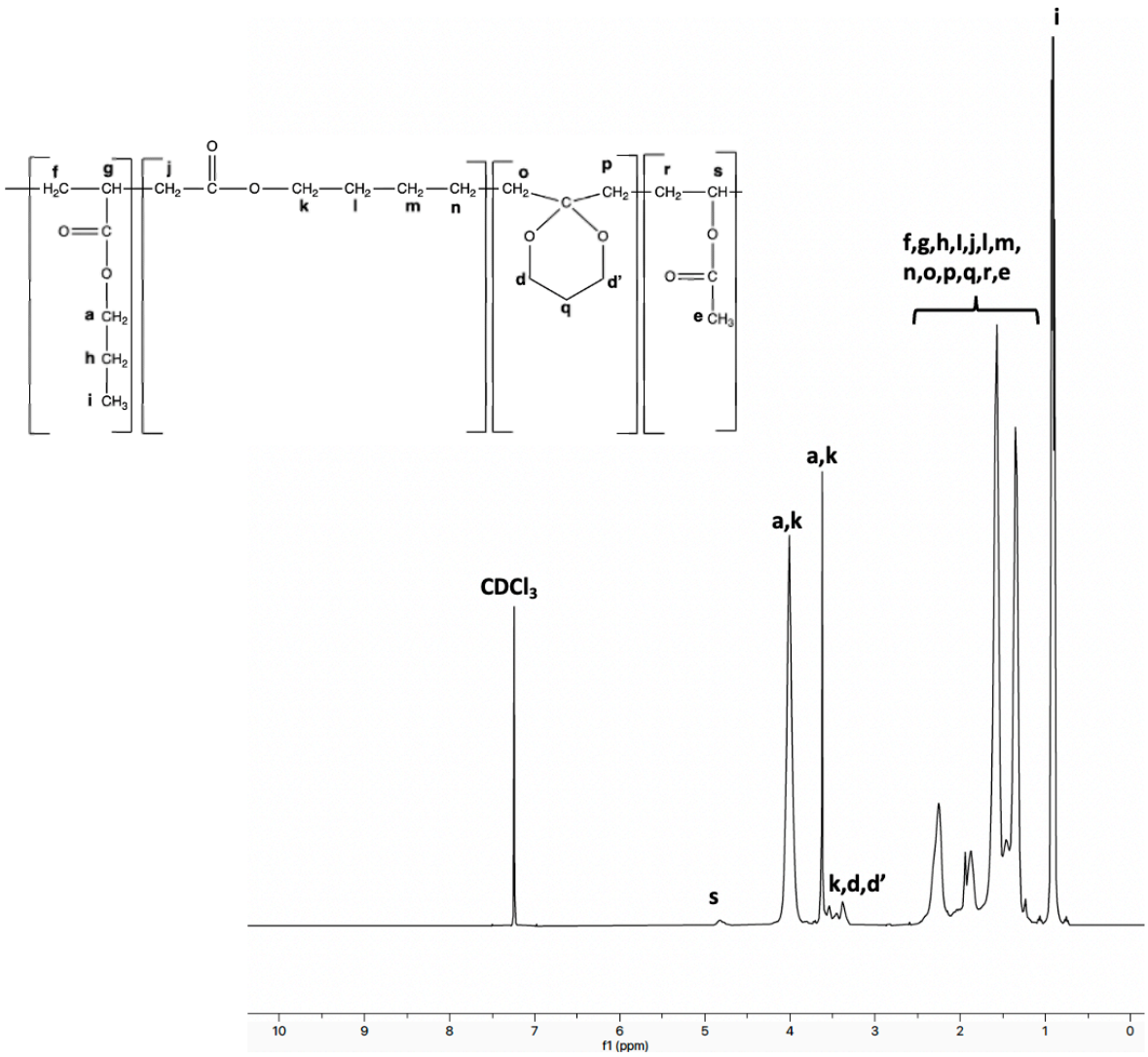

Figure II.6. ^{1}H-NMR spectrum for BMV10 in $CDCl_3$.

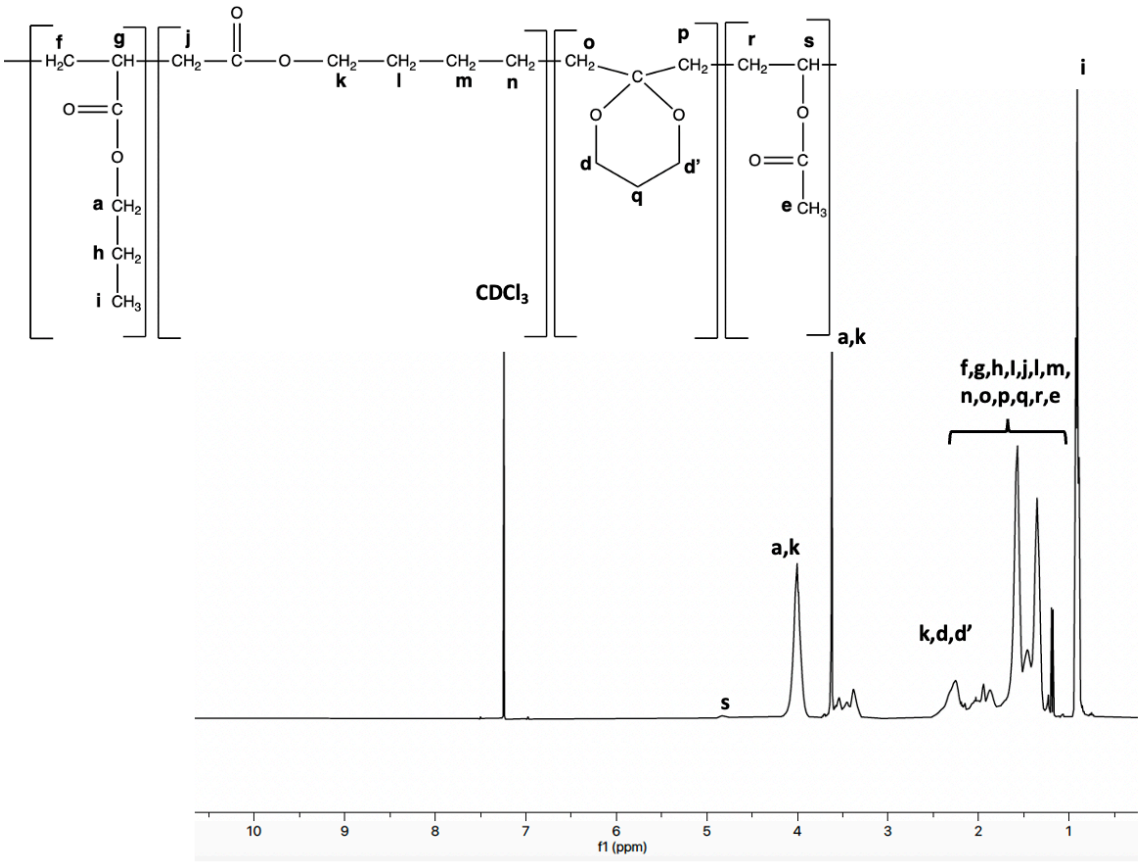

Figure II.7. ^{1}H-NMR spectrum for BMV15 in $CDCl_3$.

The BA/MDO/VAc terpolymer compositions were calculated using the following equations:

$$A_1 = H_{VAc} \quad \text{(II.1)}$$

$$A_2 = 2H_{BA} + 2H_{MDO\text{-}ro} + 4H_{MDO\text{-}rr} \quad \text{(II.2)}$$

$$A_3 = 3H_{BA} \quad \text{(II.3)}$$

$$A_4 = 7H_{BA} + 8H_{MDO\text{-}ro} + 6H_{MDO\text{-}rr} + 5H_{VAc} \quad \text{(II.4)}$$

$$F_{BA} = H_{BA} / (H_{BA} + H_{MDO\text{-}ro} + H_{MDO\text{-}rr} + H_{VAc}) \quad \text{(II.5)}$$

$$F_{MDO\text{-}ro} = H_{MDO\text{-}ro} / (H_{BA} + H_{MDO\text{-}ro} + H_{MDO\text{-}rr} + H_{VAc}) \quad \text{(II.6)}$$

$$F_{MDO\text{-}rr} = H_{MDO\text{-}rr} / (H_{BA} + H_{MDO\text{-}ro} + H_{MDO\text{-}rr} + H_{VAc}) \quad \text{(II.7)}$$

$$F_{VAc} = H_{VAc} / (H_{BA} + H_{MDO\text{-}ro} + H_{MDO\text{-}rr} + H_{VAc}) \quad \text{(II.8)}$$

where H_{BA}, $H_{MDO\text{-}ro}$, $H_{MDO\text{-}rr}$, H_{VAc} represent the BA, ring-opened MDO, ring-retained MDO and VAc protons, respectively, found in areas A_1, A_2, A_3, and A_4. Area A_1 represents the −CH protons of VAc (δ = 4.7 – 4.9 ppm), A_2 represents the $-CH_2O$ protons of BA and MDO (δ = 3.3 – 4.2 ppm), area A_4 represents the $-CH_3$ protons of BA (δ = 0.7 – 1 ppm), and A_3 encompasses the remaining protons for BA, MDO, and VAc (δ = 1 – 2.5 ppm). After solving for H_{BA}, $H_{MDO\text{-}ro}$, $H_{MDO\text{-}rr}$, and H_{VAc} (Equations II.1, II.2, II.3, and II.4), the terpolymer compositions were calculated using Equations II.5, II.6, II.7, and II.8. This composition analysis was conducted for all the BA/MDO/VAc terpolymers. For example, for the BMV20 terpolymer, the integration values were obtained as follows $A_1 = 1$, $A_2 = 42.46$, $A_3 = 115.16$, $A_4 = 47.11$; using these values in Equations II.1–II.4, we solved for H_{BA}, $H_{MDO\text{-}ro}$ $H_{MDO\text{-}rr}$, and H_{VAc}. Substituting H_{BA}, $H_{MDO\text{-}ro}$ $H_{MDO\text{-}rr}$, and H_{VAc} into Equations II.5–II.8, the molar fractions for each component in BMV20 were determined as $F_{BA} = 0.75$, $F_{MDO} = 0.20$ ($F_{MDO\text{-}ro} = 0.14$, $F_{MDO\text{-}rr} = 0.06$), and $F_{VAc} = 0.05$. This calculation process was applied consistently for all other runs, with each run's MDO contents reported in Table 5.2.

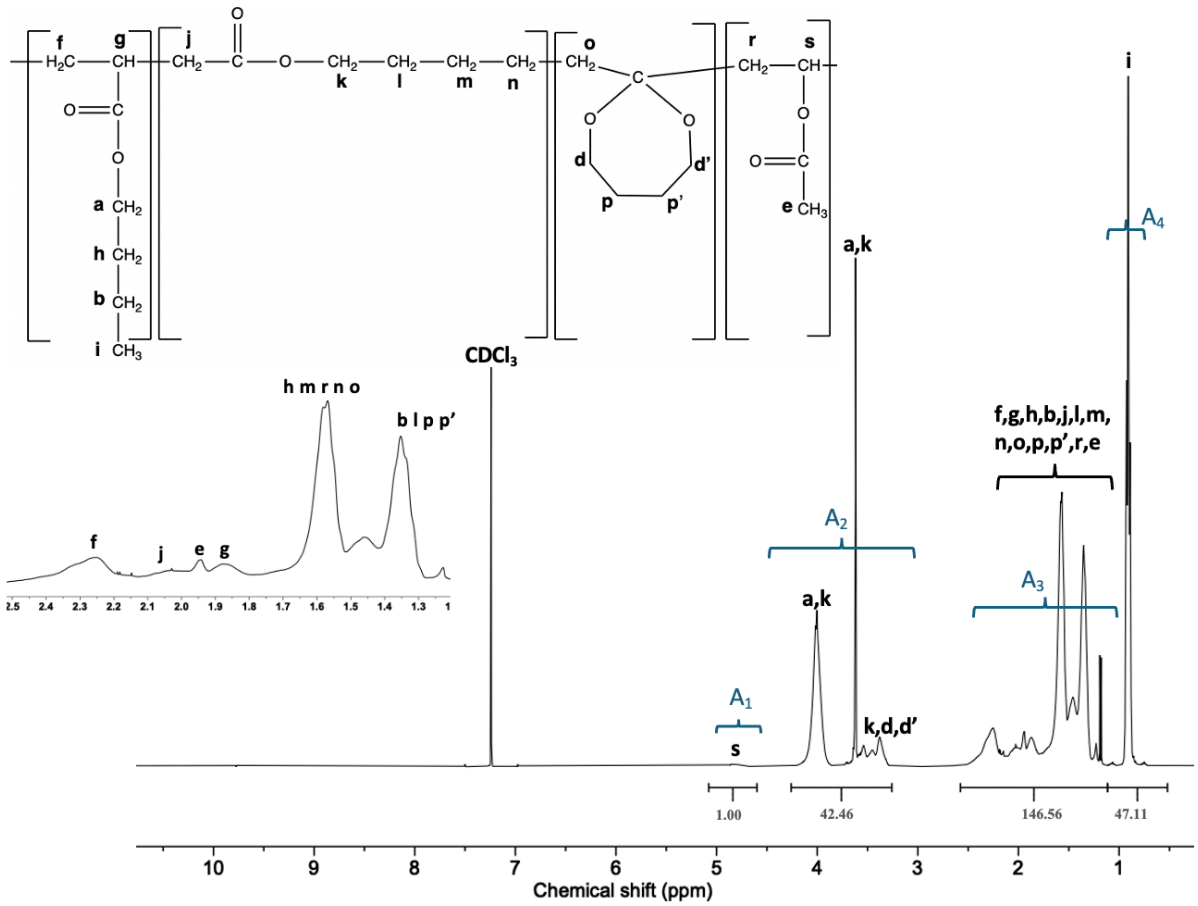

Figure II.8. ^{1}H-NMR spectrum of BMV20 in $CDCl_3$, showing peak assignments and integration values for proton environments corresponding to BA, MDO (both ring-opened and ring-retained forms), and VAc.

Equations II.9–II.11 are formulated to represent the terpolymer composition without the complexities of ratio-based responses. Here, F_i represents the instantaneous mole fraction of monomer *i* bound in the terpolymer, f_i represents the mole fraction of unreacted monomer *i* in the polymerizing mixture, and the reactivity ratios (r_{ij}). The Equations II.9–II.11 are designed to provide a representation of the terpolymer composition without the complications introduced by using ratio-based responses. Therein, F_i represents the instantaneous mole fraction of monomer *i* bound in the terpolymer, f_i represents the mole fraction of unreacted monomer *i* in the polymerizing mixture, alongside the reactivity ratios (r_{ij}).

$$F_1 - \frac{f_1\left(\frac{f_1}{r_{21}r_{31}}+\frac{f_2}{r_{21}r_{32}}+\frac{f_3}{r_{31}r_{23}}\right)\left(f_1+\frac{f_2}{r_{12}}+\frac{f_3}{r_{13}}\right)}{\begin{pmatrix} f_1\left(\frac{f_1}{r_{21}r_{31}}+\frac{f_2}{r_{21}r_{32}}+\frac{f_3}{r_{31}r_{23}}\right)\left(f_1+\frac{f_2}{r_{12}}+\frac{f_3}{r_{13}}\right) \\ +f_2\left(\frac{f_1}{r_{12}r_{31}}+\frac{f_2}{r_{12}r_{32}}+\frac{f_3}{r_{13}r_{32}}\right)\left(f_2+\frac{f_1}{r_{21}}+\frac{f_3}{r_{23}}\right) \\ +f_3\left(\frac{f_1}{r_{13}r_{21}}+\frac{f_2}{r_{23}r_{12}}+\frac{f_3}{r_{13}r_{23}}\right)\left(f_3+\frac{f_1}{r_{31}}+\frac{f_2}{r_{32}}\right) \end{pmatrix}} = 0 \quad \text{(II.9)}$$

$$F_2 - \frac{f_2\left(\frac{f_1}{r_{12}r_{31}}+\frac{f_2}{r_{12}r_{32}}+\frac{f_3}{r_{13}r_{32}}\right)\left(f_2+\frac{f_1}{r_{21}}+\frac{f_3}{r_{23}}\right)}{\begin{pmatrix} f_1\left(\frac{f_1}{r_{21}r_{31}}+\frac{f_2}{r_{21}r_{32}}+\frac{f_3}{r_{31}r_{23}}\right)\left(f_1+\frac{f_2}{r_{12}}+\frac{f_3}{r_{13}}\right) \\ +f_2\left(\frac{f_1}{r_{12}r_{31}}+\frac{f_2}{r_{12}r_{32}}+\frac{f_3}{r_{13}r_{32}}\right)\left(f_2+\frac{f_1}{r_{21}}+\frac{f_3}{r_{23}}\right) \\ +f_3\left(\frac{f_1}{r_{13}r_{21}}+\frac{f_2}{r_{23}r_{12}}+\frac{f_3}{r_{13}r_{23}}\right)\left(f_3+\frac{f_1}{r_{31}}+\frac{f_2}{r_{32}}\right) \end{pmatrix}} = 0 \quad \text{(II.10)}$$

$$F_3 - \frac{f_3\left(\frac{f_1}{r_{13}r_{21}}+\frac{f_2}{r_{23}r_{12}}+\frac{f_3}{r_{13}r_{23}}\right)\left(f_3+\frac{f_1}{r_{31}}+\frac{f_2}{r_{32}}\right)}{\begin{pmatrix} f_1\left(\frac{f_1}{r_{21}r_{31}}+\frac{f_2}{r_{21}r_{32}}+\frac{f_3}{r_{31}r_{23}}\right)\left(f_1+\frac{f_2}{r_{12}}+\frac{f_3}{r_{13}}\right) \\ +f_2\left(\frac{f_1}{r_{12}r_{31}}+\frac{f_2}{r_{12}r_{32}}+\frac{f_3}{r_{13}r_{32}}\right)\left(f_2+\frac{f_1}{r_{21}}+\frac{f_3}{r_{23}}\right) \\ +f_3\left(\frac{f_1}{r_{13}r_{21}}+\frac{f_2}{r_{23}r_{12}}+\frac{f_3}{r_{13}r_{23}}\right)\left(f_3+\frac{f_1}{r_{31}}+\frac{f_2}{r_{32}}\right) \end{pmatrix}} = 0 \quad \text{(II.11)}$$

To address the full conversion trajectory of the polymerization process, a cumulative ternary was introduced. This model, detailed in Equations II.12–II.14, connects the cumulative composition of each comonomer in the terpolymer ($\overline{F_i}$) with the initial feed's monomer mole fraction ($f_{i,0}$), the mole fraction of unreacted monomer within the polymerizing mixture (f_i), and the total molar conversion (X_n).

$$\overline{F_1} = \frac{f_{1,0} - f_1(1-X_n)}{X_n} \quad \text{(II.12)}$$

$$\overline{F_2} = \frac{f_{2,0} - f_2(1-X_n)}{X_n} \quad \text{(II.13)}$$

$$\overline{F_3} = \frac{f_{3,0} - f_3(1-X_n)}{X_n} \quad \text{(II.14)}$$

When a constant composition cannot be assumed, particularly when composition drift becomes significant, f_i needs to be assessed with respect to the conversion trajectory, as depicted in Eqs. (II.15)– (II.17).

$$\frac{df_1}{dX_n} = \frac{f_1 - F_1}{1 - X_n} \tag{II.15}$$

$$\frac{df_2}{dX_n} = \frac{f_2 - F_2}{1 - X_n} \tag{II.16}$$

$$\frac{df_3}{dX_n} = \frac{f_3 - F_3}{1 - X_n} \tag{II.17}$$

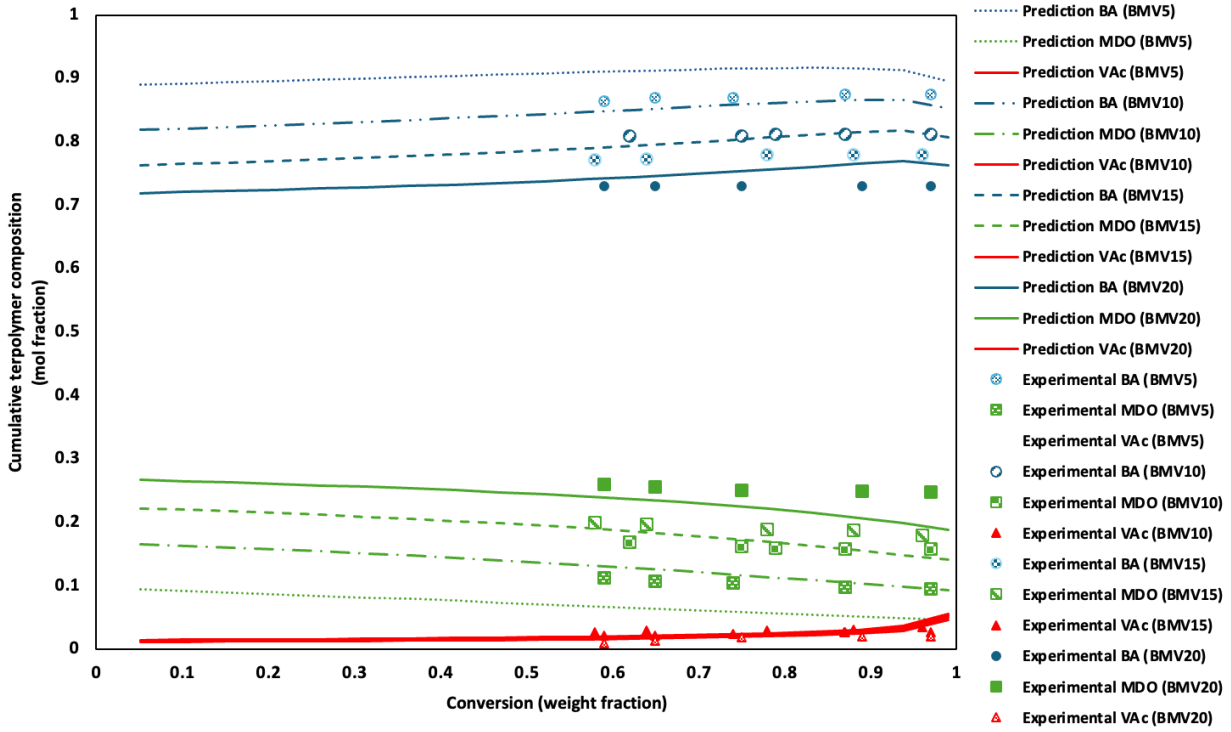

Figure II.9. Model predictions and experimental data of cumulative terpolymer composition vs. conversion using ternary reactivity ratios for all terpolymers (BMV5, BMV10, BMV15, and BMV20).

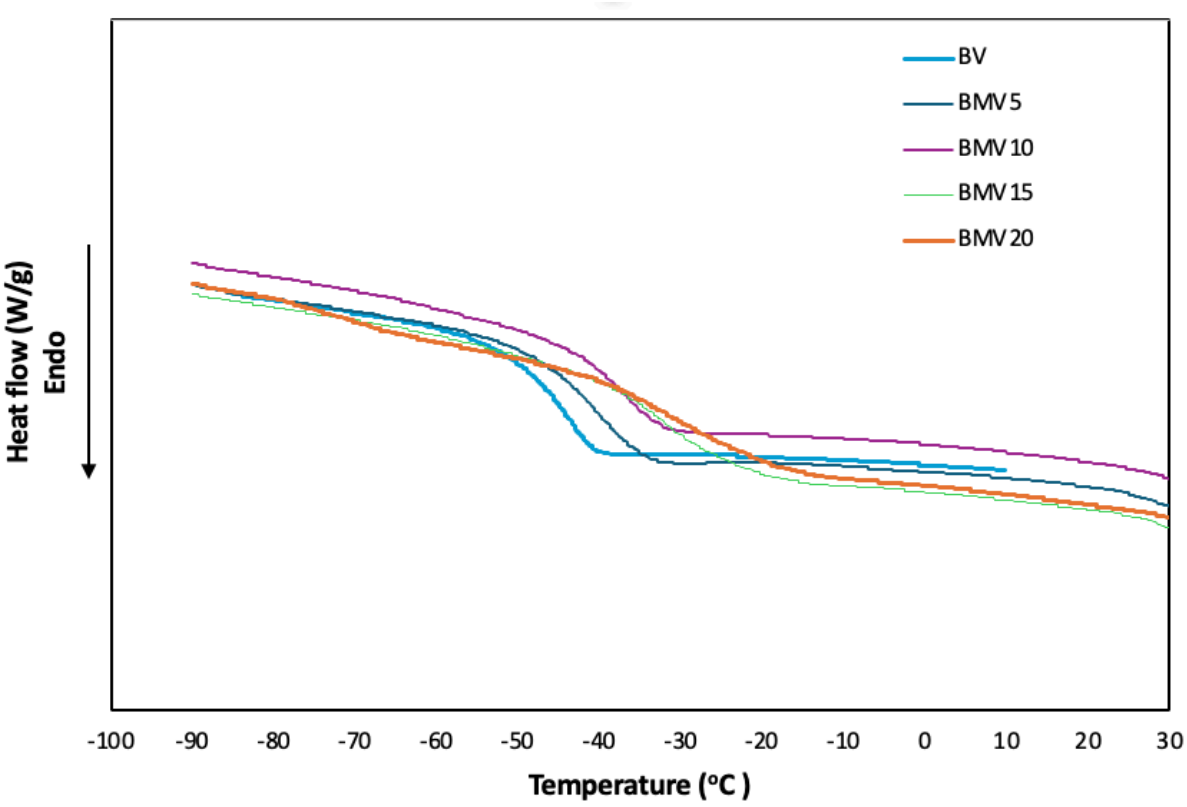

Figure II.10. DSC thermograms of BV, BMV5, BMV10, BMV15, and BMV20 show each T_g with a single transition peak.

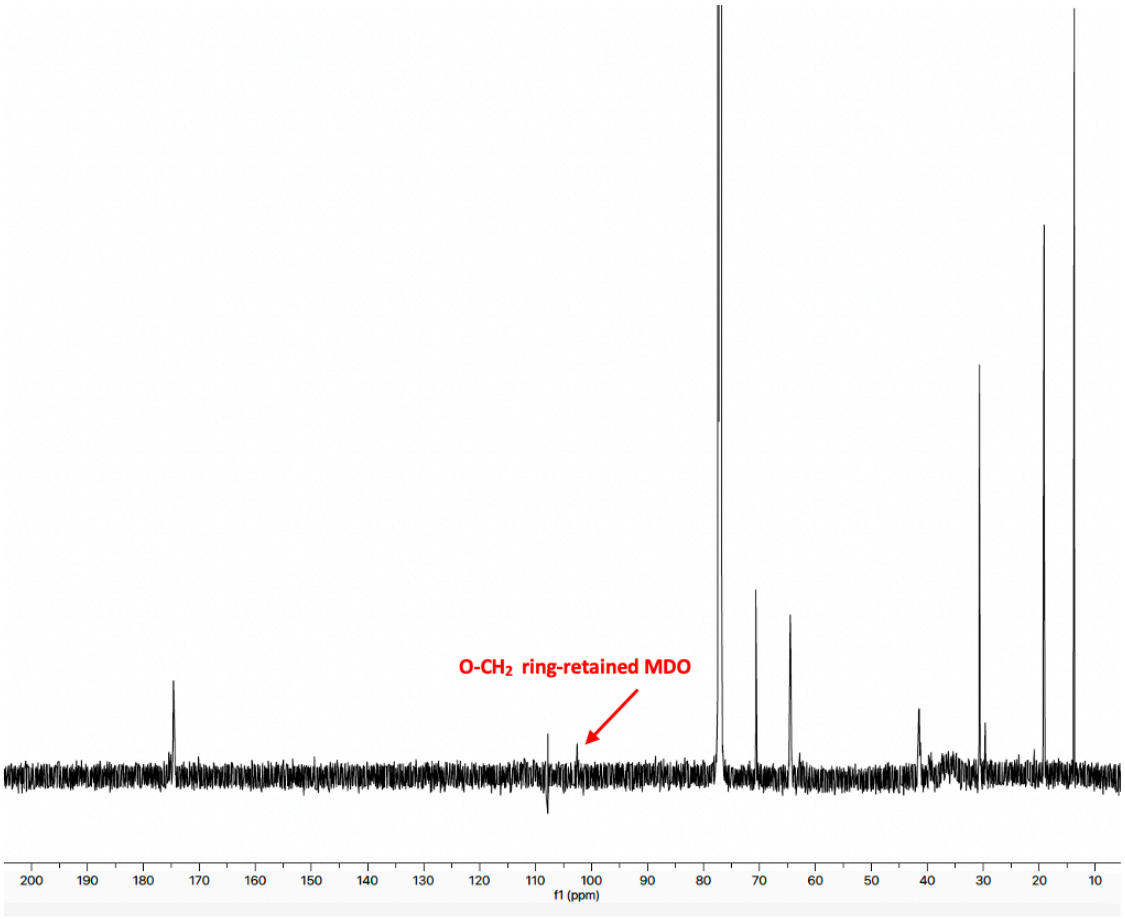

Figure II.11. ^{13}C-NMR spectrum for BMV5 in $CDCl_3$. The peak at 105 ppm is a narrow artifact observed in our ^{13}C-NMR results using the AVIII600 NMR instrument.

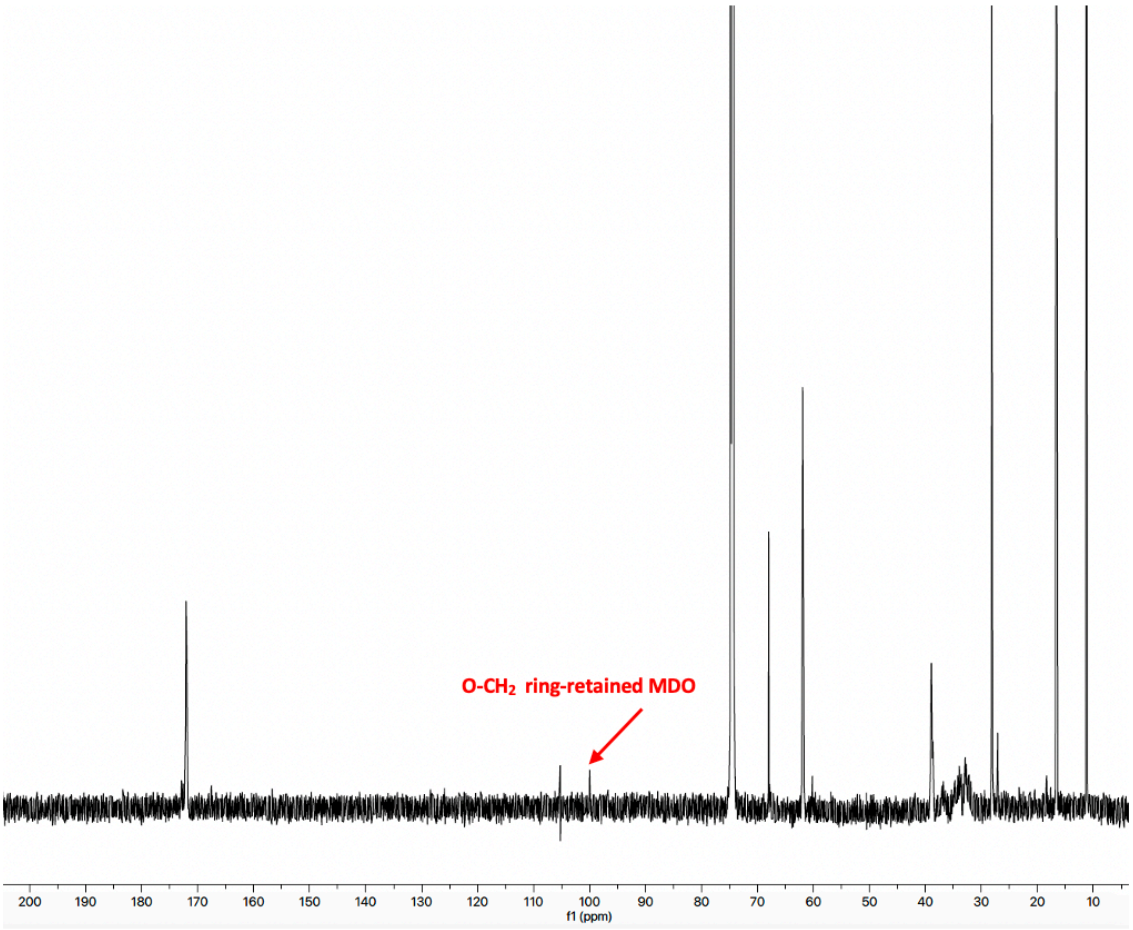

Figure II.12. ^{13}C-NMR spectrum for BMV10 in $CDCl_3$. The peak at 105 ppm is a narrow artifact observed in our ^{13}C-NMR results using the AVIII600 NMR instrument.

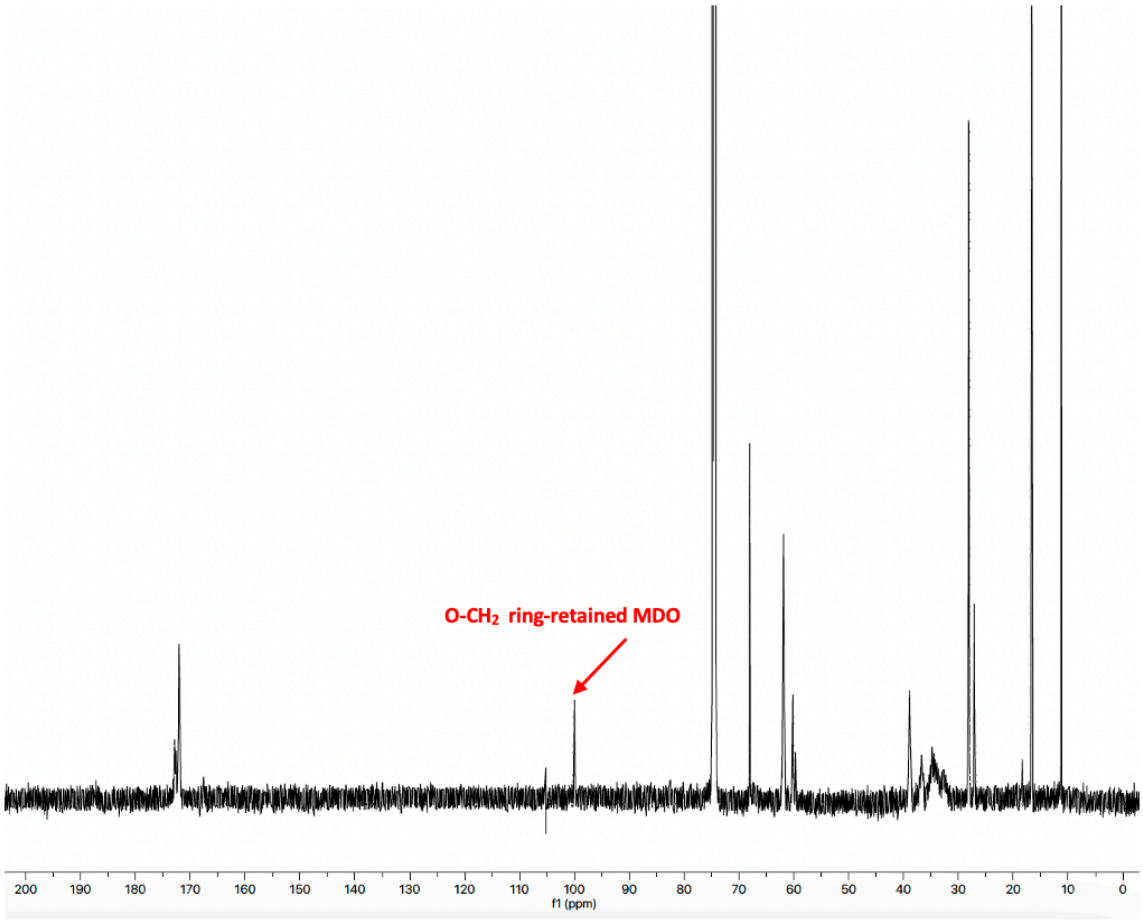

Figure II.13. ^{13}C-NMR spectrum for BMV15 in $CDCl_3$. The peak at 105 ppm is a narrow artifact observed in our ^{13}C-NMR results using the AVIII600 NMR instrument.

The MDO ring-retention using ^{13}C-NMR spectroscopy was calculated using four peaks shown in Figure 5.5 in the main manuscript. The peak at 100 ppm represents ring-retained MDO. By integrating each peak that represents the selected carbon atoms in the figure:

$$A_1 = n \quad \text{(II.7)}$$

$$A_2 = h \quad \text{(II.8)}$$

$$A_3 = k \quad \text{(II.9)}$$

$$A_4 = j \quad \text{(II.10)}$$

$$F_{\text{ring-retained MDO}} = n / (n + h + k + j) \quad \text{(II.11)}$$

where n, h, k and j relate to the ring-retained MDO, the ring-opened MDO, BA, and VAc carbons, respectively, found in areas A_1, A_2, A_3 and A_4. Area A_1 represents the carbon of ring-retained MDO ("d" in Figure 5.5 in the main manuscript), A_2 represents the ring-opened MDO ("b" in

Figure 5.5), area A_3 represents the carbon of BA ("a" in Figure 5.5 in the main manuscript) and area A_4 represents the carbon of VAc ("e" in Figure 5.5 in the main manuscript). After solving for *n*, *h, k* and *j* (Equations II.7, II.8, II.9, and II.10), ring-retained MDO was calculated using equation II.11.

a)

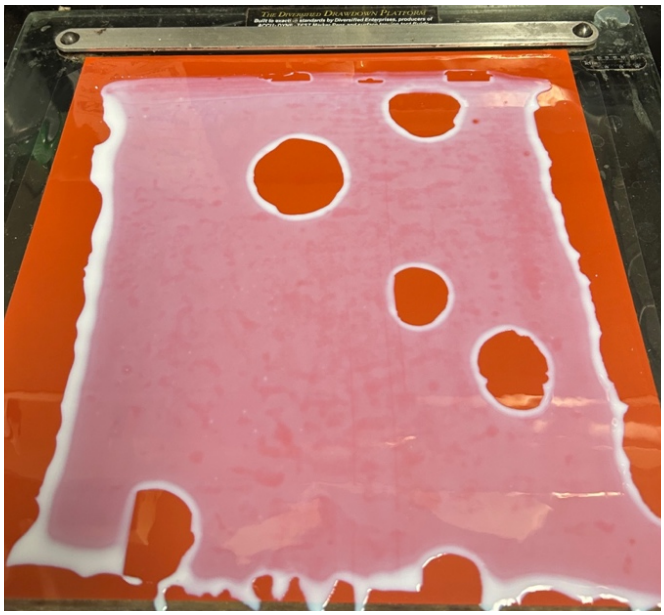

b)

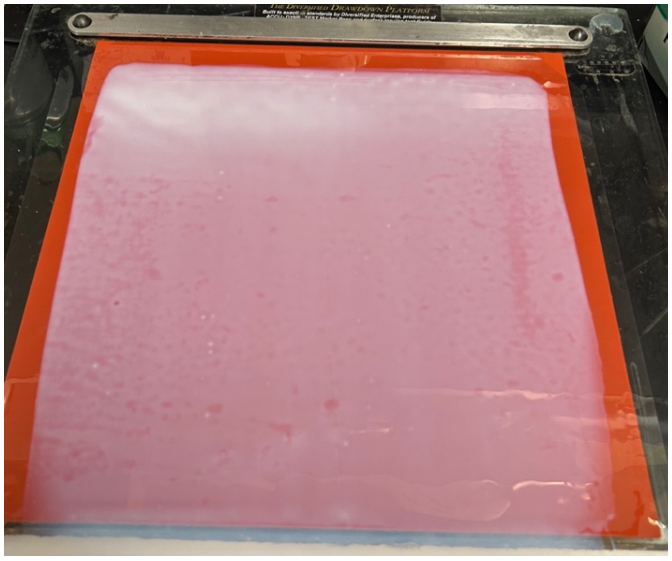

Figure II.14 Cast films of BMV20 a) before and b) after adding wetting agent.

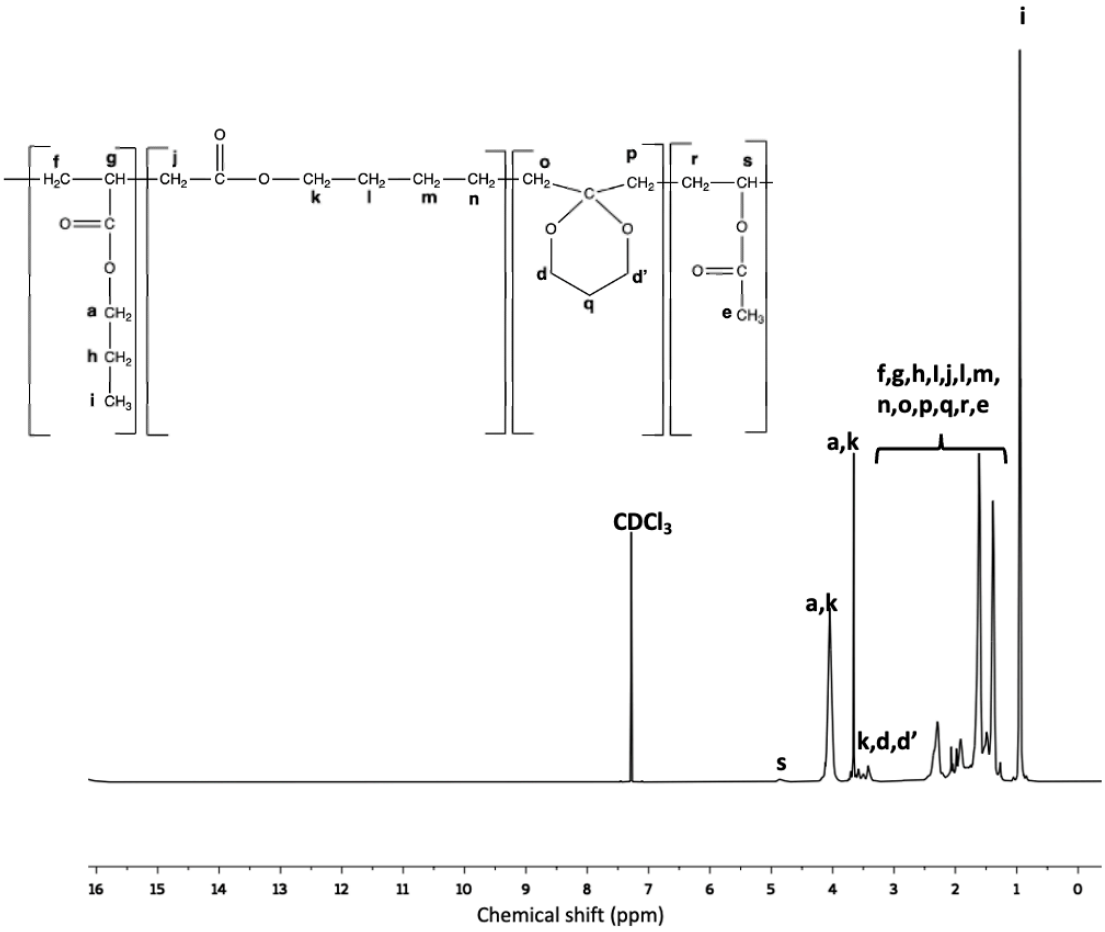

Figure II.15 ^{1}H-NMR spectrum for BMV10-NEW in $CDCl_3$.

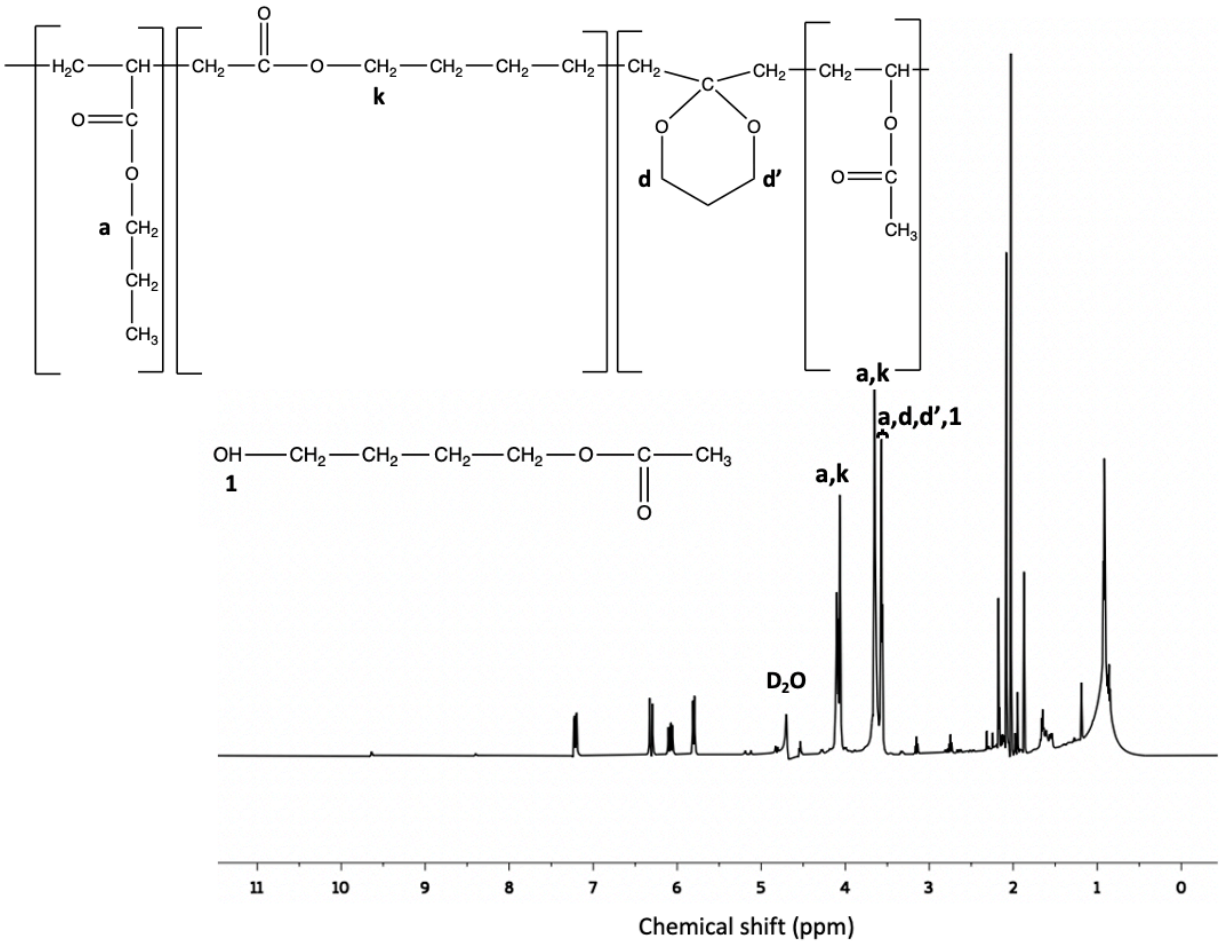

Figure II.16 ^{1}H-NMR Watergate spectrum of BMV10-NEW latex in D_2O.

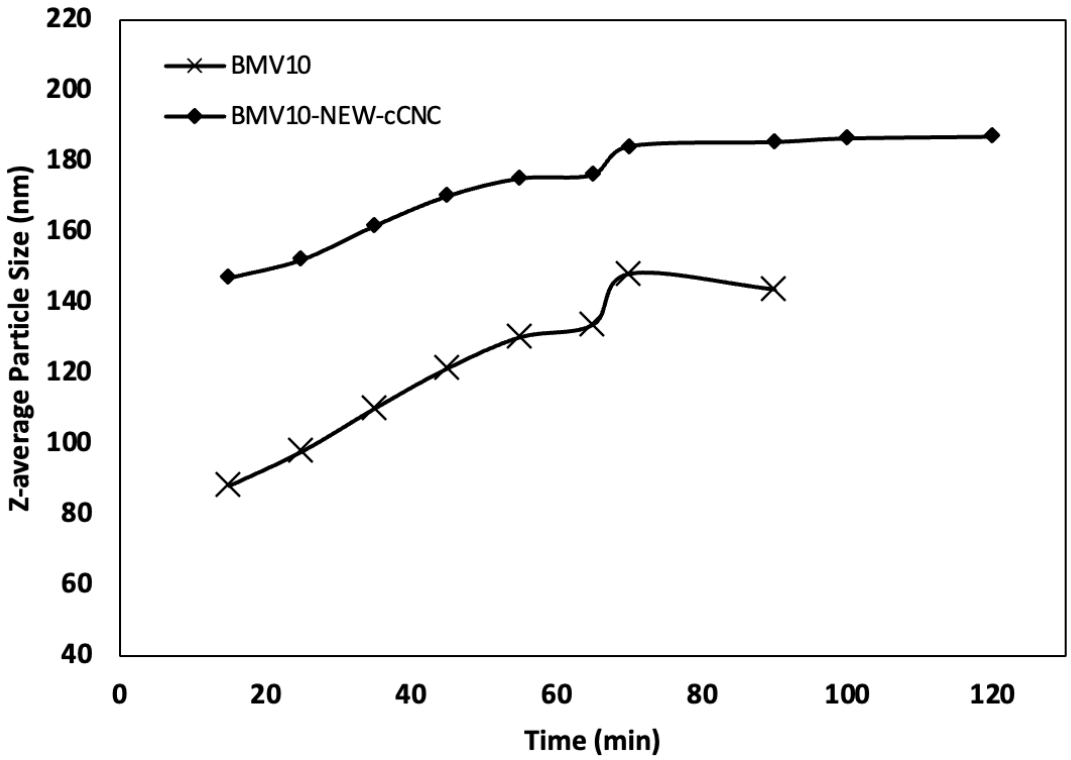

Figure II.17 Z-average particle size versus time for BMV10 and BMV10-NEW

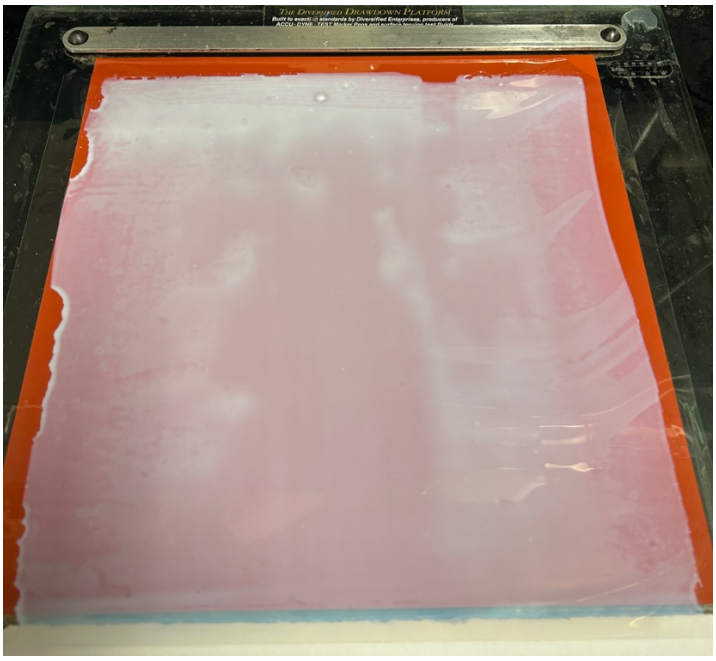

Figure II.18 Cast film of BMV10-NEW-cCNC. No wetting agent was added.

Appendix III
Supporting Information for "Chapter 6: Assessing the Biodegradability of 2-Methylene-1,3-Dioxepane (MDO)-Based Multicomponent Polymers Under Aerobic Composting Conditions"

III.1 Design of a lab-scale composting test apparatus

We designed and built a series of 15 bioreactors capable of simulating the enclosed aerated static pile, common to municipal composting facilities, to measure the aerobic degradation based on the D5338 ASTM standard. The apparatus also includes sensors, a temperature control bath, and a ventilation system. Data acquisition software was developed using LabVIEW to automate communication with the sensors to measure temperature, humidity and CO_2 concentrations and infer the degree and rate of aerobic degradation.

III.2 Bioreactor design

The bioreactors were custom-built in-house in the University of Ottawa's Chemical Engineering Department workshop to obtain a suit ab-scale set-up and reduce overall costs. The bioreactors were designed to be robust (e.g., made from durable materials, able to withstand temperatures and pressures far greater than required). Each bioreactor body was made from a 4.5" outer diameter stainless steel tube (thickness = ⅛") cut to 12" in height with a total inner volume of approximately 3.1 L. Each bioreactor had two port holes for ¼" Yor-Lok adaptors suitable for the tubing used for the active aeration (discussed later); one hole was located near the top of the vessel and the other near the bottom. The lid, made from ½" thick polycarbonate, was secured to the flange via six bolts and wing nuts passing through ¼" holes drilled into the flange and lid. Note that there was a 0.06" deep groove that was etched into the lid to house an O-ring to ensure an airtight seal. The sensor (described later) was affixed, using adhesive, to the underside of the lid and the cable used to power the sensor and transmit data to the computer was passed through the lid via a compression fitting sealed with silicone.

III.3 Temperature-controlled bath

A temperature-controlled bath was required to simulate the natural temperature cycles of composting. Environmental chambers could also have been used to simulate these temperatures. A temperature-controlled bath made from a 60-gallon galvanized steel stock tank and a heating element were used. The bioreactors were placed inside the water bath (Figure III.1) to ensure uniform heat distribution throughout the experiment. An immersion water bath circulator (Figure III.2) was used to regulate the water bath temperature, maintaining the desired thermal conditions necessary for composting. To ensure that the desired temperatures were reached and maintained throughout the experiment, the stock tank was wrapped with a ½" thick layer of isoprene insulation, and to avoid bulk water evaporation and heat loss, the bioreactors and temperature-controlled bath were covered with a Plexiglas lid (Figure III.3).

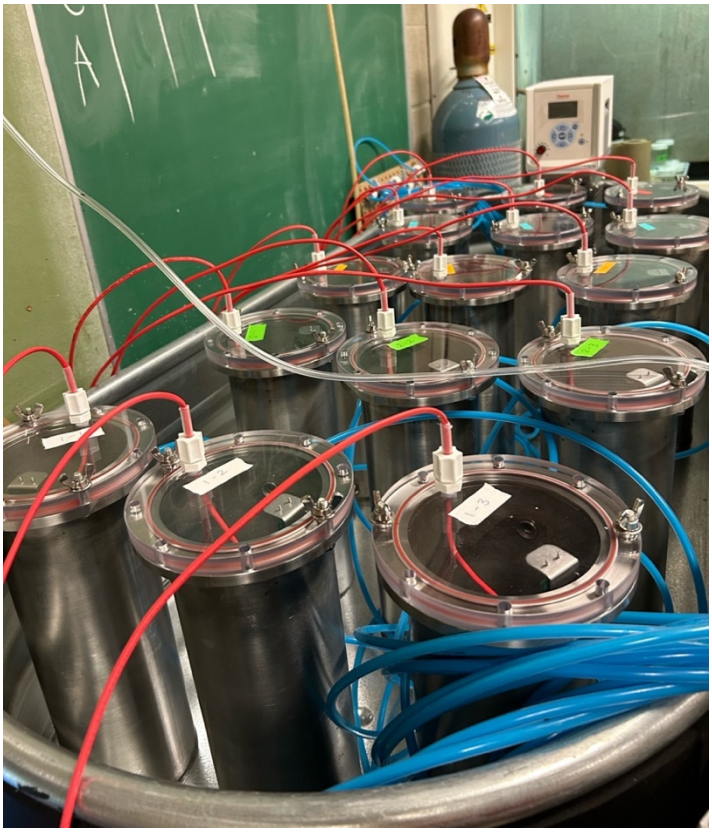

Figure III.1. 15 bioreactors and water bath

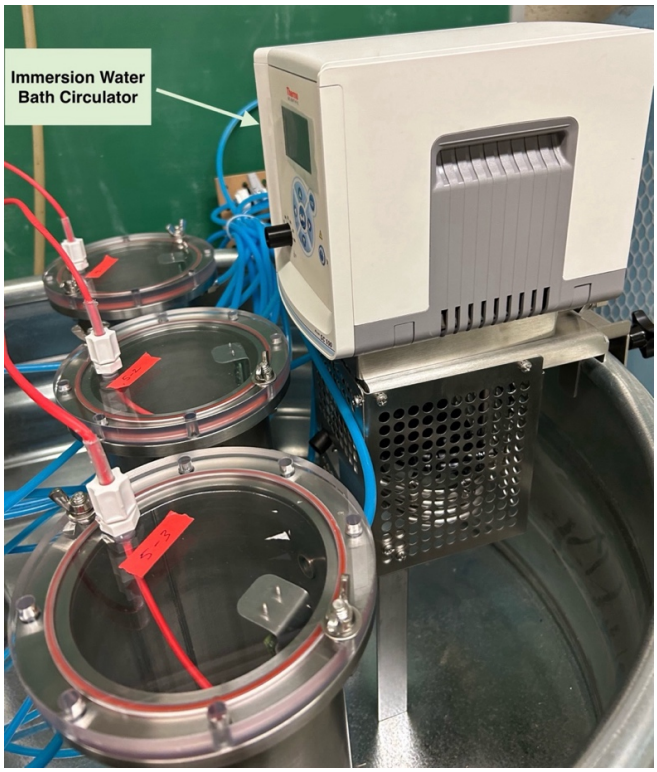

Figure III.2. Immersion water bath circulator attached to the water bath's wall

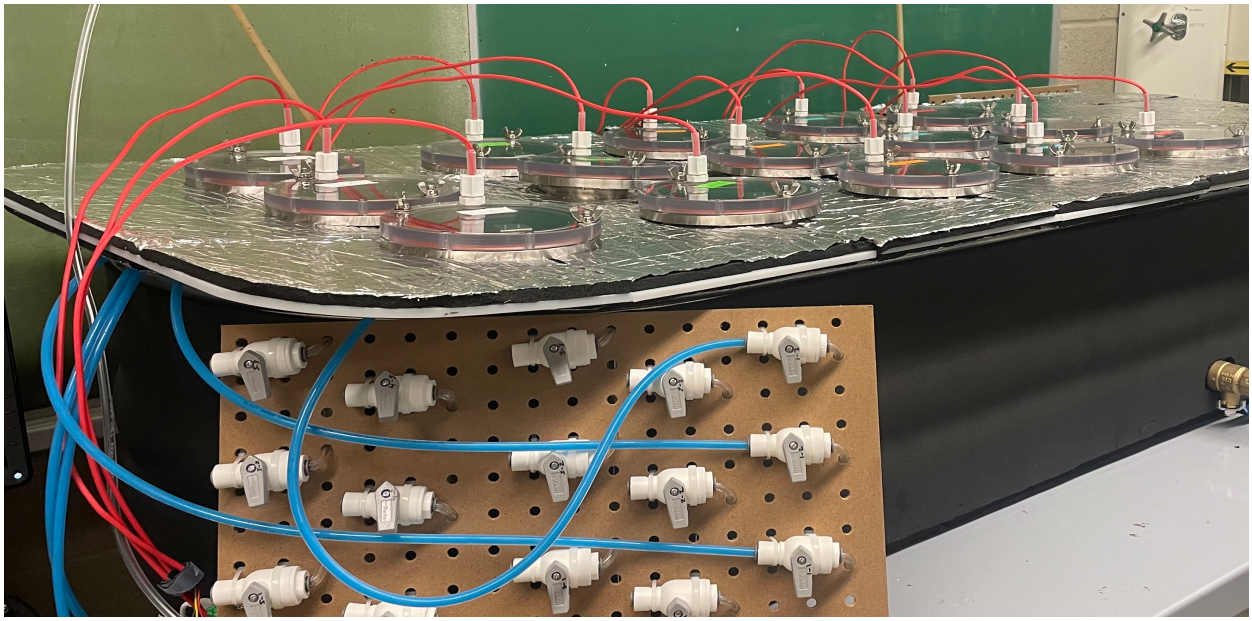

Figure III.3. Water bath with Plexiglas lid covering the bioreactors to minimize heat loss and evaporation.

III.4 CO_2, relative humidity, and temperature sensor

Instead of using cumbersome methods for determining CO_2 evolution (e.g., titrating a caustic solution periodically), an automatic data acquisition platform was designed in LabVIEW to record the CO_2 evolution in real-time, thereby reducing manual labour for the duration of the experiment. Each bioreactor was equipped with a measurement device comprised of a Sensirion SCD30 sensor (which measures CO_2 concentration (in ppm), relative humidity, and temperature) and an Adafruit 5V microcontroller board called a Trinket. The Trinket transmitted the data from the sensor to LabVIEW via a standard I2C protocol through the Arduino integrated development environment (Arduino IDE). The code used to program the SCD30 (i.e., the library manager in the Arduino IDE) was obtained online and the toolkit needed to establish communication between the Trinket and LabVIEW was downloaded from the National Instruments website (www.ni.com). Cables capable of withstanding the experimental conditions (e.g., high temperature and high humidity) were purchased from McMaster-Carr. Note that the Trinket was plugged directly into the computer via a micro USB cable which provided power to and transmitted data from the sensor.

III.5 Positive aeration system

The ASTM D5338 standard requires that the bioreactors be opened and aerated periodically to ensure that the microorganisms had sufficient oxygen. To minimize experimental error, reduce the amount of labour, and to eliminate unpleasant odours that are released every few days during aeration, an airflow system designed to mimic the positive aeration used in municipal composting facilities was used, which were vented directly into a fume hood. Briefly, CO_2-free air (Zero Air, Messer) flowed through the vessels to purge the bioreactor headspace via a series of tubes and valves (Figure III.4). The number of moles of CO_2 was calculated by taking the integral of the CO_2 curve between each reactor purge to determine the degree of biodegradation. These calculations were automated in LabVIEW.

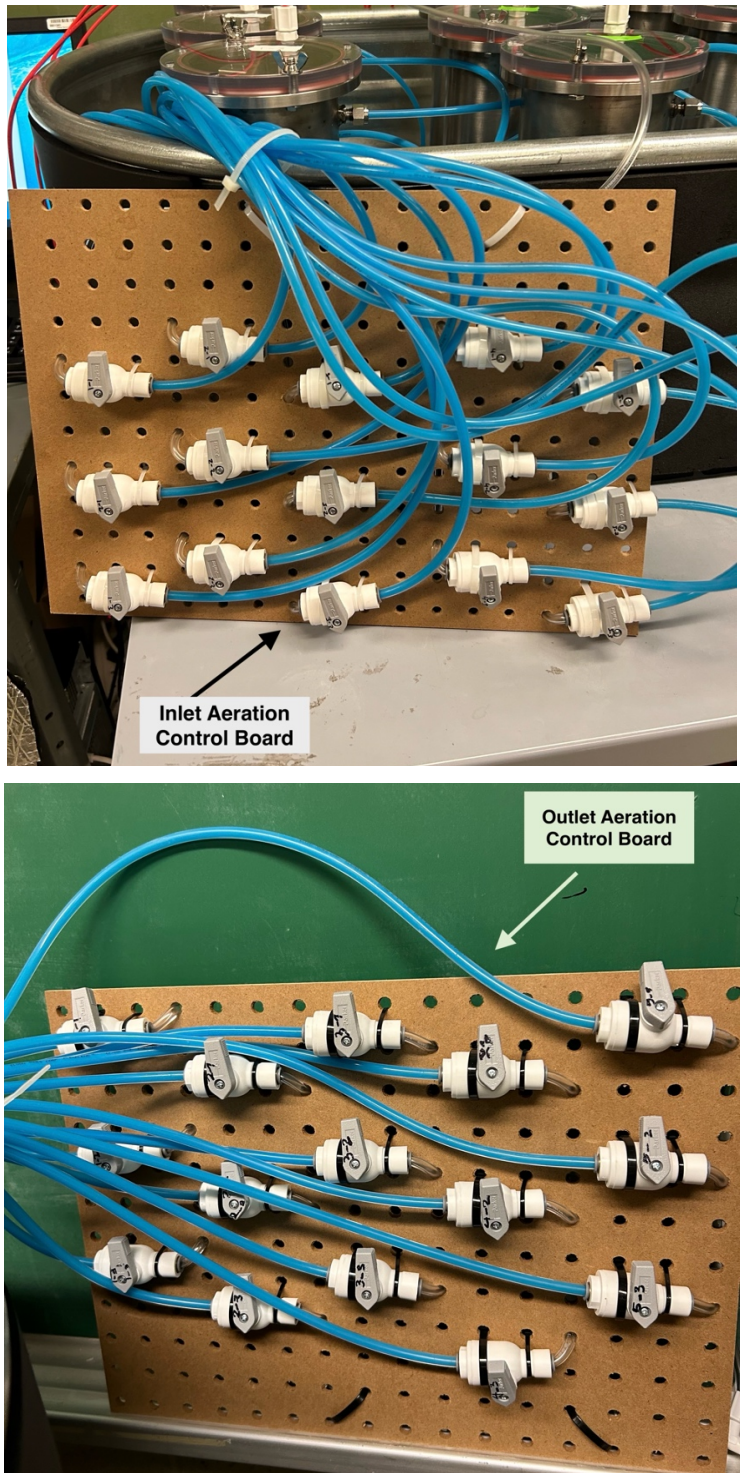

Figure III.4. Inlet and outlet aeration control boards

a)

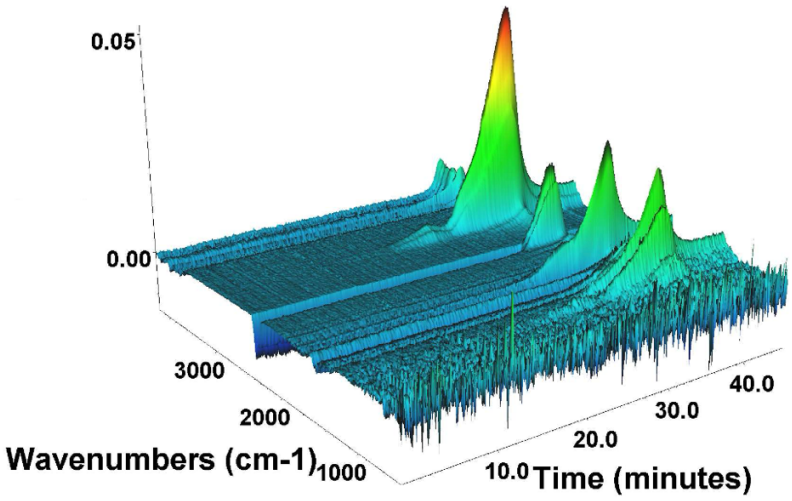

b)

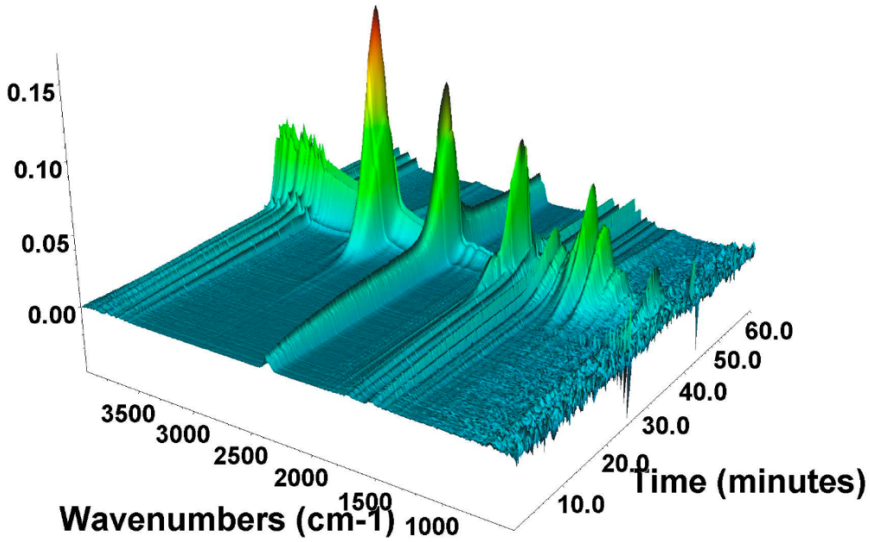

Figure III.5. 3D surface plots of TGA-FTIR spectra for the evolved gaseous products of BMV10-NEW-cCNC: (a) before and (b) after composting.

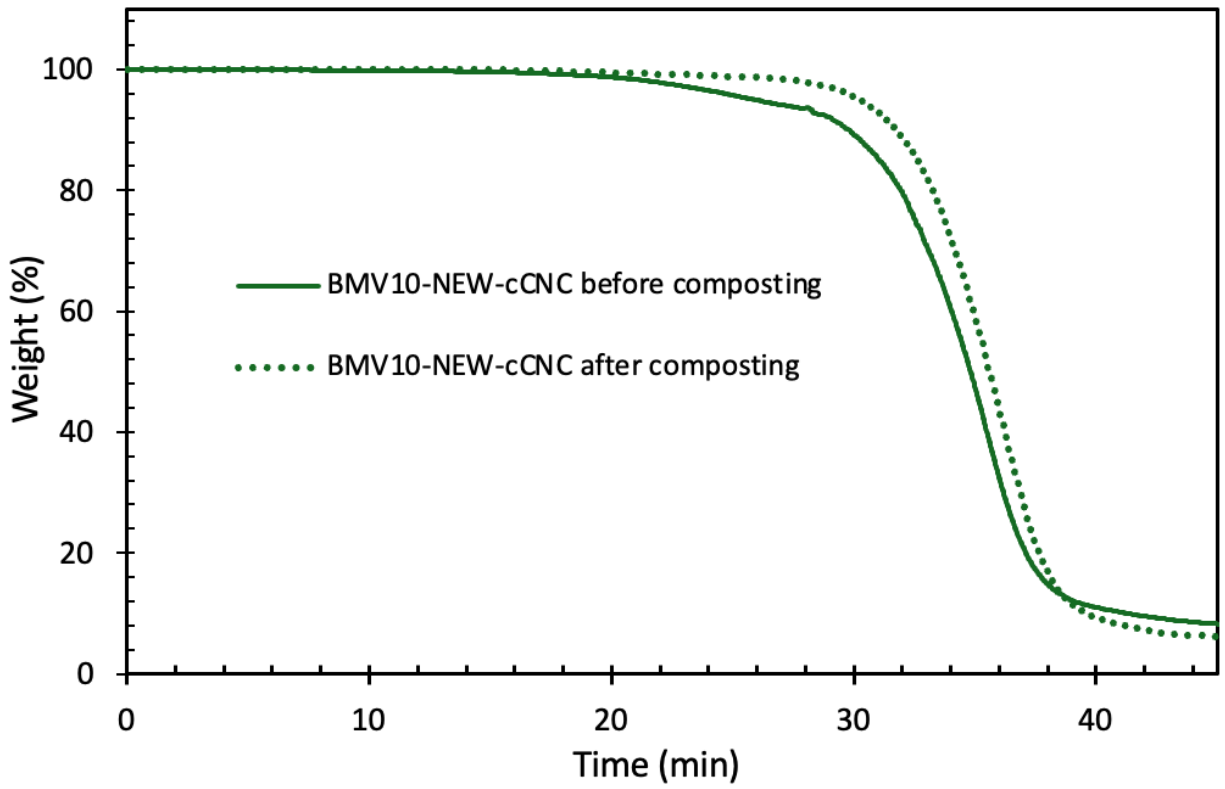

Figure III.6. TGA curves showing the weight loss as a function of time for BMV10-NEW-cCNC and BMV20, before and after composting.

Appendix V
List of Publications and Conferences

V.1 List of Publications

1. **Movafagh, M.,** Meek, K. M., Bayat, P., Cranston, E. D., Cunningham, M., Champagne, P., Morse, T., Kiriakou, M. V., George, S. R., & Dubé, M. A., Improved Pressure-Sensitive Adhesive Performance Using Carboxylated Cellulose Nanocrystals via Blending, *Polymer Engineering & Science*, 64(2), 798-816 (2024).

2. **Movafagh, M.,** Meek, K. M., Scott, A. J., Penlidis, A., & Dubé, M. A., Bulk Free Radical Terpolymerization of Butyl Acrylate, 2-Methylene-1,3-Dioxepane and Vinyl Acetate: Terpolymer Reactivity Ratio Estimation, *Polymers*, 16(10), 1330 (2024).

3. Bayat, P., Meek, K. M., **Movafagh, M.,** Cranston, E. D., Cunningham, M. F., Champagne, P., Morse, T., Kiriakou, M. V., George, S. R., & Dubé, M. A., The Effect of Cellulose Nanocrystal Reassembly on Latex-Based Pressure-Sensitive Adhesive Performance, *Biomacromolecules*, 25(5), 3018-3032 (2024).

4. **Movafagh, M.,** Dubé, M. A., & Meek, K. M., Butyl Acrylate/2-Methylene-1,3-Dioxepane/Vinyl Acetate Emulsion Terpolymerization: Incorporating Backbone Degradable Linkages into Adhesive Applications, *ChemSusChem* (2025).

5. **Movafagh, M.,** Gabriel, V. A., Meek, K. M., & Dubé, M. A., Assessing the Biodegradability of 2-Methylene-1,3-Dioxepane (MDO)-Based Multicomponent Polymers Under Aerobic Composting Condition, *Polymer Degradation and Stability* (to be submitted).

V.2 List of Conference Contributions

1. **Movafagh, M.,** Meek, K. M., & Dubé, M. A. (October 2024). Butyl Acrylate/2-Methylene-1,3-Dioxepane/Vinyl Acetate Emulsion Terpolymerization: Incorporating Backbone Degradable Linkages into Adhesive Applications. *Canadian Society of Chemical Engineering (CSChE) Conference*, Toronto, Canada.

2. **Movafagh, M.,** Meek, K. M., Scott, A. J., Penlidis, A., & Dubé, M. A. (October 2024). Butyl Acrylate/2-Methylene-1,3-Dioxepane/Vinyl Acetate Emulsion Terpolymerization: Incorporating Backbone Degradable Linkages into Adhesives. *Canadian Society of Chemical Engineering (CSChE) Conference*, Toronto, Canada.

3. Meek, K. M., **Movafagh, M.,** & Dubé, M. A. (August 2024). Towards a Compostable Pressure Sensitive Adhesive: Synthesis, Characterization, and Compostability. *American Chemical Society (ACS) Conference*, Denver, USA.

4. **Movafagh, M.,** Meek, K. M., Bayat, P., Cranston, E. D., Cunningham, M., Champagne, P., Morse, T., Kiriakou, M., George, S. R., & Dubé, M. A. (June 2023). The Effect of Carboxylated Cellulose Nanocrystals on a Latex-Based Pressure-Sensitive Adhesive via Blending. *The International Polymer Colloids Group (IPCG) Conference*, Kingston, Canada.

5. **Movafagh, M.,** Meek, K. M., Bayat, P., Cranston, E. D., Cunningham, M., Champagne, P., Morse, T., Kiriakou, M., George, S. R., & Dubé, M. A. (June 2023). The Effect of Carboxylated Cellulose Nanocrystals on a Latex-Based Pressure-Sensitive Adhesive via Blending. *The International Conference on Nanotechnology for Renewable Materials (TAPPI Nano)*, Vancouver, Canada.

6. Bayat, P., Meek, K. M., **Movafagh, M.,** Cranston, E. D., Cunningham, M. F., Champagne, P., Morse, T., Kiriakou, M. V., George, S. R., & Dubé, M. A. (June 2023). The Effect of Cellulose Nanocrystal Reassembly on Latex-Based Pressure-Sensitive Adhesive Performance, *The International Conference on Nanotechnology for Renewable Materials (TAPPI Nano)*, Vancouver, Canada.

Appendix IV
Laboratory Safety Considerations

The hazards and required personal protective equipment (PPE) for all the chemicals used in this project were obtained from the manufacturer's safety data sheets and are summarized below. In general, solutions were prepared in a fume hood, and PPE, including a respiratory mask, safety goggles, nitrile gloves, and a lab coat, were used during reaction preparation and polymerization because of possible contact with monomer (during reactor charging and sampling). The reactor temperature was automatically controlled (max ~ 65-70°C) in a jacketed stainless-steel reactor, connected to a condenser which liquefied the monomer vapours.

Table IV.4 Hazards and personal protective equipment required for chemicals in this project.

Chemicals	Manufacturer	Hazards	Personal protective equipment (PPE)
Acetone	Fischer Scientific	Highly flammable liquid and vapor Causes serious eye irritation May cause drowsiness	Protective clothing and gloves, eye protection
Ammonium persulfate (APS)	Sigma-Aldrich	Oxidizing solids May cause eye, skin, and respiratory irritation	Protective clothing and gloves, eye protection
2,2'-Azobis isobutyronitrile (AIBN)	Sigma-Aldrich	Flammable Toxic if swallowed Skin, eye and respiratory irritation	Protective clothing and gloves, eye protection, and full face respirator
Butyl acrylate (BA)	Sigma-Aldrich	Flammable liquid and vapour Cause skin irritation	Protective clothing and gloves, eye protection, and full face respirator
Butyl hydroperoxide (t-BHP)	Sigma-Aldrich	Oxidizing liquid May cause eye, skin, and respiratory irritation	Protective clothing and gloves, eye protection
Carboxylated cellulose nanocrystals (cCNCs)	Anomera Inc.	No significant hazard	Protective clothing and gloves, eye protection
Deuterated chloroform ($CDCl_3$)	Sigma-Aldrich	Highly flammable liquid and vapor Causes serious eye irritation May cause drowsiness	Protective clothing and gloves, eye protection

2-methylene 1,3-dioxepane (MDO)	Wacker Chemie	Flammable liquid and vapour Cause skin irritation	Protective clothing and gloves, eye protection, and full-face respirator
Nitrogen gas (N_2)	Messer	High pressure May cause suffocation by displacing the oxygen in air	Storage upright and secure cylinders all time while in use and use appropriate hand truck designed for cylinder
Sodium dodecyl sulfate (SDS)	Sigma-Aldrich	Flammable and toxic in contact with skin May cause serious eye damage and may cause skin and respiratory irritation	Protective clothing and gloves, eye protection
Sodium hydroxide (NaOH)	Sigma-Aldrich	Causes severe skin burns and eye damage	Protective clothing and gloves, eye protection and respirator
Tetrahydrofuran (THF)	Caledon Chemicals	Flammable May cause mild skin and serious eye irritation	Protective clothing and gloves, eye protection
Triton X-405, 70% solution in water	Fisher Scientific	Not considered hazardous by the 2012 OSHA Hazard Communication Standard	Protective clothing, gloves, eye protection
Vinyl acetate (VAc)	Sigma-Aldrich	Flammable liquid and vapour Cause skin irritation	Protective clothing and gloves, eye protection, and full face respirator